UNIVERSITY OF SOUTHAMPTON

FACULTY OF NATURAL AND ENVIRONMENTAL SCIENCES

Chemistry

REPROGRAMMING THE CELLULAR RESPONSE TO HYPOXIA

by

Ishna N Mistry

Thesis for the degree of Doctor of Philosophy

2016

UNIVERSITY OF SOUTHAMPTON

ABSTRACT

FACULTY OF NATURAL AND ENVIRONMENTAL SCIENCES

Chemistry

Thesis for the degree of Doctor of Philosophy

REPROGRAMMING THE CELLULAR RESPONSE TO HYPOXIA

Ishna N Mistry

HIF-1 is a heterodimeric transcription factor comprising HIF-1α and HIF-1β subunits. Cellular response to hypoxia relies on the dimerisation of HIF-1α and HIF-1β in the nucleus, forming HIF-1, which then initiates transcription of target genes. Both subunits are constitutively expressed, but the α subunit is degraded in an oxygen-dependent manner, so it is only stabilised in hypoxia. HIF-1 expression is deregulated in many cancers and has been associated with resistance to chemotherapy. Therefore, understanding the molecular mechanisms of hypoxic response is key to developing cancer therapeutics.

This thesis describes the construction and validation of a novel method to study the HIF-1 pathway by reprogramming cellular behaviour. This is achieved by targeting HIF-1α/HIF-1β dimerisation with an endogenously expressed molecular inhibitor. The compound, cyclo-CLLFVY, was previously identified through screening of a library of biologically synthesised cyclic peptides. In this study, the peptide sequence was genetically-encoded, between split *Nostoc punctiforme* DnaE inteins, onto the chromosome of a mammalian cell line, to allow inducible expression and *in situ* cyclisation of the peptide. The utility of this methodology was demonstrated via identification of genes specifically transactivated by HIF-1 or HIF-2 transcription factors in hypoxia, in the integrated cell line. Furthermore, cell viability assays showed that specific inhibition of HIF-1 dimerisation in these cells increased cellular sensitivity to glucose deprivation and to inhibition of glycolysis.

In addition, the epigenetic regulation of HIF-1α was studied. HIF-1 transactivates the expression of its α-subunit resulting in positive autoregulation, which contributes to the build up of HIF-1α at the onset of hypoxia. This autoregulation is dependent on an unmethylated CpG site in the hypoxia response element (HRE) within the promoter of the HIF-1α gene. Given the key role of HIF-1 in the development of the mammalian embryo, the methylation status of the HIF-1α HRE in developing tissue was sought. The HIF-1α HRE was unmethylated in several embryonic tissues, suggesting that transactivation of HIF-1α plays a role in HIF-1-mediated gene expression during development.

Table of Contents

List of Tables

List of Figures

DECLARATION OF AUTHORSHIP

I, ISHNA N MISTRY

declare that this thesis and the work presented in it are my own and has been generated by me as the result of my own original research.

Reprogramming the cellular response to hypoxia.

I confirm that:

1. This work was done wholly or mainly while in candidature for a research degree at this University;
2. Where any part of this thesis has previously been submitted for a degree or any other qualification at this University or any other institution, this has been clearly stated;
3. Where I have consulted the published work of others, this is always clearly attributed;
4. Where I have quoted from the work of others, the source is always given. With the exception of such quotations, this thesis is entirely my own work;
5. I have acknowledged all main sources of help;
6. Where the thesis is based on work done by myself jointly with others, I have made clear exactly what was done by others and what I have contributed myself;
7. Parts of this work have been published as:

   Mistry, I. N.; Smith, P. J. S.; Wilson, D. I.; Tavassoli, A. *Mol Biosyst* 2015, *11* (10), 2780-2785.

Signed: .....

Date:.....

Acknowledgements

Thank you to my parents, who cultivated my passion for knowledge and supported me in indulging it. Everything I have achieved I owe to you.

I would also like to thank Prof Ali Tavassoli for the opportunity to carry out this research and the advice and guidance given to me throughout my PhD, and Prof Peter Smith for useful discussions. I am thankful to Dr Noel Wortham for the HEK cells that turned my project around and Ms. Julie Herniman and Dr. John Langley for help and advice with MS.

In addition, I am hugely grateful to Dr. Daniel Asby who taught me everything I know about cell culture and a little bit about life in general, you have supported me as a colleague, a mentor and a friend. I would like to extend this thanks to the Tavassoli group past and present and to my friends and family for immeasurable support and encouragement. Particularly Dr. Charlotte Lawrence for being menthol and Dr Charlotte Mardle for being sane. Nobody understands the trials of a PhD like someone trying finish one themself. So to my comrades in the Tavassoli lab: If I can do it, anyone can.

Also, thanks to Krishan, Parv and Priyesh, for their constant backing and reassurance, you helped me believe it was all worthwhile. Thank you to Hayley Nash and Joe Plummer for putting a roof over my head when I most needed it, and to Catherine Burd for fun times under mine. I have made friends during my time at Southampton who I will cherish for life.

Most of all I would like to thank Dr. Christopher Mallinson, who was there for every up and down, all the tears and tantrums, who listened to every rant and replied with support and patience. You encourage me and challenge me. I never could have done it without you.

Definitions and Abbreviations

18S rRNA	18S ribosomal RNA
2-DG	2-deoxy-d-glucose
4E-BP	4E binding protein
5mC	5-methylcytosine
ADM	Adrenomedullin
ADRP	Adipose differentiation-related protein
αKG	Alpha-ketoglutarate
αHIF	Antisense HIF-1α
Akt	Protein kinase B
ALDA	Aldolase A
AMP	Ampicillin
ANGPT	Angiopoietin
ANGPTL4	Angiopoietin-like 4
AP-1	Activator protein-1
AraC	Arabinose promoter
Arg	Arginine
ARH	Aryl hydrocarbon receptor
ARNT/2	Aryl hydrocarbon receptor nuclear translocator/2
Asn	Asparagine
ATP	Adenosine triphosphate
ATP1B1	ATPase, Na+/K+ transporting beta 1 polypeptide
bHLH	Basic helix-loop-helix
bHLHB2	Basic helix-loop-helix domain containing, class B, 2
BNIP	BCL2/Adenovirus E1B 19kDa Interacting Protein
bp	Base pairs
BS	Bisulfite sequencing
C-TAD	C-terminal transactivation domain
CAIX	Carbonic anhydrase IX
CBD	Chitin binding domain
CBP	CREB binding protein
cDNA	Complementary DNA
CHIP	Carboxyl terminus of HSP70 interaction protein
CK	Casein kinase
CMV	Cytomegalovirus
CpG	Cytosine preceding guanine
CtBP1/2	C-terminal binding protein 1/2
CUL2	Cullin 2
Cys	Cysteine
DAPI	4',6-diamidino-2-phenylindole
DCM	Dichloromethane
DDIT4	DNA-damage-inducible transcript 4
DDIT4L	DNA-damage-inducible transcript 4-like
Dhfr	Dihydrofolate reductase
DMEM	Dulbecco's Modified Eagle Medium

DMF	Dimethylformamide
DMSO	Dimethyl sulfoxide
DNA	Deoxyribonucleic acid
DNMT	DNA methyl transferase
dNTP	Deoxynucleotide triphosphate
Dox	Doxycycline
DTT	Dithiothreitol
E	Embryonic day
EDN1	Endothelin 1
EDTA	Ethylenediaminetetraacetic acid
EGTA	Ethyleneglycoltetraacetic acid
ENO1	Enolase 1
EP300	E1A binding protein p300
EPAS1	Endothelial PAS-domain protein 1
EPO	Erythropoietin
eq	Equivalents
ESI	Electrospray ionisation
FBS	Foetal bovine serum
FIH	Factor inhibiting HIF
Flp	Flippase
Fmoc	Fluorenylmethyloxycarbonyl
FP	Forward primer
FRAP1	FK506 binding protein 12-rapamycin associated protein 1
FRT	Flp Recombination Target
GAPDH	Glyceraldehyde-3 phosphate dehydrogenase
GDF	Growth and differentiation factor
GFP	Green fluorescent protein
Gln	Glycine
Glu	Glutamine
GLUT1/8	Glucose transporter1/8
GOI	Gene of interest
GPI	Glucosephosphate isomerase
GSK	Glycogen synthase kinase
GUSB	Glucuronidase beta
HAF	Hypoxia-associated factor
HAT	Histone acetyltransferase
HDAC	Histone deacetylase
HDM	Histone demethylase
HEK	Human embryonic kidney
HIF1/2/3	Hypoxia Inducible Factor1/2/3
HIG2	Hypoxia-inducible protein 2
His	Histidine
HK	Hexokinase
hmC	5-hydroxymethylcytosine
HMOX1	Heme oxygenase 1
HMT	Histone methyltransferase
HO	Heme-oxygenase
HOBt	Hydroxybenzotriazole

HRE	Hypoxia response element
Hsp	Heat-shock protein
HYOU1	Hypoxia up-regulated 1
Ic	C-intein
IGF2	insulin growth factor 2
IGFBP1	Insulin-like growth factor binding protein 1
In	N-intein
ING4	Inhibitor of growth family member 4
IRES	Internal ribosome entry site
ISWI	Imitation switch
JmjC	Jumonji-domain containing
kb	Kilobases
kDa	Kilo Daltons
L1CAM	L1 cell adhesion molecule
LB	Luria broth
LC-MS	Liquid chromatography-mass spectrometry
LDHA	Lactate dehydrogenase A
LIMD	LIM domain containing
LNA	Locked nucleic acid
lncRNA	Long non-coding RNA
Luc	Luciferase
Lys	Lysine
LZIP	Leucine zipper
m/z	Mass to charge ratio
MAPK	Mitogen-activated protein kinase
MAT1A/ 2A	Methionine adenosyltransferase 1A/ 2A
MB	Myoglobin
MCF-7	Michigan Cancer Foundation-7
MeCP	Methylcytosine binding protein
MEF	Mouse embryonic fibroblasts
minutes	Minute (s)
miRNA	MicroRNA
Mlh	MutL homolog
MMP9	Matrix metallopeptidase 9
MPI	Moxi population index
mRNA	Messenger RNA
MSP	Methylation specific PCR
MSP	Methylation specific PCR
MT3	Metallothionein 3
mTOR	Mammalian target of rapamycin
MTT	3-(4,5-dimethylthiazol-2-yl)-2-5-diphenyltetrazolium bromide
N-TAD	N-terminal transactivation domain
NF-κB	Nuclear factor κB
NGRG1	N-myc downstream regulated gene
NOS1	Nitric oxide synthase 1
NOS2A	Nitric oxide synthase 2A
NOS3	Nitric oxide synthase 3
NOTCH1	Notch homolog 1, translocation-associated (Drosophila)

Npu	Nostoc punctiforme
Oct	Octamer binding transcription factor
ODDD	Oxygen-dependent degradation domain
P1	Name of the peptide sequence: CLLFVY
PAS	Per-Arnt-Sim
PBS	Phosphate buffered saline
PCAF	p300/CBP associated factor
PCR	Polymerase chain reaction
PDB	Protein data bank
PDK1	Pyruvate dehydrogenase kinase
PFK	Phosphofructokinase
PGC	Primordial germ cell
PGK1	Phosphoglycerate kinase 1
PHD	Prolyl hydroxylase domain
PI3K	Phosphoinositide 3-kinase
PIK3CA	Phosphoinositide-3-kinase catalytic alpha polypeptide
PLA	Proximity ligation assay
PLK	Polo-like kinase
PPi	Protein-protein interactions
PRKAA1	Protein kinase, adenosine monophosphate-activated, alpha 1 catalytic subunit
PRKAA2	Protein kinase adenosine monophosphate-activated alpha 2 catalytic subunit
PTEN	Phosphatase and tensin homolog
qRT-PCR	Quantitative reverse transcriptase polymerase chain reaction
RACK1	Receptor of activated protein C kinase
RBX1	Ring-box 1
RBX1	RING-box protein 1
REDD1/2	Regulated in development and DNA damage response
RIPA	Radioimmunoprecipitation assay
RISC	RNA-induced silencing complex
RNA	Ribonucleic acid
RP	Reverse primer
RP-HPLC	Reverse-phase high performance liquid chromatography
RPMI	Roswell Park Memorial Institute
RTHS	Reverse two-hybrid system
SAM	S-adenosyl methionine
SD	Standard deviation
SDM	Site-directed mutagenesis
SDS-PAGE	Sodium Dodecyl Sulfate-Polyacrylamide Gel Electrophoresis
SEM	Standard error of the mean
Ser	Serine
SICLOPPS	Split-intein circular ligation of peptides and proteins
siRNA	Short interfering RNA
SIRT1	Sirtuin 1
sncRNA	Short non-coding RNA
SOC	Super optimal broth containing glucose
Spy	Aldrithiol protecting group
Ssp	Synechocystis sp. strain PCC6803
SWI/SNF	Switch/sucrose nonfermentable

TAE	Tris-acetate-EDTA
TBP	TATA-binding protein
Tc	Tetracycline
TCEP	Tris (2-carboxyethyl) phosphine
TDG	Thymine DNA glycosylase
TET	Ten-eleven translocation
TetO2	Tetracycline operator
TetR	Tet repressor
TF	Transcription factor
TFA	Trifluoroacetic acid
TGFa	Transforming growth factor a
TGFBR2	Transforming growth factor beta receptor 2
Thr	Threonine
TIS	Triisopropylsilane
Tm	Melting temperature
TOP	topoisomerase
TOS	TOR signalling
TP53	Tumour protein p53
TPI	Triosephosphate isomerase
TSAP	Thermosensitive alkaline phosphatase
TSS	Transcription start site
Val	Valine
VEGF	Vascular endothelial growth factor
VHL	Von Hippel-Lindau

Chapter 1: Introduction

1.1 Hypoxia inducible factors

Maintaining cellular oxygen levels is vital for cell function and survival. In conditions of low oxygen, hypoxia, organisms trigger a response at cellular and systematic levels in order to recover oxygen homeostasis. At the transcriptional level this response is principally mediated by the hypoxia inducible factor 1 (HIF-1) transcriptional complex.[1, 2] HIF-1 is a heterodimer consisting of an oxygen-sensitive alpha (α) subunit and a constitutively expressed beta (β) subunit, also known as the aryl hydrocarbon receptor nuclear translocator (ARNT).[3, 4] HIF-1β (encoded by two genes, ARNT1 and ARNT2) is stably expressed and is also an obligate partner for the aryl hydrocarbon receptor (ARH).[4, 5] In mammals, there are three genes that encode the α subunits giving rise to three isoforms, HIF-2α (also known as EPAS1) and HIF-3α, in addition to HIF-1α, which are able to dimerise with HIF-1β.[6, 7] The HIF family of transcription factors mediate the expression of a vast number of genes, including those involved in formation of new blood vessels, production of erythrocytes, and metabolic reprogramming of hypoxic cells. Therefore HIF function is vital during embryonic development.[3, 8-12] However, these functions can be exploited by cancer cells during the progression of solid tumours, as cells proliferate so rapidly they outstrip their local oxygen and nutrient supplies.[12-15]

1.1.1 Structure of HIF subunits

Both α and β subunits are members of the basic helix-loop-helix Per/Arnt/Sim (bHLH-PAS) transcription factor family (Figure 1).[4, 9, 16] Structurally, HIF-1α and HIF-2α are closely related, there is 83% sequence similarity in their bHLH domains and 67% similarity in their PAS motifs.[9] HIF-3α also shares 74% and 52-58% identity in its bHLH and PAS domains with HIF-1α and HIF-2α, respectively. Crystal structures of the HIF-1α/HIF-1β and HIF-2α/HIF-1β heterodimers suggest that their overall architectures are indistinguishable.[17] The PAS domains enable dimerisation of the α and β subunits which interact via the exposed face of the central β-sheets on the α-subunit (Figure 2).[18, 19] Both PAS-A and PAS-B domains of the α-subunits are required for heterodimer formation.[20]

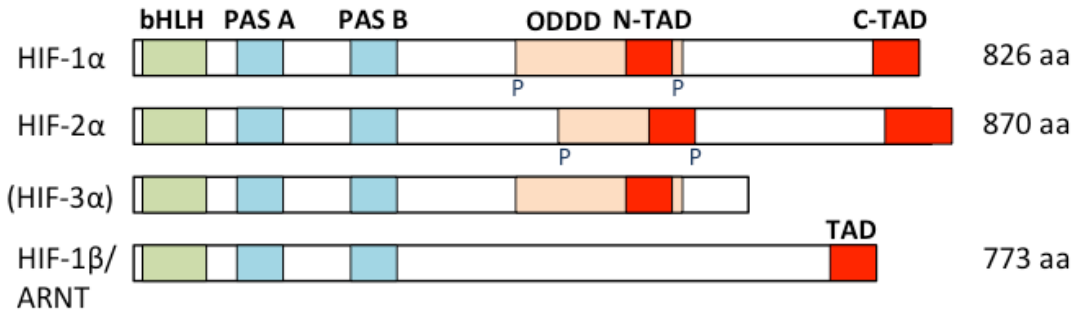

Figure 1: Structure of HIF-1α, its isoforms HIF-2α and HIF-3α and its binding partner HIF-1β. ODDD: oxygen-dependent degradation domain; TAD: transactivation domain.

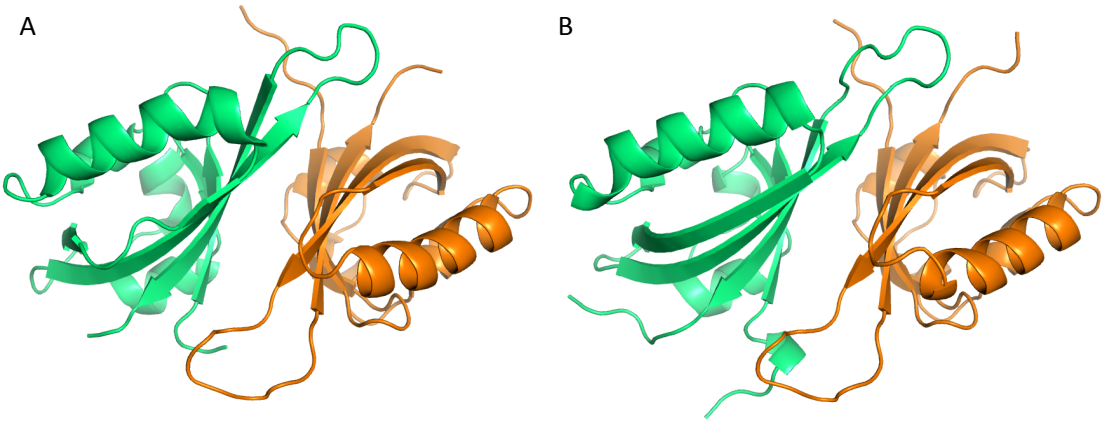

Figure 2: Crystal structures of HIF-α PAS-B and HIF-1β PAS-B dimerisation interfaces. (A) HIF-1α PAS-B (green) and HIF-1β PAS-B (orange) RCSB protein data bank (PDB) structure PDB 4H6J.[21] (B) HIF-2α PAS-B (green) and HIF-1β PAS-B (orange) PDB 3F1P.[22] Both α isoforms interact with HIF-1β via the exposed central β-sheets in these PAS-B domains.

The N-terminal bHLH domain is required for binding to DNA, with specific amino acids in the bHLH domains of HIF-α and HIF-β subunits engaging with a specific sequence of DNA, the hypoxia response element (HRE): TACGTG (Figure 3A).[17, 23] The bHLH domains insert α-helices into the major groove faces of the HRE sequence, allowing the formation of base-specific hydrogen-bonds and van der Waals interactions with residues from these helices (Figure 3B). His94 and Arg102 of HIF-1β interact with the first and second guanine residues, respectively, of the HRE on the sense strand of DNA (Figure 3D). A third residue of HIF-1β, Glu98, and Arg27 of HIF-1α interact with cytosine and guanine residues, respectively, of the HRE on the opposing DNA strand (Figure 3C). Additional basic residues from HIF-1α (Lys16 and 18 and Arg20, 24 and 26) and HIF-1β (Arg91, 99 and 101) can interact with DNA through the phosphate backbone.[17] Binding to DNA induces a stark change in conformation of the bHLH domains of both α and β subunits. The α1 helices elongate to bind DNA and the α2 helices, which link the bHLH domains of the proteins to the remainder of the structure, rotate

to facilitate DNA binding.[17] The PAS-A domain of both HIF-1α and HIF-2α cooperates with the bHLH domain to allow DNA binding.

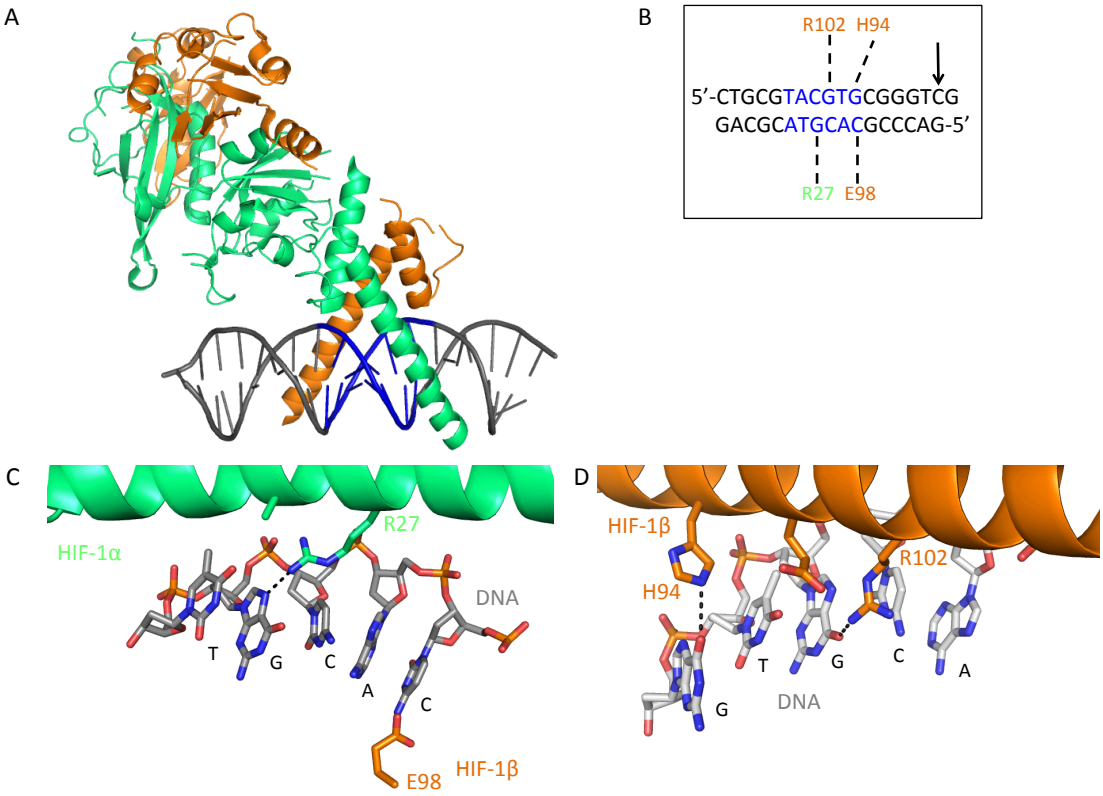

Figure 3: Recognition of the HRE by bHLH domains of HIF-1α/HIF-1β. (A) Overview of the interaction of the HIF-1 dimer with DNA. *Mus musculus* HIF-1α and HIF-1β (which are analogous to the human HIF-1 isoforms) bound to DNA with the HRE highlighted, PDB 4ZPR.[17] The α helices of the bHLH domains of HIF-1α and HIF-1β extend into the major groove at HRE sequences in DNA.(B) Diagram of the recognition of the HRE sequence by HIF-1α/HIF-1β. The arrow indicates the nucleotide that interacts with the PAS-A domain of HIF-1α and HIF-2α. (C) Detailed interactions of HIF-1α and HIF-1β with the HRE on the antisense DNA strand. (D) Detailed interactions of HIF-1β with the HRE on the sense DNA strand. For all, HIF-1α: green; HIF-1β: orange; DNA: A, B black; C, D grey; HRE: blue; dotted black lines represent hydrogen bonds. Adapted from Wu *et al.* 2015.[17]

Interaction of co-activators with HIF-1 and HIF-2, and activation of transcription, is mediated by two transactivation domains in the C-terminal region of HIF-1α and HIF-2α: the N-terminal and the C-terminal transactivation domains (TAD) (Figure 1).[24, 25] Although the sequences of the N-TADs of HIF-1α and HIF-2α are highly conserved (70% similarity), these regions are thought to confer HIF-1 target gene specificity through their interaction with different co-factors.[26] In contrast, the C-TADs, which are more divergent in sequence (67% similarity), mediate the transactivation of genes regulated by both HIF-1α and HIF-2α.[26, 27]

HIF-3α mRNA is alternatively spliced to give a number of different isoforms, the roles of which are unclear, but have been shown to include negative regulation of other HIF

complexes and modulation of hypoxic gene induction by HIF-1α.[28-30] The human splice variants HIF-3α1 and HIF-3α2 have similar domain organisation to the other HIF-α subunits, except they lack the C-TAD (Figure 4). HIF-3α1 instead comprises a leucine zipper (LZIP) at its C-terminus. HIF-3α1 and HIF-3α2 were shown to dimerise with HIF-1β but were unable to induce expression of a HRE reporter. Therefore, they may act to limit gene induction by HIF-1α and HIF-2α by competing for HIF-1β.[28] A shorter variant, HIF-3α4, lacks the CTAD, NTAD and oxygen-dependent degradation domain (ODDD) (Figure 4) and was reported to dimerise with HIF-1α and inhibit its nuclear translocation.[28] Expression of HIF-3α mRNA has been shown to be upregulated in hypoxia in a HIF-1α-dependent manner.[30] In contrast, the predominant mode of HIF-1α and HIF-2α regulation occurs at the protein level.

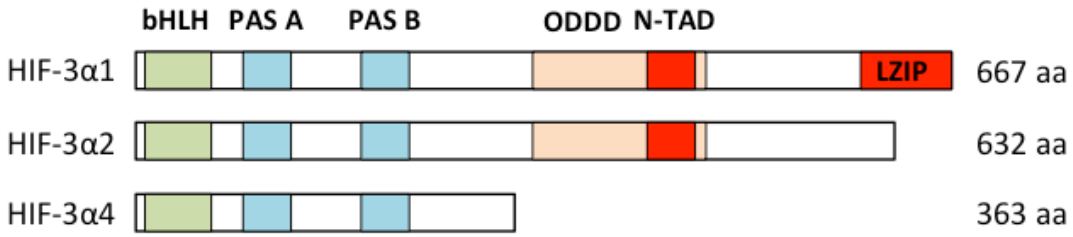

Figure 4: Illustration of three of the more characterised HIF-3α isoforms.

1.1.2 Oxygen-dependent regulation of HIFs

Regulation of protein stability by oxygen occurs via the ODDD, a highly conserved domain that partly overlaps the N-TAD (Figure 1).[24, 31] HIF-1α and HIF-2α have a high degree of similarity in their ODDDs, and are both post-transcriptionally regulated in a similar way.[32] In normoxia (normal levels of oxygen), the oxygen-sensitive HIF-1α subunit is degraded. Prolyl hydroxylase domain (PHD) enzymes catalyse the hydroxylation of two proline residues (P402 and P564 in HIF-1α and P405 and P531 in HIF-2α) within the ODDD, at the γ carbon of the pyrrolidine ring (Figure 5).[33-35] PHDs are dioxygenases that require α-ketoglutarate (αKG) and iron as co-factors in order to function, and utilise oxygen as a co-substrate, so they act as cellular oxygen sensors.[33, 36] Binding of oxygen to the enzyme-co-factor complex causes oxidative decarboxylation of αKG to succinate, and generation of an Fe (IV)-oxo species that allows hydroxylation of proline (Figure 6).[36, 37]

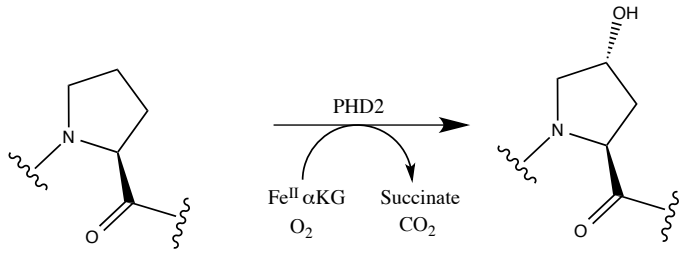

Figure 5: Hydroxylation of proline residues in HIF-1α leads to its oxygen-dependent regulation. PHD2 catalyses the hydroxylation of P402 and P564 in HIF-1α at the γ carbon of the pyrrolidine ring.

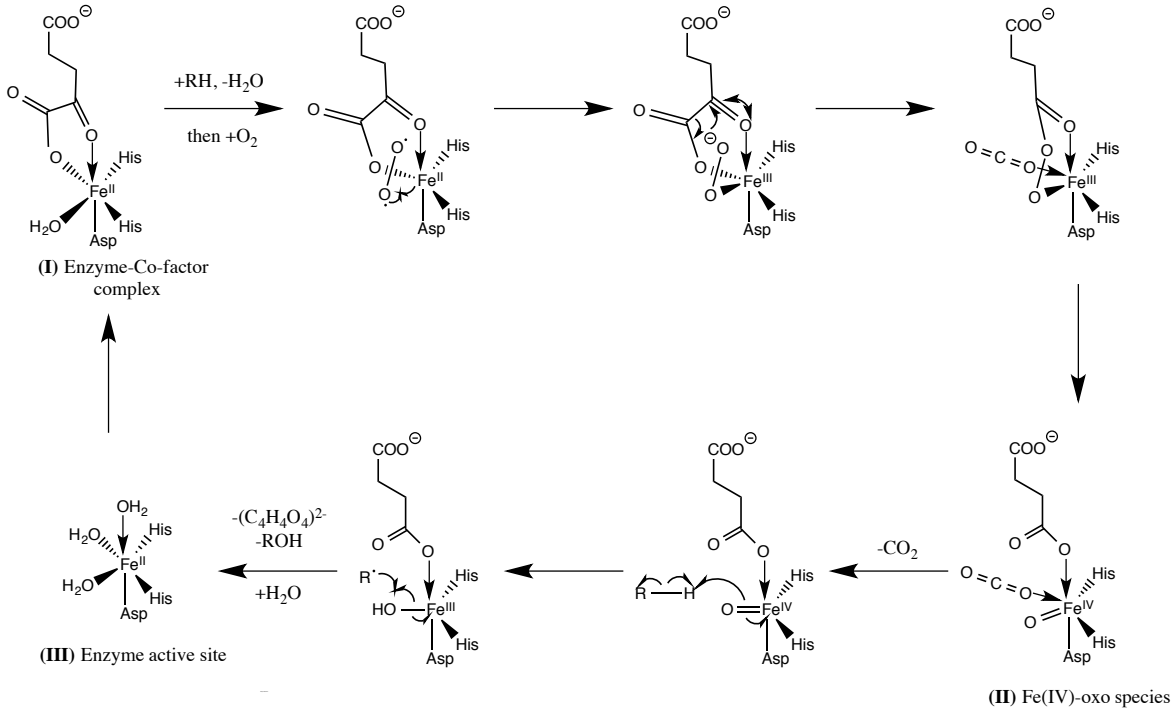

Figure 6: General mechanism for catalytic hydroxylation by αKG dependent enzymes. Once the enzyme-co-factor complex (**I**) has formed, dioxygen binds, resulting in oxidative decarboxylation of αKG to succinate and the generation of an Fe (IV)-oxo species (**II**). This species enables the hydroxylation of the substrate. Amino acid residues shown are catalytic resides of the enzyme. In the case of HIF-1α, for PHD2 R=P402 or P564 and for factor inhibiting HIF (FIH) R=N803.

Of the three PHD isoforms that have been identified and shown to hydroxylate HIF-α subunits in mammalian cells (PHD1, 2 and 3), PHD2 has been identified as the main dioxygenase of HIF-1α.[38, 39] The expression of PHD isoforms is varied in different cell types and although PHD2 has more influence on HIF-1α than HIF-2α, PHD3 has been shown to have more influence on HIF-2α than HIF-1α.[39] Prolyl hydroxylation initiates the binding of pVHL, the protein product of the von Hippel-Lindau (VHL) tumour suppressor gene that serves as a recognition component of the E3 ubiquitin ligase complex.[40-42] This promotes poly-ubiquitination of HIF-α, which targets it for proteasomal degradation.[42] The protein LIMD1 (LIM domain containing 1) is able to bind PHD and VHL simultaneously, assembling a multi-enzyme complex to allow efficient degradation of HIF-1α.[43]

Secondary oxygen sensing is provided by the enzyme factor inhibiting HIF (FIH), which hydroxylates a conserved asparagine residue in the C-TAD of HIF-1α and HIF-2α (N803 for HIF-1α and N-851 for HIF-2α) (Figure 7).[44, 45] Like PHD enzymes, FIH is a Fe (II)-dependent hydroxylase that uses molecular oxygen and αKG as substrates.[46] Hydroxylation of HIF-2α by FIH is less efficient than that of HIF-1α.[47] Asparagine hydroxylation inhibits HIF-1α transactivation function by inhibiting interaction of the C-TAD with the CREB binding protein (CBP)/p300 transcription co-activator (Figure 8). Structural analysis of the interaction between HIF-1α and CBP revealed that the Asn-803 side chain is buried deep within the molecular interface of the two proteins, where hydroxylation would likely destabilise the interaction.[48] In addition, FIH has been shown to bind to VHL, and functions as a transcriptional co-repressor by recruiting histone deacetylases (HDACs) to further inhibit HIF-1α mediated transactivation.[44]

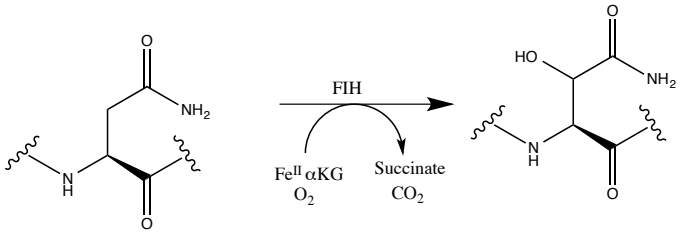

Figure 7: Hydroxylation of asparagine residues in the C-TAD in HIF-1αand HIF-2αprevents recruitment of transcriptional co-activators. FIH catalyses the hydroxylation of asparagine at the β carbon of the side chain.

Under hypoxia, HIF-α subunits are stabilised because oxygen becomes rate limiting for prolyl and asparaginyl hydroxylation, there is a decrease in ubiquitination and degradation of HIF-1α and HIF-2α so they accumulate in the cytoplasm (Figure 8). Interestingly, the K_M of FIH for oxygen was one third of that of PHDs, so FIH is able to maintain hydroxylation activity at lower oxygen concentrations than PHDs.[47] This suggests that even when HIFs are stabilised by reduced PHD activity, their transactivation activity is still regulated by oxygen availability through FIH. In addition, PHD2 and PHD3 themselves are targets of HIF-1 which may result in a negative regulatory loop which prevents accumulation of HIF-1α and accelerates its degradation upon re-oxygenation.[49] However, succinate, a product of hydroxylation by PHDs, and fumarate, a chemically similar metabolite, inhibit PHD activity leading to increased HIF-1α stabilisation independent of oxygen.[50, 51]

Once HIF-α accumulates in the cytoplasm, it translocates to the nucleus. Although HIF-α/HIF-1β dimerisation is necessary for DNA binding and transactivation activity, HIF-1β is not required for HIF-α translocation into the nucleus.[52, 53] HIF-1α and HIF-2α contain a nuclear translocation signal within the C-terminal region, which binds to nuclear transport receptors

importin-α/β and leads to translocation.[54] HIF-1β itself is a nuclear protein and as such is located in the nucleus in most cell types.[53]

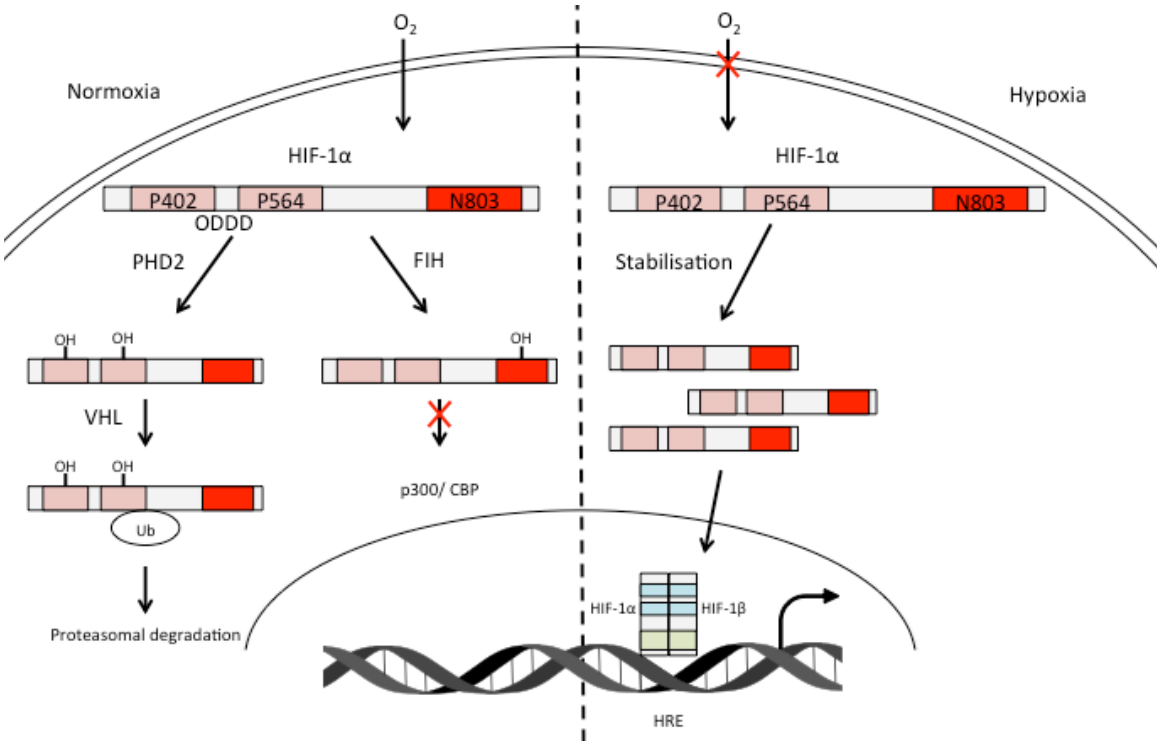

Figure 8: Oxygen-dependent, post-translational regulation of the HIF-1α subunit. In normoxia HIF-1α is hydroxylated which targets it for degradation or prevents its interaction with transcriptional co-activators. In hypoxia HIF-1α is stabilised and dimerises with HIF-1β in the nucleus to form HIF-1, which binds to HREs in DNA, activating the transcription of target genes.

It is important to note that in many studies normoxia is defined as 20% oxygen, which is approximately equivalent to atmospheric oxygen concentrations, and hypoxia as 1-5% oxygen. The definition of hypoxia has been well established as such but the definition of normoxia *in vivo* varies depending on cell type. Normal oxygen levels vary from 0% in bone marrow to 14% in many organs (including lung, liver, kidney and heart) and are approximately 10-12% in circulation.[55] This distinction may affect oxygen-dependent regulation of HIF-1 and be an important consideration for developing therapeutics targeting the hypoxia response pathway.

In addition to regulation by oxygen sensitivity of the HIF-1α protein, transcriptional regulation of HIF-1α mRNA in hypoxia has been reported. Transcriptional activation of HIF-1α has been shown in Hep3B and HepG2 liver cancer cell lines as well as rat cardiomyocytes, brain, and kidney.[4, 56] However, its expression is constitutive in HeLa and HeLaS3 cervical cancer and LN229 brain cancer cell lines.[57] This cell line specificity of hypoxic HIF-1α transcriptional induction may be due to epigenetic effects at the HIF-1α gene promoter.

1.1.3 Oxygen-independent regulation of HIFs

A number of other oxygen-independent pathways can also lead to HIF-1 stabilisation (Figure 9). For example, mammalian target of rapamycin (mTOR) has been shown to be an upstream activator of HIF-1 function. Binding of mTOR to a TOR signalling motif located in the N-terminus of HIF-1α enhances HIF-1-mediated transcription, linking HIF stabilisation to growth factor signalling.[58, 59] However, this activity is also modulated through a negative feedback loop where hypoxic activation of HIF-1 leads to upregulation of REDD1/2 (regulated in development and DNA damage responses, also known as DDIT4/ DDIT4L), which inhibit mTOR activity.[60] In addition to regulation by PHD stabilisation through the metabolites succinate and fumarate, build up of lactate and pyruvate have been shown to stabilise HIF-1 in a oxygen-independent manner.[61] This suggests that high rates of anaerobic glycolysis can lead to malignant transformation of cancer cells through HIF-1 activity.

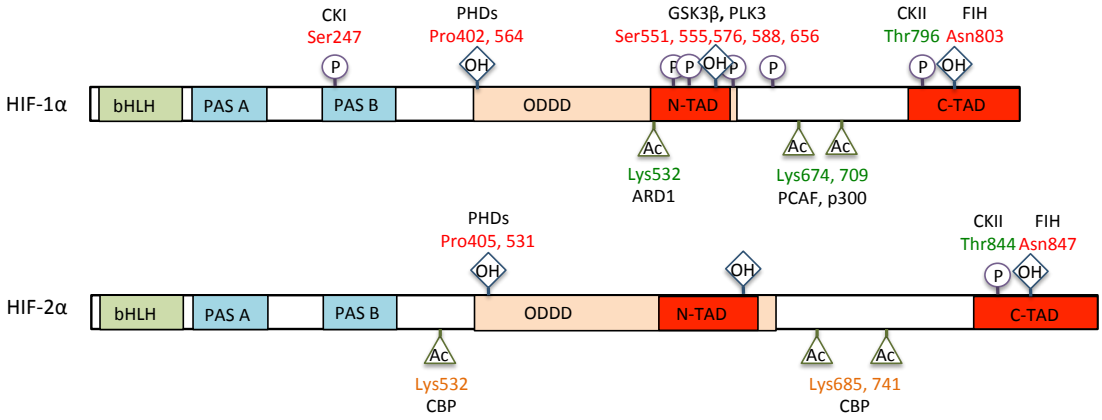

Figure 9: Summary illustration of post-transcriptional modifications to HIF-1α and HIF-2α that regulate stability and activity of the proteins. Modifications are represented by symbols and letters for phosphorylation (P), hydroxylation (OH) and acetylation (Ac). Labels for each modification show its amino acid position coloured to represent the overall effect of the modification: positive (green), negative (red) or both (orange). Modifications are also labelled with the enzyme responsible for them. Adapted from Dengler *et al.* 2015.[62]

Phosphorylation of HIF-1α and HIF-2α has also been shown to play a role in HIF-1 function and stability. Phosphorylation of HIF-1α through the p42/44 mitogen-activated protein kinase (MAPK) pathway promotes HIF-1 transcriptional activity, providing a further link between growth factor signalling and HIF-1 activation.[63] The p42/44 MAPK pathway has also been implicated in activation of HIF-2, but through an indirect mechanism, possibly by recruiting co-factors necessary for HIF-2-mediated transactivation, rather than direct phosphorylation of the subunit.[64] Direct activation of transcriptional activity of HIF-1α and HIF-2α by phosphorylation has been noted at a conserved threonine residue in the C-TAD (Thr796 for HIF-1α and Thr844 for HIF-2α) via casein kinase II (CKII).[65]

Other phosphorylation events have been shown to reduce HIF stability or activity. Phosphorylation of Ser247 in the PAS-B domain of HIF-1α, by casein kinase I (CKI), destabilised the HIF-1α/HIF-1β complex and diminished HIF-1 transactivation activity in HeLa cells, demonstrating the importance of HIF-1 dimerisation for activity.[66] A number of key serine residues have been identified as phosphorylation targets leading to decreased stability of HIF-1α by increasing oxygen sensitivity by phosphorylation in the ODDD. These are Ser551, 555 and 589 by glycogen synthase kinase 3 (GSK-3) and Ser576 and 659 by polo-like kinase 3 (PLK3).[67, 68] Specifically, increased degradation of HIF-1α after phosphorylation by GSK-3 was shown to be independent of the VHL complex.[67]

A key role of regulation by acetylation at a number of lysine residues in HIF-1α and HIF-2α is emerging, but current evidence is contradictory and unclear.[62] Acetylation appears to positively and negatively regulate HIF, and these effects vary depending on cell line and residue. For example, acetylation at Lys709 increased HIF-1α protein stability, and this acetylation could be opposed by HDAC1.[69] Interestingly, acetylation at Lys709 was mediated by p300, indicating a novel role for p300 in hypoxic response.[69] In addition, acetylation of HIF-1α by p300/CBP associated factor (PCAF) activated HIF-1 activity, and deacetylation of this site by sirtuin 1 (SIRT1) acetylase repressed HIF-1 activity.[70] SIRT1 is a redox sensor that is downregulated by increased NAD+ levels. Therefore, in hypoxia, SIRT1expression is reduced due to increased glycolysis, and HIF-1α activation is favoured. Conversely, acetylation of Lys10, 11, 12, 19 and 21 of HIF-1α decreased stability and deacetylation by HDAC4 increased HIF-1α protein levels.[71] Acetylation of HIF-1α at Lys532 by arrest defective 1 acetyltransferase also decreased HIF-1αstability, possibly by enhancing its interaction with pVHL.[72]

Cross talk of oxygen-independent mechanisms with the oxygen/VHL mediated HIF-1α degradation pathway has been demonstrated through a number of other proteins with E3 ubiquitin ligase activity. The receptor of activated protein C kinase (RACK1) interacts with HIF-1α, binds to Elongin C and recruits Elongin B and other E3 ubiquitin ligase components. This leads to polyubiquitination and proteasomal degradation of HIF-1α in a VHL independent manner.[73] RACK1 activity was shown to prevent heat shock protein (Hsp)90 (a molecular chaperone) mediated stabilisation of HIF-1α.[73-75] Similarly, Hsp70 interacts with HIF-1α and recruits the ubiquitin ligase carboxyl terminus of Hsp70-interacting protein (CHIP), which promotes ubiquitination and subsequent degradation of HIF-1α.[76] This mechanism is thought to contribute to the decrease in HIF-1α protein after long periods of hypoxia. In addition, the Hsp70-CHIP degradation pathway was shown to be specific to HIF-1α and not affect HIF-2α protein levels.[76] Another E3 ubiquitin ligase, hypoxia-associated factor (HAF), has also been identified to promote degradation of HIF-1α through an

oxygen/VHL independent pathway.[77] HAF was shown to bind to HIF-1α between amino acids 269-400, upstream of the ODDD, and induce its ubiquitination.[77] Conversely, HAF was shown to bind to HIF-2α downstream of the N-TAD and increase its transactivation activity.[78] Therefore, this mechanism may be an effector of differential activity of the HIF isoforms.

1.1.4 The hypoxia response element

When stabilised, HIF-α subunits accumulate in the cytoplasm then translocate to the nucleus where they dimerise with the constitutively expressed HIF-1β, to form the heterodimeric transcription factor HIF. HIF binds to the core consensus sequence (5' (T)RCGTG 3', where R is A or G) of 50 base pair HREs in the promoter or enhancer regions of target genes, and recruits co-activators to activate their transcription.[79, 80] In the first position of the HRE, A is preferred to G for HIF binding and T is favoured in the -1 position.[23, 81] Although the core sequence was found to be abundant in gene promoters, it is very selective, only a small proportion (<1%) of DNA sequences containing the motif bound HIF-1α or HIF-2α.[82] No significant features of the sequences surrounding the HREs were identified that dictated HIF-1 binding, suggesting there are factors other then DNA sequence that determine HIF-1 binding such as epigenetic regulation.

In addition to the core consensus sequence, a HIF-1 ancillary sequence (HAS) has been identified in a number of HIF-1 target genes (Table 1). This is an imperfect inverted repeat of the core HRE, CACG(T/C) or CACA(G/T), and has been shown to be critical for vascular endothelial growth factor (VEGF) and erythropoietin (EPO) reporter induction in response to hypoxia.[79, 83] The spacing between the HRE and HAS is critical for activity of the promoters, a requirement of 8 or 9 nucleotide spacing, depending on the gene.[79]

Table 1: The HREs of several HIF target genes contain a core HIF binding site and a HAS, with a spacing of 8-9 nucleotides between the two elements. ALDA: aldolase A; ENO-1: enolase 1; LDHA: lactate dehydrogenase A; GLUT-1: glucose transporter 1; HO-1: heme oxygenase 1. Adapted from Kimura *et al*. 2001.[79]

Gene	HRE (Core binding sequence + HAS)	Spacing (nt)	HAS
VEGF	5'-CATACGTGGGCTCCAACAGGTCCT-3'	8	CAGGT
EPO	5'-CCTACGTGCTGTCTCACACAGCCT-3'	8	CACAG
ALDA	5'-GGGATGTGGTCCGGTCACGTCCG-3'	8	CACGT
ENO-1	5'-CGCACGTGCCCCGGACACGCAGC	8	CACGC
LDHA	5'-CACACGTGGGTTCCCGCACGTCCG-3'	8	CACGT
GLUT-1	5'-CAGGCGTGCCGTCTGACACGCATC-3'	8	CACGC
HO-1	5'-CGGACGTGCTGGCGTGGCACGTCCT-3'	9	CACGT

HIF binding sites were found to cluster in two distinct regions, ~0.5 kb upstream and 1 kb downstream of target gene transcription start sites (TSS), which may be a result of co-operation with other factors that enhance HIF binding in these regions.[82] Although functional HREs tend to localise in the proximal promoters of target genes, they may also function over long ranges. Functional analysis of HIF transcripts compared to binding data revealed that whereas >20% of gene activation was induced by direct HIF binding to promoters, almost all HIF dependent gene repression was indirect.[82] HIF bound preferentially to gene loci that were transcriptionally active at a low level in normoxic conditions, aided by permissive chromatin structure (H3 lysine 4 methylation, DNaseI hypersensitivity and presence of RNA polymerase II).[84] This may allow HIFs to launch a rapid transcriptional response on the onset of hypoxia and contribute to the cell type specificity of HIF activity.

1.1.5 HIF target genes

HIFs regulate the expression of target genes in diverse biological pathways. Over 100 direct targets of HIF-1 and HIF-2 have been identified, but genome wide transcript profiling of the hypoxic response, and siRNA-mediated knockdown of HIF-1α or HIF-1β, has led to the identification of hundreds of genes that are targeted directly or indirectly by the HIF-1 pathway.[32, 81, 84, 85] This includes oxygen-related genes involved in erythropoiesis (e.g. EPO), iron metabolism (e.g. transferrin), oxygen transport and vascularisation (e.g. VEGF, and adrenomedullin, ADM).[2, 3, 86-88] In order to adapt to low oxygen conditions, HIFs co-ordinate a

switch in energy metabolism away from aerobic metabolism to anaerobic glycolysis.[89] The vast majority of genes encoding glycolytic enzymes are direct targets of HIF-1.[90, 91]

In addition to recovering oxygen homeostasis, HIFs have roles in cell differentiation, apoptosis, cell growth and renewal, inflammation, immunity, metastasis, invasion and more.[23, 82, 85] HIFs are involved in maintaining pluripotency of stem cells; HIF-2 has been shown to regulate octamer binding transcription factor 4 (Oct4) and HIF-1α has been shown to bind to Notch1 and increase its downstream signalling.[92, 93] Recently, HIF-1α itself has also been identified as a target of HIF-1, allowing positive autoregulation of HIF signalling in an epigenetically regulated manner.[94, 95]

1.1.6 HIF isoform specificity

Though HIF-1α and HIF-2α are very similar in structure, and HIF-1 and HIF-2 transcription factors are able to bind the same HRE, they have both shared and distinct target genes (Table 2). The selectivity of HIF-1 and HIF-2 targets may vary with cell type, duration and severity of hypoxia, and the presence of functional VHL.

Table 2: Summary table displaying some HIF target genes that are HIF-1α specific, HIF-2α specific, or a target of both isoforms.

HIF isoform	Target gene function	Target Genes	Cell line
HIF-1α only	Glycolysis	Hexokinase 2 (HK2), glucosephosphate isomerase (GPI), phosphofructokinase (PFK), ALDA, aldolase C (ALDC), triosephosphate isomerase (TPI), glyceraldehyde-3 phosphate dehydrogenase (GAPDH), phosphoglycerate kinase 1 (PGK1), ENO1, LDHA	HEK-293[32] RCC (RCC4)[96]
	pH regulation (also resistance to treatment)	Carbonic anhydrase IX (CAIX)	HEK-293[32] RCC (primary cells)[97]
	Apoptotic factor	BNIP3L, BNIP3	HEK-293[98]
HIF-2α only	Cell migration	Matrix metallopeptidase 9 (MMP9)	Glioblastoma (U87, LN229)[78] RCC (786-O)[78]

	Stem cell factor	Oct4	Glioblastoma (U87, LN229)[78] RCC (786-O)[78]
HIF-1α and HIF-2α	Glucose uptake	GLUT1, GLUT3	HEK-293[32]
	Differentiation	Adipose differentiation-related protein (ADRP), N-myc downstream regulated gene 1 (NDRG1)	HEK-293[32] RCC (primary cells)[99]
	pH regulation (also invasion/ migration)	Carbonic anhydrase XII (CAXII)	Breast cancer (MDA-MB-231)[100]
	Vascular	ADM, EPO, VEGF	HEK-293[32] ESC[101] RCC (primary cells)[99] Mouse hepatocytes[102]

Whereas HIF-1α is ubiquitously expressed, HIF-2α expression is thought to be limited to a subset of cell types. HIF-2α expression was first identified in embryonic endothelial cells and identified to play a key role in lung and vascular development.[6, 9, 11] Later work identified hypoxia induced HIF-2α expression in distinct cell populations of a variety of tissues in postnatal rats, revealing an important role for HIF-2α in hypoxic response not confined to its function in vasculature.[103] In contrast, almost all transformed cell lines express HIF-2α.[103] It should be noted that HIF-2α expression does not always equate to HIF-2 transcriptional activity; for example, HIF-2α was shown to be expendable for the response to hypoxia in embryonic stem cells.[104]

There is also evidence of temporal differences in HIF-1α and HIF-2α expression. Levels of both isoforms were found to be similar after short-term exposure to hypoxia (<12 or 24 h) and target gene activation was primarily mediated by HIF-1 in a number of cell lines.[78, 105] However, after prolonged periods of hypoxia, HIF-1α levels decreased whereas HIF-2α levels remained high and stable, and HIF-2 became the prominent driver for hypoxic gene induction.[78, 105] Therefore HIF-1 is thought to mediate the response to acute hypoxia whereas HIF-2 exerts more of an influence during longer periods of hypoxic exposure. This is an interesting difference, as although solid tumours exhibit chronic hypoxia, most hypoxia studies focus on the transcriptional response before 24 h exposure. It has been suggested that the switch from HIF-1- to HIF-2-led transactivation is regulated by HAF, the overexpression of which induced HIF-1α degradation, but enhanced HIF-2α transactivation, in a number of

cell lines.[78] Levels of HAF expression were shown to initially decrease with exposure to hypoxia, then peak after 48 h exposure.

In agreement with its role in response to acute hypoxia, HIF-1α specifically regulated glycolytic genes in Hep3B cells, allowing alteration of cellular metabolism to an anaerobic mechanism to allow survival.[32] Glycolytic genes are not induced in HIF-1α deficient 786-O cells suggesting HIF-2α is not able to upregulate genes involved in glucose metabolism.[32] In addition, reconstitution of HIF-1α in this cell line restored glycolytic gene expression. Carbonic anhydrase IX (CAIX, a zinc metalloenzyme involved in pH regulation) and genes involved in apoptosis (BNIP3L and BNIP3) are also specifically regulated by HIF-1.[97, 98] Consistent with this finding, knockout of the HIF-1α gene in mouse embryonic fibroblasts (MEF) prevented metabolic reprogramming of cells in hypoxia.[106] Glucose transporters 1 and 3 (GLUT-1 and 3) are targets of both HIF-1 and HIF-2, suggesting HIF-2 can activate some means of metabolic adaptation by increasing glucose uptake in hypoxic cells.[32] A number of other gene targets are also shared by the two transcription factors, including VEGF and ADM.[98, 101]

HIF-2-specific targets include matrix metallopeptidase 9 (MMP9) and the stem cell factor Oct4.[78, 92] A switch from HIF-1α- to HIF-2α-driven hypoxic response was associated with a more aggressive, invasive tumour phenotype in cultured cells.[78] In addition, there is evidence that HIFs have contrasting effects on the expression of some genes. For example, in glioma stem cells, HIF-1α was shown to activate Notch signalling (in agreement with other studies in cultured cells) whereas HIF-2α repressed Notch expression.[107, 108] Notch signalling functions to maintain stem/progenitor cell state and so HIF-2α repression of Notch seems in contrast to its upregulation of Oct4.

1.1.7 Aberrant expression of HIF-1 in cancer

Hypoxic cells are at risk of oxidative DNA damage: DNA strand breaks and genetic aberrations that retard cell growth and eventually lead to cell death. Cancer cells show a range of genetic changes that improve survival and enable adaptation to hypoxic conditions allowing them to continue to proliferate, to metastasise and making them resistant to radiotherapy and chemotherapy (Figure 10). This response to hypoxia is primarily modulated by HIF-1, which is deregulated in many human cancers, often due to the overexpression of HIF-1α. HIF-1α overexpression has been recorded in a number of cancers including skin, ovarian, prostate, gastric, colon, breast and renal carcinomas and this overexpression was associated with increased cell proliferation.[109] Overexpression can be

caused by disruption of the regulatory pathway- for example loss of function mutations in the VHL protein lead to increased HIF-1α stabilisation.[40]

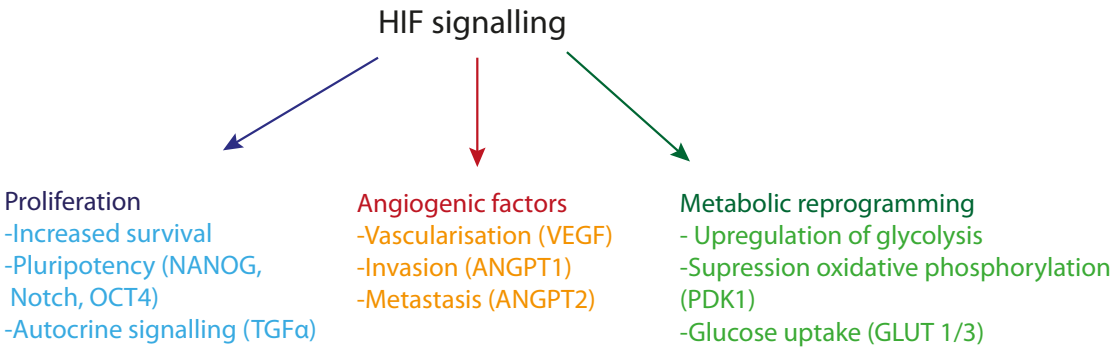

Figure 10: Summary illustration of some of the key effects of HIF-1α overexpression or HIF-1 deregulation in cancer, with examples of HIF-1 target genes whose upregulation lead to these effects.

HIF target genes code for proteins involved in key stages of cancer progression. For example, cancer cells often exhibit autocrine signalling to allow increased cell proliferation and survival. A number of HIF regulated genes have been shown to participate in autocrine signalling including transforming growth factor α (TGFα) in clear cell renal carcinoma,[99] VEGF in colorectal and pancreatic cancer,[88] ADM in pancreatic and prostate cancer,[110, 111] and EPO in breast, prostate and renal cancer.[112] In addition, HIFs transactivate pluripotency factors such as NANOG, Notch and Oct, allowing immortalisation.[108, 113]

Several angiogenic factors are HIF targets such as VEGF, angiopoietin 1 and 2 (ANGPT1/2), the expression of which promotes tumour vascularisation.[86, 114] VEGF and ANGPT2 are also involved in increasing vascular permeability, and promoting invasion of cancer cells into blood vessels. In addition, targets of HIF-1 L1 cell adhesion molecule (L1CAM) and AGNPTL4 enable extravasation of cancer cells to metastatic sites such as the lung.[115] HIF-1 has also been implicated in the activation of metalloproteinases (MMPs) that degrade the extracellular matrix, facilitating metastasis.[78]

As discussed, HIF-1 mediates the expression of genes encoding glucose transporters and glycolytic enzymes, and has a key role in metabolic reprograming of tumour cells. HIF-1 also directly supressed oxidative respiration through upregulation of pyruvate dehydrogenase kinase 1 (PDK1) in MEF, which induced the phosphorylation and deactivation of pyruvate dehydrogenase, the enzyme that converts pyruvate to acetyl coenzyme-A for entry to the tricarboxylic acid cycle.[96]

High HIF-1α expression has been associated with low survival rates in renal cell carcinoma and breast carcinoma.[116, 117] In a study of rectal cancer patients, HIF-1α overexpression correlated with cancer specific mortality and cancer reoccurrence. In contrast, no correlation

was found between HIF-2α expression and cancer reoccurrence or mortality in these patients. However, HIF-1α overexpression is not always linked to decreased survival; HIF-1α overexpression was shown to indicate a positive prognosis in early stage squamous carcinomas,[118] exemplifying the complexity of the HIF pathway in cell proliferation and survival.

In renal cell carcinoma, HIF-1α and HIF-2α had contrasting roles in target gene activation. HIF-2α was shown to activate pro-tumorigenic genes encoding cyclin D1, TGFα and VEGF, whereas the pro-apoptotic gene BNIP3 was activated by HIF-1α.[99] In tumour xenografts of renal cell carcinoma cells, HIF-1α retarded growth whereas HIF-2α enhanced growth of tumours.[99] Therefore investigation into the overexpression of specific HIF isoforms could lead to a greater understanding of cancer progression. In addition, the specific functions of HIF-isoforms should be taken into account when targeting the HIF system therapeutically.

1.1.8 Targeting HIF-1 for cancer therapy

HIF activity is crucial for cancer progression, and has been correlated to poor patient prognosis and resistance to chemo and radiotherapy. Therefore, it presents a key target for cancer therapeutics, however, HIF-1 has proven challenging to target specifically. The hypoxia response pathway, principally regulated by HIF-1, relies on a number of protein-protein interactions (PPi) to function. Interactions between proteins are central to almost all biological processes and therefore present attractive targets for therapeutic intervention. This intervention would ideally be with small 'drug like' molecules that are often cheap to produce and can be administered orally, but the nature of protein-protein interfaces present a number of challenges.[119] Whereas the size of contact surfaces involved in protein-small molecule interactions are ~300-1,000 Å, the contact surfaces of PPi are much larger: ~1,500-3,000 Å.[120-122] Protein-protein interfaces are also relatively featureless; X-ray structures of protein-protein pairs do not show small deep cavities, grooves and pockets that look like small molecule binding sites.[123] However, these interactions often involve binding 'hotspots': a small subset of interacting residues in centralised regions of the interface that account for the majority of the binding free energy.[124, 125] An interesting feature of hotspots is their functional and structural plasticity, allowing 'promiscuous' binding of one hotspot to several targets.[126]

A number of chemical compounds have been shown to inhibit HIF-1 activity and reduce tumour xenograft growth. These target the HIF-1 pathway at a number of different levels to inhibit HIF-1 activity, including HIF-1α mRNA expression, HIF-1α protein synthesis and stability, HIF-1α/HIF-1β dimerisation and binding to DNA, and HIF-1 transactivation activity

(Figure 11). The identification, mechanisms and clinical relevance of these inhibitors have been reviewed recently and extensively.[55, 127-129] A number of these inhibitors are described below, to illustrate the complexity of targeting the hypoxia pathway and the challenges that are yet to be overcome.

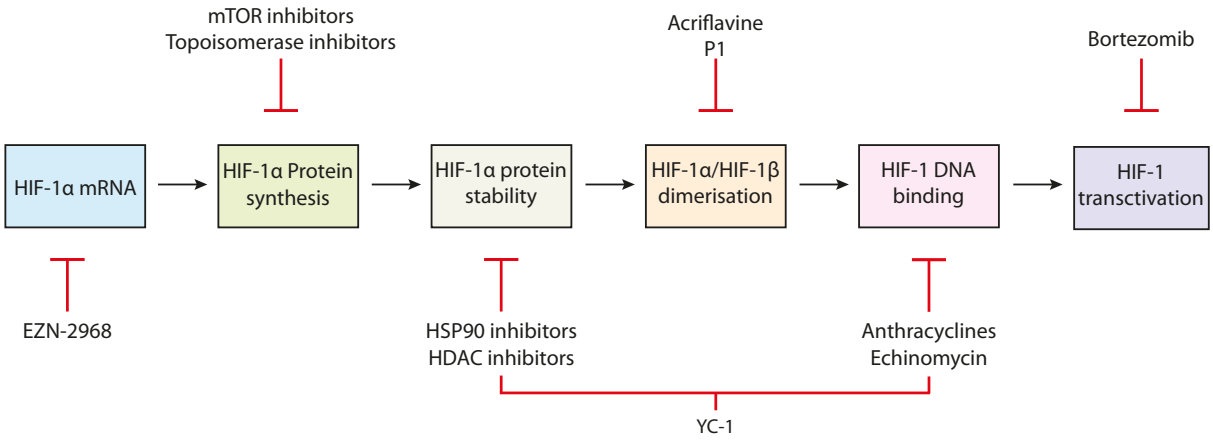

Figure 11: Summary illustration of the various levels of the HIF-1 pathway that have been targeted for therapeutics. The inhibitors discussed here, and their level of action, are labelled.

1.1.8.1 Inhibition of HIF-1α mRNA expression

EZN-2968 is an RNA antagonist that specifically binds to, and inhibits the expression of, HIF-1α mRNA.[130] The inhibitor is a 'third generation' oligonucleotide consisting of both DNA and locked nucleic acid (LNA) of which residues have a methylene bridge between the 2'oxygen and 4' carbon of the ribose sugar, increasing oligonucleotide stability and specificity. EZN-2968 was shown to antagonise HIF-1α mRNA and protein expression in human prostate and glioblastoma cells and downregulated HIF-1α and VEGF expression in mice. In a pilot clinical trial, the compound reduced HIF-1α protein and mRNA levels of some target genes in patients and the inhibitor is currently in phase I trials.[131] This illustrates that effective inhibitors are not limited to small molecules.

1.1.8.2 Inhibitors of HIF-1α protein expression

Camptothecin analogues topotecan and irinotecan (Figure 12) have topoisomerase I (TOP1) inhibitor activity. TOP1 relaxes DNA supercoiling by forming single strand breaks, unwinding and re-ligating DNA. Camptothecins irreversibly intercalate into the DNA/enzyme interface and prevent re-ligation of DNA strands.[132] TOP1 is an upstream activator of HIF-1 and its inhibition leads to a decrease in HIF-1α translation, which is independent to its DNA damage activity.[132] Knowledge of the mechanism of action of TOP1 inhibitors has allowed optimisation of pharmokinetic properties, and a number of camptothecin derivatives have been approved for clinical use.[55]

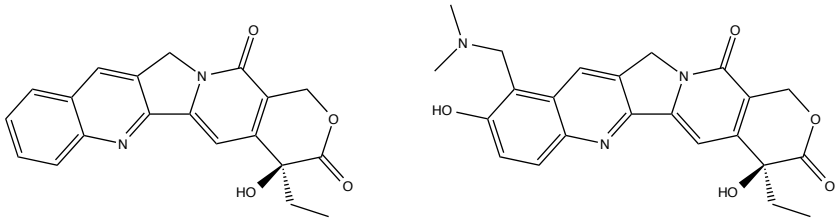

(1) Camptothecin

(2) Topotecan

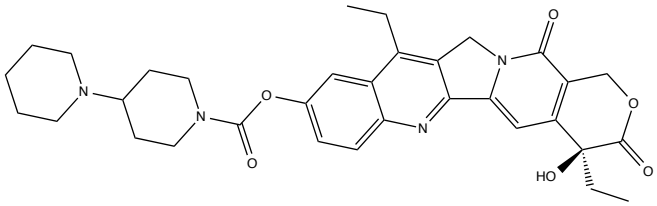

(3) Irinotecan

Figure 12: Structure of topoisomerase inhibitor Camptothecin (1) and its analogues topotecan (2) and irinotecan (3).

Temsirolimus (Figure 13), a derivative of rapamycin, is an inhibitor of mTOR and was approved for therapy for renal cell carcinoma in the US in 2008.[133] The compound reduced HIF-1α expression by inhibition of the mTOR-dependent translational cascade required for HIF-1α expression, and prevented tumour development.[133] Temsirolimus inhibited HIF-1α mediated VEGF production in MDA-MB-231 breast cancer cells, suggesting that anti-angiogenic effects may play a substantial role in the anti-cancer activity of temsirolimus in breast cancer.[134] The overlapping pathways of HIF-1 activation can lead to efficacy of drugs via different mechanisms of action in different cell types.

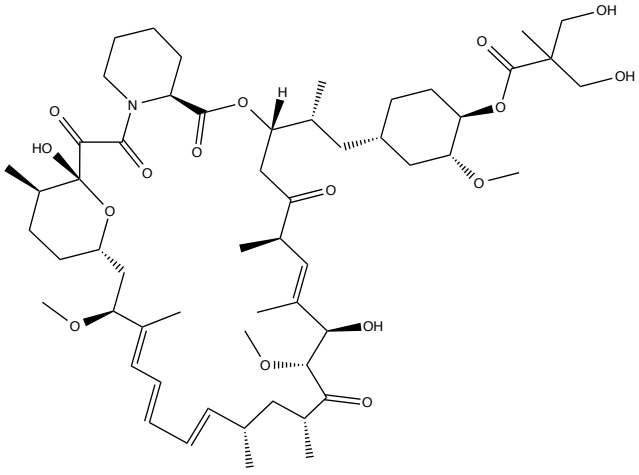

(4) Temsirolimus

Figure 13: Structure of mTOR inhibitor Temsirolimus (4), a rapamycin analogue.

1.1.8.3 Inhibition of HIF-1α stabilisation

Geldanamycin (Figure 14) is an ansamycin antibiotic that is able to disrupt binding of Hsp90 to its target proteins by competition with the ATP binding site of Hsp90. Geldanamycin was shown to disrupt the HIF-1α/Hsp90 interaction and promote ubiquitination and proteasomal degradation of HIF-1α. A number of geldanamycin derivatives are currently in phase I and II clinical trials.[135]

As discussed earlier, acetylation of HIF-1α can modulate HIF-1 activity. Class II HDAC inhibitors, for example LAQ824, have been shown to antagonise HIF-1α transactivation activity and stimulate its ubiquitination and degradation in a VHL independent manner, but the mechanism of these inhibitors is as yet unclear.[136] Most inhibitors of HIF α-subunit stability show similar activity against HIF-1α and HIF-2α.[137]

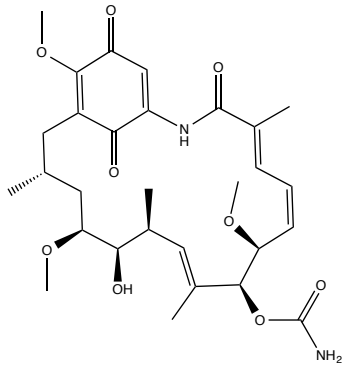

(5) Geldanamycin

Figure 14: Structure of Hsp90 inhibitor Geldanamycin (5).

1.1.8.4 Inhibition of HIF-1 dimerisation

Despite a range of compounds targeting the HIF-1α subunit, and more still targeting DNA binding and transactivation activity of HIF-1, there is a lack of inhibitors targeting HIF-1α/ HIF-1β dimerisation. Targeting this interaction could allow greater specificity as it directly interferes with the HIF-1 transcription factor compared to, for example, geldanamycins which inhibit the interaction of Hsp90 with a wide range of client proteins rather than HIF-1α specifically. In addition, such inhibitors may be highly potent in cancer types where HIF-1α overexpression leads to tumour progression.

Overexpression of the HIF-1α PAS-A domain was shown to inhibit hypoxia induced expression of HIF-1, identifying this domain as a valid target for a small molecule inhibitor of the PPi.[138] Screening of a chemically synthesised library identified compound NSC 50352 (Figure 15), a derivative of tetracycline, as an inhibitor of the HIF-1α PAS-A and HIF-1β PAS-A

interaction, however, cell based assays revealed that NSC 50352 did not significantly inhibit the interaction between HIF-1α and HIF-1β proteins under normoxia or hypoxia.

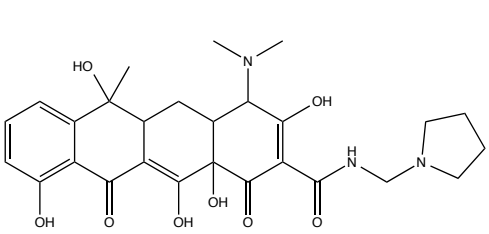

(6) NSC 50352

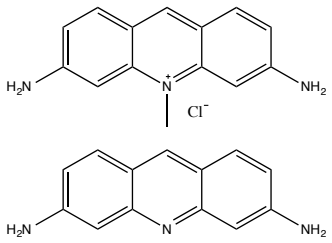

(7) Acriflavine

Figure 15: Structure of NSC 50352 (6), an inhibitor of HIF-1α/HIF-1β PAS-B dimerisation and acriflavine (7) an inhibitor of full length HIF-1α/HIF-1β and HIF-2α/ HIF-1β dimerisation.

Acriflavine, a mixture of trypaflavine (3,6-diamino-10-methylacridinium) and proflavine (3,6-diaminoacridine) (Figure 15), was the first small molecule reported to inhibit HIF-1 dimerisation.[139] Acriflavine was identified by high-throughput screening and shown to bind to the PAS-B domain of HIF-1α and HIF-2α, inhibiting HIF-α/HIF-1β dimerisation and HIF-1-mediated transcriptional activity. In mice bearing prostate cancer xenografts, acriflavine prevented tumour growth. Interestingly, acriflavine did not affect the HIF-1α/Hsp90 interaction or myc-max mediated transcription, suggesting specificity of the compound.

Recently, a second HIF-1 dimerisation inhibitor was identified through screening of a biologically synthesised library of cyclic peptides in a bacterial reverse two-hybrid system (RTHS). The inhibitor, Tat-cyclo-CLLFVY (P1) (Figure 16) was shown to specifically bind to the PAS-B domain of HIF-1α and inhibit HIF-1 dimerisation specifically over HIF-2.[140] Tat-cyclo-CLLFVY disrupted HIF-1 transcriptional activity in MCF7 breast cancer and U2OS osteosarcoma cells.

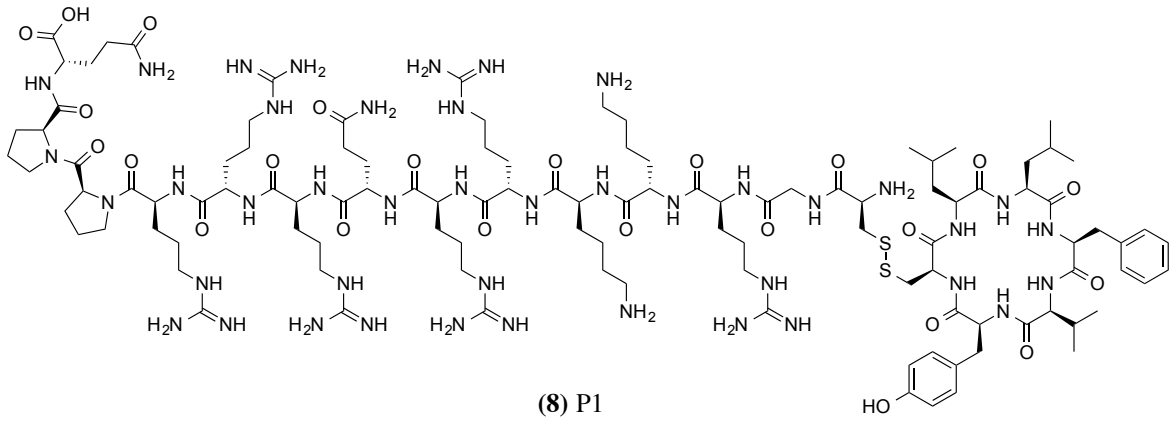

(8) P1

Figure 16: Structure of the specific inhibitor of HIF-1α/HIF-1β dimerisation Tat-cyclo-CLLFVY, P1 (8).

1.1.8.5 Inhibition of DNA binding

Echinomycin is a cyclic peptide antibiotic (Figure 17) that is known to bind to DNA in a sequence specific fashion. It binds specifically to the core recognition sequence of HIF-1 5'-CGTG'-3' disrupting HIF-1 binding, but not binding of nuclear factor κB (NF-κB) or activator protein-1 (AP-1), which have shared target promoters with HIF-1.[141] As HIF-2 binds to the same consensus sequence, the compound is unlikely to discriminate between the two. Echinomycin inhibited hypoxic induction of VEGF in U251 cells, however, earlier clinical trails of echinomycin in mice and beagle dogs had revealed major toxic effects, limiting further clinical evaluation of this agent.[142]

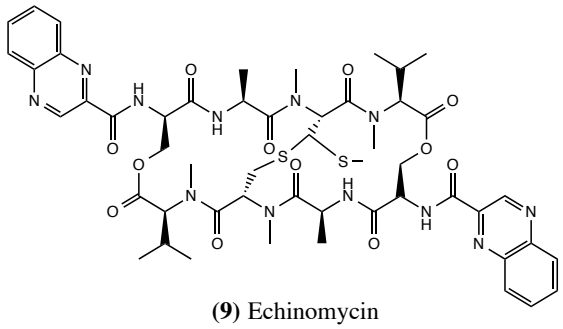

(**9**) Echinomycin

Figure 17: Structure of the HIF-1 DNA binding inhibitor Echinomycin.

The anthracyclines doxorubicin, daunorubicin, epirubicin and idarubicin (Figure 18) are potent chemotherapeutic agents that are used in the clinic. Their anticancer effect was attributed to their ability to intercalate DNA and induce TOP2 mediated strand breaks, but doxorubicin was shown to inhibit tumour growth through antiangioagenic activity.[143] Later, anthracyclines were shown to disrupt HIF-1 binding to DNA and potently inhibit HIF-1 transcriptional activity and tumour growth.[144] New understanding on the mechanism of action of current chemotherapeutics can allow tailored drug regimes for patients depending on cancer expression profiles.

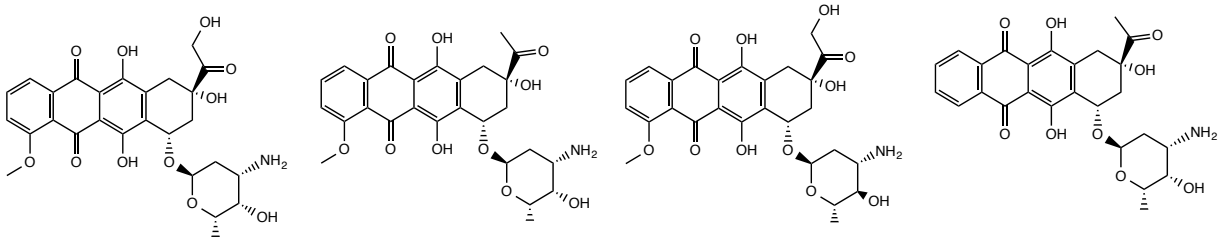

(**10**) Doxorubicin (**11**) Danuorubicin (**12**) Epirubicin (**13**) Idarubicin

Figure 18: Structure of anthracyline DNA binding inhibitors, Doxorubicin (10), daunorubicin (11), epirubicin (12) and Idarubicin (13).

1.1.8.6 Inhibition of HIF transactivational activity

Bortezomib (Figure 19) is a proteasome inhibitor that is in clinical use for multiple myeloma and prostate cancer. Bortezomib targets the C-TAD of HIF-1α and promotes the interaction of Asn803 in the C-TAD with FIH under hypoxic conditions.[145] This stimulates hydroxylation of Asn803 by FIH, inhibiting the interaction between p300/CBP and HIF-1α and attenuating the hypoxic induction of EPO and VEGF in cancer cell lines. In addition, bortezomib has been shown to inhibit HIF-1α protein synthesis by dephosphorylation of, key components of the PI3K/Akt/mTOR pathway, which is known to be required for HIF-1α expression.[146] Bortezomib also suppresses the p44/42 MAPK pathway by inhibiting phosphorylation, leading to a reduction in nuclear translocation of HIF-1α.[146] Together, these effects lead to reduction of HIF-1α protein levels under normoxic and hypoxic conditions and attenuate downstream VEGF expression.

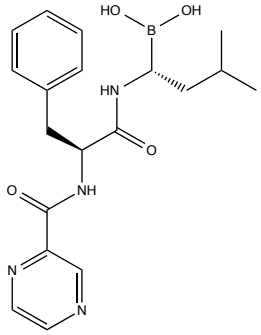

(**14**) Bortezomib

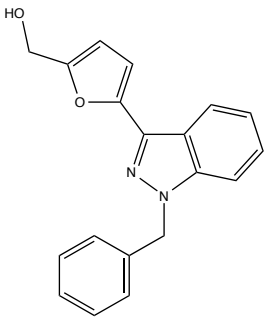

(**15**) YC-1

Figure 19: Structure of bortezomib, which inhibits HIF-1 transactivation activity and YC-1, which inhibits HIF-1 at multiple levels.

1.1.8.7 Targeting HIF-1 at multiple levels

Clearly there are many routes to HIF-1 inhibition, but targeting multiple pathways simultaneously could allow increased potency of chemotherapeutic agents. EZN-2986 and bortezomib are examples of agents that target HIF-1 multiple effects on the HIF pathway. YC-1 is a benzylindazole derivative that inhibits HIF-1-mediated hypoxic response. YC-1 was shown to inhibit binding of HIF-1 to DNA, reduce hypoxia-induced HIF-1α accumulation, and induce binding of FIH to the C-TAD of HIF-1α and preventing the HIF-1α/p300 interaction.[147, 148] In addition, YC-1 was found to supress the PI3K/Akt/mTOR/4E-BP pathway and prevent HIF-1α and HIF-1β accumulation in hypoxia in prostate cancer cells.[149]

In recent years, discovery and development of inhibitors targeting the HIF-1 pathway has been an extremely active area of research. However, none of the recently discovered inhibitors have been translated to a clinical setting, although some previously approved

chemotherapeutic agents have been found to function via HIF-1 inhibition. A large obstacle to new inhibitors is specificity, as HIF-1 in involved in many cellular pathways and so interacts with many other proteins and cofactors. Further work is needed to identify more selective HIF-1 inhibitors, study their mechanism of action and progress them to the clinic. Alternatively, these compounds could hold potential as bioprobes to identify direct targets and study the molecular mechanisms of the HIF-1 pathway in more detail. For example, study of the mechanism of YC-1 in prostate cancer cells revealed a role for NF-κB in Akt-mediated HIF-1α accumulation during hypoxia.[149]

The importance of HIFs in biological pathways is undisputed, and in recent decades many of the functional activities and mechanisms of regulation of HIFs (principally HIF-1) have been identified.[62, 129] In addition, there is strong evidence that HIF-1 overexpression and de-regulation leads to cancer progression and resistance to currently available therapeutics.[150, 151] In response, the HIF pathway has been targeted, but the development of effective, specific inhibitors remains challenging. A more detailed understanding of the molecular mechanisms that regulate HIF-1 and of the role of HIF-1 in hypoxic response is vital. In addition, a deeper analysis of the roles of HIF-2α and HIF-3α is necessary to most effectively manipulate each isoform for optimum therapeutic outcome. This body of work aims to address two of these research gaps with the overall goal of advancing the understanding of HIF biology. These aims require understanding of two vastly different research areas: Intein splicing and its use to produce cyclic peptides in vivo, and epigenetics and its relationship to hypoxia and regulation of HIF-1α. More information on these topics is given in the following sections.

1.2 Inteins and SICLOPPS

Targeting HIF-1 dimerisation can allow greater specificity, and even distinction between HIF-1 and HIF-2 isoforms, so it is an attractive target for therapeutic intervention. As discussed in section 1.1.8, targeting PPi is challenging due to the large interaction interface between the dimerisation partners. Traditional high-throughput screening methods can be limited in their potential for finding inhibitors of PPi as the libraries are often biased towards a small number of protein classes and lack the structural diversity required.[123]

One of the challenges of chemically synthesised small molecule libraries is that the path to identify the active members is often convoluted. Biologically synthesised libraries, however, can be several fold larger and rapidly and easily screened against a chosen target.[152] SICLOPPS is a method of biosynthesising a cyclic peptide library of up to 10^8 members, which when combined with a bacterial reverse two-hybrid system (RTHS), has been used to identify inhibitors of PPi, including Tat-cyclo-CLLFVY, the specific HIF-1 inhibitor.[140, 153-155]

The method was developed in *Escherichia coli* (*E. coli*) and uses cyanobacterium *Synechocystis sp.* strain PCC6803 (Ssp) DnaE split inteins to produce cyclic peptides *in vivo*.[156] Inteins are internal protein elements that can self-excise from their host protein, and in doing so, catalyse the ligation of flanking protein sequences with a peptide bond (Figure 20). Intein splicing is a post-translational process that requires no external enzymes or cofactors. In addition to cyclic peptide library production, inteins have been used in a variety of applications including protein cyclisation, protein purification, and conditional (inducible) protein splicing.[157-159]

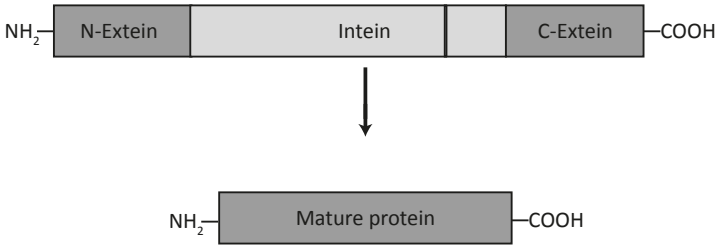

Figure 20: Illustration of intein splicing. The intein element is able to self-excise from the precursor protein, ligating the two flanking ends to give the mature protein.

1.2.1 Intein structure

Three types of naturally occurring inteins have been identified: maxi inteins, minimal (mini) inteins, and split inteins (Figure 21).[160,161] Maxi inteins are bifunctional proteins consisting of a protein splicing domain and a central homing endonuclease domain (Figure 21A). Homing endonucleases, usually encoded for by an open reading frame within the intein, cause site specific hydrolysis of double stranded DNA at the "homing" site in intein-less alleles. This

promotes a recombination process through which the intein is copied into the break site.[162] This domain, however, is not thought to affect protein splicing.[162] Mini inteins lack the homing endonuclease domain and their N- and C- terminal splicing domains form a horseshoe-like 12-β-strand structure, similar to that of the hedgehog autoprocessing domain (Figure 21B).[163, 164]

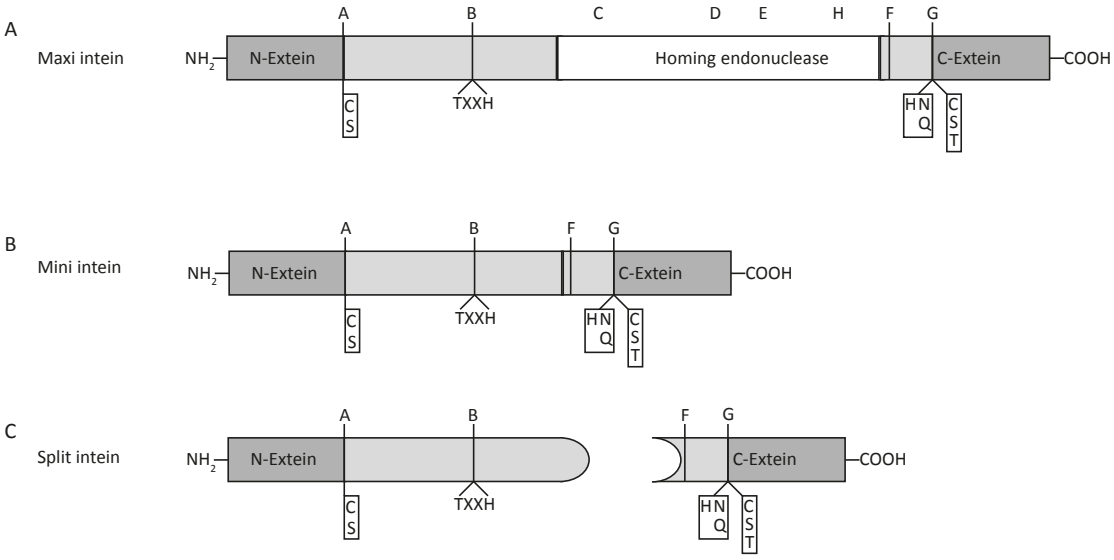

Figure 21: Structure of the three types of naturally occurring inteins. Maxi (A), mini (B) and split (C) inteins are structurally similar but mini and split inteins lack the homing endonuclease domain and split inteins exist as two separate fragments. The conserved sequence blocks A-H are labelled along with key residues at splice junctions.

Split inteins exist as two fragments that are encoded by two separate genes (Figure 21C). The inteins are transcribed and translated separately then they self associate and catalyse protein-splicing activity in *trans*.[164] Ssp DnaE inteins are trans splicing. The N (upstream) and C (downstream) terminal halves of the *Synechocystis* alpha subunit of DNA polymerase III DnaE are encoded by *dnaE-n* and *dnaE-c* genes, which are more than 700 kb apart.[161] The SICLOPPS methodology uses a plasmid that encodes the elements of the Ssp intein in a rearranged order, resulting in an active *cis*-intein (Figure 22A). The C- and N-inteins flank the central extein sequence such that splicing yields cyclisation of the target peptide or protein sequence (Figure 21B).

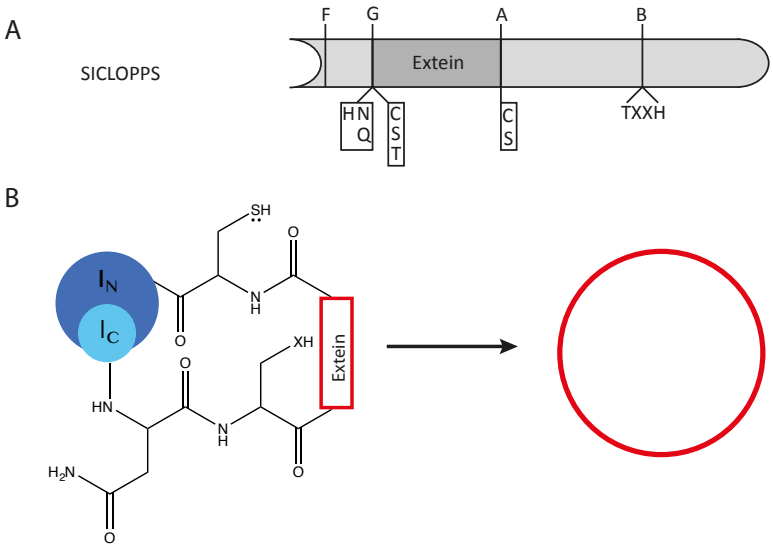

Figure 22: Inteins in SICLOPPS. (A) Structure and arrangement of split inteins in the SICLOPPS methodology. The conserved blocks A, B, F and G with mini inteins as well as the key residues at splice junctions are labelled. (B) The single extein flanked by inteins in the SICLOPPS arrangement allows extein cyclisation upon intein splicing.

Known inteins share little overall identity but do contain conserved residues at the N and C splice junctions (Figure 21). Most inteins start with a Ser or Cys at the N-terminus of the intein and end in His-Asn or His-Gln at the C terminus, this is usually followed by a nucleophilic residue (Cys, Ser or Thr) in the first position of the C extein.[165] In addition, inteins show a significant degree of conservation of short sequence motifs with functionally or structurally similar amino acids, rather than a single predominant residue, termed blocks A-H.[165, 166] Block A, which contains the conserved N splice junction, is followed by block B which contains a polar residue three amino acids prior to a highly conserved His residue which may be involved in N-terminal splice junction cleavage.[167] Blocks C, D, E and H are present in the homing endonuclease domain and therefore only feature in maxi inteins. The C-intein compromises block F, which contains several acidic and hydrophobic residues, including a Val that has been shown to donate an essential hydrogen bond during C-terminal cleavage.[168] In addition, the imidazole ring of a conserved His residue in block F has been shown to contribute to activation of the side chain N atom of the C-terminal Asn residue, leading to Asn cyclisation.[164, 169] The C- terminal splice junction with its conserved motif, is contained within block G.

1.2.2 SICLOPPS intein splicing

Intein *cis*-splicing is a rapid process involving four nucleophilic attacks that rely on the conserved residues at the splice junctions and are aided by surrounding residues in the conserved blocks (Figure 23). Splicing is initiated by nucleophilic attack by the intein residue

at the N intein/extein splice junction (Ser, Cys or Thr) causing an N-O or N-S acyl shift of the peptide bond at the N-terminus and forming an ester or thioester bond at the N-intein/extein junction (I). Next, the –OH or –SH group of the first residue of the extein (nucleophilic Ser or Cys) attacks the (thio) ester bond leading to transesterification and cyclising the extein, forming a branched intermediate (II). In step 3, the C-terminal intein residue Asn cyclises, cleaving the peptide bond between the extein and C-intein, releasing the cyclised extein (III). The final step is a spontaneous N-O or N-S acyl shift, affecting a rearrangement of the (thio)ester to a peptide bond (IV).

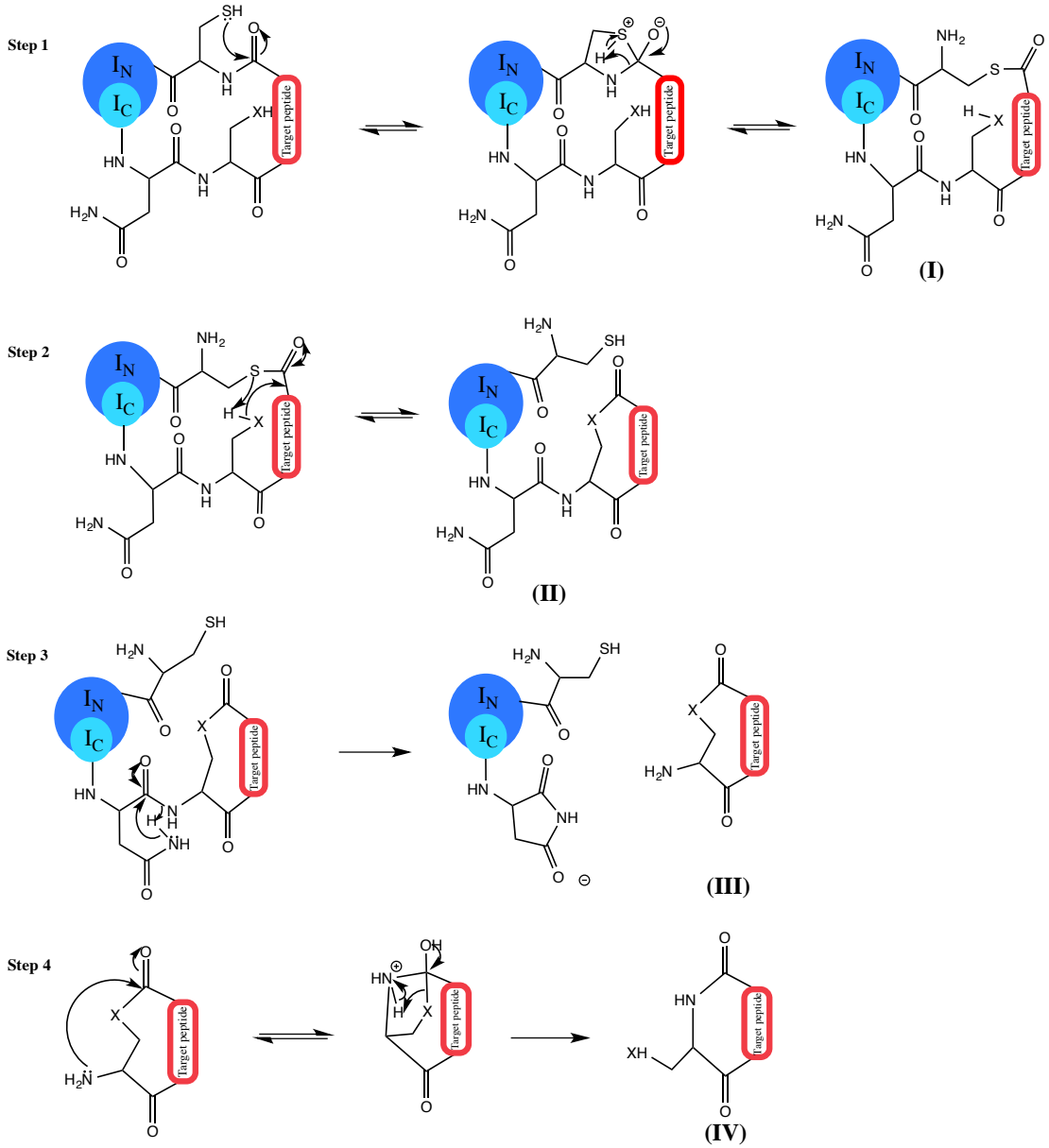

Figure 23: Mechanism of SICLOPPS intein splicing to give the cyclic peptide. X= OH (Ser/ Thr) or SH (Cys). Splicing proceeds via four nucleophilic attacks, step 1: N-[S/O] acyl shift, step 2: transesterification, step 3: Asn cyclisation, step 4: [S/O]-N acyl shift.

This standard splicing mechanism of (Class I) inteins requires the conserved nucleophilic residue at the intein N terminus, however, inteins that lack this residue but still achieve

protein splicing have been described. These inteins (termed class II and class III) cannot perform the initial acyl shift that initiates splicing in class I inteins so instead follow an alternative splicing pathway. In class II inteins, such as the archeal KlbA proteins, the first residue of the C-extein, a nucleophilic Cys residue, directly attacks the amide bond at the N-terminal splice junction, leading to the branched intermediate formed in class I splicing.[170] In class III inteins, the –SH group of a conserved Cys residue in the F block of the intein attacks the peptide bond at the N-terminal splice junction.[171, 172] This forms an intermediate with an unstable thioester linkage. Transesterification of the first residue of the C-extein then transfers the N-extein to form the standard branched intermediate.

A number of naturally occurring split inteins with superior splicing efficiencies and speeds compared to Ssp DnaE have been identified.[173, 174] Of these, the *Nostoc punctiforme* (Npu) DnaE split intein is homologous to the Ssp DnaE intein and shares 70% structural similarity, with 67% sequence identity between the N-terminal inteins and 53% between the C terminal inteins (Figure 24).[174] Npu DnaE inteins display robust trans-splicing activity with an estimated ligation efficiency of more than 98%.[174] *In vitro* characterisation of these inteins revealed superior trans-splicing activity of Npu DnaE with a half life of 63 s compared to 175 minutes for Ssp DnaE.[175] In addition, whereas the Ssp intein has a reduced splicing rate at 37°C compared to 30°C, the rate of splicing of the Npu intein was largely unaffected by temperature (6-37°C).[175]

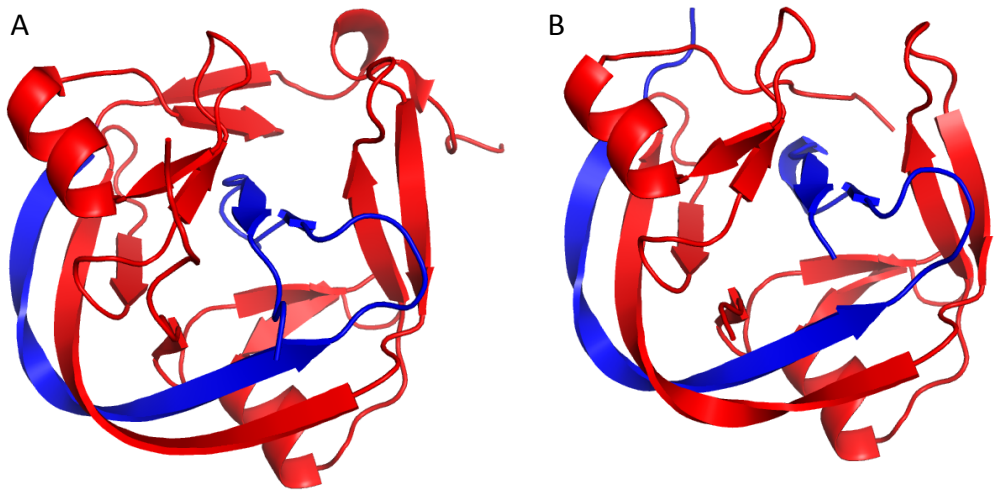

Figure 24: Crystal structures of Ssp and Npu DnaE split inteins. The splicing conformations of the Ssp DnaE intein (A) PDB 1ZDE[164] and Npu DnaE intein (B) PBD 4LX3[176] are remarkably similar. For both N-intein: red and C-intein: blue.

Furthermore, compared to the Ssp intein, the Npu intein showed greater flexibility in the amino acids at the ligation splice junction. Substitution of the Phe residue in the +2 position of the C-extein adjacent to the splice junction (after the necessary Ser or Cys at +1) to each of the 20 naturally occurring amino acids revealed the greater tolerance of the Npu intein than

the Ssp intein to the extein sequence (Figure 25).[174] Aromatic and hydrophobic residues were relatively more preferred for protein splicing activity and hydrophilic side chains significantly reduced splicing.

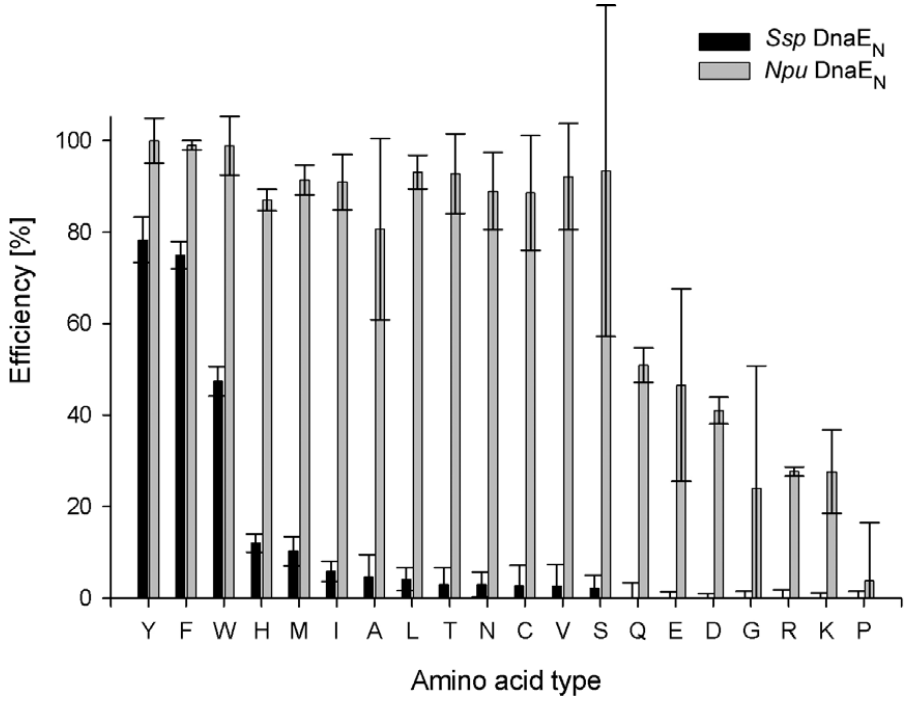

Figure 25: Splicing efficiency of Ssp DnaE and Npu DnaE inteins with variation of the +1 position of the extein. Npu inteins are much more tolerant to amino acid variation than Ssp inteins. Reproduced from Iwai 2006 with permissions from the rights holder Wiley and Sons.[174]

The Npu inteins were mutated using random mutant oligonucleotides in PCR and variants with even greater tolerance for varied amino acids at the C-intein splice junction were selected.[177] A second generation SICLOPPS plasmid was constructed in the Tavassoli laboratory with these mutated Npu inteins.[178] In the context of library production, the amino acid tolerance is highly valuable, allowing the production of a less biased, more varied library of cyclic peptides. In addition, higher splicing efficiency (particularly at 37°C) allows more peptide production.

1.2.3 Use of inteins in mammalian cells

Inteins have also been introduced to mammalian cells in a range of applications. Inteins have been shown to facilitate antibody production in mammalian cells by allowing separation of heavy and light polypeptide chains during translation, which are later joined together through splicing.[179] In addition, conditional splicing of inteins in mammalian cells has been demonstrated through the use of a bio-molecular scaffold, via the small molecule 4-hydroxy tamoxifen or by light.[180-182] The feasibility of genetically encoding inteins onto the mammalian

chromosome was demonstrated with expression and splicing of green fluorescent protein (GFP).[180] The SICLOPPS methodology has also been used in mammalian cells to produce biologically active cyclic peptides. Retroviral delivery of genetic constructs encoding randomised sequences between Ssp DnaB split inteins allowed the production of a cyclic peptide library in a human B cell line (BJAB).[183] Treatment of cells with interleukin-4 (IL-4) allowed detection of peptides that inhibited the IL-4 signalling pathway. Similarly, transient transfection of cyclic peptide In-Box fragments produced using SICLOPPS allowed the identification of inhibitors of the Aurora B-In-Box interaction.[184]

These applications reveal the potential for using inteins to produce cyclic peptides that alter cellular function in cells. The evolved Npu inteins could be particularly advantageous for this application because of their ability to splice efficiently at 37°C.[177] However, cyclisation of peptides via Npu inteins has not previously been shown in mammalian cells. In addition, expression of an inhibitor peptide in mammalian cells from a genetically-encoded construct has not been shown. In the development of a cell line with reprogrammed function via inhibition of HIF-1 dimerisation by cyclo-CLLFVY, it will be necessary to demonstrate intein expression and cyclisation in the cell line.

1.3 Epigenetics

There is increasing evidence that epigenetic changes are essential for determining the hypoxic response.[94, 185-187] Epigenetics describes the study of heritable changes in gene expression that occur independent of changes in the primary DNA sequence.[188] There are four main epigenetic mechanisms: DNA methylation, covalent histone modification, non-covalent modifications and non-coding RNAs. Epigenetic modifications at the DNA and histone level have the ability to dictate HIF binding to target gene promoters.[94, 185, 186] In addition, epigenetic marks are dynamic and therefore can respond to changes in physiological conditions (e.g. hypoxia) and contribute to tumour progression.

1.3.1 Non-coding RNAs

Non-coding RNAs are transcripts that do not code for proteins, and a key role for such sequences in regulation of transcription is emerging.[189, 190] Non-coding RNAs include short non-coding (snc) RNAs (such as short-interfering (si)RNA and micro (mi)RNA) and long non-coding (lnc) RNAs (such as antisense mRNA). miRNAs are single-stranded, regulatory RNAs that are transcribed as longer immature transcripts and undergo extensive splicing to molecules of approximately 21-25 nucleotides in length.[189] They have been identified in almost all metazoan genomes and implicated in the regulation of stability and translation of hundreds of genes.[189] miRNAs are bound by the RNA-induced silencing complex (RISC) and direct the complex to target complementary mRNA transcripts (Figure 26). Perfect complementarity between the guide sequence and the target mRNA leads to transcript degradation whereas imperfect complementarity and binding to the 3'UTR of the target mRNA can lead to translation inhibition.[189]

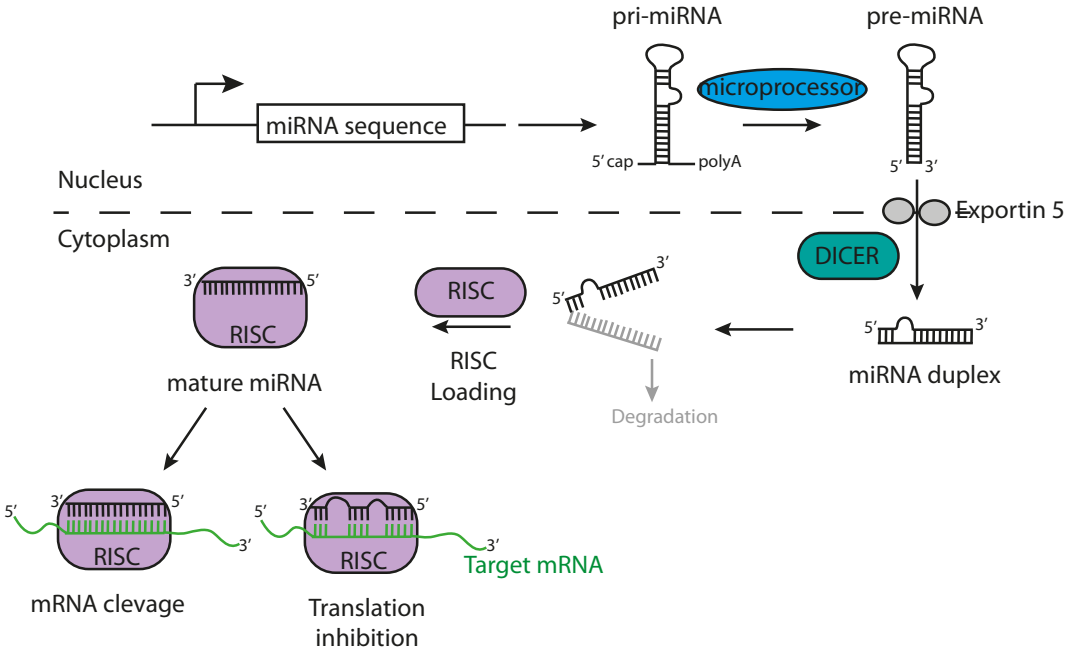

Figure 26: Illustration of the RISC pathway that leads to miRNA control of gene expression. Short RNA sequences that do not code for proteins but code for hairpin loop pri-mRNA structures are transcribed in the nucleus by RNA polymerase II. The hairpin is liberated from the pri-mRNA structure by the microprocessor complex, forming pre-miRNA typically 11 nucleotides from hairpin to base. The pre-miRNA is exported from the nucleus then further processed in the cytoplasm by the RNase III enzyme Dicer, which cleaves the hairpin from the miRNA duplex. One strand of the miRNA is loaded on to the RISC complex and acts as a guide sequence to target mRNAs. The level of complementarity between the miRNA and the target mRNA can determine the mode of action of RISC.

A number of miRNAs have been shown to be upregulated in hypoxia, and to be direct targets of HIFs.[191] In particular, miR-210 is a consistent feature in the hypoxic response. It has been shown to be a direct target of HIF-1 and is overexpressed in a variety of hypoxic disease states.[192] High levels of miR-210 have been associated with poor prognosis in breast and pancreatic cancer patients.[193] miR-210 has been implicated in a wide range of targets that contribute to the hypoxic response, including genes involved in the cell cycle, angiogenesis, DNA damage response, apoptosis and mitochondrial metabolism.[194]

Although some classes of sncRNAs have been established as key players in gene regulation, there is still relatively little known about lncRNAs such as antisense RNA. Antisense transcripts are transcribed from the opposite strand of that of the sense transcript of protein coding or non-protein coding genes.[190] Antisense transcripts can interact with other gene loci and mediate gene expression in a 'trans' process, or remain at their transcription site and affect gene expression through 'cis' processes such as stalled polymerases or triple helices.[190] Genomic analysis of non-coding transcripts identified a number of lncRNAs that were upregulated by hypoxia.[187] In combination with HIF-1 binding analysis these lncRNAs were defined as a new group of HIF-1α target genes.[187] Specifically, prolonged hypoxia has been

shown to induce an increase in an antisense HIF-1α (aHIF) transcript to which HIF-1α and HIF-2α could bind.[105] This increase in aHIF led to destabilisation of HIF-1α mRNA and has been implicated in target gene specificity between HIF-1 and HIF-2.

1.3.2 Chromosome modification

Chromosomal DNA is packaged into chromatin, a highly ordered DNA-protein complex. Histones, the major protein components of chromatin, are small, basic proteins that bind tightly to DNA. There are four families of core histones H2A, H2B, H3 and H4, which form an octamer (made up of two of each of the four core histone types), and associate tightly with DNA to form nucleosomes; approximately 200 bp of DNA is associated with each histone octamer. A single molecule of a fifth family of histones, H1, binds to the nucleosome and stabilises the point at which DNA enters and leaves the nucleosome core. Histone modifications are an essential mechanism for the condensation and relaxation of chromatin to allow DNA replication and gene expression. The core histone proteins are modified in their N-terminal regions and transcriptional states are associated with particular histone modifications (Figure 27). There are many histone modifications with complex potential combinations, but in general, acetylation of H3 and H4 and methylation of the Lys-4 residue of H3 (H3K4) is associated with gene activation.[195] Hypoacetylation of histones and methylation of H3K9 or H3K27 is associated with inactive genes.[195]

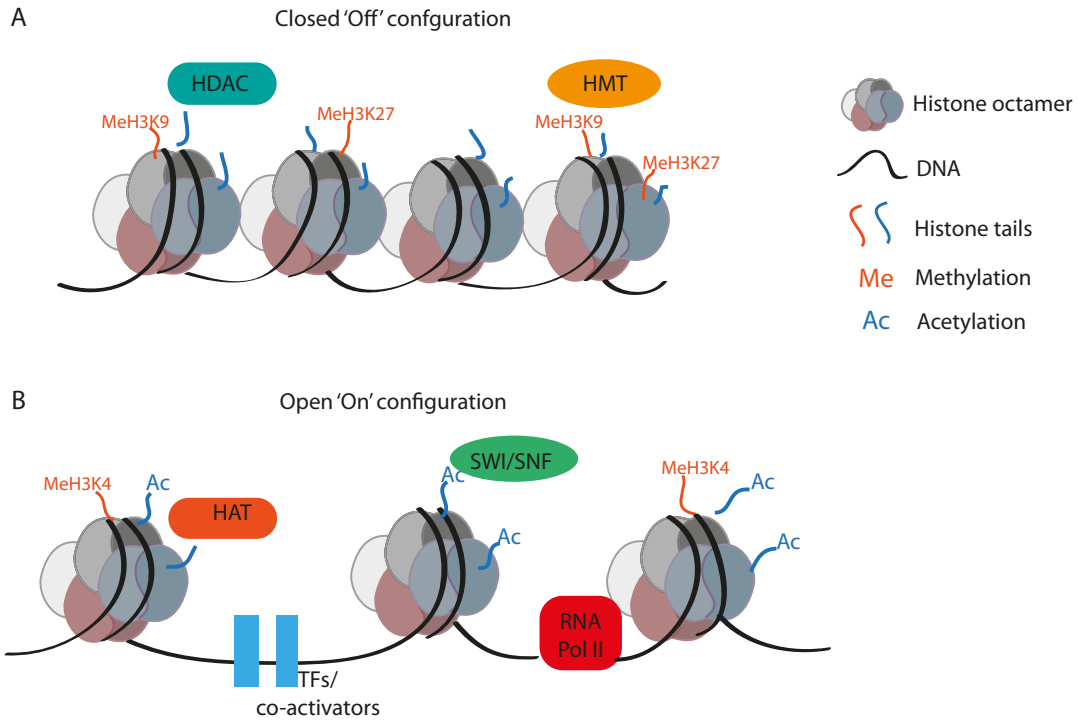

Figure 27: Dynamic chromatin remodelling regulates transcription. (A) DNA is wrapped tightly around basic histones in a condensed state, where transcription factors and polymerase cannot access genes. Histone deacetylation and methylation at H3K9 and H3K27 is associated with inactive genes. (B) Histone acetylation leads to disassociation of DNA from the histone, allowing access of transcription factors and co-activators to gene promoters, of RNA polymerase II to genes, and association of other chromatin remodellers. Genes are actively transcribed. In addition methylation of H3K4 is associated with active genes. HDAC: Histone deacetylase; HMT: Histone methyltransferase; HAT: Histone acetyltransferase; TFs: Transcription factors; SWI/SNF: switch/sucrose nonfermentable.

1.3.2.1 Effect of hypoxia on histone modifications

Chromatin immunoprecipitation assays have shown that histones are modified in a gene specific manner under hypoxia.[186, 196] Despite overall repression, hypoxia induces H3K4 methylation at the core promoters of hypoxia active genes, and H3K27 methylation at the promoters of genes repressed in hypoxia.[196] De-regulation of histone methyltransferases (HMT) and histone demethylases (HDM) has been associated with a number of cancer types, including breast, prostate, lung and brain.[197] The expression and activity of HMT G9a was increased under hypoxia, leading to increased H3K9me2 by inhibiting H3K9 demethylation.[198] This histone methylation was specifically increased in the promoter regions of hypoxia-repressed genes such as MutL homolog 1 (Mlh1, involved in mismatch repair) and dihydrofolate reductase (Dhfr), correlating with their repression.

Histone modifications have also be implicated in tumour progression in VHL negative renal cell carcinoma. Loss of VHL leads to overexpression of HIFs; in the first stages of carcinogenesis HIF-1α is the dominant isoform but later HIF-2α increases and results in a

more aggressive tumour type. A reverse hypoxia response element was identified in the promoter of HIF-1α, which is able to bind HIF-1α or HIF-2α and activate H3K27me3 and repress HIF-1α expression.[199] Indicating that epigenetic changes can dictate temporal changes in HIF isoform expression. Jumonji-domain containing (JmjC) proteins are histone demethylases that are upregulated in hypoxia. JMJD1A and JMJD2B are direct transcriptional targets of HIF-1α and maintain their histone lysine demethylase activity in hypoxia and so are able to impact hypoxic gene expression.[200] Depending on their target, JmjC proteins can induce transcriptional repression or activation. JMJDC1A was reported to regulate expression of HIF-1 target genes ADM and growth and differentiation factor 15 (GDF15) under hypoxia in renal cell carcinoma, HCT116 cells and MEFs by decreased histone methylation.[201] In addition, loss of JMJDA1 was shown to reduce tumour growth. Thus hypoxic induction of JMJDA1 by HIF-1 allows signal amplification to facilitate hypoxic gene induction leading to tumour growth.

Chromatin remodelling can also be achieved through non-covalent means through the action of multiprotein complexes, which use the energy of ATP hydrolysis to bring about structural changes in the nucleosome. The switch/sucrose nonfermentable (SWI/SNF) chromatin remodelling complex was found to associate with the HIF-1α promoter and positively impact the expression of HIF-1α and its ability to transactivate hypoxia responsive genes in U2OS cells.[202] In contrast, the imitation switch (ISWI) complex represses HIF activity through controlling expression of FIH.[203] In U2OS cells, ISWI was found to change RNA polymerase II loading to the FIH promoter and was required for full expression of FIH.

1.3.3 DNA methylation

The process of DNA methylation mainly occurs at the C5 position of cytosine residues in cytosine preceding guanine (CpG) dinucleotides, to form 5-methylcytosine (5-mC). These dinucleotides are not evenly distributed across the mammalian genome but are clustered in areas called CpG islands. CpG islands are preferentially located at the 5' end of genes and co-localise with 88% of human gene promoters.[204] Around 80% of the cytosine residues in CpG dinucleotides not in CpG islands are methylated. However, those dinucleotides in CpG islands are usually unmethylated; this is particularly true of those located in gene promoters regardless of whether on not the gene is being actively transcribed.[205]

Methylation of cytosine is catalysed by enzymes from the DNA methyltransferase (DNMT) family, which has four members: DNMT1, 2, 3a and 3b. DNMT1 is responsible for the maintenance of the existing DNA methylation pattern by adding methyl groups to hemimethylated DNA after DNA replication (Figure 28).[206] DNMT2 mediates methylation of t-RNAs, which prevents proteasomal cleavage of t-RNAs and contributes to ensuring codon

fidelity.[207, 208] DNMT3a and DNMT3b are essential for *de novo* methylation of CpG sites and play an important role in mammalian development.[209] DNA methylation can cause gene silencing by preventing or promoting the recruitment of regulatory proteins to DNA.[210]

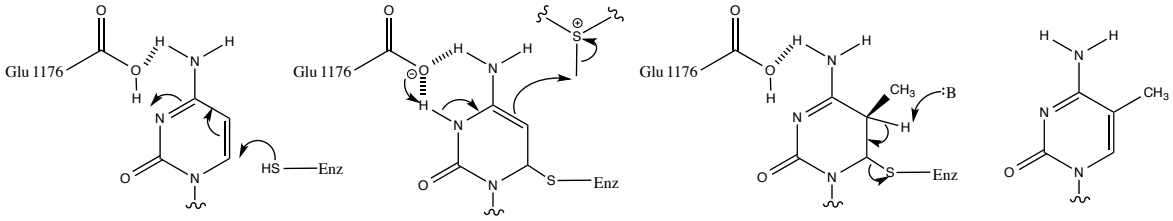

Figure 28: Mechanism of the methylation of cytosine to form 5-methylcytosine. The reaction is catalysed by DNMT1.

Transcriptional repression is mediated by methyl-cytosine binding protein 2 (MeCP2), which binds specifically to methylated DNA.[211] MeCP2 associates with a co-repressor complex containing the transcriptional repressor mSin3A and HDACs, therefore eliminating access of transcription factors (Figure 29).[211] In addition, the presence of DNA methylation directs methylation of H3K9, causing transcriptional repression through the interaction between DNMT1 and G9a.[212] There is interplay between DNA methylation and histone modifications such that genes may not be expressed despite unmethylated DNA or acetylated histones, as both should be in an 'open' configuration to allow gene expression.

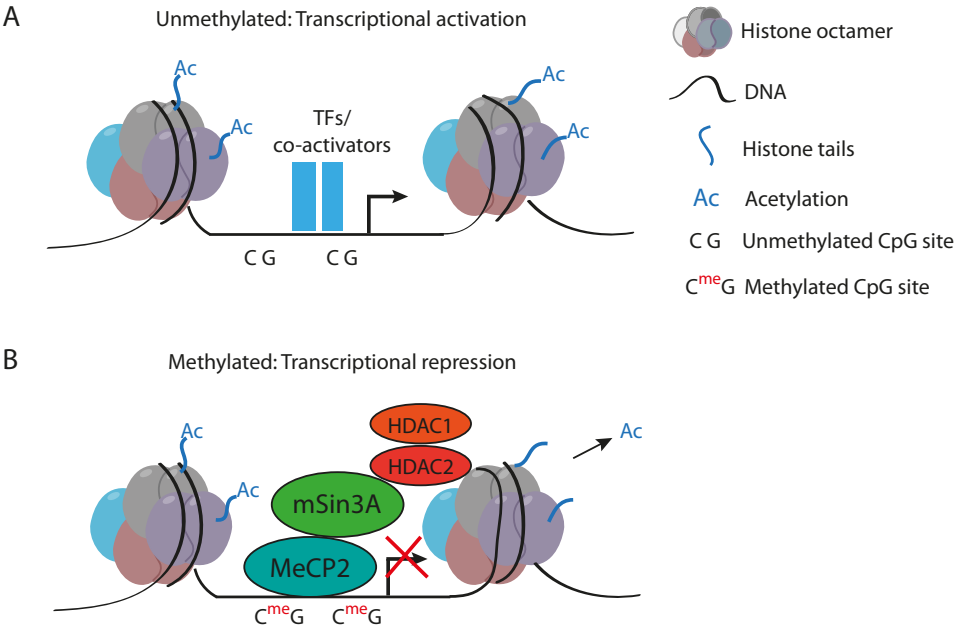

Figure 29: Illustration of transcription repression by co-ordination between DNA and histone modifications. (A) When CpG dinucleotides in gene promoters are unmethylated and histones are acetylated, chromatin is in an 'open' configuration and transcription can proceed. (B) Methylated CpG dinucleotides recruit MeCP2, which associates with transcriptional repressor mSin3A that recruits HDACs, leading to a 'closed' chromatin formation and transcriptional repression.

The majority of DNA methylation occurs in non-coding regions of DNA. Heavily methylated DNA is replicated later than non-methylated DNA; this late replication is associated with formation of inactive chromatin, facilitating the silencing of non-coding regions.[213] DNA methylation is also important in preventing transcription of repeat elements, inserted viral sequences and transposons. In addition, DNA methylation maintains the silencing of imprinted genes; genes for which only one allele is expressed, either that from the mother or father or on the inactive X chromosome in females.

1.3.3.1 DNA methylation in development

During mammalian development, differentiation of cells is directed by transcription factors that establish gene expression in response to developmental cues. Once their expression is established, transcription factors ensure unidirectional development towards differential cell types. Alongside this, epigenetic mechanisms function to reinforce cell fate and to establish safeguards against reversion to previous cellular states.[214]

At fertilisation, a genome wide demethylation event occurs in the zygote. This may occur via conversion of 5mC to 5-hydroxymethyl cytosine (hmC) by ten-eleven translocation (TET) proteins.[215] TET proteins are αKG dependent dioxygenases and hydroxylate cytosine in a mechanism akin to that of PHD2 hydroxylation of proline in HIF-1α (Figure 6).[215] Three TET proteins have been identified: TET1, TET2 and TET3. Iterative oxidation of hmC by TET proteins can form 5-formyl cytosine and 5-carboxyl-cytosine which could then be removed by base pair excision and repair by the enzyme thymine-DNA glycosylase (TDG) (Figure 30).[216, 217] Alternatively, conversion of 5mC to hmC could facilitate passive removal of 5mC in a replication dependent manner, whereby hmC blocks the binding of DNMT1 and the maintenance of DNA methylation patterns.[218] During the demethylation at fertilisation, sequences that are associated with imprinted genes remain methylated, as do some tandem repeats and other DNA sequences.[219, 220]

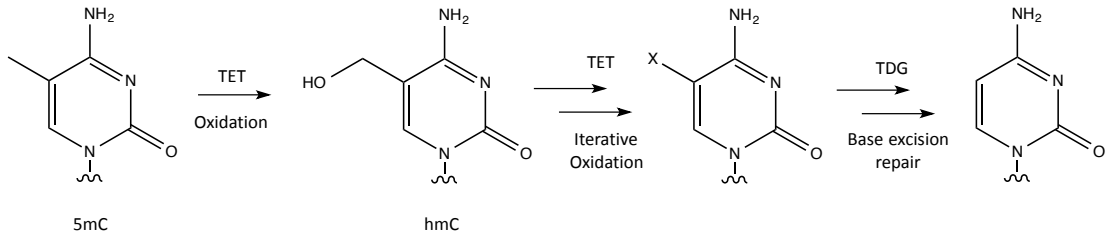

Figure 30: Proposed mechanism of active DNA demethylation by TET proteins. DNA demethylation may proceed via TET mediated oxidation of 5-methylcytosine (mC) to 5-hydroxy-methylcytosine (hmC) and then to 5-formylcytosine or 5-carboxylcytosine. Base excision repair initiated by thymine-DNA glycosylase (TDG) replaces the modified base with unmodified cytosine.

Pluripotent cells are established upon completion of demethylation, which occurs around embryonic day (E) 3.5, and then *de novo* methylation by DNMT3A and DNMT3B begins, which locks in cellular identity.[209] At E6.5 cells either continue to develop towards a somatic fate, or are specified as primordial germ cells (PGCs) and undergo another phase of demethylation (Figure 31).[220] PGCs then gain a gamete-specific methylome during gametogenesis.

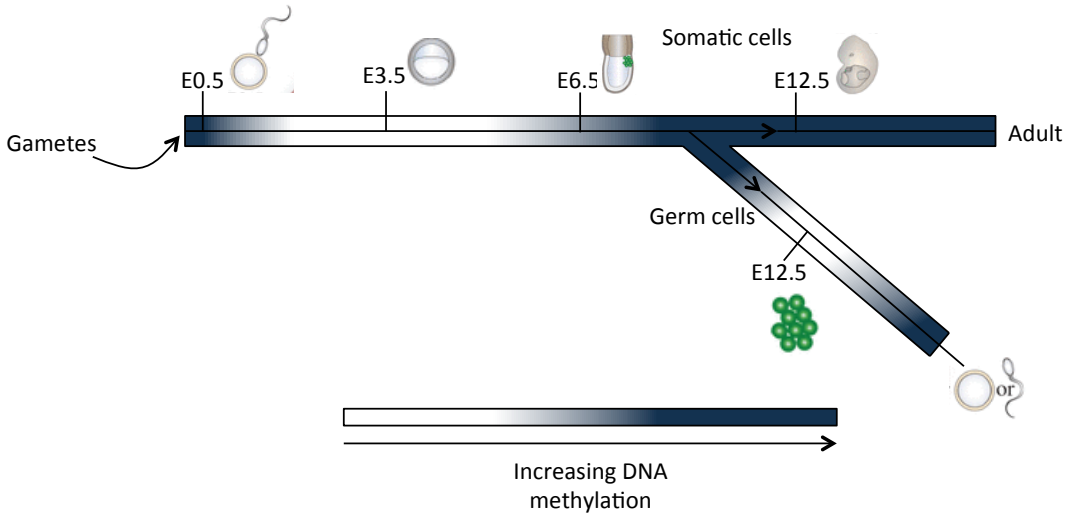

Figure 31: DNA methylation dynamics during the mammalian life cycle. Post-fertilisation, a major demethylation event establishes pluripotent cells at E3.5, then de novo methylation locks in cell fate. Germ cells undergo further demethylation before gaining a gamete specific methylation pattern. Methylation is represented by colour with increasing methylation with darker colour.

TET mediated hydroxylation of cytosine to 5mC has been demonstrated to play an important role in epigenetic regulation of transcription in stem cells. Expression of TET1 is high in embryonic stem cells (ESC) and its upregulation is key to the generation of induced pluripotent stem cells.[221, 222] TET2 also transcriptionally upregulates pluripotency factors in ESC and is required for normal differentiation of hematopatic stem cells.[223, 224] TET3 has been implicated in the reprogramming of cells in oocytes and after fertilization.[225, 226]

1.3.3.2 DNA methylation in cancer

Aberrant patterns of DNA methylation are characteristic of cancer; the cancer epigenome is marked by the occurrence of global hypomethylation and site-specific hypermethylation at CpG islands in gene promoters. This global change in epigenetic marks, including DNA methylation and histone modifications, is associated with a number of malignancies.[227] Hypomethylation mostly occurs at DNA repetitive elements and this may contribute to genomic instability.[228] It can also lead to the overexpression of oncogenic proteins such as insulin growth factor 2 (IGF2) due to loss of imprinting.[229] The mechanism of demethylation is unclear, but it may proceed via an hmC intermediate in a process involving TET proteins, akin to DNA demethylation during embryonic development.[215] Hypermethylation of CpG

islands in the promoters of tumour suppressor genes can lead to silencing of these genes, contributing to tumourigenesis. The silencing of transcription factors and DNA repair genes can also indirectly silence additional classes of genes.[210] For example in colon cancer, increased methylation on chromosome 17p corresponds to the loci of the tumour suppressor gene p53 and precedes allelic loss characteristic to development of colorectal carcinogenesis.[230]

1.3.3.3 The effect of hypoxia on DNA methylation

Regions of solid tumours are transiently or chronically exposed to hypoxic conditions; these conditions contribute to tumour progression and may be the cause of aberrant DNA methylation. For example, severe hypoxic conditions induced a loss in global DNA methylation in human colorectal and melanoma cancer cell lines.[231] Hypoxia has also been reported to induce the downregulation of DNMT1 and DNMT3 in human colorectal cancer cells, contributing to DNA hypomethylation.[232] In hepatocellular carcinoma, hypoxia resulted in genomic demethylation with a bias for CpG islands through activation of methionine adenosyltransferase 2A (MAT2A).[233] MAT2A catalyses the synthesis of S-adenosyl methionine (SAM), a major biological methyl donor. Hypoxia-induced MAT2A expression was shown to be HIF-1α dependent and a consensus HRE was confirmed in the MAT2A promoter.[233] A switch from MAT1A to MAT2A is frequently observed during malignant liver transformation and plays an important role in facilitating liver cancer progression but it is unclear how MAT2A decreases intracellular SAM level.[234] TET1 has also been implicated in the hypoxic response; TET1 upregulation in hypoxia led to an increase in global 5hmC levels and 5hmC density in the promoter elements of HIF-1 target genes.[235] TET1 was required for full expression of hypoxia response genes, suggesting 5hmC facilitates demethylation and HIF binding at promoters of target genes.[235]

A HRE is located within a CpG island in the promoter of the HIF-1α gene itself. It has been suggested that this HRE is normally repressed by methylation of a CpG dinucleotide in the core element.[94] However, in colon cancer cell lines, this element is frequently demethylated, allowing positive auto-regulation of HIF-1α and resulting in amplification of hypoxia-induced transactivation of HIF-1α target genes.[94] This autoregulation of HIF-1α was also shown in MCF7s cells that have an unmethylated HIF-1α HRE, but was absent in HCT-116 cells, which comprise a methylated HIF-1α HRE. In addition, the level of DNA methylation in the HIF-1α promoter region in HMC1, LAD, Hep G2 and A549 cell lines negatively correlated with HIF-1α expression, supporting positive autoregulation of HIF-1α in cancer cell lines.[236] However, despite the importance of HIF signalling in embryonic development, the epigenetic status of the HIF-1α HRE, or the HREs of HIF target genes, has not been studied in embryonic tissues.

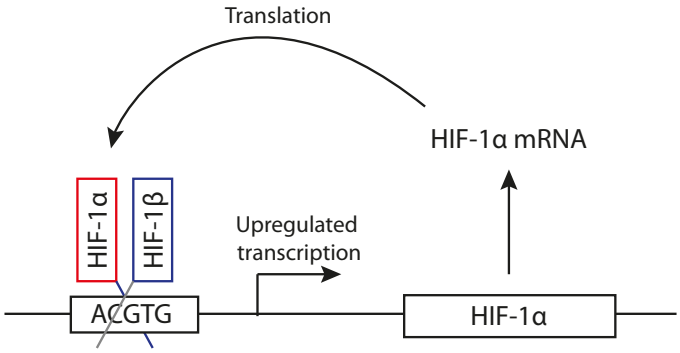

Figure 32: Illustration of proposed positive autoregulation of HIF-1α through the HRE in the promoter the HIF-1α gene. Methylation of the CpG within this HRE has been shown to inhibit this positive autoregulation.

1.1 Aims

The aim of the work presented in this thesis was to improve the current understanding of HIF biology. This was achieved by studying the role of HIF-1 dimerisation in the HIF-1 pathway and by developing knowledge of epigenetic regulation of HIF-1α expression, as described in the following sections.

1.1.1 Developing understanding of the role of HIF-1 dimerisation in hypoxic response.

HIF-1 functions as a part of multiple complex gene networks. As well as having over 100 direct and possibly hundreds of indirect gene targets itself, it is also a member of other key protein cascades such as the PI3K/Akt/mTOR and p44/42 MAPK pathways.[32, 59, 64, 82, 146] Modulation of gene function can allow de-convolution of complex gene networks. There are multiple possible points for intervention in the hypoxia response network but as dimerisation of HIF-1α and HIF-1β is essential for DNA binding and transcriptional activity of HIF-1, this PPi provides an attractive target for interception.

Previous approaches to explore the HIF pathway by disrupting HIF-1 have targeted transcription with techniques such as siRNA and antisense mRNA, but these methods prevent expression of HIF-1α or HIF-1β entirely, rather than specifically modulating their role in hypoxia.[237, 238] HIF-1 dimerisation has been targeted with dominant negative HIF-1α (dnHIF-1α): mutant HIF-1α protein lacking the DNA binding domains and ODDD domain, which can still dimerise with HIF-1β but does not activate transcription of downstream genes.[239, 240] This technique has yielded new information on the HIF-1 pathway, for example transfection of dnHIF-1α in pancreatic cancer cells revealed increased sensitivity of transfected cells to glucose withdrawal.[239] However, dnHIF-1α will also prevent dimerisation of HIF-2α or HIF-3α with HIF-1β and so is not specific to HIF-1.

A number of small molecule inhibitors that target the HIF pathway have been identified and these could be used to study hypoxic response (1.1.8).[127, 137] However, these are limited by the need to synthesise and deliver the compounds. Also, these inhibitors tend to lack specificity, particularly in distinguishing between HIF isoforms.[241] To address this, the first aim of this project was to develop a novel mechanism of reprogramming cellular behaviour by targeting HIF-1 dimerisation with an endogenously expressed small molecule inhibitor. The HIF-1α/HIF-1β interaction was targeted with the specific inhibitor cyclo-CLLFVY.[140] The intein construct encoding this inhibitor was genetically-encoded onto the chromosome of a mammalian cell line downstream of an inducible promoter. *In situ* peptide cyclisation was

achieved via split-intein circular ligation of proteins and peptides (SICLOPPS).[153] This method of cyclic peptide production in mammalian cells was validated by detection of peptide expression and the use of assays to assess peptide activity. The cell line was used to explore the effect of inhibition of HIF-1 dimerisation on the transcriptional profile and the growth and survival of hypoxic tumorigenic cells.

1.1.2 Expanding knowledge of HIF-1 regulation.

The oxygen-dependent regulation of HIF-1α protein has been well characterised (Figure 8).[38, 42, 43, 46] In addition, a number of other post-transcriptional mechanisms of regulation of HIF-1α stability and function have been described (Figure 9).[62] More recently, evidence of transcriptional regulation of HIF-1 has been reported, modulated through epigenetic changes at the HIF-1α promoter. It was shown that demethylation of the HIF-1α gene promoter in HCT-116 cells led to positive auto-regulation of HIF-1α expression by HIF-1.[94] This was supported by identification of a positive HIF-1α feedback loop in MCF7, A549 and HepG2 cells.[95, 236] Hypoxia is often associated with tumour biology but the development of the mammalian embryo takes place in a low oxygen environment where HIF signalling plays a significant role.[242, 243] Understanding of transcriptional regulation of HIF-1α in developing tissue may give insights into the potential significance of the HIF-1α transactivation loop in cancer. Therefore, this section of work aimed to identify the previously unknown methylation status of the HIF-1α promoter in embryonic tissue by methylation specific PCR and bisulfite sequencing. In addition, the methylation status of the EPO enhancer in embryonic tissue and the HIF-1α promoter in adult tissue was sought.

Chapter 2: Reprogramming the cellular response to hypoxia with a genetically-encoded inhibitor of HIF-1 dimerisation

The HIF-1 dimerisation inhibitor cyclo-CLLFVY has great potential to serve as a valuable tool to study HIF biology by interrupting the hypoxic response pathway at this key PPi. However, the cyclic peptide cyclo-CLLFVY has poor aqueous solubility and low cell membrane permeability because it contains many hydrophobic amino acid side chains, and no acidic or basic side chains. Therefore, the peptide has to be conjugated to a 14 amino acid 'Tat' tag for cellular assays, so its synthesis is complicated, low yielding and time consuming. The SICLOPPS methodology used to identify the peptide demonstrates that the peptide can be expressed and cyclised directly in *E. coli* from a genetically-encoded DNA plasmid. The current project aimed to adapt the SICLOPPS methodology to a mammalian expression construct, which would facilitate *in situ* peptide expression and cyclisation within mammalian cells, thus circumventing issues relating to solubility and cell permeability. Stable integration of this construct into mammalian cells would result in a cell line that cannot initiate a response to hypoxia via the HIF-1 transcription factor, hence reprogramming hypoxic cellular behaviour. This system will be a novel tool in the study of HIF biology, enabling analysis of the central role of HIF-1 dimerisation in the hypoxic response and a deeper understanding of the individual roles of the HIF-α isoforms.

2.1 Inducible expression of a cyclic peptide in mammalian cells

2.1.1 Construction of Npu-CLLFVY bacterial expression vector

A genetic cassette encoding the peptide sequence (CLLFVY) as the extein between *Nostoc punctiforme* (Npu) DnaE split inteins (Figure 33), was first constructed in a bacterial expression vector (pARCBD) adapted from the intein encoding vector pARCBD-Npu previously constructed in the Tavassoli laboratory.[178] pARCBD also encodes a chitin binding domain (CBD) sequence in frame with the inteins, at the C-terminus of the N-intein. Expression and splicing of the construct was first demonstrated in *E. coli*. Expression of the construct from the bacterial expression vector pARCBD was induced with L-arabinose (0.5% final concentration) and the inteins isolated using chitin bead pull-down. SDS-PAGE of proteins eluted from chitin beads indicated intein expression and splicing (Figure 34).

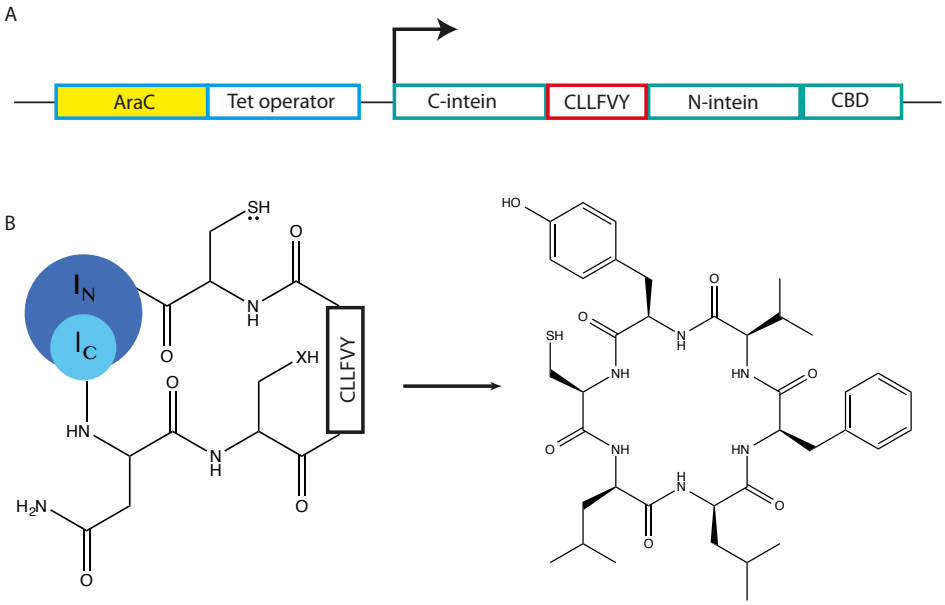

Figure 33: *In situ* expression of cyclo-CLLFVY (A) Representation of the plasmid pARCBD-Npu-CLLFVY. The peptide sequence is encoded between split Npu inteins and is tagged with a CBD sequence. Expression of the open reading frame is under the control of the arabinose promoter (AraC). (B) Illustration of the expressed intein construct splicing to give the cyclic peptide CLLFVY.

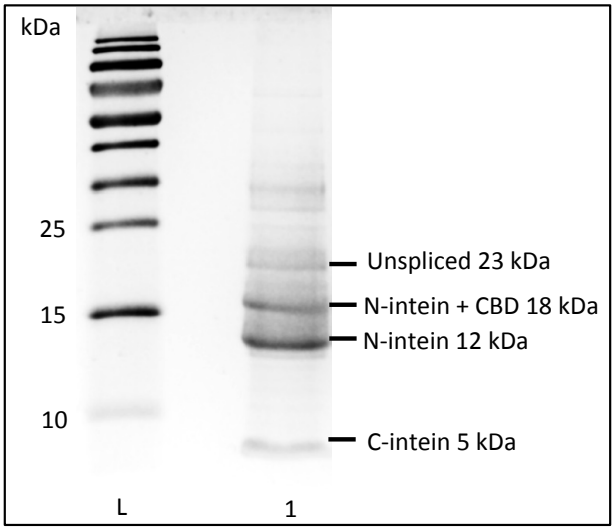

Figure 34: SDS-PAGE analysis of splicing of the Npu-CLLFVY construct expressed in *E. coli*. Lane 1shows the proteins eluted from chitin bead purification of intein expression in *E. coli:* bands corresponding to the unspliced construct (23 kDa), N-intein (18 kDa and 12 kDa) and C-intein (5 kDa) were visualised. Lane L contains the 10-170 kDa protein ladder

2.1.2 Integration of the Npu-CLLFVY construct into HEK-293 cells

The intein-peptide construct was cloned into the vector pcDNA5/FRT/TO to enable expression in mammalian cells. The DNA fragment encoding the peptide between Npu inteins, which included the 3' fusion sequence encoding the CBD, was amplified from pARCBD-Npu-CLLFVY, introducing a 5' Kozak consensus sequence (GCCGCCACC).

pcDNA5/FRT/TO is an inducible expression vector encoding a cytomegalovirus (CMV) promoter, followed by two copies of the tetracycline operator (TetO2) upstream of a multiple cloning site. The vector also encodes a flippase recombination target (FRT) site upstream of a hygromycin resistance gene to permit site-specific flippase-FRT (Flp-FRT) recombination into a suitable cell line, and polyclonal selection using hygromycin.[244, 245] The amplified sequence was cloned into pcDNA5/FRT/TO downstream of the TetO2 giving pcDNA5/FRT/TO/Npu/CLLFVY (pcDNA5/CLLFVY) (Figure 35A). An internal ribosome entry site (IRES) followed by the gene encoding green fluorescent protein (GFP) was then cloned into pcDNA5/CLLFVY downstream of the N-intein, to permit visualisation of successful integrants (giving pcDNA5/GFP) (Figure 35B).

Stable transfection, as opposed to transient transfection, was chosen as it typically leads to more consistent results when testing construct expression and activity, as transfection efficiency would not be a concern. However, isolation of stable transfectants from a mixed population of untransfected or transiently transfected cells is a laborious process requiring many weeks of selection with a well-optimised selection agent. Stably transfected genes are integrated into the host genome and so transgene expression is sustained in daughter cells following mitosis. In contrast, transiently transfected genes are introduced to the host nucleus, but are not integrated onto the chromosome. Therefore, transiently transfected genes are expressed only for a limited period of time and are not maintained after cell replication. Flp-FRT recombination was chosen for integration as it results in integration into a predetermined site on the cell chromosome to avoid integration into open reading frames.

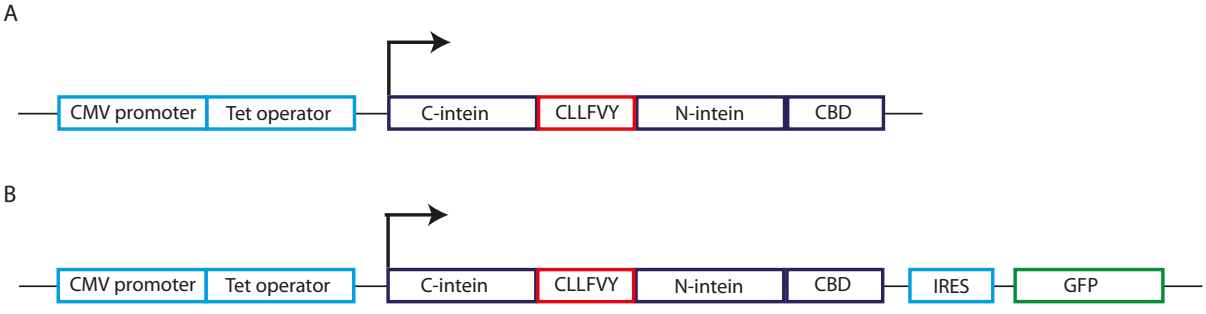

Figure 35: Illustration of the genetic constructs cloned into pcDNA5/FRT/TO and integrated onto the chromosome of T-REx-293 cells. (A) The peptide CLLFVY is encoded as the extein sequence between Npu split inteins and fused with a CBD. The construct is under the control of a CMV promoter and repressed by the TetO2. (B) An IRES was cloned downstream of the Npu-CLLFVY construct followed by the gene encoding GFP.

Both pcDNA5/CLLFVY and pcDNA5/GFP were each co-transfected, separately, into Flp-In T-REx-293 cells with pOG44, which expresses Flp-In recombinase. The cell line is a variant of human embryonic kidney (HEK)-293 that expresses the Tet repressor (TetR) from pcDNA6/TR and contains a single integrated FRT site. Hygromycin (200 µg / mL) was used

for polyclonal selection of positive integrants. The hygromycin resistance gene on the plasmid lacks a promoter and the ATG translation initiation codon (Figure 36). Therefore transient transfection of the plasmid does not confer hygromycin resistance, and only integrated cells are selected. Furthermore, this ensures that only integration at the specific FRT site, and not random integration onto the chromosome, imparts hygromycin resistance.

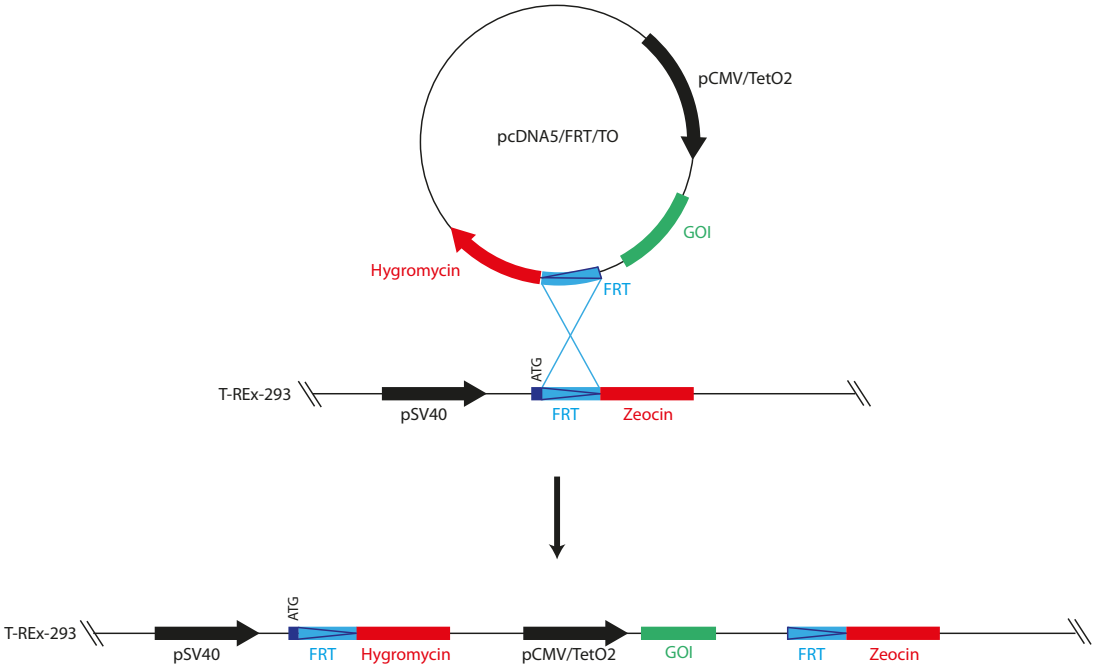

Figure 36: Graphical representation of Flp-FRT recombination. Specific integration of a genetic construct, encoding the gene of interest (GOI), onto the chromosome of T-REx-293, is achieved via Flp-FRT recombination, catalysed by the enzyme Flp-In recombinase. The gene encoding hygromycin resistance lacks the start codon 'ATG' on the plasmid, which it gains upon integration at the target site, facilitating selection of site-specific integrants only.

The presence of the TetO, in combination with TetR expression, permits inducible expression of the gene of interest (GOI), in this instance the Npu-CLLFVY construct (Figure 37). The system is adapted from the bacterial resistance mechanism to the broad-spectrum antibiotic Tetracycline (Tc). Tc functions via inactivation of the bacterial ribosome, interrupting protein synthesis and causing the bacteria to die.[246] Gram-negative bacteria have developed resistance against Tc, principally through the membrane embedded protein TetA that exports Tc out of the bacterial cell before it can inhibit translation.[247, 248] However, in the absence of Tc, overexpression of TetA can result in loss of membrane integrity and damage the cell.[249] Therefore, expression of TetA is tightly controlled by the homodimeric Tet repressor TetR. In the absence of Tc, TetR binds to the TetO with high affinity and specificity, blocking transcription of TetA.[250, 251] When Tc diffuses into the cell it chelates Mg^{2+} forming a $[MgTc]^{+}$ complex that binds to the TetR homodimer. Binding of $[MgTc]^{+}$ induces a conformational

change in TetR which greatly reduces its affinity for the TetO, leading to TetA expression and bacterial resistance to Tc.[251, 252]

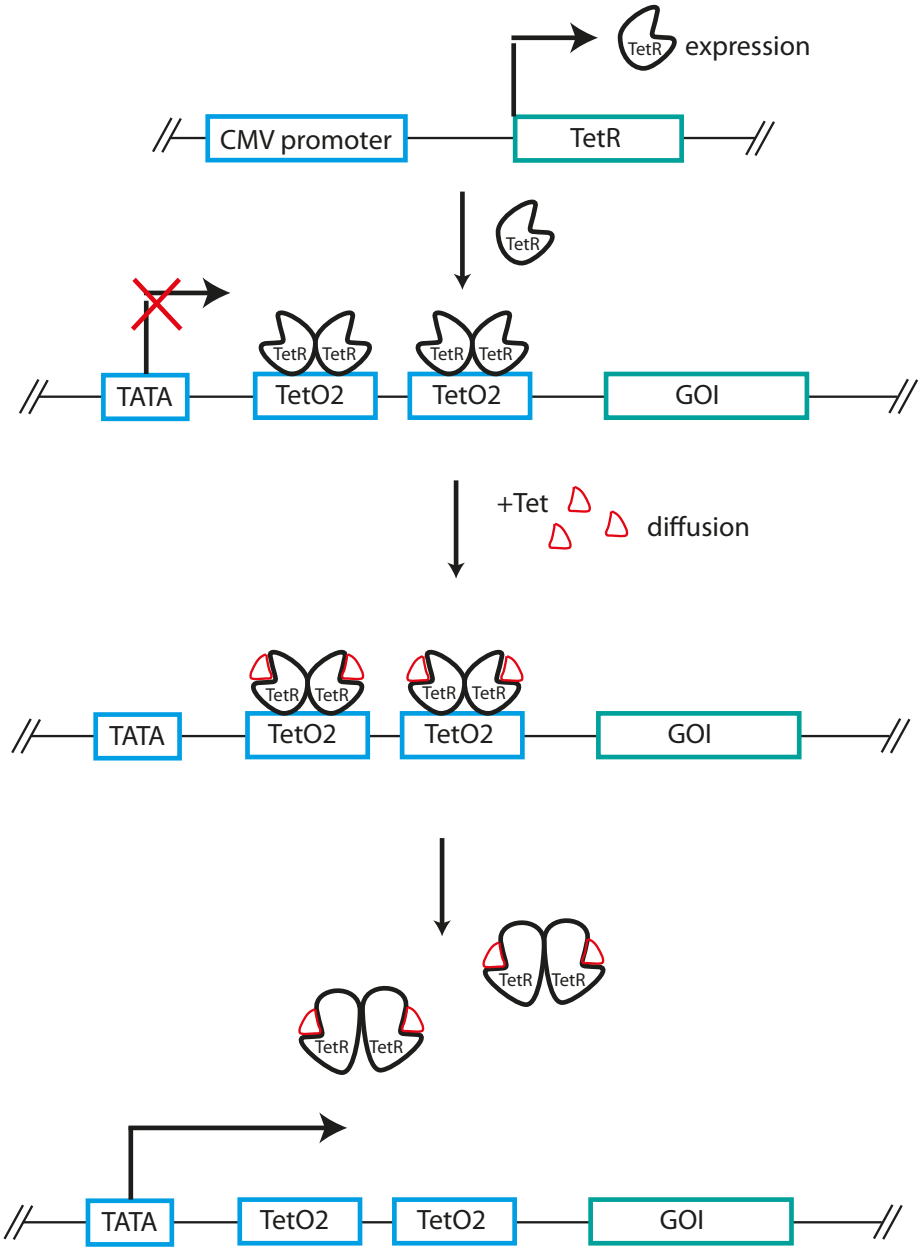

Figure 37: Graphical representation of gene repression by the Tetracycline operator (TetO2). The gene encoding the Tetracycline repressor protein (TetR) is integrated on to the chromosome of T-REx-293 cells and is constitutively expressed. TetR dimerises and binds to the TetO2 with high affinity, blocking the progress of RNA polymerase and inhibiting expression of the GOI. Upon addition, tetracycline (Tet, red shape) diffuses into the cell and binds to TetR with high affinity, causing a change in conformation of TetR, which reduces the affinity of TetR for TetO2 by nine orders of magnitude. TetR therefore leaves TetO2 and the GOI is expressed.

The precise, sensitive control mediated by TetR has been exploited for use as a transcriptional regulator in eukaryotic cells.[253] In the T-REx System, the expression of the GOI is under the control of a CMV promoter, but in the absence of Tc, TetR binds to the TetO2 and

transcription of the gene is blocked. Upon addition of Tc and subsequent binding of Tc to TetR, TetR changes conformation and dissociates from TetO2, leading to expression of the GOI. An analogue of tetracycline, doxycycline (Dox), can be used as an alternative inducing agent. Doxycycline exhibits a similar mechanism of action to tetracycline, but confers more sensitive induction, as TetR has a stronger binding constant for $[Dox.Mg]^+$ compared to $[tc.Mg]^+$ (Ka $\approx 10^{10}$ M^{-1} and Ka $\approx 10^9$ M^{-1}, respectively).[254, 255] Induction with Dox can also lead to longer lasting effects because Dox has a longer half-life than Tc, 48 h and 24 h respectively.[254, 255]

2.1.3 Confirmation of integration: Detection of intein expression in T-REx-CLLFVY cells

Fluorescence microscopy was used to visualise expression of GFP in T-Rex-GFP cells, to confirm integration of the construct. Treatment of T-REx-GFP cells with 1 µg / mL Dox induced expression of GFP, indicating integration of the construct into the cell line (Figure 38). GFP appeared to be expressed in all cell visualised, demonstrating that only integrated cells had been selected. This also suggests successful integration of the Npu-CLLFVY construct in T-Rex-CLLFVY cells, as both cell lines were obtained via the same methodology.

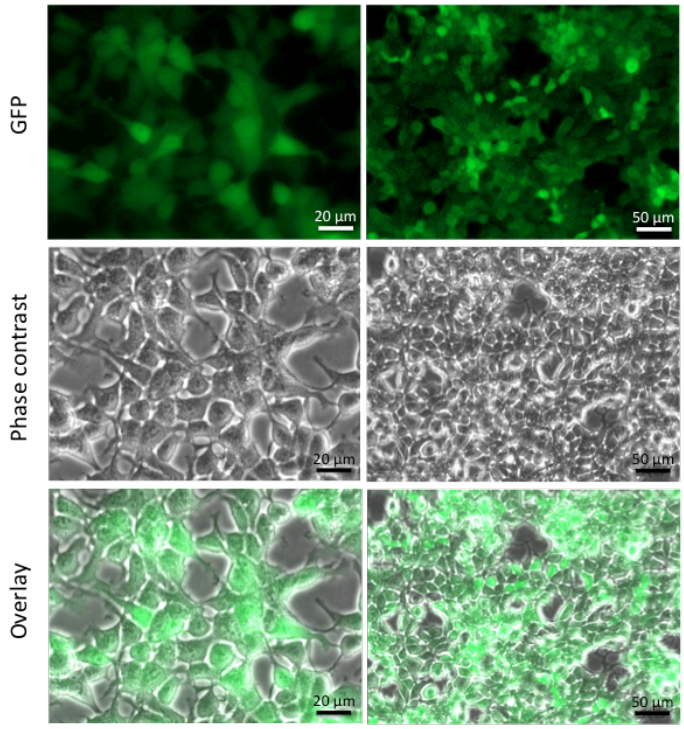

Figure 38: Expression of T-REx-CLLFVY in T-REx cells treated with 1 µg / mL Dox. Top row demonstrates strong GFP expression indicative of successful integration of the Npu-CLLFVY construct. Middle and bottom rows demonstrate widespread integration of the construct in cells.

To optimise the dosage of Dox, T-REx-GFP cells were treated with Dox (0-100 μg / mL) for 24 h and the fluorescence intensity measured (excitation 480 nm / emission 520 nm). Induction of construct expression increased up to 1 μg / mL Dox dosage, then decreased at higher concentrations (Figure 39). Characterisation of the TetO2 integrated into HeLa cells with the reporter gene luciferase demonstrated that maximal activation of expression was achieved at 1 μg / mL Dox and plateaued.[256] However in T-REx-GFP cells, above 1 μg / mL Dox, induction of construct expression was reduced, suggesting possible toxic effects of higher concentrations of Dox in this cell line. Therefore 1 μg / mL was chosen as the optimal Dox concentration and used for the remainder of this work unless otherwise stated.

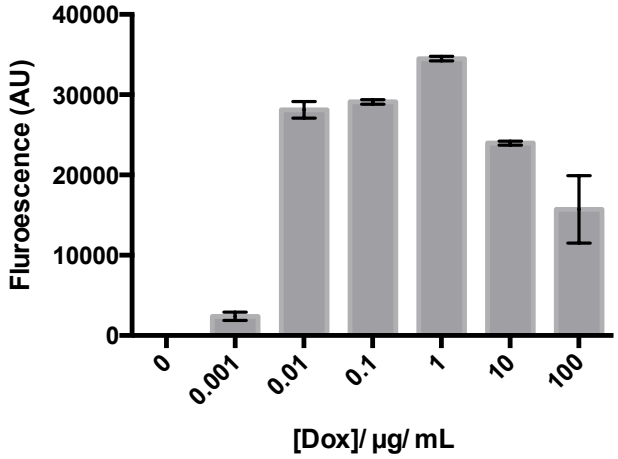

Figure 39: Effect of Dox treatment on T-REx-GFP cells. T-REx-GFP cells were treated with 0-100 μg / mL Dox for 24 h, then expression of GFP measured at 520 nm (excitation 480 nm). Experiments were performed in triplicate (n=2) and normalised to the untreated cells. Error bars represent ±SEM.

Integration and expression of the Npu-CLLFVY construct in T-Rex-CLLFVY was then confirmed by detection of intein mRNA expression. Following treatment with Dox for 16 h, qRT-PCR analysis was conducted on RNA extracted from T-REx-CLLFVY cells with primers specific for the integrated inteins. There was a 38-fold increase in expression following treatment with 1 μg / mL Dox, compared to untreated cells, in both normoxia and hypoxia (Figure 40). Melt curve analysis of the qRT-PCR products showed an equivalent melting temperature for all samples, indicating the same oligonucleotide had been amplified in both samples.

A

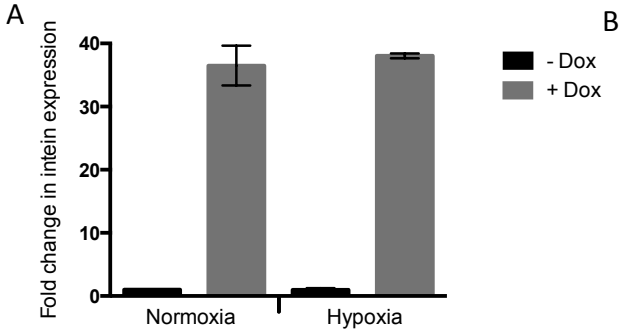

B

Treatment	Mean Tm (°C)	SD of Tm (°C)
Normoxia – Dox	85.7	0.8
Normoxia + Dox	85.5	0.9
Hypoxia – Dox	85.7	0.7
Hypoxia +Dox	85.7	0.8

Figure 40: Dox induces expression of the Npu-CLLFVY construct in normoxia and hypoxia in T-REx-CLLFVY cells. T-REx-CLLFVY cells were treated with vehicle (-Dox) or 1 µg / mL Dox (+Dox) in normoxia or hypoxia for 24 h. (A) RNA was extracted and construct expression analysed using qRT-PCR with primers specific for the integrated inteins. Experiments were performed in triplicate (n=3) and results were normalised to expression of β-actin. Error bars represent ±SEM. (B) Melting temperatures of qRT-PCR products amplified by primers specific for the integrated inteins.

To demonstrate that the construct was being translated correctly, CBD-labelled proteins were isolated from protein extracted, via pull-down assay, from T-REx-CLLFVY cells treated with Dox for 24 h. SDS-PAGE analysis of the isolated proteins demonstrated that a band corresponding to the spliced intein was present (Figure 41). There appeared to be no unspliced construct, suggesting complete turnover of the SICLOPPS construct in cells. The bands were weak because of low cell numbers compared to culture in *E. coli*. Therefore, Western blotting was used, with an antibody specific to the CBD, to detect intein expression.

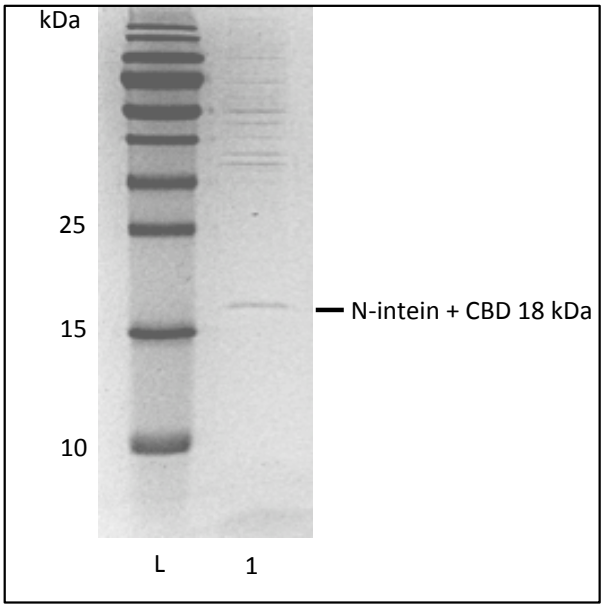

Figure 41: SDS-PAGE analysis of intein expression in T-REx-CLLFVY cells. Lane 1 shows proteins eluted from chitin bead pull-down from T-REx-CLLFVY cells. A band corresponding to the N-intein (18 kDa) and a weak band corresponding to the C-intein (5 kDa) are visible. Lane L shows 10-170 kDa protein marker ladder.

Following treatment of T-REx-CLLFVY and the T-REx-293 parent cell line with 1 μg / mL Dox for 16 h, a product approximately 18 kDa in size was detectable (Figure 42). This is consistent with the size of the CBD-labelled N intein, denoting Npu intein expression and indicating splicing of the Npu-CLLFVY construct. No unspliced protein was detectable, supporting full splicing of the SICLOPPS construct in cells.

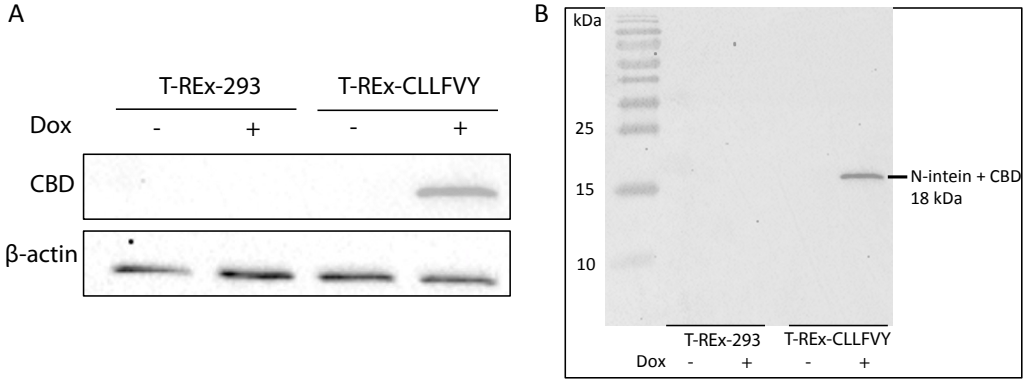

Figure 42: Western blot analysis of Npu-CLLFVY expression in T-REx-CLLFVY cells. (A) Npu-CLLFVY expression was detected in T-REx-CLLFVY cells treated with Dox further demonstrating successful integration and inducible expression of the construct. (B) A band was detected at 18 kDa corresponding to the N-intein, indicating splicing of the Npu-CLLFVY construct.

Cyclo-CLLFVY inhibits hypoxia-induced HIF-1 dimerisation, therefore in order for it to function as a genetically-encoded inhibitor, it must be expressed and cyclised (by intein splicing) under hypoxia, as well as normoxia. Following treatment of T-REx-CLLFVY cells with 1 μg / mL Dox and incubation in hypoxia for 24 h, a band consistent with the size of the N-intein (18 kDa) was detected (Figure 43). Further demonstrating expression of Npu-CLLFVY in hypoxia and indicating splicing of the construct. In contrast to other inteins, Npu inteins have been shown to splice with high efficiency at 37 °C.[177] This is supported by the absence of any detectable unspliced product in cell lysates of T-REx-CLLFVY cells treated with Dox.

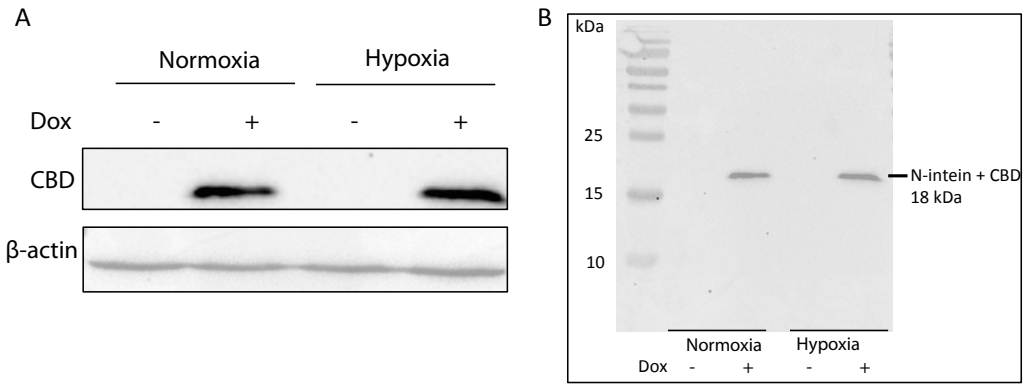

Figure 43: Western blot analysis of Npu-CLLFVY expression in T-REx-CLLFVY cells in normoxia and hypoxia. (A) Npu-CLLFVY expression was detected in T-REx-CLLFVY cells treated with Dox in normoxic and hypoxic conditions, demonstrating successful integration and inducible expression of Npu-CLLFVY in T-REx-CLLFVY cells. (B) A band corresponding to the N-intein (18 kDa) was detected, indicating splicing of the Npu-CLLFVY construct in normoxia and hypoxia.

A time course was carried out to assess the level of expression of Npu-CLLFVY protein over time. In the absence of Dox, there was no detectable construct expression. Addition of Dox induced peptide expression after 2 h, which increased up to 24 h, indicating that Dox is stable and active after 24 h (Figure 44A). Intein expression increased two-fold between 24 and 32 h. Following 32 h of treatment, the level of inteins stabilised (Figure 44B). Previously, characterisation of TetO mediated gene expression in HeLa cells demonstrated maximal induction of reporter gene expression within 24 h.[256] The increase in construct expression that was observed in T-REx-CLLFVY cells following incubation for more than 24 h could suggest that once expressed, the inteins are stable and accumulate in the cell.

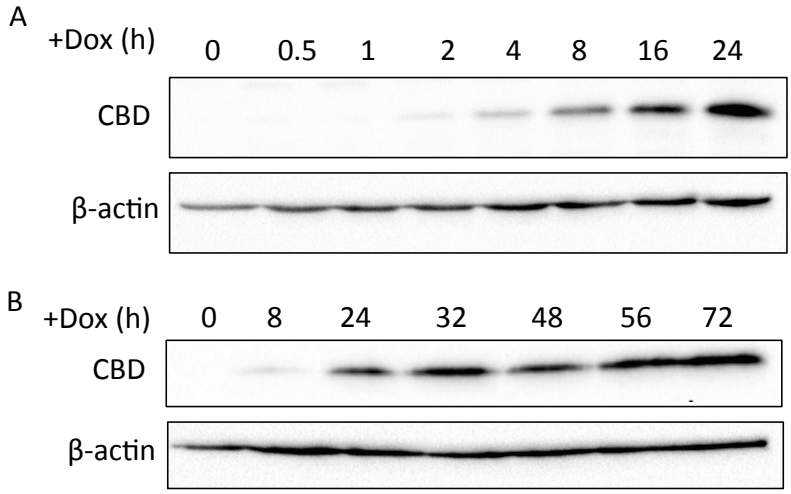

Figure 44: Western blot analysis of Npu-CLLFVY expression in T-REx-CLLFVY cells. Anti-CBD was used to detect of the CBD-labelled N-intein in T-REx-CLLFVY cells treated with 1 μg / mL Dox for (A) 0-24 h or (B) 0-72 h. β-Actin was used as a loading control.

2.1.4 Detection of cyclo-CLLFVY expression from T-REx-CLLFVY cells

Cyclo-CLLFVY was synthesised by solid-phase peptide synthesis to use as a standard to compare to cyclo-CLLFVY expressed *in vivo.* Dilutions of the synthetic peptide in methanol were analysed by LC-MS to assess the detection limits of the instrument for the peptide. The peptide was observed at dilutions up to 1 μg / mL.

Cell lysates from T-REx-CLLFVY and T-REx-293 cells treated with Dox for 24 h were analysed by RP-HPLC. 1 mL fractions were collected for five minutes either side of the retention time (RT) of the synthetic equivalent (24.5 minutes, Figure 45A). In this analysis period, no peaks were visualised from the T-REx-293 cell lysate, but a peak was detectable at RT 23.9 minutes for T-REx-CLLFVY cell lysate (Figure 45B). Analysis of collected fractions by liquid chromatography mass spectrometry (LC-MS) led to the detection of a molecule with the same retention time and a mass equivalent to that of the synthetic peptide, in T-REx-CLLFVY cell lysate (Figure 46, Figure 47). There was no such peak from T-REx-293 cell lysate. This confirms the expression of cyclo-CLLFVY from the genetically-encoded Npu-CLLFVY construct in T-REx-CLLFVY cells.

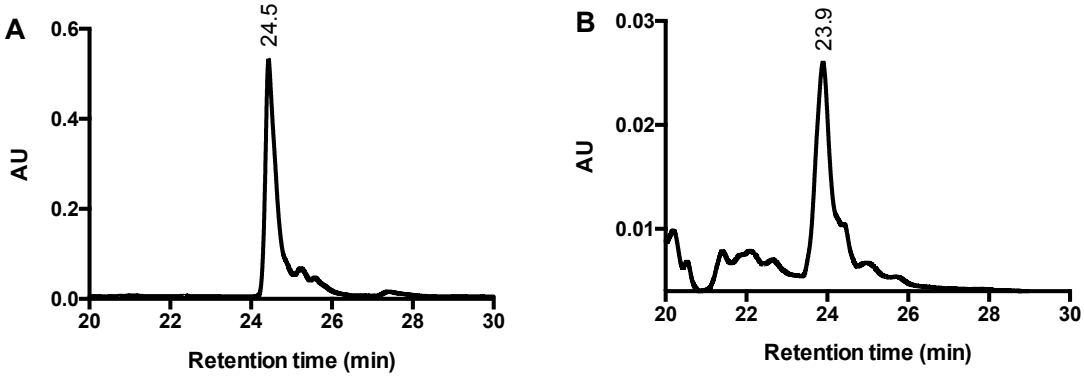

Figure 45: Analytical RP-HPLC of cyclo-CLLFVY. UV traces from analytical RP-HPLC of (A) synthetic cyclo-CLLFVY in methanol and (B) filtered cell lysate from T-REx-CLLFVY cells treated with 1 μg / mL Dox, for 24 h, showing a peak from the lysate (RT: 23.9 minutes) corresponding to that of the synthetic peptide (RT: 24.5 minutes).

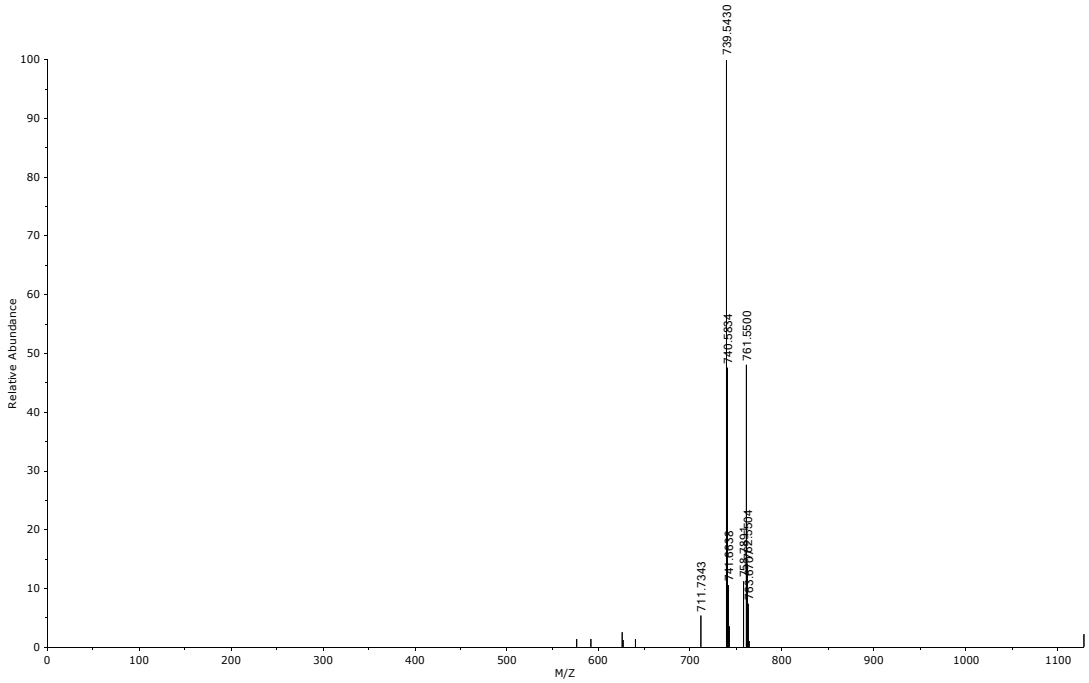

Figure 46: ESI+ MS trace of synthetic cyclo-CLLFVY. LC-ESI-MS (ESI^+, AcCN, 200 nm) RT 2.99 minutes shows: 739.2 ($[M+H]^+$)

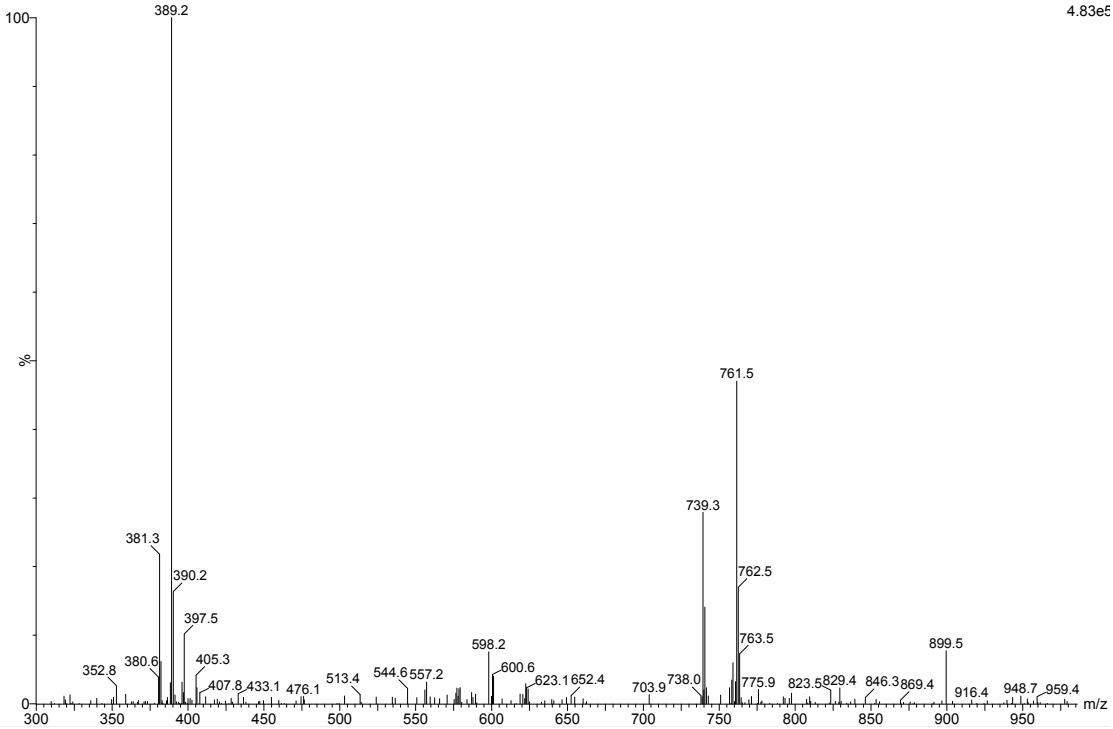

Figure 47: ESI+ MS trace of cyclo-CLLFVY expressed in T-REx-CLLFVY cells. T-REx-CLLFVY cells were treated with 1 µg / mL Dox for 24 h. LC-ESI-MS (ESI^+, AcCN, 200 nm) RT 2.95 minutes shows: 761.5 ($[M+Na]^+$) and 739.2 ($[M+H]^+$).

2.1.5 Activity of the genetically-encoded peptide in T-REx-CLLFVY cells

Having demonstrated that the inhibitor was expressed, its activity was then analysed. Cyclo-CLLFVY has been shown to inhibit the dimerisation of HIF-1α and HIF-1β, preventing the formation of the HIF-1 transcription factor.[140] Assessment of downstream effects of inhibition of HIF dimerisation via cyclo-CLLFVY expression will indicate peptide activity *in vivo*.

2.1.5.1 HRE dependent luciferase assay

A hypoxia response element (HRE) dependent luciferase assay was used to probe the activity of the integrated inhibitor construct. HIF-1 dimerisation has previously been monitored using a HRE-dependent luciferase assay.[257-260] The assay, first developed by Rapisadra *et al.* (2002),[260] places the transcription of firefly (*Photinus pyralis*) luciferase under the control of three copies of the nitric oxide synthase promoter canonical HRE in the plasmid pGL2-TK-HRE (HRE-Luc). Firefly luciferase catalyses the oxidation of luciferin to oxyluciferin and in doing so, releases light (Figure 48). This bioluminescence can be linked to gene expression and therefore to promoter activation. HRE-Luc has previously been used in HEK-293 cells to study HIF-1 transcriptional activity.[59] The assay has also been used to measure inhibition of HIF-1 dimerisation by cyclo-CLLFVY; treatment of MCF-7 cells with 50 μM Tat-cyclo-CLLFVY under hypoxic conditions decreased luciferase expression 5-fold.[140]

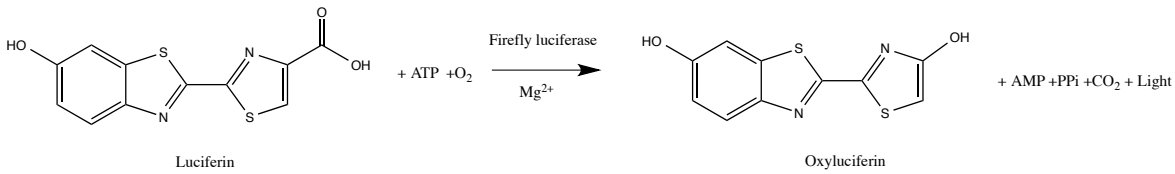

Figure 48: Firefly luciferase catalyses a bioluminescent reaction. Luciferin is oxidised to oxyluciferin by firefly luciferase, releasing light. ATP: adenosine triphosphate; AMP: adenosine monophosphate; PPi: inorganic phosphate.

The HRE-dependent luciferase assay was adapted to analyse the effect of inhibition of HIF-1 dimerisation in T-REx cells. The reporter construct used was HRE-Luc where the expression of luciferase is controlled by a HRE. Luciferase expression is only induced in hypoxic conditions where HIF-1α is stabilised and can dimerise with HIF-1β forming the HIF-1 transcription factor. However, if cyclo-CLLFVY were expressed (with Dox treatment of cells), inhibition of HIF subunit dimerisation would prevent formation of the HIF-1 transcription factor and prevent luciferase expression (Figure 49). The reporter vector, pGL3-SV40-Luc (SV40-Luc), was used as a control, because expression of luciferase in this construct is under an SV40 promoter, which does not rely on HIF-1 for expression and therefore should not be affected by cyclo-CLLFVY expression.

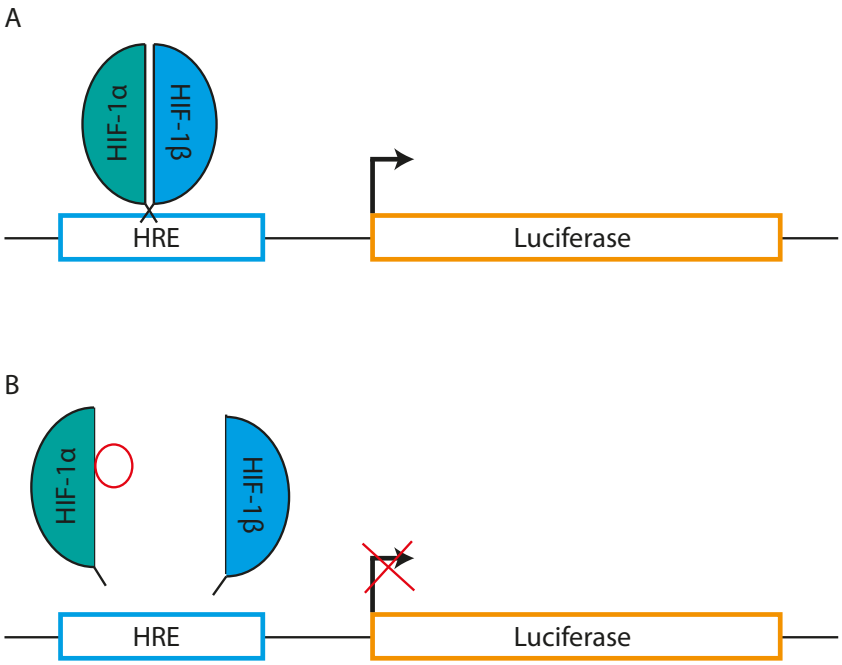

Figure 49: Illustration of the HRE dependent luciferase assay. (A) HIF-1α and HIF-1β dimerise, forming the HIF-1 transcription factor, and bind to the HRE upstream of the gene encoding firefly luciferase, leading to luciferase expression. (B) Expression of cyclo-CLLFVY inhibits HIF-1 dimerisation and the subunits cannot bind to the HRE. Luciferase expression is supressed.

T-REx-CLLFVY cells were transfected with HRE-Luc or SV40-Luc and treated with 1 µg / mL Dox under normoxia or hypoxia. HRE dependent luciferase expression was increased eight-fold in hypoxia (Figure 50). Treatment of cells with Dox resulted in a 1.9-fold decrease in luciferase expression in hypoxia but no significant change in HRE controlled luciferase expression in normoxia. This suggests that expression of the peptide in hypoxia inhibits HIF-1 dimerisation. SV40 controlled luciferase expression was the same in normoxia and hypoxia. Dox treatment had no significant impact on SV40 controlled luciferase expression in normoxia or hypoxia indicating the effect of the peptide on HRE controlled luciferase expression was a result of inhibition of HIF-1 dimerisation rather than inhibition of luciferase activity.

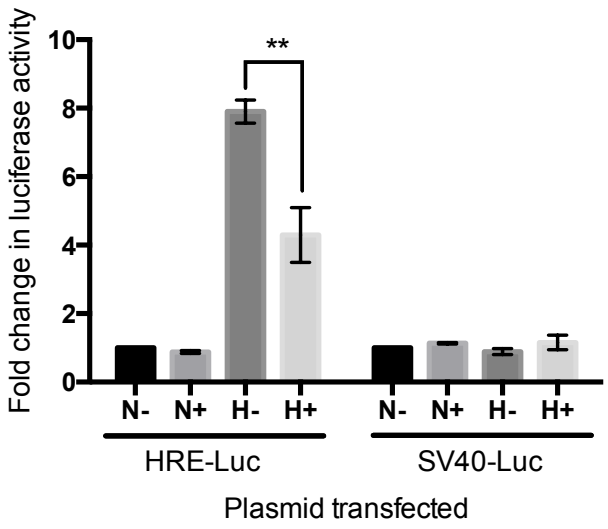

Figure 50: Expression of cyclo-CLLFVY in T-REx-CLLFVY cells suppressed HRE-dependent luciferase expression in hypoxia. T-REx-CLLFVY cells were transfected with HRE-Luc or SV40-Luc. Cells were incubated with vehicle (-) or 1 µg / mL Dox (+) for 16 h in normoxia (N) or hypoxia (H). Experiments were performed in triplicate (n=3). Error bars represent ±SEM. Stars denote significant differences between means: **$p \leq 0.01$.

2.1.5.2 qRT-PCR analysis of expression of HIF-1 target genes

To investigate if expression of cyclo-CLLFVY affected HIF-1-mediated gene expression, the transcription of one of the HIF-1 target genes, VEGF, was analysed. The VEGF gene contains a HRE in its promoter, where binding of HIF-1 activates VEGF expression.[88] Previous studies have shown that inhibition of HIF-1 dimerisation in HEK-293 cells, using the inhibitor acriflavine, blocked hypoxic induction of VEGF expression.[139]

Incubation of T-REx-293 and T-REx-CLLFVY cells in hypoxic conditions for 16 h resulted in a 2.7-fold increase in VEGF expression when compared to cells cultured in normoxic conditions (Figure 51A). This finding suggests VEGF expression represents a useful proxy for monitoring alterations in the hypoxia response pathway in these cell lines. In addition, the similarity in VEGF induction in these cell lines demonstrates that integration of the construct itself does not affect the cellular response to hypoxia, when its expression has not been induced. In contrast, treatment of T-REx-CLLFVY cells with Dox resulted in a 1.4-fold decrease in VEGF expression under hypoxia indicating cyclo-CLLFVY expression and inhibition of HIF-1 dimerisation (Figure 51B).

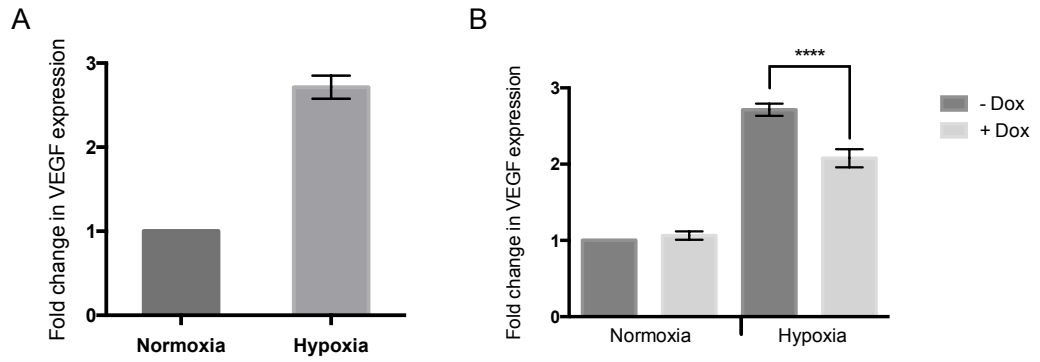

Figure 51: VEGF is upregulated in hypoxia in T-REx cell lines and upregulation is dampened in T-REx-CLLFVY cells by Dox treatment in hypoxia. (A) T-REx-293 cells were incubated in normoxia or hypoxia for 16 h and (B) T-REx-CLLFVY cells were treated with vehicle (-Dox) or 1 μg / mL Dox (+Dox) in normoxia or hypoxia for 16 h. For both, RNA was extracted and VEGF expression analysed by qRT-PCR. Experiments were performed in triplicate ((A) n=3, (B) n=6) and results were normalised to expression of 18S and β-actin. Error bars represent ±SEM. Stars denote significant differences between means: ****$p \leq 0.0001$.

The effect of cyclo-CLLFVY expression on the transcription of another HIF-1 target gene, CAIX, was also analysed to ensure the inhibitory effect was not limited to VEGF. CAIX expression was induced 80-fold in hypoxia compared to normoxia, this result agrees with previous reports of hypoxic induction of CAIX expression in HEK-293 cells.[261] Dox treatment resulted in a 1.5-fold decrease in CAIX expression (Figure 52). CAIX was induced more strongly than VEGF by hypoxia in T-REx-CLLFVY cells; incubation of cells in hypoxia resulted in an 80-fold increase in CAIX expression in contrast to a 2.7-fold increase in VEGF expression compared to normoxia. However, the inhibitory effect of the peptide was similar. Previous studies with synthetic cyclo-CLLFVY also showed that in MCF-7 breast cancer and U2OS osteosarcoma cells, hypoxic induction of CAIX expression was greater than that of VEGF. VEGF was induced ~three-fold whereas CAIX was induced ~25-fold. However, treatment of MCF-7 and U2OS cells with 50 μM cyclo-CLLFVY resulted in a five-fold decrease in expression of both VEGF and CAIX.[140]

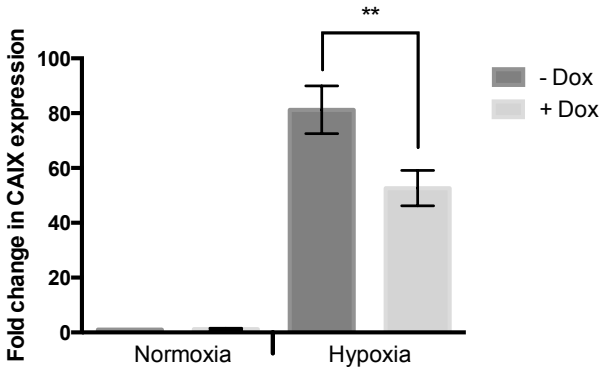

Figure 52: Hypoxic induction of CAIX expression is dampened by Dox treatment in T-REx-CLLFVY cells. T-REx-CLLFVY cells were treated with vehicle (-Dox) or Dox (+Dox) in normoxia or hypoxia for 16 h. RNA was extracted and CAIX expression analysed by qRT-PCR. Experiments were performed in triplicate (n=3) and results were normalised to expression of 18S and β-actin. Error bars represent ±SEM. Stars denote significant differences between means: **p ≤ 0.01.

The time course of Npu-CLLFVY expression showed more protein after 24 h than 16 h hypoxic treatment (Figure 44). To assess if this resulted in increased inhibition of HIF-1 dimerisation, the expression of VEGF and CAIX in T-REx-CLLFVY cells treated with Dox in hypoxic conditions for 24 h was analysed by qRT-PCR. The hypoxic induction of VEGF and CAIX was similar at 16 h and 24 h. However, Dox treatment resulted in increased inhibition of target gene expression: 1.5-fold for VEGF and 1.7-fold for CAIX (Figure 53), suggesting increased inhibition of HIF-1 dimerisation after 24 h compared to 16 h. This may be a result of higher peptide concentration at the longer incubation period.

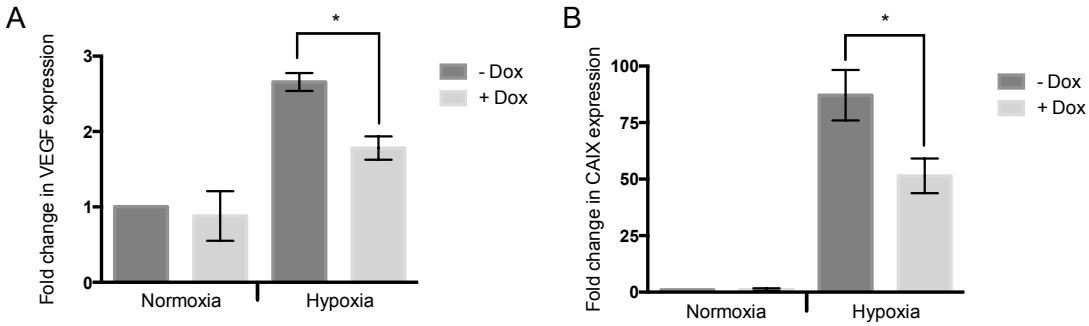

Figure 53: VEGF and CAIX expression is inhibited after 24 h Dox treatment in hypoxic T-REx-CLLFVY cells. T-REx-CLLFVY cells were incubated with vehicle (-Dox) or 1 µg / mL Dox (+Dox) in normoxia or hypoxia for 24 h. RNA was extracted and VEGF (A) and CAIX (B) expression was analysed by qRT-PCR. Experiments were performed in triplicate (n=3) and results were normalised to expression of 18S and β-actin. Error bars represent ±SEM. Stars denote significant differences between means: *p ≤ 0.05.

2.1.6 Investigation of a scrambled peptide control

To investigate whether the change in gene expression in T-REx-CLLFVY cells was a result of cyclo-CLLFVY activity rather than expression of the inteins or Dox itself, a scrambled peptide cell line was constructed. Previously in the Tavassoli laboratory, alanine scanning of CLLFVY derivatives, where each amino acid in turn was replaced with an alanine and assessed for activity, suggested that proximity of the aromatic side chains of phenylalanine and tyrosine in the cyclic peptide contributed to peptide activity. Therefore these residues were separated in the scrambled peptide sequence.

The peptide sequence CFVLYL was encoded as the extein between split Npu inteins in the bacterial expression vector pARCBD-Npu. Expression of Npu-CLLFVY and Npu-CFVLYL in *E. coli*, from pARCBD-Npu-CLLFVY and pARCBD-Npu-CFVLYL respectively, was induced with L-arabinose (0.5% final concentration). The inteins were isolated using chitin bead pull-down. SDS-PAGE of proteins eluted from chitin beads suggested equivalent expression and splicing of the two intein-peptide constructs (Figure 54). Therefore, expression of the Npu-CFVLYL construct would give an accurate comparison of inhibitor and scrambled peptide activity *in vivo*.

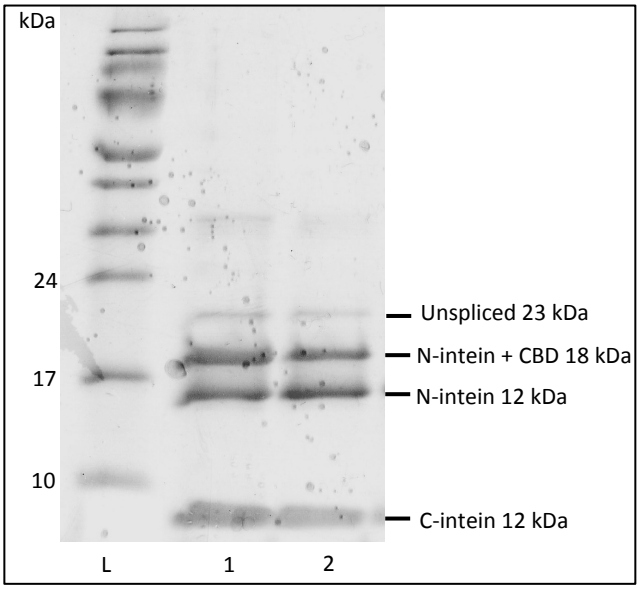

Figure 54: SDS-PAGE analysis of Npu-CLLFVY and Npu-CFVLYL splicing in *E. coli*. Proteins eluted from chitin bead purification of intein expression in *E. coli* from pARCBD-Npu-CLLFVY (Lane 1) and pARCBD-Npu-CFVLYL (Lane 2). Bands corresponding to the unspliced construct (23 kDa), N-intein (18 kDa and 12 kDa) and C-intein (5 kDa) were visualised. Lane L contains the 10-170 kDa protein ladder.

The Npu-CFVLYL construct was then cloned into the mammalian expression vector pcDNA5/FRT/TO and integrated into T-REx-293 cells via Flp-FRT recombination. The T-REx-CFVLYL cell line was obtained by selection of positive integrants with hygromycin (Figure 55). Expression of Npu-CFVLYL was detected in T-REx-Scram cells following treatment with

Dox with 1 µg / mL for 24 h under normoxia and hypoxia (Figure 56A). The presence of a band at ~18 kDa, corresponding to the N-intein, indicated splicing of the integrated construct *in vivo* (Figure 56B).

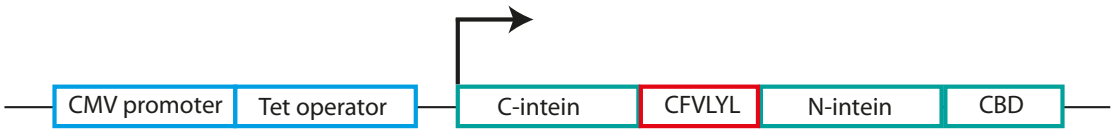

Figure 55: Illustration of the genetic construct encoded into the vector pcDNA5/FRT/TO and integrated onto the chromosome of T-REx-293 cells. The peptide CFVLYL is encoded as the extein sequence between Npu split inteins and a CBD is fused to the C-terminus of the N-intein. Construct expression is under the control of a CMV promoter and repressed by the TetO2 in the absence of Dox.

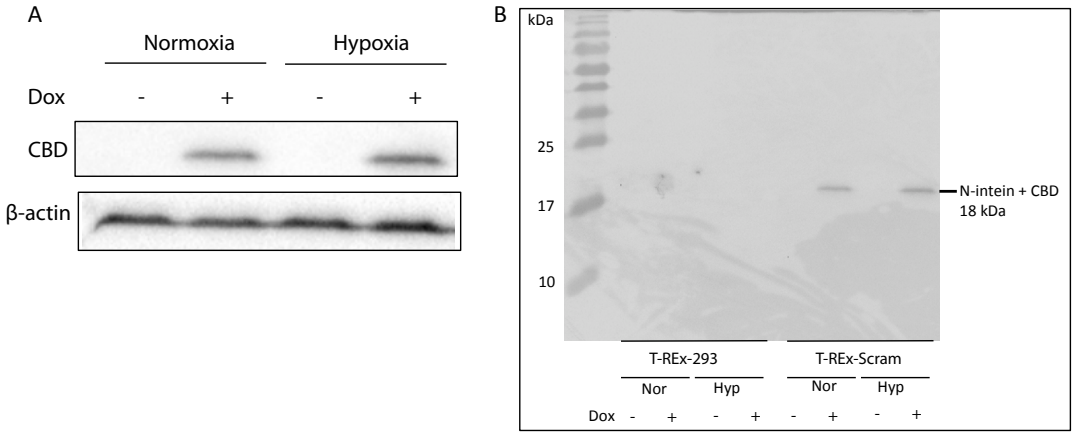

Figure 56: Western blot analysis of Npu-CFVLYL expression in T-REx-Scram cells. Anti-CBD was used to detect expression of the integrated construct in T-REx-Scram cells. (A) Npu-CFVLYL expression was detected in T-REx-CLLFVY cells treated with vehicle (-) or 1 µg / mL Dox (+) in normoxic and hypoxic conditions, demonstrating successful integration and inducible expression of Npu-CFVLYL in T-REx-CFVLYL cells. (B) A band corresponding to the N-intein (18 kDa) was detected, indicating splicing of the Npu-CLLFVY construct in normoxia and hypoxia.

The activity of the expressed scrambled peptide for inhibition of HIF-1 dimerisation was assessed with the HRE-dependent luciferase assay described in section 2.1.5.1. T-REx-Scram cells were transfected with HRE-Luc or SV40-Luc and treated with Dox under normoxia or hypoxia. HRE dependent luciferase expression increased ~seven-fold in hypoxia (Figure 57). Following treatment with Dox, there was no significant change HRE controlled luciferase expression in normoxia or hypoxia, suggesting the scrambled peptide has no effect on HIF-1 activity. SV40 controlled luciferase expression appeared to increase in hypoxia, but this change was not statistically significant. Treatment of T-REx-Scram cells with Dox had no significant impact on SV40 controlled luciferase expression.

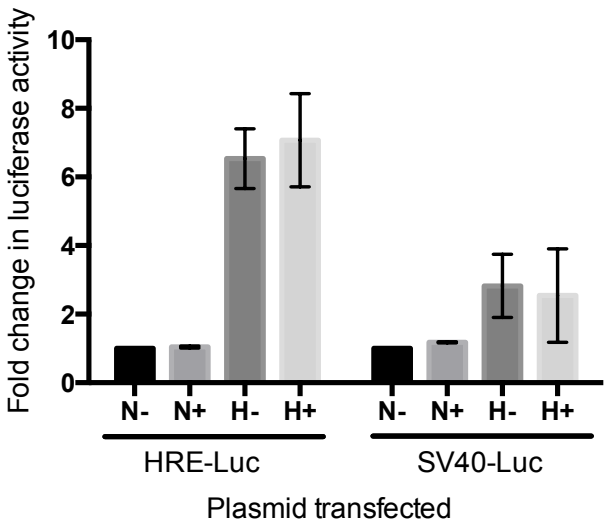

Figure 57: Expression of cyclo-CFVLYL in T-REx-Scram cells does not affect HRE-dependent luciferase expression. T-REx-CFVLYL cells were transfected with HRE-Luc or SV40-Luc. Cells were incubated with vehicle (-) or 1 μg / mL Dox (+) for 16 h in normoxia (N) or Hypoxia (H). Experiments were performed in triplicate (n=3). Error bars represent ±SEM.

The affect of the scrambled peptide on VEGF and CAIX expression was then assessed by qRT-PCR. T-REx-Scram cells were treated with Dox and incubated in normoxia or hypoxia for 24 h. The longer treatment period was used as it gave a larger effect in T-REx-CLLFVY cells than 16 h. Incubation in hypoxia resulted in a two-fold increase in VEGF expression and ~80-fold increase in CAIX expression. Treatment of T-REx-Scram cells with Dox did not significantly impact VEGF or CAIX expression (Figure 58). In normoxia too, expression of cyclo-CFVLYL made no significant difference to VEGF and CAIX expression. Together, these results suggest that the change in luciferase expression in the HRE dependent luciferase assay, and the change in HIF-1 target gene expression in T-REx-CLLFVY cells was a result of cyclo-CLLFVY expression, not of intein expression or integration.

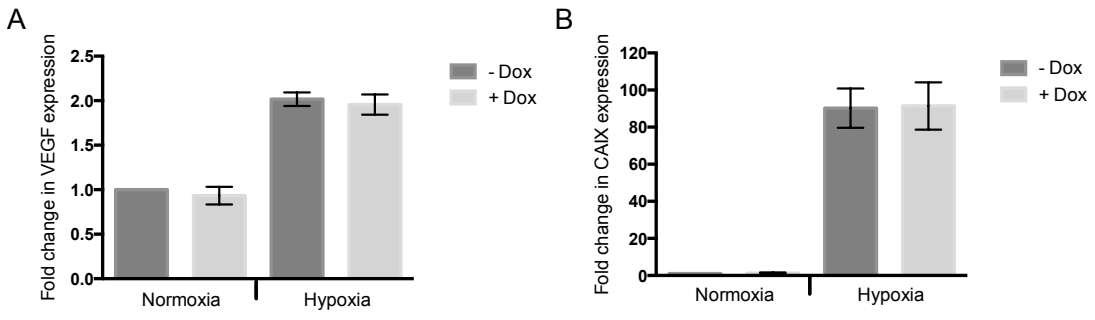

Figure 58: VEGF and CAIX expression is not changed by cyclo-CFVLYL expression. T-REx-Scram cells were incubated with vehicle (-Dox) or 1 μg / mL Dox (+Dox) in normoxia or hypoxia for 24 h. qRT-PCR experiments were performed in triplicate (n=3) and results were normalised to expression of 18S and β-actin. Error bars represent ±SEM.

2.2 Hypoxia-controlled, inducible expression of cyclo-CLLFVY in mammalian cells

The genetic cassette was adapted such that expression was under the control of a HRE promoter. The HRE promoter requires binding of the HIF-1 heterodimer to activate transcription of downstream genes.[260] In this system, the HRE promoter provides a second level of control of peptide expression. The construct should only be expressed in the presence of Dox *and* hypoxia. This would result in a negative feedback loop, whereby hypoxia induces the expression of the peptide, but presence of the peptide blocks HIF-1 dimerisation and prevents further peptide expression, preventing excessive build up of the inteins and peptide.

2.2.1 Construction of a hybrid HRE/TetO2 promoter

The CMV sequence in pcDNA5/CLLFVY was replaced with 3 copies of the HRE (5'-GTGACTACGTGCTGCCTAG-3') from the inducible nitric synthase promoter from the pGL2-TK-HRE plasmid,[260] to generate pcDNA5/FRT/HRE/TO/Npu/CLLFVY (pcDNA5/HRE) (Figure 59). The plasmid was integrated into T-REx-293 cells via Flp-FRT recombination, and positive integrants selected using hygromycin (Figure 60). A scrambled peptide version was not produced as cyclo-CFVLYL had already been shown to have no significant effect on HIF-1 activity in T-REx cells.

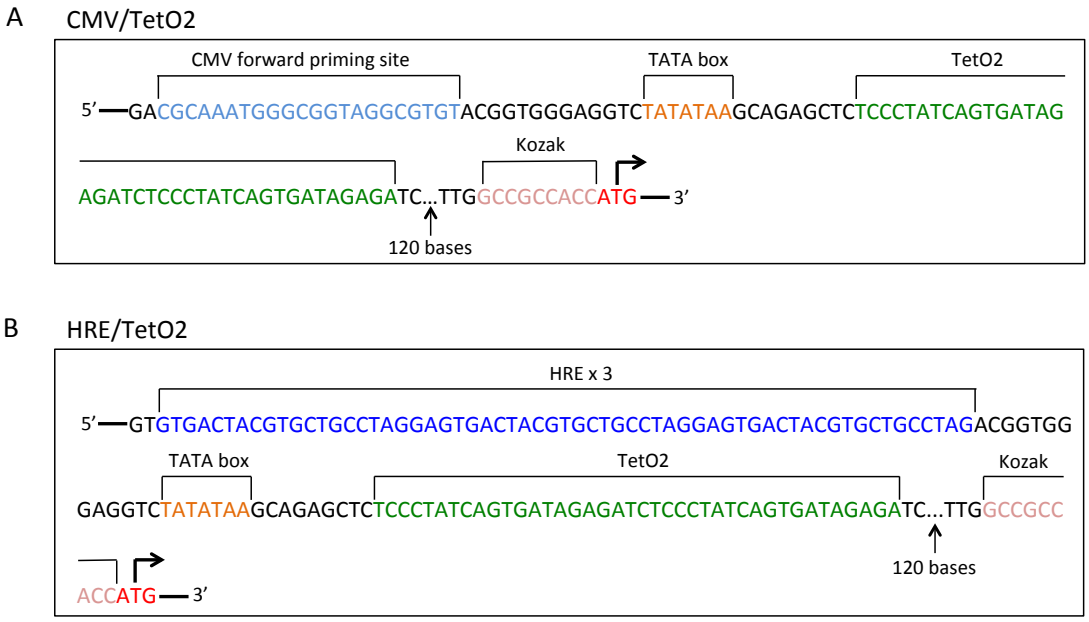

Figure 59: Illustration of the CMV/TetO2 and HRE/TetO2 hybrid promoters. In the construction of the HRE/TetO2, the CMV promoter from CMV/TetO2 was replaced with three copies of the iNOS HRE (HRE x 3). The spacing between the promoter and the TetO2, and between the TetO2 and the TSS, was maintained.

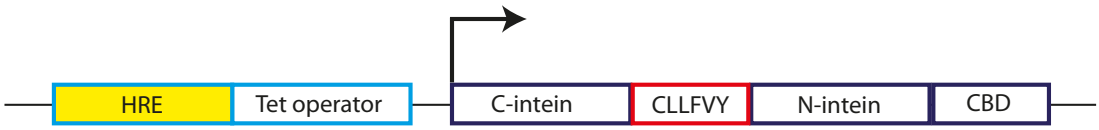

Figure 60: Illustration of the HRE gene construct encoded in the vector pcDNA5/HRE and integrated into T-REx-293 cells to make the T-REx-HRE cell line. The peptide CLLFVY is encoded between Npu inteins and tagged with a CBD for identification of construct expression. The construct is under the control of a HRE promoter and modulated by a TetO2, therefore expression only occurs in hypoxic conditions and in the presence of Dox.

2.2.2 Control of expression by the hybrid promoter

Integration and inducible expression of the Npu-CLLFVY construct was demonstrated by qRT-PCR of the intein mRNA. Following treatment of T-REx-HRE cells with 1 µg / mL for 16 h, Npu-CLLFVY mRNA expression was increased nine-fold in hypoxia, indicating integration of the construct and inducible expression by Dox and hypoxia (Figure 61). There was no significant induction of intein expression in normoxic conditions following treatment of cells with Dox. Transcription of the Npu-CLLFVY construct under hypoxia was lower in T-REx-HRE cells than in T-REx-CLLFVY cells. This may partly be due to the higher level of background expression of Npu-CFVLYL in T-REx-HRE cells masking the level of construct expression as the results are normalised to normoxic expression. In addition, the peptide inhibits HIF-1 dimerisation yet relies on HIF-1 dimerisation for its own expression. This negative feedback loop leads to lower total expression compared to the CMV promoted expression. Prevention of normoxic Npu-CLLFVY expression in the presence of Dox may avoid excessive build up of the compound or inteins.

A

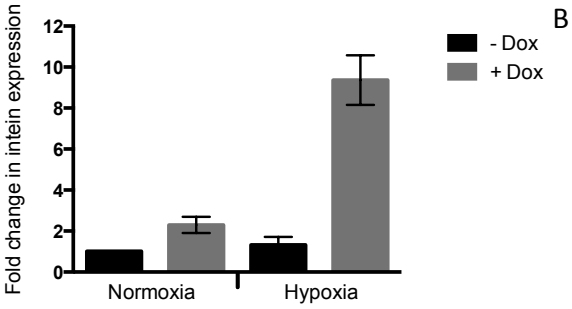

B

Treatment	Mean Tm (°C)	SD of Tm (°C)
Normoxia – Dox	85.7	0.7
Normoxia + Dox	85.5	0.9
Hypoxia – Dox	85.6	0.7
Hypoxia +Dox	85.7	0.8

Figure 61:Dox induces Npu-CLLFVY expression in hypoxia in T-REx-HRE cells. T-REx-HRE cells were treated with vehicle (-Dox) or 1 µg / mL Dox (+Dox) in normoxia or hypoxia for 24 h. (A) Construct expression analysed by qRT-PCR with primers specific for the integrated inteins. Experiments were performed in triplicate (n=3) and results were normalised to β-actin expression. Error bars show ±SEM. Melting temperatures of PCR products amplified by primers specific for the integrated inteins from RNA extracted from T-REx-HRE cells.

Expression of Npu-CLLFVY protein was then assessed by Western blotting. Following treatment of T-REx-HRE cells with 1 μg / mL Dox for 24 h in hypoxia, Npu-CLLFVY protein was detected (Figure 62). The presence of a band only at ~18 kDa indicated complete splicing of the inteins *in vivo*. There was no detectable expression of the integrated construct in normoxic conditions or under hypoxia in the absence of Dox, demonstrating that the HRE/TetO2 promoter functioned as designed.

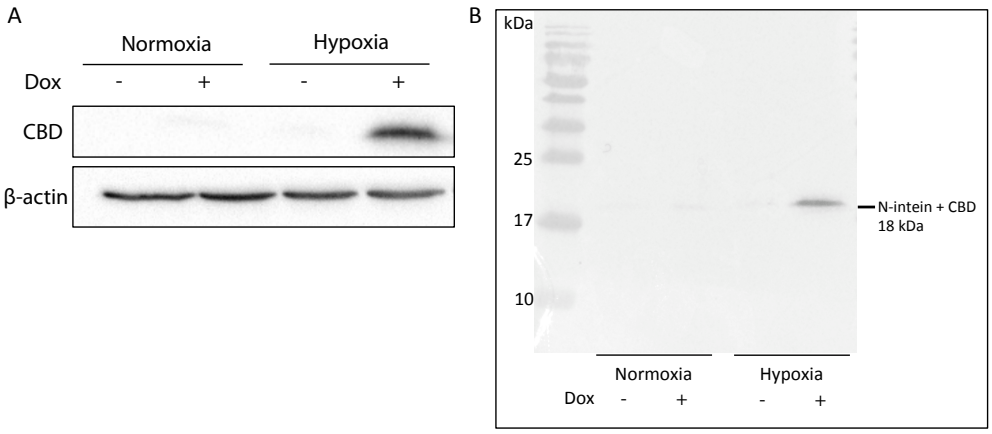

Figure 62: Western blot analysis of expression of Npu-CLLFVY in T-REx-HRE cells. (A) Anti-CBD was used to detect expression of the integrated construct in T-REx-HRE cells treated with vehicle (-) or 1 μg/ mL Dox (+) for 16 h in normoxia or hypoxia. Npu-CLLFVY expression was detected in hypoxia with Dox treatment, indicating control of expression by the HRE/TetO2 promoter. β-Actin was used as a loading control.(B) A band corresponding to the N-intein (18 kDa) was detected, indicating splicing of the Npu-CLLFVY construct in normoxia and hypoxia.

2.2.3 Comparison of CMV controlled expression and HRE controlled expression

Expression of Npu-CLLFVY protein in T-Rex-CLLFVY and T-Rex-HRE cells was then directly compared by Western blot. Densitometry was conducted on the bands visualised with the anti-CBD antibody corresponding to the inteins and normalised to the intensity of β-actin bands for each sample. Following treatment with Dox for 24 h, expression of Npu-CLLFVY in the T-REx-CLLFVY cells was nearly eight-fold greater than that in T-REx-HRE cells (Figure 63). The CMV promoter has previously been shown to induce higher levels of transgene expression than the HRE promoter.[262, 263] In addition, peptide expression in T-REx-HRE cells may be limited by the negative feedback loop of inhibition of HIF-1 dimerisation, which is necessary for peptide expression.

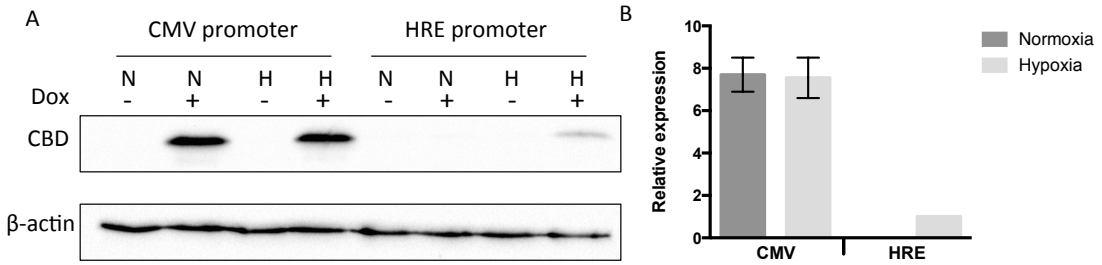

Figure 63: Comparative Western blot of Npu-CLLFVY expression in T-REx-CLLFVY and T-REx-HRE cells. Anti-CBD was used to detect integrated construct expression under the control of a CMV promoter (in T-REx-CLLFVY cells) or a HRE promoter (in T-REx-HRE cells). Cells were incubated with vehicle (-) or 1 μg / mL Dox (+) in normoxia (N) or hypoxia (H) for 16 h. (A) Representative Western blot with Anti-CBD and β-actin as a loading control (B) Densitometry of Npu-CLLFVY expression relative to β-actin expression (n=2). Data is give normalised to expression in T-REx-HRE cells under hypoxia = 1. Error bars represent ±SEM.

The expression of the construct at the mRNA and protein level in T-REx-HRE cells over time was then analysed. qRT-PCR of intein mRNA expression showed an increase in Npu-CLLFVY after 2 h exposure to hypoxia to 3.5-fold that in normoxic cells (0 h incubation in hypoxia) (Figure 64). Expression continued to increase to 8.5-fold after 8 h and nine-fold after 16 h hypoxia, compared to normoxic cells. After 24 h incubation in hypoxia, Npu-CLLFVY expression was 7 fold that in normoxic cells. Expression of the construct appeared to decrease between 16 h and 24 h incubation, but this decrease was not statistically significant.

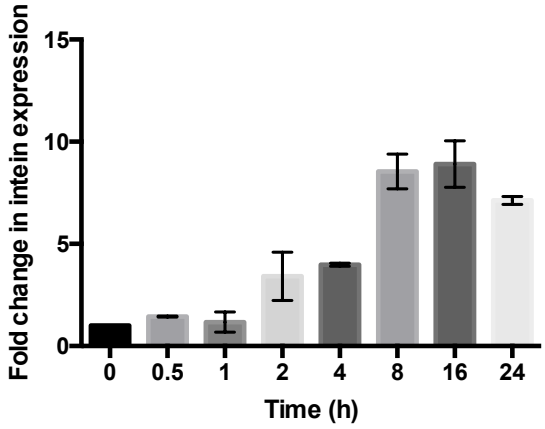

Figure 64: Dox induced Npu-CLLFVY mRNA expression increases after 2 h exposure to hypoxia. T-REx-HRE cells were treated with 1 μg / mL Dox hypoxia for 0-24 h. RNA was extracted and construct expression analysed by qRT-PCR with primers specific for the integrated inteins. Experiments were performed in triplicate (n=3) and results were normalised to β-actin expression. Error bars show ±SEM.

At the protein level, in the absence of Dox there was no detectable Npu-CLLFVY expression. Npu-CLLFVY protein was detected after 2 h treatment and increased construct expression was seen after 8 h treatment in hypoxia (Figure 65A). Expression of Npu-CLLFVY was two-

fold greater after 24 h treatment than 16 h. In T-REx-HRE cells, expression of the construct continued to increase up to 72 h (Figure 65B). In contrast, Npu-CLLFVY expression appeared to stabilise after 36 h Dox treatment in T-REx-CLLFVY cells, indicating a difference in kinetics of the CMV/TetO2 and HRE/TetO2 promoters.

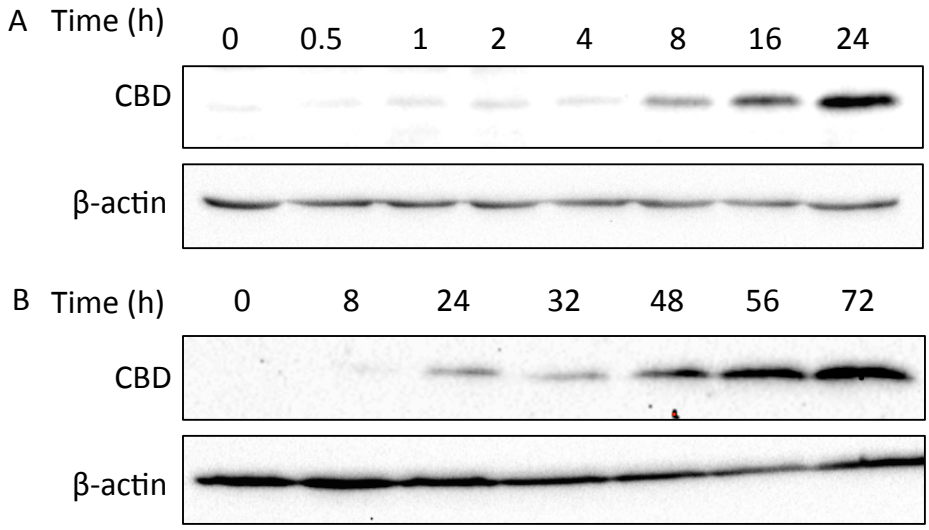

Figure 65: Npu-CLLFVY expression increases up to 72 h. Anti-CBD was used to detect Npu-CLLFVY expression in T-REx-HRE cells treated with 1 µg / mL Dox for 0-24h (A) or 0-72h (B). β-actin was used as a loading control.

A comparative Western blot was conducted to compare Npu-CLLFVY protein expression over time in T-REx-HRE cells and T-REx-CLLFVY cells (Figure 66). Although Npu-CLLFVY expression was detectable after 8 h treatment and incubation under hypoxia, it is not visualised on the comparative blot as there is higher expression of the construct in T-REx-CLLFVY cells. In addition, although expression of the integrated inteins appeared to stabilised after 36 h Dox treatment whereas it continued to increase in T-REx-HRE cells, at 72 h, there was higher expression of the construct in T-REx-CLLFVY cells than T-REx-HRE cells.

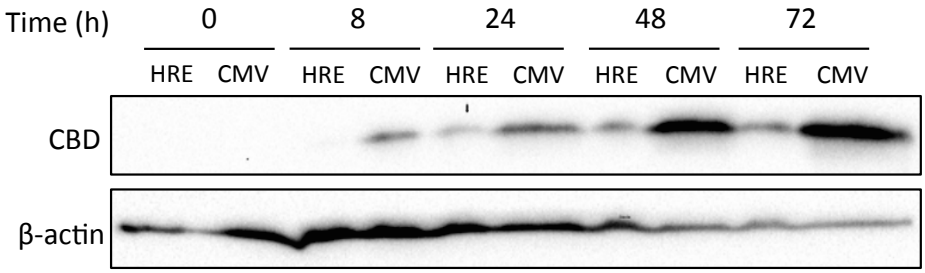

Figure 66: Comparative Western blot of expression of the integrated construct in T-REx-HRE and T-REx-CLLFVY cells. Anti-CBD was used to detect construct expression in T-REx-HRE and T-REx-CLLFVY cells (left and right respectively at each time point) treated with Dox for 0-72 h. β-actin was used as a loading control.

Abundance of HIF-1α over 24 h in T-REx-HRE cells treated with Dox was then analysed. It should be noted that HIF-1α is known to be ubiquitously expressed but regulated post-translationally such that it is degraded in normoxia.[38] Therefore, the Western blot of HIF-1α represents changes in stability rather than expression of the protein. There was a low level of HIF-1 protein in normoxia (0 h hypoxia). HIF-1α abundance increased after 1 h exposure to hypoxia, peaked at 4-8 h and then decreased. However, abundance at 16 to 48 h hypoxia remained higher than that in normoxia (Figure 67 A). When T-REx-HRE cells were treated with Dox, a peak in HIF-1α was still identified at 4-8 h hypoxic treatment. There appeared to be less HIF-1α present in Dox treated than untreated T-REx-HRE cells after 8h hypoxia. The time course of Npu-CLLFVY expression shows the cascade response of HIF-1α stabilisation in hypoxia and HIF-1-mediated expression of the construct.

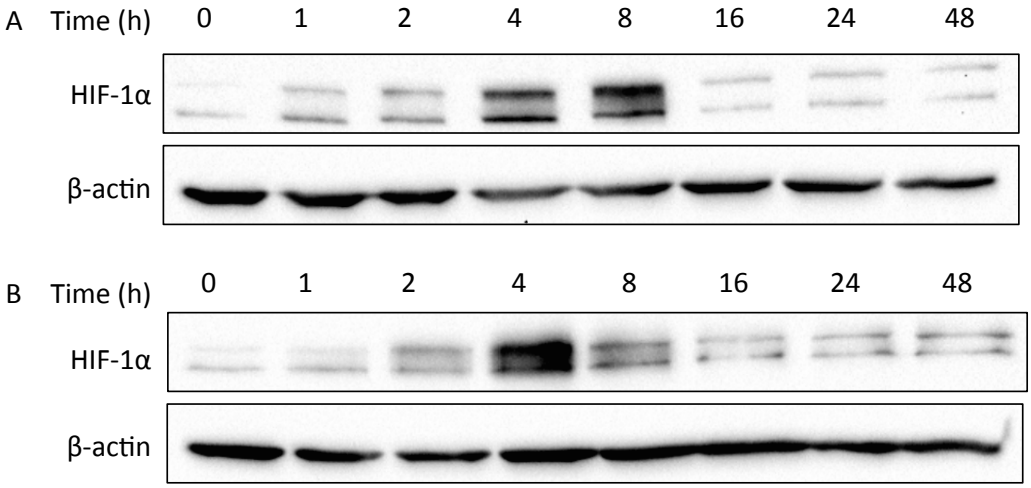

Figure 67: Western blot showing abundance of HIF-1α peaks at 4-8 h in T-REx-HRE cells. Anti-HIF-1α was used to detect HIF-1α expression in T-REx-HRE cells untreated (A) or treated with 1 μg / mL Dox (B) for 0-48 h. β-actin was used as a loading control.

2.2.4 Analysis of activity of peptide expressed in T-REx-HRE cells

2.2.4.1 Proximity ligation assay

A proximity ligation assay (PLA) was employed to directly detect inhibition of HIF-1 dimerisation by the genetically-encoded peptide (Figure 68). Dimerisation of protein subunits (in this instance, HIF-1α and HIF-1β) is detected using specific primary antibodies raised in different animal species (in this study rabbit and mouse). These are then conjugated to secondary antibody PLA probes specific for each species. The secondary antibodies are labelled with complementary oligonucleotides. When the antibodies are in close proximity, the oligonucleotides are able to ligate and can be amplified to produce a 'mini-plasmid' that binds a red fluorescent dye. HIF-1 dimerisation can therefore be visualised as red dots in cells. The Duolink In situ assay has previously been used to study inhibition of HIF-1 dimerisation by synthetic Tat-cyclo-CLLFVY in MCF-7 cells.[140]

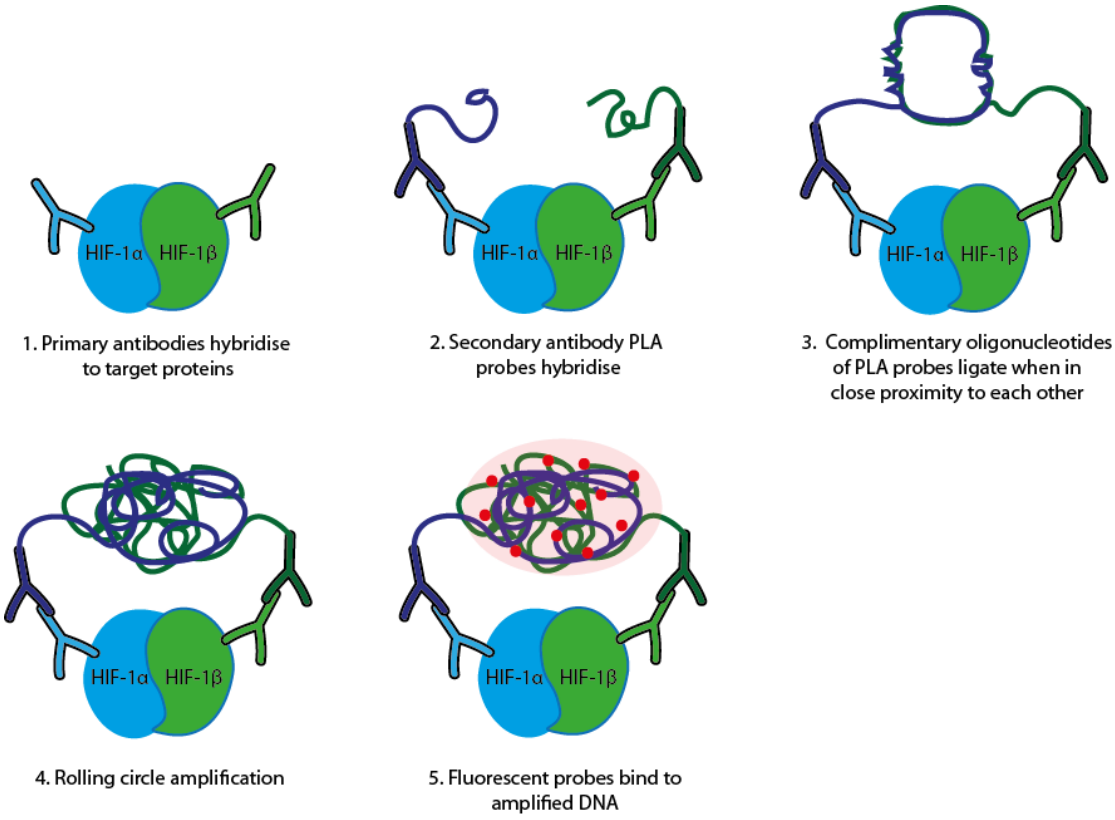

Figure 68: Illustration of the PLA used to visualise HIF-1 dimerisation in T-REx-HRE cells. When the interacting proteins are in close proximity, complementary oligonucleotides hybridised to the secondary antibodies are able to ligate and promote rolling circle amplification of the circular DNA molecule. Then, the fluorescent probes are able to bind to the amplified DNA and indicate protein dimerisation. When protein dimerisation is inhibited, oligonucleotides cannot ligate (step 3), amplification cannot proceed and no fluorescent signal is visualised.

The binding of the primary antibodies to their targets in fixed cells was evaluated using immunofluorescent labelling. Cells probed with HIF-1α antibody only gave a signal when incubated with the fluorescently labelled (Dylight 550) anti-rabbit secondary antibody (Figure 69A) and not with the anti-mouse antibody (Figure 69B). Similarly, a fluorescent signal was only detected in cells probed with HIF-1β antibody when incubated with the Dylight 488 anti-mouse secondary antibody (Figure 69F), an important specificity for the Duolink assay as identification of individual binding partner proteins relies on specific hybridisation of the secondary antibodies to their primary antibody targets. The successful immunofluorescent labelling of the proteins also suggested that the fixation and permeablisation methods were suitable for this cell line.

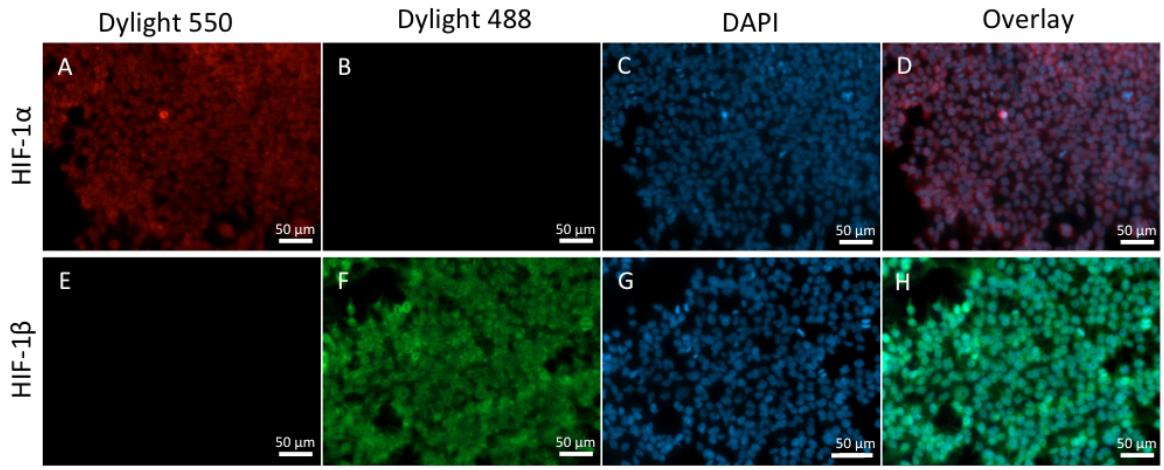

Figure 69: Secondary anti-rabbit and anti-mouse antibodies specifically detect rabbit-anti-HIF-1α and mouse-anti-HIF-1β primary antibodies respectively. T-REx–HRE cells were exposed to hypoxia for 24 h then incubated with primary and secondary antibodies. Top row demonstrates the specificity of the anti-rabbit Dylight 550 secondary antibody the HIF-1α primary antibody. Bottom row shows that the anti-mouse Dylight 488 secondary antibody only detects the HIF-1β primary antibody.

When both antibodies were incubated together in the same well, they each hybridised to their specific protein and were detectable by secondary antibodies (Figure 70A and B), suggesting that the antibodies did not interfere with each other and were suitable for the assay. Both HIF-1α and HIF-1β were visualised in cells incubated in normoxic and hypoxic conditions for 24 h. This result is in agreement with the stabilisation of HIF-1α protein in normoxia visualised by Western blot.

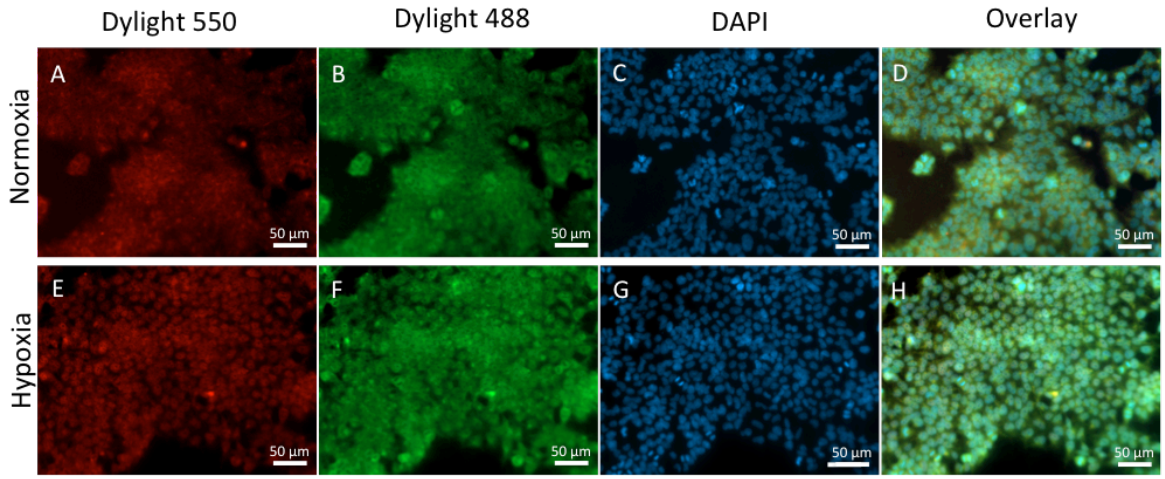

Figure 70: HIF-1α and HIF-1β expression is detected in normoxia and hypoxia in T-REx-HRE cells. T-REx–HRE cells were exposed to normoxia or hypoxia for 24 h then incubated with HIF-1α and HIF-1β primary antibodies then anti-rabbit Dylight 550 and anti-mouse Dylight 488 secondary antibodies. Micrographs indicate that HIF-1α and HIF-1β are detectable in normoxia (top row) and hypoxia (bottom row).

In the PLA, cells would be treated with Dox to induce expression of Npu-CLLFVY to assess its activity. Therefore it was necessary to verify that Dox did not impede binding of primary HIF-1α and HIF-1β antibodies to their targets, which could lead to false positive results. Incubation of cells with 1 µg / mL Dox for 24 h did not appear to affect binding of antibodies, both HIF-1α and HIF-1β were visualised following treatment (Figure 71).

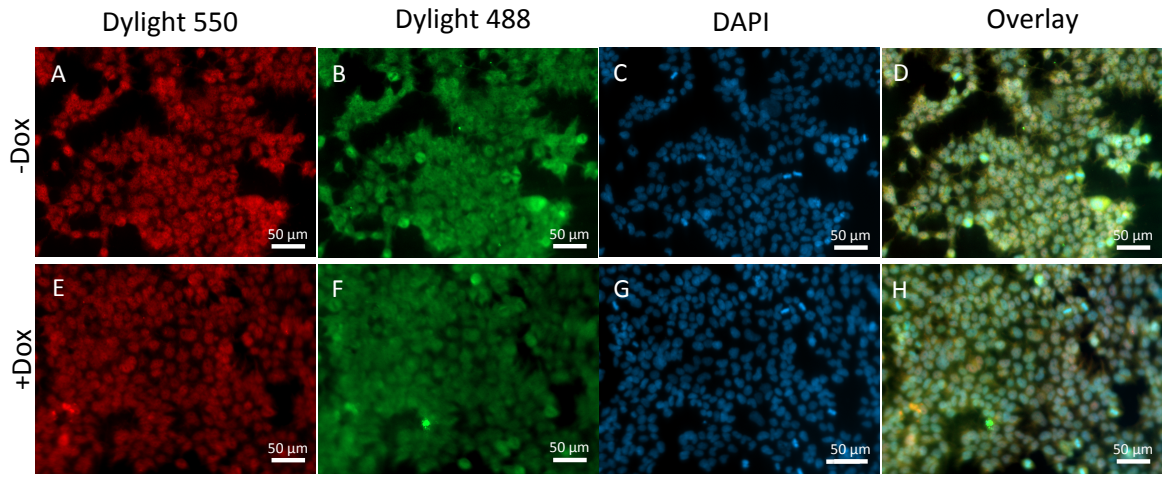

Figure 71: Dox treatment does not impede detection of HIF-1α and HIF-1β in T-REx-HRE cells. T-REx –HRE cells were treated with vehicle (-Dox) or 1 µg / mL Dox (+Dox), exposed to hypoxia for 24 h then incubated with HIF-1α and HIF-1β primary antibodies then anti-rabbit Dylight 550 and anti-mouse Dylight 488 secondary antibodies. HIF-1α and HIF-1β proteins are detected in the absence (top row) or presence (bottom row) of Dox.

HIF-1α was detected in both normoxic and hypoxic cells (Figure 70A and E), this was expected as a low level of HIF-1α protein was previously detected in normoxia (Figure 67A).

Interestingly, HIF-1α in normoxic cells appeared to be located mostly in the cytoplasm where as HIF-1α in hypoxic cells appeared to be mostly in the nucleus (Figure 72). Although HIF-1α is ubiquitously expressed, it is not stable in normoxia, it is hydroxylated by PHD enzymes and targeted for ubiquitination and degradation.[34, 264] Therefore, it does not have time to translocate to the nucleus before degradation, and is visualised in the cytosol. In hypoxia, where oxygen becomes rate limiting for PHD enzymes, HIF-1α is stabilised and is able to translocate to the nucleus.[38, 53] Addition of Dox had no visible effect on these processes. HIF-1β was visible in the nucleus and cytosol of normoxic and hypoxic cells, with and without Dox treatment (Figure 71B and F).

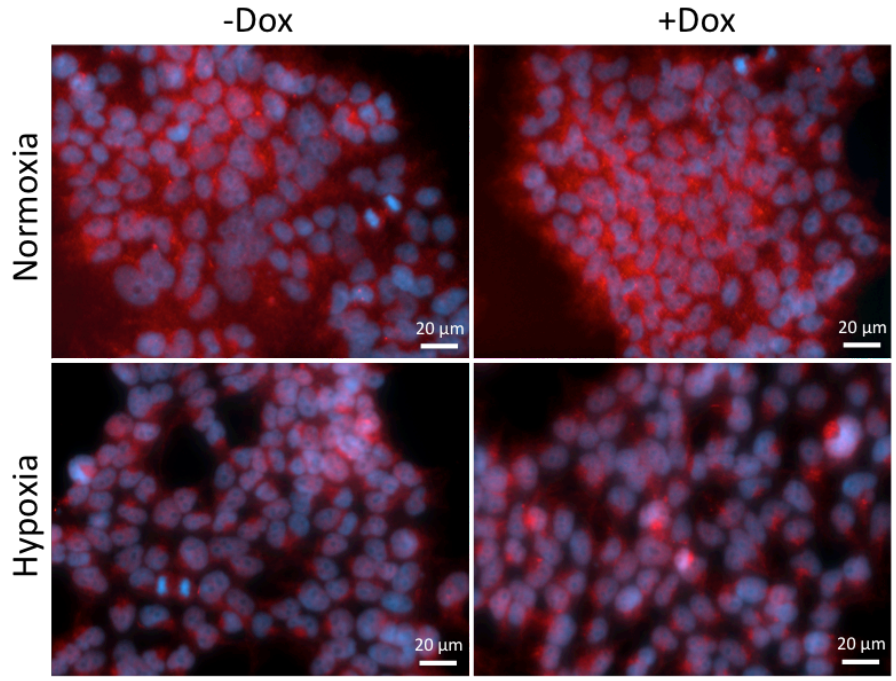

Figure 72: Sub-cellular localisation of HIF-1α changes in hypoxia in T–REx-HRE cells. T-REx-HRE cells were treated with vehicle (-Dox) or 1 µg / mL Dox (+Dox) in normoxia or hypoxia for 24 h then incubated with HIF-1α primary antibody then anti-rabbit Dylight 550 secondary antibody. Top row demonstrates cytosolic localisation of HIF-1α in normoxia. Bottom row demonstrates nuclear localisation of HIF-1α in hypoxia, indicative of HIF-1α stabilisation.

Having shown the suitability of the primary antibodies, they were then used in the PLA in T-REx-HRE cells. On each slide, a negative control that was untreated and a technical control that was incubated with anti-HIF-1β antibody only, were included (Figure 73). There was no PLA signal in negative control cells, indicating that in the absence of primary antibodies, secondary antibody-PLA probes were unable to bind to proteins and probe oligonucleotides were unable to ligate. In addition, there was no PLA signal in cells incubated with anti-HIF-1β only, demonstrating that PLA signal only results from binding of both sets of primary and secondary antibodies and that secondary antibodies could not ligate when not each bound to

a dimerisation partner. When cells were visualised by fluorescence microscopy, the negative control sample was used to adjust exposure and brightness settings so as to remove any background fluorescence, the other samples were then imaged with the same settings.

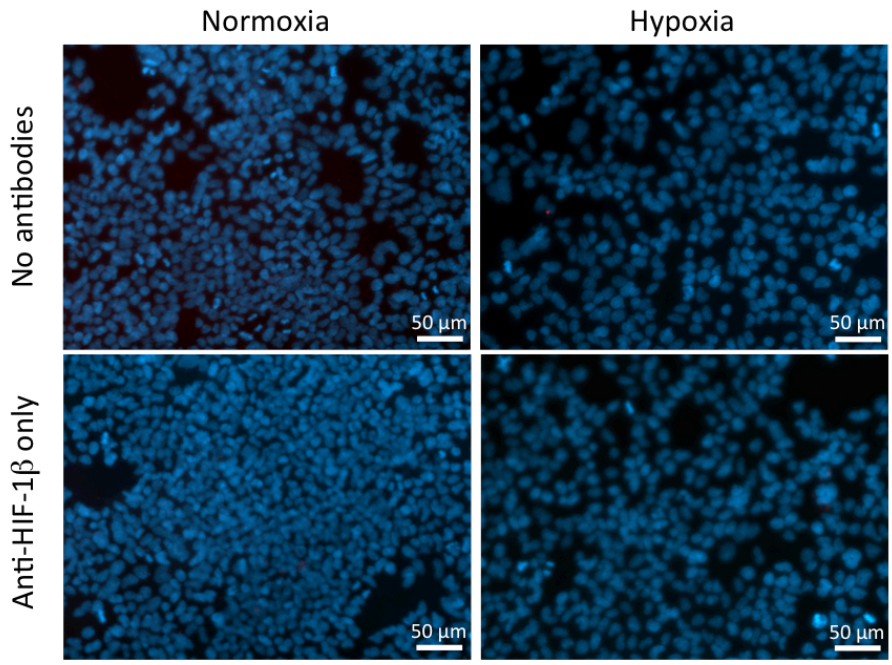

Figure 73: PLA reagents specifically detect HIF-1α / HIF-1β dimerisation. Top row demonstrates that no PLA signal is detected when both primary antibodies (anti-HIF-1α and anti-HIF-1β) are excluded from the assay, providing a negative control. Bottom row demonstrates that no PLA signal is detected when only one primary antibody (anti-HIF-1α) is excluded from the assay, providing a technical control.

In normoxia, where HIF-1α is quickly degraded and is not able to dimerise with HIF-1β, there was no visible PLA signal (Figure 74). However in hypoxia, HIF-1α was stabilised and was able to dimerise to HIF-1β forming the PLA complex and a visible signal in cells. Treatment of cells with Dox diminished the PLA signal in hypoxic cells, suggesting inhibition of the HIF-1α/HIF-1β interaction by cyclo-CLLFVY. It should be noted that a low level of red signal was visible in Dox treated cells, suggesting incomplete inhibition of HIF-1 dimerisation by cyclo-CLLFVY expression. There was no PLA signal in cells probed with anti-HIF-1β only (Figure 73).

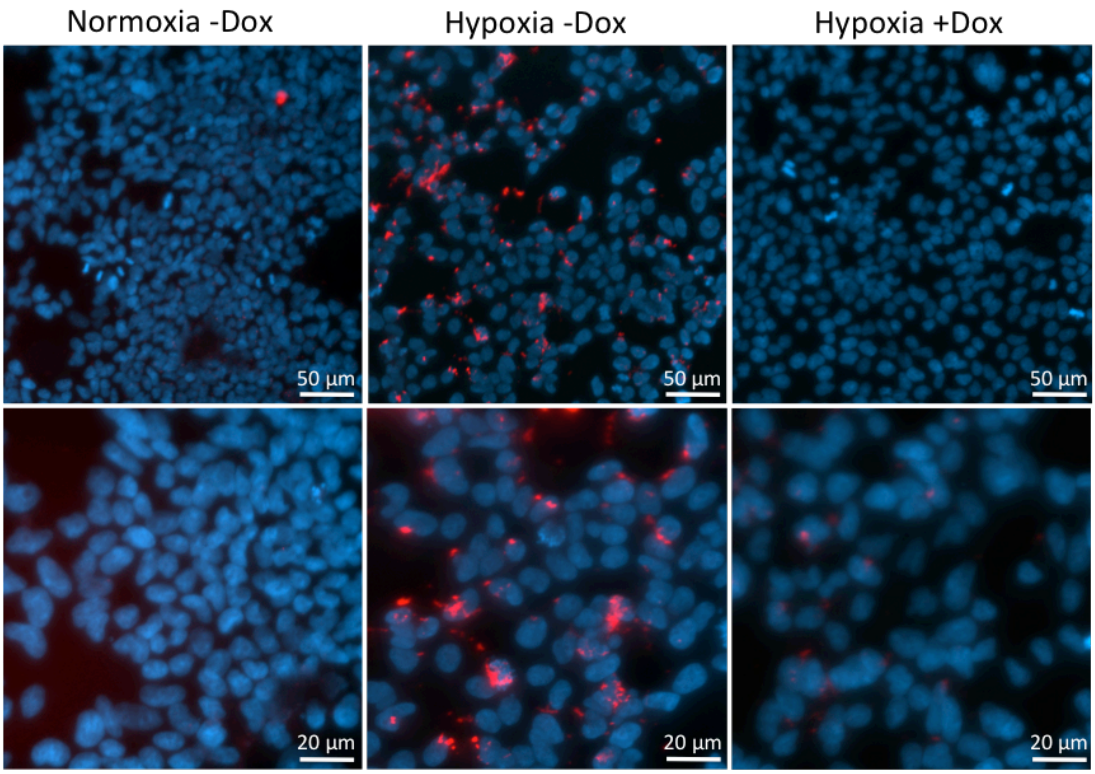

Figure 74: Fluorescence micrographs of HIF-1 dimerisation visualised in T-REx-HRE cells using a PLA assay. T-REx-HRE cells were treated with vehicle (-Dox) or Dox (+Dox) and incubated in normoxia or hypoxia for 24 h. Cells were fixed, permeablised and incubated with primary antibodies. Cells were then incubated with Duolink reagents and visualised by fluorescence microscopy.

2.2.4.2 HRE dependent luciferase assay

The HRE dependent luciferase assay described in section 2.1.5.1 was used to assess the activity of the expressed peptide in T-REx-HRE cells. T-REx-HRE cells were transfected with HRE-Luc or SV40-Luc and treated with Dox under normoxia or hypoxia. Hypoxia induced approximately an eight-fold increase in HRE controlled luciferase expression compared to normoxia. However, this hypoxic induction of luciferase expression was not significantly impacted by Dox treatment of T-REx-HRE cells (Figure 75). Dox treatment had no impact on SV40 controlled luciferase expression.

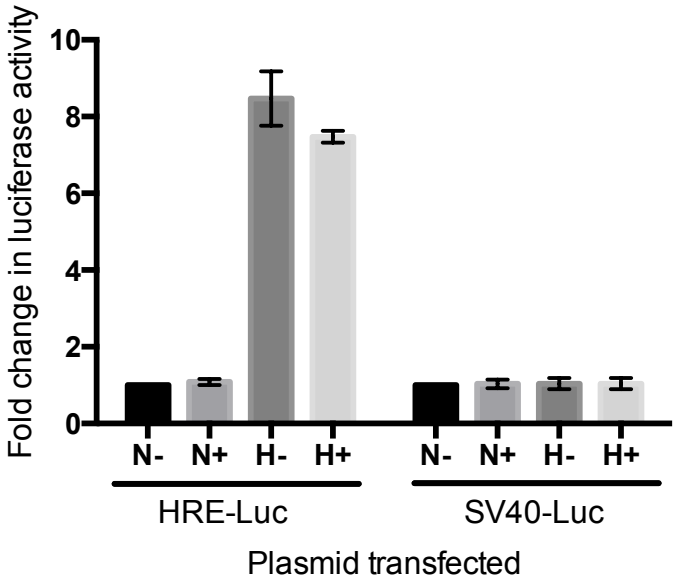

Figure 75: Effect of expression of cyclo-CLLFVY on luciferase expression in T-REx-HRE cells. T-REx-HRE cells were transfected with HRE-Luc or SV40-Luc. Cells were incubated with vehicle (-) or 1 μg / mL Dox (+) for 16 h in normoxia (N) or Hypoxia (H). Experiments were performed in triplicate (n=3). Error bars represent ±SEM.

In contrast to the luciferase assay, the PLA suggested inhibition of HIF-1 dimerisation by peptide expression in T-REx-HRE cells. Peptide expression reduced HRE controlled luciferase expression 1.9-fold in T-REx-CLLFVY cells (Figure 50). This could suggest that the smaller amount of peptide expression in T-REx-HRE cells is insufficient to inhibit HIF-1 dimerisation, but this disagrees with the result of the PLA. Alternatively, the lack of inhibition of luciferase expression could be a result of the promoter controlling peptide expression. In the assay, luciferase expression is under the control of a HRE promoter and so there is low expression in normoxia and increased expression in hypoxia when HIF-1α is stabilised. In T-REx-CLLFVY cells, peptide expression is ubiquitous, so the peptide is expressed and present before the cells are exposed to hypoxia and before hypoxic luciferase expression in induced. Therefore, the peptide can inhibit HIF-1 dimerisation and luciferase induction in hypoxia.

However, in T-REx-HRE cells, peptide expression also relies on HIF-1 and so is not expressed until cells are exposed to hypoxia. In fact, peptide expression is only increased after 8 h exposure to hypoxia (Figure 65A). Therefore luciferase can be expressed before the peptide, and build up, masking any later effect of the peptide on HIF-1 activity. Furthermore, it has been shown that HIF-1 preferentially binds to gene loci with permissive chromatin structure,[84] and so luciferase (as plasmid DNA) may be preferentially expressed over the peptide (on the chromosome). It would be interesting conduct a time course of HRE controlled luciferase expression from transiently transfected HRE-Luc and compare this to timing of peptide expression.

2.2.4.3 qRT-PCR analysis of HIF-1 target genes

To clarify whether lower peptide expression in T-REx-HRE cells than T-REx-CLLFVY cells would result in less inhibition of HIF-1, the expression of the HIF-1 target genes VEGF and CAIX was analysed. Incubation of T-REx-HRE cells under hypoxia resulted in a three-fold increase in VEGF expression and a ~100-fold increase in CAIX expression compared to normoxia. Treatment with 1 µg / mL Dox for 16 h resulted in a 1.3-fold decrease in VEGF and CAIX expression compared to untreated cells (Figure 76). This was similar to T-REx-CLLFVY cells, where Dox treatment resulted in a 1.4-fold decrease in VEGF and 1.5-fold decrease in CAIX, despite the lower amount of Npu-CLLFVY expression.

Detection of Npu-CLLFVY protein expression had shown a band corresponding to the size of the spliced product and no band for the unspliced construct, suggesting that all of the expressed construct successfully splices *in vivo* (Figure 62). Therefore, despite lower expression levels seen, equivalent inhibition activity is not likely a result of limitation of peptide quantity by the amount of intein splicing. This suggests that the dosage of peptide at 16 h in both cell lines is in excess and produces the maximum dampening of VEGF expression by inhibition of HIF-1 dimerisation.

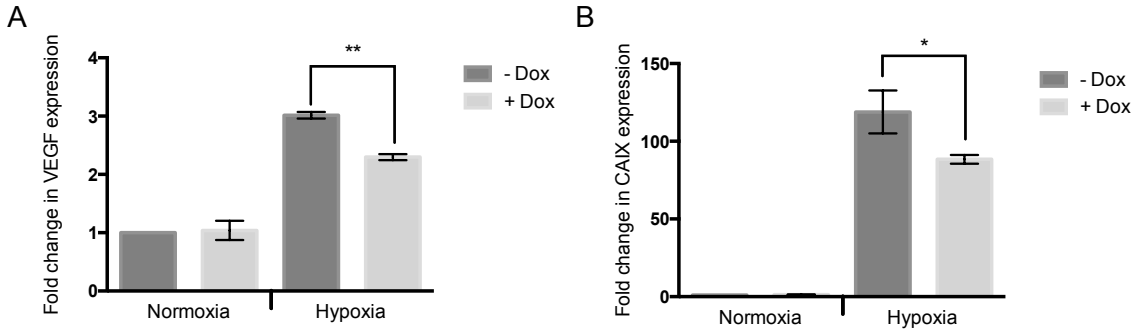

Figure 76: Expression of cyclo-CLLFVY supresses HIF-1 target gene expression in T-REx-HRE cells. T-REx-HRE cells were incubated with vehicle (-) or 1 µg / mL Dox (+) in normoxia or hypoxia for 16 h. VEGF (A) and CAIX (B) expression was analysed by qRT-PCR. qRT-PCR experiments were performed in triplicate (n=3) and results were normalised to expression of 18S and β-actin. Error bars represent ±SEM. Stars denote significant differences between means: *$p \leq 0.05$, **$p \leq 0.01$.

Western blotting had shown that there was a greater amount of peptide expression after 24 h Dox treatment. If peptide dosage is in excess, this greater quantity of peptide expressed should not have any greater effect on the expression of HIF-1 targets. Following 24 h Dox treatment, VEGF and CAIX expression in hypoxia were reduced 1.7 and two-fold respectively (Figure 77), a greater decrease than that after 16 h treatment. This suggests that increased inhibition may be a result of the expression of HIF-1α over time compared to the expression of the peptide and HIF-1 target genes and not to increased dose of the peptide.

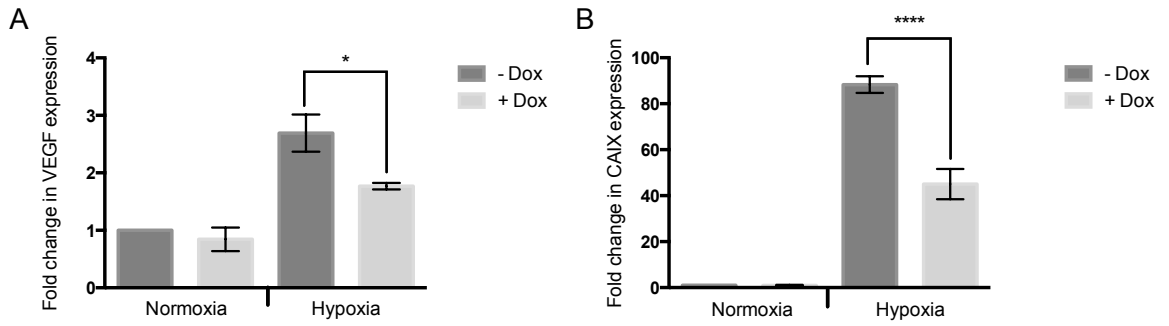

Figure 77: Expression of cyclo-CLLFVY supresses expression of HIF-1 targets by a greater degree after 24 h than 16 h in T-REx-HRE cells under hypoxia. T-REx-HRE cells were incubated with vehicle (-) or Dox (+) for 24, (A) VEGF and (B) CAIX expression was analysed by qRT-PCR. qRT-PCR experiments were performed in triplicate (n=4) and results were normalised to expression of 18S and β-actin. Error bars represent ±SEM. Stars denote significant differences between means: *$p \leq 0.05$, ****$p \leq 0.0001$.

To further investigate the relationship between length of hypoxic exposure, the expression of HIF-1 target genes and cyclo-CLLFVY activity in T-REx-HRE cells, transcription of VEGF and CAIX at 4 and 8 h was assessed (Figure 78). Incubation of T-REx-HRE cells in hypoxia for 4 h or 8 h resulted in a 1.7-fold and 1.3-fold increase in VEGF expression, respectively. Dox treatment made no significant change to VEGF expression at these incubation periods. Npu-CLLFVY protein expression increased after 8 h Dox treatment, so no inhibitory effect of the peptide would be expected before this time. After 16 h in hypoxia, when peptide expression had increased, and following the peak in HIF-1α stabilisation, VEGF expression was upregulated compared to normoxic expression (three-fold) and Dox treatment inhibited VEGF expression. Inhibition of VEGF expression by cyclo-CLLFVY increased at 24 h, as discussed above.

This trend was also seen for induction of CAIX expression by hypoxia, and its inhibition by cyclo-CLLFVY. After 4 h hypoxic exposure, CAIX expression was induced five-fold compared to normoxia, and Dox treatment had no effect on hypoxic induction. Similarly, at 8 h, CAIX expression was nine-fold higher than normoxic expression and expression of the peptide had no significant impact. However, after 16 h exposure to hypoxia, CAIX expression was increased to 118-fold, and Dox treatment resulted in a 1.3-fold decrease. Although hypoxia-induced CAIX expression is lower at 24 h than 16 h (88-fold compared to 118-fold), Dox treatment of cells had a bigger impact on CAIX expression. Referring back to the Western blot of construct expression over time, construct expression increased at 8 h then continued to increase over time, therefore the peptide was available to inhibit CAIX expression from 8 h forward (Figure 65A). Therefore at 24 h, although CAIX expression was lower in -Dox cells, its expression at 8 h forward (including 16 h) could be inhibited, leading to a cumulative inhibitory effect.

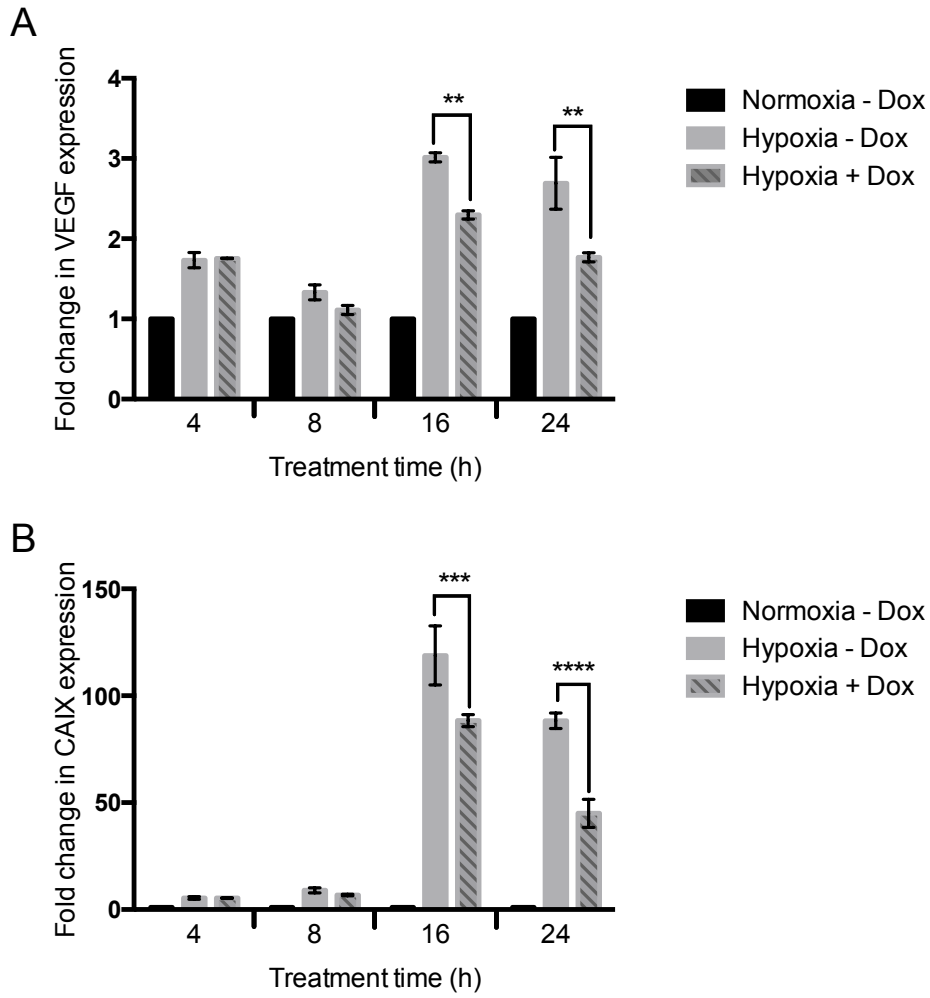

Figure 78: Expression of, and suppression by cyclo-CLLFVY, of HIF-1 target genes increases over time. T-REx-HRE cells were incubated in normoxia or in hypoxia, with vehicle (-Dox) or 1 μg / mL Dox (+ Dox) for 4, 8, 16 or 24 h, (A) VEGF and (B) CAIX expression was analysed by qRT-PCR. qRT-PCR experiments were performed in triplicate (n=3 for 4, 8, 16 h; n=4 for 24 h) and results were normalised to expression of 18S and β-actin. Error bars represent ±SEM. Stars denote significant differences between means: **$p \leq 0.01$, ***$p \leq 0.001$, ****$p \leq 0.0001$.

2.2.5 Role of HIF-2α in construct expression

Analysis of HIF-1α protein in T-REx-HRE cells over time had showed a peak in HIF-1α abundance at 4-8 h hypoxia, which was followed by an increase in Npu-CLLFVY construct expression at 8-16 h hypoxic exposure. HIF-2α is an isoform of HIF-1α and can dimerise with HIF-1β to form the HIF-2 transcription factor.[9] HIF-1 and HIF-2 have been shown to have many overlapping target genes.[32, 91] As construct expression results in the expression of the HIF-1 dimerisation inhibitor, it is interesting to know whether construct expression is mainly driven by HIF-1 or HIF-2 to assess the extent of any feedback loops. HIF-2 binds to DNA at the same consensus HRE as HIF-1[6] and specifically, the expression of genes under the control of the HRE from the nitric synthase promoter, used in the expression Npu-CLLFVY construct,

have been shown to be induced by HIF-2,[59, 140] suggesting that HIF-2 could also drive the expression of Npu-CLLFVY in T-REx-HRE cells. In renal cells, HIF-1α and HIF-2α expression was found to be similar after exposure to hypoxia for 12-24 h.[78]

Knockdown of HIF-2α expression was used to assess the role of HIF-2α in driving the upregulation of genes promoted by a HRE in hypoxia. T-REx-HRE cells were transiently transfected with HIF-2α siRNA then pre-treated cells were then exposed to hypoxia for 24 h with and without Dox treatment. Following HIF-2α siRNA treatment, HIF-2α expression was depleted regardless of treatment with Dox (Figure 79). Also, Dox treatment of cells in the absence of HIF-2α siRNA had no significant effect on HIF-2α mRNA expression.

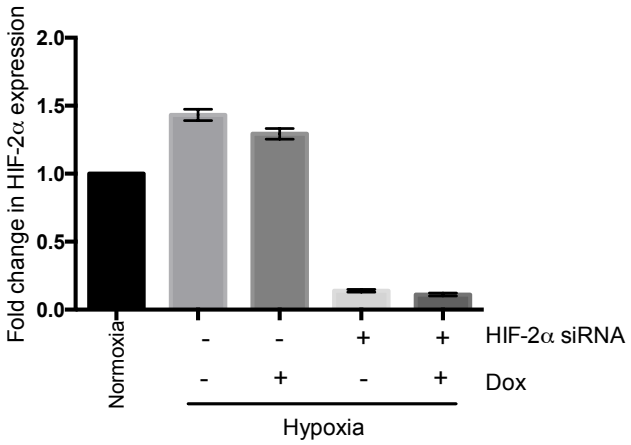

Figure 79: Transfection of HIF-2α siRNA prevents HIF-2α mRNA expression in hypoxia. T-REx-HRE cells were transfected with negative control siRNA (-) or HIF-2α siRNA (+) for 24 h then exposed to hypoxia for 24 h with vehicle (-) or 1 μg / mL Dox (+). qRT-PCR experiments were performed in triplicate (n=3). Data was normalised to expression of 18S and β-actin. Error bars represent ±SEM.

HIF-1α and HIF-2α are closely related isoforms and share 83% sequence similarity.[9] Therefore it was a concern that the siRNA targeting HIF-2α may also affect HIF-1α expression. qRT-PCR analysis of HIF-1α mRNA expression in cells treated with HIF-2α siRNA was conducted. Treatment of T-REx-HRE cells with HIF-2α siRNA did not significantly change the expression of HIF-1α mRNA, verifying the specificity of the siRNA (Figure 80A). In addition, Western blot analysis of protein extracted from T-REx-HRE cells treated with HIF-2α siRNA showed no difference in HIF-1α protein levels compared with untreated cells (Figure 80B). Treatment of cells with Dox made no change to HIF-1α mRNA or protein levels in the presence or absence of HIF-2α siRNA.

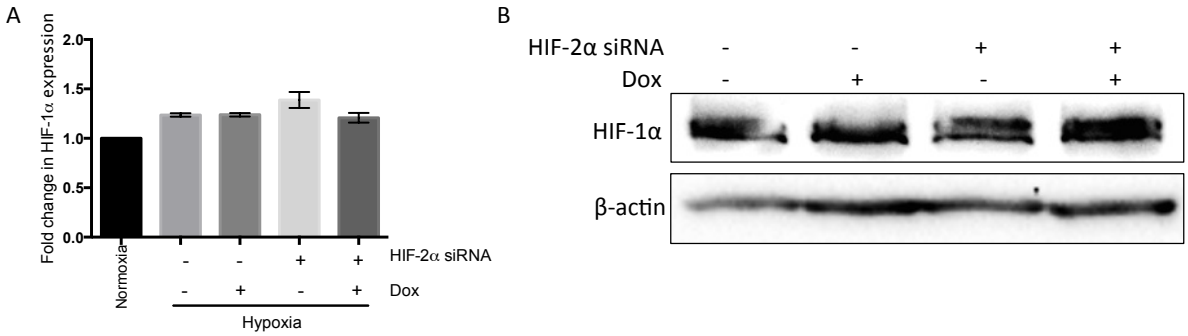

Figure 80: HIF-2α siRNA is specific for HIF-2α over HIF-1α. T-REx-HRE cells were transfected with negative control siRNA (-) or HIF-2α siRNA for 24 h then exposed to hypoxia for 24 h with vehicle (-) or 1 μg / mL Dox (+). (A) qRT-PCR experiments were performed in triplicate (n=2). Data was normalised to expression of 18S and β-actin. Error bars represent ±SEM. (B) Western blot analysis of HIF-1α levels. Anti-HIF-1α was used to detect HIF-1α protein. β-actin was used as a loading control.

A luciferase reporter assay was used to assess the effect of HIF-2α siRNA on induction of genes from the HRE promoter. Cells were co-transfected with HRE-Luc and HIF-2α siRNA. Luciferase expression in the plasmid HRE-Luc is under the control of the same HRE in the HRE/TetO2 promoter in T-REx-HRE cells, therefore analysis of the effect of HIF-2α siRNA on luciferase expression will give an indication of the role of HIF-2α in transactivation at this promoter. As the plasmid and HIF-2α siRNA were co-transfected, the transfection efficiency of HIF-2α siRNA could be affected, preventing knockdown of HIF-2α siRNA. Therefore, as a control, expression of HIF-2α and HIF-1α mRNA in cells co-transfected with HIF-2α siRNA and HRE-Luc was assessed by qRT-PCR. Co-transfection of the reporter plasmid with the siRNA did not prevent HIF-2α knockdown and did not significantly affect HIF-1α expression (Figure 81).

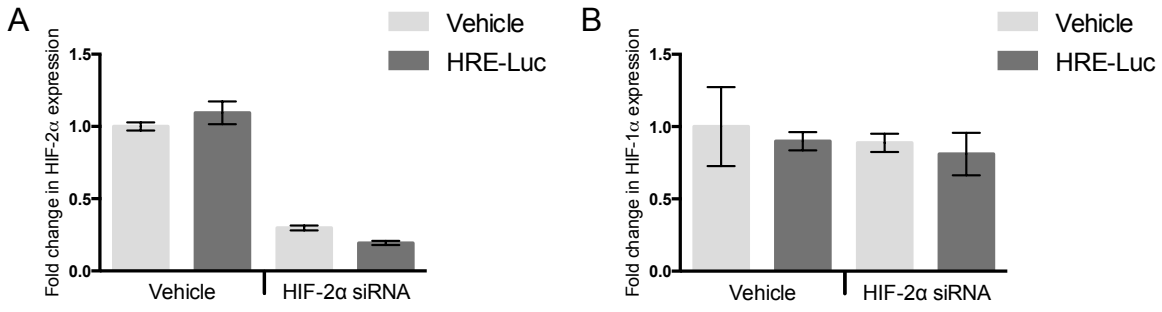

Figure 81: Co-transfection of HRE-Luc with HIF-2α siRNA does not prevent HIF-2α knockdown. T-REx-HRE cells were co-transfected with vehicle or HRE-Luc and vehicle or HIF-2α siRNA for 24 h. RNA was extracted from treated cells and expression of HIF-2α (A) and HIF-1α (B) was analysed by qRT-PCR. qRT-PCR experiments were conducted in triplicate (n=1), data was normalised to expression of 18S and β-actin. Bars show means of triplicate wells ±error according to upper and lower limits of fold change in expression between triplicate wells.

Having confirmed the experimental format did not prevent siRNA-mediated knockdown of HIF-2α, following co-transfection of HRE-Luc and HIF-2α siRNA for 24 h, T-REx-HRE cells were incubated under normoxia or hypoxia for 24 h. Levels of luciferase expression were then assessed by measuring luciferase activity. In normoxia, there was low expression of luciferase, as expected, as a HRE promoter drives luciferase expression. Incubation of cells in hypoxic conditions resulted in a ~18 fold increase in luciferase expression, which was not significantly impacted by knockdown of HIF-2α(Figure 82). This suggests that in the absence of HIF-2α, expression of genes under the control of the HRE promoter is maintained by the HIF-1 transcription factor in T-REx-HRE cells.

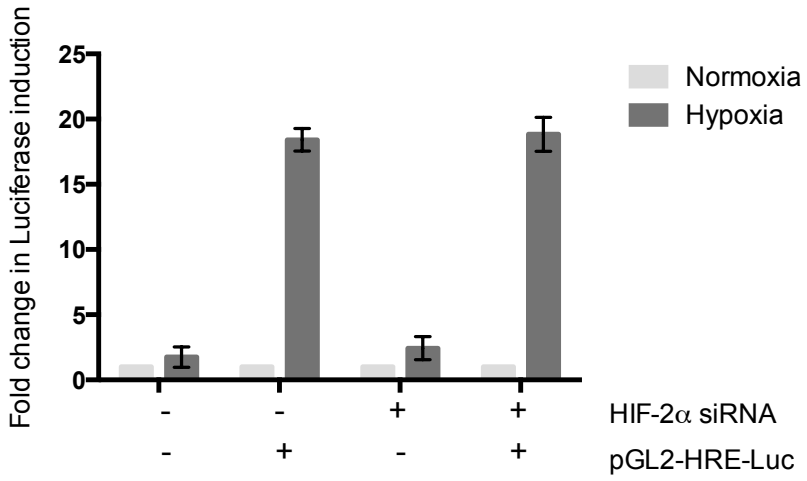

Figure 82: HIF-2α siRNA does not impact expression of HRE controlled luciferase expression. T-REx-HRE cells were co-transfected with HRE-Luc and HIF-2α siRNA for 24 h. Transfected cells were then incubated in normoxia or hypoxia for 24 h. Cells were then incubated with luciferase assay substrate and luminescence recorded. Results are shown as fold change in expression relative to normoxia. Bars show mean (n=2) ± SEM.

The effect of HIF-2α siRNA treatment on expression of Npu-CLLFVY in T-REx-HRE cells was assessed by Western blot of the inteins. Expression of Npu-CLLFVY in T-REx-HRE cells is under the same HRE promoter as luciferase in HRE-Luc, but combined with the TetO2, and integrated onto the chromosome rather than expressed off of a plasmid. Following incubation in hypoxia for 24 h, treatment of cells with HIF-2α siRNA did not change Dox-induced Npu-CLLFVY expression (Figure 83), further supporting that HIF-1 controls expression of genes under the HRE promoter in the absence of HIF-2α. Dox treatment of T-REx-HRE cells results in the production of the HIF-1 dimerisation inhibitor cyclo-CLLFVY, which was shown to inhibition HIF-1-mediated transactivation of genes (section 2.2.4). However, following treatment with Dox and HIF-2α siRNA, expression of cyclo-CLLFVY in T-REx-HRE cells, under the control of the HRE/TetO2 promoter was not inhibited. This supports earlier conclusions that the inteins are stable and accumulate over time.

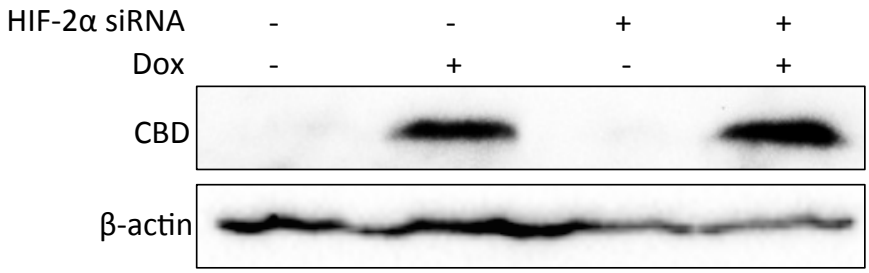

Figure 83: Treatment of T-REx-HRE cells with HIF-2α siRNA results in an increase in Npu-CLLFVY expression. T-REx-HRE cells were treated with HIF-2α siRNA (+) or negative control siRNA (-) for 24 h. Pre-treated cells were then treated with vehicle (-) or 1 μg / mL Dox (+) and exposed to hypoxia for 24 h. Expression of Npu-CLLFVY was detected by Western immunoblotting using Anti-CBD antibody. β-actin was used as a loading control.

2.2.6 Role of HIF-2α in hypoxic gene expression in T-REx-HRE cells

The effect of HIF-2α knockdown on the expression of HIF target genes VEGF and CAIX was analysed to assess the role of HIF-2α siRNA in the expression of native genes in T-REx-HRE cells. Despite the PLA assay suggesting almost complete inhibition of HIF-1 dimerisation in Dox treated cells after 24 h incubation under hypoxia, the expression of HIF-1 target genes VEGF and CAIX was still significantly higher than normoxic expression. HIF-2 may also activate the expression of VEGF and CAIX in T-REx-HRE cells, preventing complete inhibition of their expression and therefore HIF-2α siRNA would be expected to decrease their expression in this scenario.

T-REx-HRE cells were treated with HIF-2α siRNA and 1 μg / mL Dox for 24 h, then VEGF expression was analysed by qRT-PCR. Knockdown of HIF-2α expression in T-REx-HRE cells inhibited VEGF expression 1.5-fold, a similar level of inhibition by peptide expression (Figure 84A). Previous work with synthetic cyclo-CLLFVY showed the compound to be specific to HIF-1α over HIF-2α. Also, this study (section 2.4) showed that the compound had no effect in HIF-2α positive but HIF-1α deficient 786-O cells. Therefore, inhibition of VEGF by HIF-2α knockdown suggests that VEGF is a target of the HIF-1 and HIF-2 transcription factors in T-REx cells, which is in agreement with reports in various other cell lines and mouse studies.[6, 9, 16]

The combination of HIF-2α knockdown and Dox treatment had a cumulative effect on VEGF expression, resulting in a 2.4-fold decrease, which was significantly higher than Dox treatment alone (1.7-fold). The combination of treatments reduced VEGF expression to normoxic levels. This supports that HIF-2 has a role in the activation of VEGF expression in hypoxia because disrupting both HIF-1 and HIF-2 transactivation pathways had a larger effect.

Analysis of mRNA MCF-7 and U2OS cells treated with synthetic Tat-cyclo-CLLFVY suggested that 50 μM of the compound was sufficient to reduce hypoxia-induced VEGF expression to below that in normoxic conditions, but 25 μM was not, suggesting that the dosing of expressed peptide is equivalent to between 25-50 μM synthetic peptide.[140] However, the extent of the effect of the peptide is likely to be different in T-REx cells, as it was different in MCF-7 and U2OS cells.[140]

In contrast to VEGF, HIF-2α knockdown did not significantly impact CAIX expression (Figure 84B), suggesting that expression of CAIX is mediated by only HIF-1 in T-REx cells. This is supported by earlier results that expression of CAIX was more impacted by inhibition of HIF-1 dimerisation than VEGF (two-fold compared to 1.7-fold respectively). Previous studies have shown that CAIX is specifically regulated by HIF-1 in renal cell carcinoma cells.[97, 265] In addition, CAIX was not expressed in HIF-1α deficient 786-O cells (section 2.4) or in Ka13 cells where co-transfection of HIF-1α, but not HIF-2α, restored CAIX expression.[265] This selectivity has been shown to be a result of differential recruitment of cofactors to transactivation domains in the C-terminal regions of HIF-1α and HIF-2α, not to DNA binding, as both HIF-1 and HIF-2 bind to the CAIX HRE.[26, 27, 266]

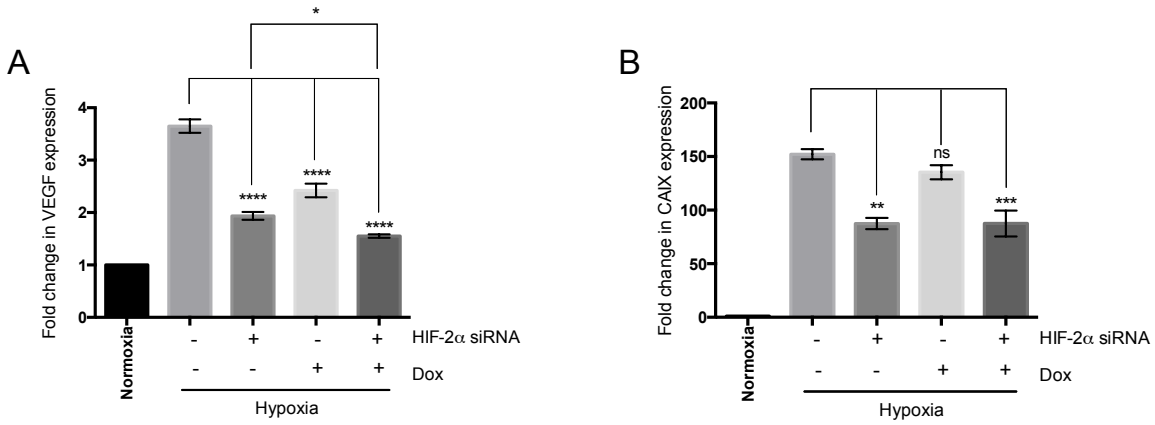

Figure 84: Knockdown of HIF-2α expression inhibits expression of VEGF. T-REx-HRE cells were transfected with negative control siRNA (-) or HIF2α siRNA (+) for 24 h then exposed to hypoxia for 24 h with vehicle (-) or 1 μg / mL Dox (+). RNA was extracted and VEGF (A) and CAIX (B) expression was analysed by qRT-PCR. Experiments were performed in triplicate (n=3). Error bars represent ±SEM. Stars denote significant differences between means: **p ≤ 0.01, ***p ≤ 0.001, ****p ≤ 0.0001.

Earlier results had shown that expression of cyclo-CLLFVY in T-REx cells had a similar effect on VEGF expression whether promoted by a CMV or HRE promoter (section 2.1.5.2). To assess if HIF-2α siRNA also had a similar effect in T-REx-CLLFVY cells as in T-REx-HRE cells, qRT-PCR analysis of VEGF expression in T-REx-CLLFVY cells treated with HIF-2α siRNA and Dox was conducted. Knockdown of HIF-2α expression in T-REx-CLLFVY cells by HIF-2α siRNA was demonstrated by qRT-PCR of HIF-2α (Figure 85A). Knockdown of HIF-2α in T-

REx-CLLFVY cells resulted in a 1.2-fold decrease in VEGF expression, and the combination of HIF-2α knockdown and Dox treatment further reduced VEGF expression to 1.8 fold that in untreated cells. This was a smaller impact than that seen in T-REx-HRE cells.

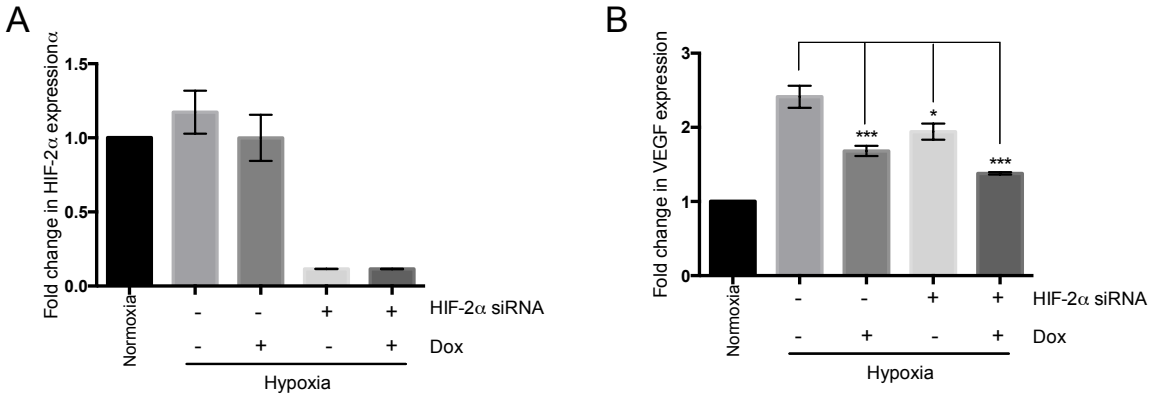

Figure 85: Knockdown of HIF-2α expression inhibits expression of VEGF in T-REx-CLLFVY cells. T-REx-CLLFVY cells were transfected with negative control siRNA (-) or HIF-2α siRNA (+) for 24 h then exposed to hypoxia for 24 h with vehicle (-) or 1 μg / mL Dox (+). RNA was extracted and HIF-2α (A) and VEGF (B) expression was analysed by qRT-PCR. Experiments were performed in triplicate (n=3). Error bars represent ±SEM. Stars denote significant differences between means: *p ≤ 0.05, ***p ≤ 0.001.

2.2.7 Control of the transcriptional response to hypoxia by HIFs in T-REx–HRE cells

2.2.7.1 Effect of cyclo-CLLFVY expression on hypoxic gene induction

To gain an overall view of the effect of inhibition of HIF-1α dimerisation on the transcriptome of T-REx-HRE cells, a hypoxia-focused microarray was conducted. The array was performed using mRNA extracted from untreated cells incubated under normoxia, untreated cells incubated under hypoxia, and cells treated with 1 μg / mL Dox incubated under hypoxia, for 24 h. The relative expression of key genes involved in the hypoxia response network is summarised in Table 3. Cyclo-CLLFVY had wide-ranging effects on the expression of hypoxia-related genes in T-REx-HRE cells. Following treatment with 1 μg / mL Dox for 24 h, the expression of 37 genes decreased and the expression of five genes increased compared to untreated cells. Of note was the change in the expression of VEGF, which decreased 1.7-fold when cyclo-CLLFVY was expressed, reflecting what was detected via qRT-PCR analysis (also a 1.7-fold decrease) (Figure 77A).

Expression of HIF-1α and HIF-2α decreased in T-REx-HRE cells treated with Dox compared to untreated cells, which is contrary to the qRT-PCR results that demonstrated that Dox

treatment had no significant effect on HIF-1α or HIF-2α expression (Figure 79, Figure 85A). This is a reflection of the inaccuracies possible when drawing conclusions from a single biological repeat. Therefore, although the array results give an interesting overview of changes in the expression of hypoxia-related genes, it is preferential to validate interesting trends in the array data. This was achieved via qRT-PCR analysis of further independent repeats of the experiments analysed in the hypoxia array.

Table 3: Effect of inhibition of HIF-1 dimerisation on hypoxic gene expression in T-REx-HRE cells. T-REx-HRE cells were incubated with vehicle or 1 µg / mL Dox (+Dox) in normoxia or hypoxia for 24 h. Hypoxic gene expression was measured using the TaqMan human hypoxia array. Experiments were conducted in duplicate. Data is presented as ΔΔCt relative to 18S expression and expression of each gene in normoxia. Fold change in ΔΔCt of treated relative to untreated hypoxic cells is shown; fold decrease (red), fold increase (green) or ≤1.1-fold change (black).

	Hypoxia		Hypoxia +Dox		Fold change in expression
	ΔΔCt	Ct	ΔΔCt	Ct	
ANGPTL4	4.69	35.71	1.42	37.09	**3.29**
IGFBP1	2.16	36.57	0.77	37.71	**2.79**
RBX1	2.93	20.07	1.06	21.20	**2.77**
ADM	2.16	24.34	1.01	25.09	**2.13**
NOTCH1	0.78	25.78	0.42	26.34	**1.87**
PTEN	1.01	26.45	0.55	26.98	**1.83**
NOS3	0.94	31.90	0.55	32.32	**1.69**
TGFBR2	1.18	25.93	0.70	26.35	**1.69**
VEGFA	3.36	23.73	1.99	24.15	**1.69**
CREBBP	1.01	22.81	0.64	23.13	**1.58**
EPO	1.25	34.06	0.80	34.36	**1.56**
MB	1.35	34.15	0.90	34.40	**1.51**
ARNT2	0.97	26.31	0.66	26.54	**1.48**
NOS1	1.74	28.44	1.18	28.66	**1.47**
CUL2	0.82	22.54	0.58	22.70	**1.41**
BHLHB2	3.94	23.41	2.79	23.57	**1.41**
PRKAA2	1.07	25.41	0.76	25.56	**1.40**
PHD2	1.97	21.90	1.43	22.02	**1.38**
GUSB	0.95	23.34	0.69	23.46	**1.38**
FIH	0.89	23.57	0.65	23.69	**1.38**
ATP1B1	1.03	24.62	0.75	24.74	**1.38**
ARNT	1.24	24.81	0.91	24.92	**1.37**
GLUT8	0.93	25.93	0.68	26.03	**1.36**
PHD3	2.57	25.36	1.92	25.44	**1.34**
EDN1	1.30	31.88	0.97	31.96	**1.34**
NOS2A	1.24	27.80	0.93	27.88	**1.34**
PHD1	0.84	23.73	0.63	23.80	**1.33**
HIF1A	0.92	22.74	0.69	22.81	**1.33**
HIF3A	1.67	34.50	1.27	34.56	**1.32**
DDIT4	5.17	21.21	3.92	21.27	**1.32**
EP300	0.97	23.19	0.73	23.25	**1.32**
HIF2A	1.29	28.51	0.99	28.56	**1.31**
FRAP1	0.84	23.48	0.66	23.48	**1.27**
PRKAA1	1.11	25.06	0.89	25.04	**1.25**
HMOX1	1.18	26.18	0.95	26.15	**1.24**
HYOU1	0.82	23.72	0.69	23.64	**1.20**
DDIT4L	1.33	29.64	1.13	29.53	**1.17**
HIG2	5.98	25.15	5.24	25.00	**1.14**
GAPDH	1.21	17.40	1.11	17.19	**1.09**
ING4	1.28	25.84	1.48	25.29	**1.16**
TP53	0.78	23.15	0.95	23.11	**1.21**
PIK3CA	1.12	28.28	1.38	27.64	**1.23**
MT3	1.06	39.78	1.43	39.01	**1.35**
VHL	0.60	25.73	0.93	24.77	**1.54**

The gene whose induction was most affected by cyclo-CLLFVY expression was angiopoietin like 4 (ANGPTL4), which encodes the angiopoietin like 4 protein, an adipokine involved in the regulation of lipid and glucose metabolism.[114] ANGPTL4 has been implicated in promoting angiogenesis, metastasis and cancer growth and progression. However, the role of ANGPTL4 does vary in different types of cancer, which may be due to proteolytic processing and post-translational modifications leading to varied protein function.[114] ANGPTL4 was strongly upregulated in hypoxia, but inhibition of HIF-1 dimerisation decreased ANGPTL4 expression more than three-fold (Figure 86A). Validation of this result using qRT-PCR did not show as large an impact. However, cyclo-CLLFVY expression did reduce ANGPTL4 expression by nearly half, downregulating expression from 2.4-fold to 1.3-fold normoxic ANGPTL4 expression (Figure 86B). Therefore, expression of cyclo-CLLFVY may prevent the development of metabolic disorders and hypoxia-induced angiogenesis in tumour cells through inhibition of hypoxic ANGPTL4 induction.

A

Gene	Hypoxia - Dox	Hypoxia +Dox	Relative expression
ANGPTL4	4.69	1.42	0.30

B

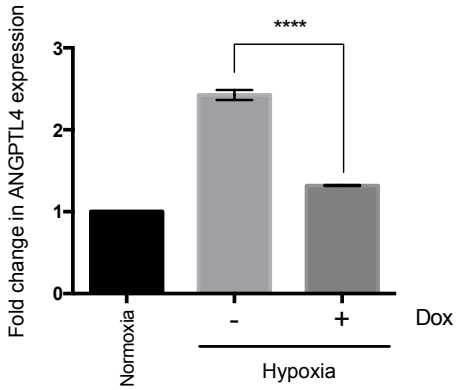

Figure 86: Inhibition of HIF-1 dimerisation prevents hypoxic induction of ANGPTL4. (A) Array results of expression of ANGPTL4 in hypoxia with and without Dox treatment, relative to normoxic expression. Experiments were conducted in duplicate and results normalised to expression of 18S. (B) qRT-PCR analysis of ANGPTL4 expression with and without Dox treatment, relative to normoxic expression. Experiments were conducted in triplicate (n=3) and results normalised to expression of 18S and β-actin. Error bars represent ±SEM. Stars denote significant differences between means: ****$p \leq 0.0001$.

The array also indicated a large decrease in expression of adrenomedullin (ADM) a pro-angiogenic factor that is highly induced by hypoxia in a range of cell types.[87, 267, 268] In the array, following treatment with 1 μg / mL Dox, ADM expression was reduced two-fold (Figure 87A). However validation via qRT-PCR showed Dox treatment resulted in only a 1.3-fold decrease in ADM expression (Figure 87B). The result from the qRT-PCR analysis is more reliable than the array data as it is based on independent repeats, rather than a single sample.

The low impact of inhibition of HIF-1 dimerisation on ADM expression suggests that ADM may be transactivated by both HIF-1 and HIF-2,as has been shown previously in other cell lines.[32, 101] Together, the inhibitory affect of cyclo-CLLFVY expression on genes involved in the promotion of angiogenesis VEGF, ANGPTL4 and ADM indicates the potential of targeting HIF-1 dimerisation as a therapeutic strategy to prevent tumour vascularisation.

A

Gene	Hypoxia - Dox	Hypoxia +Dox	Relative expression
ADM	2.16	1.01	0.47

B

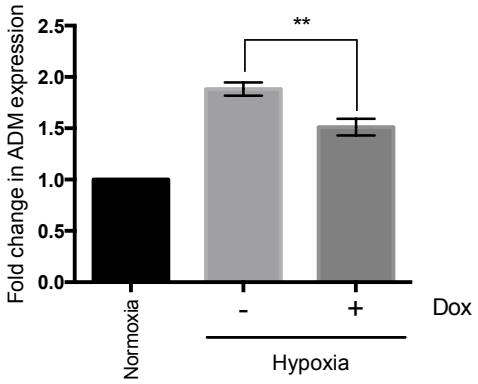

Figure 87: Inhibition of HIF-1 dimerisation decreases hypoxic induction of ADM. (A) Array results of expression of ADM in hypoxia with and without Dox treatment, relative to normoxic expression. Experiments were conducted in duplicate and results normalised to expression of 18S. (B) qRT-PCR analysis of ADM expression with and without Dox treatment, relative to normoxic expression. Experiments were conducted in triplicate (n=3) and results normalised to expression of 18S and β-actin. Error bars represent ±SEM. Stars denote significant differences between means: **$p \leq 0.01$.

Treatment of T-REx-HRE cells with Dox resulted in a two-fold decrease in ring box protein-1 (RBX1) expression (Figure 88A). This result was reflected by qRT-PCR analyses, which also showed a two-fold reduction in RBX1 expression following treatment with Dox (Figure 88B). RBX1 is a core component of the VHL complex involved in regulation of HIF-1α in normoxia.[269] Interestingly, expression of cullin 2 (CUL2), another component of the VHL complex, was also significantly reduced following treatment with Dox (Figure 88A), indicating a role for HIF-1 in the activation of pathways that lead to the degradation of HIF-1α in the presence of oxygen and αKG. It has been shown that RBX2, a closely related E3 ubiquitin ligase, is a HIF-1 target gene that contributes to regulation of HIF-1α.[270] It has been suggested that this feedback loop could comprise a cellular defence mechanism to prevent cytotoxicity caused by prolonged HIF-1 activation. In addition, although RBX2 expression was induced by hypoxia, RBX1 expression was shown to be constitutive in human colon carcinoma cells.[270] However, in the present study, the array data, supported by qRT-PCR analyses, demonstrated that hypoxia-induced RBX1 expression was significantly reduced by

cyclo-CLLFVY expression (Figure 88A and B), suggesting that RBX1 is transactivated by HIF-1 in T-REx-HRE cells.

A

Gene	Hypoxia - Dox	Hypoxia +Dox	Relative expression
RBX1	2.93	1.06	0.36
CUL2	0.82	0.58	0.71

B

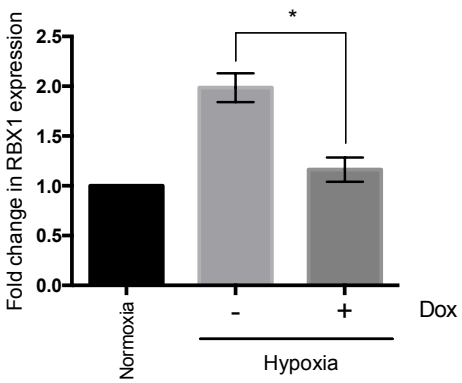

Figure 88: Inhibition of HIF-1 dimerisation prevents hypoxic induction of RBX1. (A) Array results of expression of RBX1 in hypoxia with and without Dox treatment, relative to normoxic expression. Experiments were conducted in duplicate and results normalised to expression of 18S. (B) qRT-PCR analysis of RBX1 expression with and without Dox treatment, relative to normoxic expression. Experiments were conducted in triplicate (n=3) and results normalised to expression of 18S and β-actin. Error bars represent ±SEM. Stars denote significant differences between means: *$p \leq 0.05$.

The expression of DNA-damage inducible transcript 4 (DDIT4) in T-REx-HRE cells was also decreased following Dox treatment. DDIT4 encodes the protein regulated in development and DNA damage responses 1 (REDD1), which is a conserved stress response protein that regulates mammalian target of rapamycin complex 1 (mTORC1), a critical regulator of cell proliferation.[60] DDIT4 expression was induced 5.2-fold in hypoxic conditions and expression of cyclo-CLLFVY reduced this 1.3-fold (Figure 89A). A similar effect was seen by qRT-PCR analyses of T-REx-HRE mRNA, following Dox treatment, DDIT4 expression in hypoxia decreased 1.4-foldcompared to untreated cells (Figure 89B). DDIT4 is a target of HIF-1,[271] and so a decrease in its expression following the inhibition of HIF-1 dimerisation would be expected. However, following peptide expression, DDIT4 expression was still five-fold that in normoxic cells. A HRE has been identified in the DDIT4 promoter that may also permit HIF-2-mediated transactivation.[272] Therefore, DDIT4 expression may be induced in hypoxia by the HIF-2 transcription factor when the transactivational activity of HIF-1 is inhibited.

A

Gene	Hypoxia - Dox	Hypoxia +Dox	Relative expression
DDIT4	5.17	3.92	0.76

B

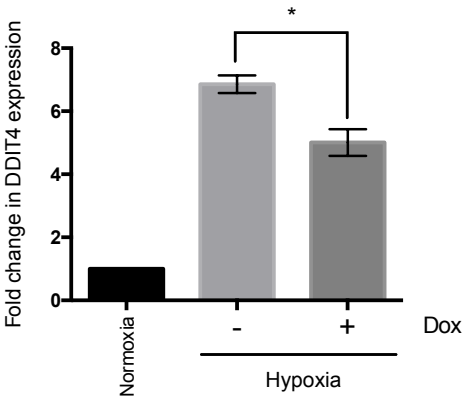

Figure 89: Inhibition of HIF-1 dimerisation reduces hypoxic induction of DDIT4. (A) Array results of expression of DDIT4 in hypoxia with and without Dox treatment, relative to normoxic expression. Experiments were conducted in duplicate and results normalised to expression of 18S. (B) qRT-PCR analysis of DDIT4 expression with and without Dox treatment, relative to normoxic expression. Experiments were conducted in triplicate (n=4) and results normalised to expression of 18S and β-actin. Error bars represent ±SEM. Stars denote significant differences between means: *$p \leq 0.05$.

In contrast to DDIT4, T-REx-HRE cells exhibited increased expression of PIK3CA, with Dox treatment, which was 1.4-fold greater in treated cells compared to untreated cells (Figure 90B). PIK3CA is the catalytic subunit of the enzyme phosphatidylinositol 3-kinase (PI3K), which phosphorylates membrane phospholipids that act as signalling messengers to mediate a diverse range of cellular functions.[273] Hypoxic activation of PIK3CA and its interaction with the serine/threonine kinase Akt has been linked to cellular protection from apoptosis.[273] The increase in PIK3CA expression following HIF-1 inhibition suggests that HIF-1 supresses PIK3CA expression. However, as PIK3CA is a component of a kinase involved in a number of signalling pathways, the increase in PIK3CA mRNA with cyclo-CLLFVY expression may be an indirect effect, and not directly a result of inhibition of HIF-1 dimerisation.

The array data also suggested an increase in VHL expression when HIF-1 dimerisation is inhibited (Figure 90A). However, the qRT-PCR analyses did not corroborate this, there was no significant difference in VHL expression between untreated and treated T-REx-HRE cells (Figure 90C). Finally, the array data indicated that the expression of MT3 was also increased in treated cells, but as the Ct values from the qRT-PCR analyses were close to the upper end of the useful range of 40 cycles, this would suggest fundamentally low expression of this gene in T-REx-HRE cells, making it difficult to draw conclusions from the relative expression following treatment of cells.

A

Gene	Hypoxia - Dox	Hypoxia +Dox	Relative expression
PIK3CA	1.12	1.38	1.23
VHL	0.60	0.93	1.54

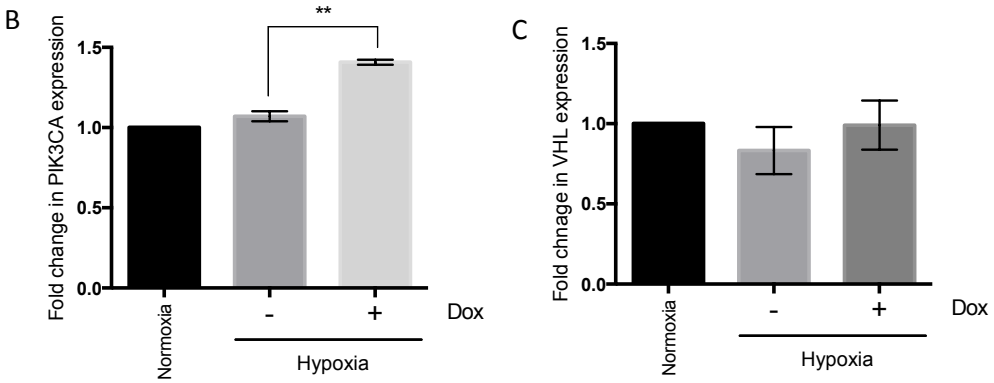

Figure 90: Inhibition of HIF-1 dimerisation suppresses hypoxic induction of PIK3CA and VHL. (A) Array results of expression of PIK3CA and VHL in hypoxia with and without Dox treatment, relative to normoxic expression. Experiments were conducted in duplicate and results normalised to expression of 18S. (B) qRT-PCR analysis of PIK3CA and (C) qRT-PCR analysis of VHL expression with and without Dox treatment, relative to normoxic expression. Experiments were conducted in triplicate (VHL: n=3; PIK3CA n=3) and results normalised to expression of 18S and β-actin. Error bars represent ±SEM. Stars denote significant differences between means: **$p \leq 0.01$.

2.2.7.2 Effect of HIF-2α siRNA on hypoxic gene induction

To compare the effect of inhibition of HIF-1 dimerisation to the effect of disruption of HIF-2-mediated transactivation, the array was repeated with mRNA extracted from cells transfected with HIF-2α siRNA for 24 h. Following siRNA treatment, cells were incubated in normoxia or hypoxia with or without 1 μg / mL Dox for a further 24 h. Treatment of cells with HIF-2α siRNA as well as Dox permits analysis of the transcriptional effect of disrupting both HIF-1 and HIF-2-mediated hypoxic response in T-REx cells (Table 4).

Table 4: Effect of HIF-2α siRNA on hypoxic gene expression in T-REx-HRE cells. T-REx-HRE cells were incubated with no treatment, HIF-2α siRNA or HIF-2α siRNA and 1 μg / mL Dox in normoxia or hypoxia for 24 h. Hypoxic gene expression was measured using the TaqMan human hypoxia array. Experiments were conducted in duplicate. Data is presented as ΔΔCt relative to 18S expression and expression of each gene in normoxia. Fold change in ΔΔCt of treated relative to untreated hypoxic cells is shown, fold decrease (red), fold increase (green) or ≤1.1-fold change (black).

	Hypoxia		Hypoxia +HIF-2α siRNA			Hypoxia +HIF-2α siRNA +Dox		
	ΔΔCt	Ct	ΔΔCt	Ct	Fold change in expression	ΔΔCt	Ct	Fold change in expression
NOS1	1.74	28.44	0.12	31.68	14.89	0.58	31.65	3.02
HIF2A	1.29	28.51	0.13	30.97	9.62	0.11	30.94	11.35
IGFBP1	2.16	36.57	0.26	38.86	8.45	0.43	38.83	5.02
MB	1.35	34.15	0.18	36.25	7.36	0.34	36.22	3.91
NOS3	0.94	31.90	0.22	33.19	4.30	0.69	33.16	1.37
ANGPTL4	4.69	35.71	1.39	36.37	3.38	1.00	36.32	4.69
HIF3A	1.67	34.50	0.53	35.32	3.13	0.41	35.29	4.11
RBX1	2.93	20.07	0.96	20.74	3.04	0.72	18.48	4.07
CASP1	0.58	39.18	0.21	39.88	2.79	0.30	39.84	1.92
HIG2	5.98	25.15	2.43	25.59	2.46	3.90	25.54	1.54
PRKAA2	1.07	25.41	0.45	25.87	2.39	0.45	25.83	2.36
GLUT8	0.93	25.93	0.43	26.23	2.16	0.81	26.20	1.14
NOS2A	1.24	27.80	0.59	28.05	2.11	0.75	28.02	1.65
ARNT2	0.97	26.31	0.47	26.57	2.09	0.77	26.53	1.27
MT3	1.06	39.78	0.53	39.85	1.99	0.66	39.78	1.61
TGFBR2	1.18	25.93	0.66	25.88	1.79	0.49	25.85	2.40
ING4	1.28	25.84	0.72	25.83	1.78	1.09	25.79	1.17
VEGFA	3.36	23.73	1.91	23.61	1.77	1.42	23.58	2.37
BHLHB2	3.94	23.41	2.24	23.42	1.76	2.46	23.39	1.60
DDIT4L	1.33	29.64	0.78	29.57	1.69	0.56	29.54	2.35
DDIT4	5.17	21.21	3.56	20.94	1.45	2.58	20.91	2.01
EDN1	1.30	31.88	0.94	31.52	1.39	1.03	31.49	1.27
PIK3CA	1.12	28.28	0.86	27.83	1.30	0.87	27.79	1.29
GUSB	0.95	23.34	0.73	22.91	1.29	0.70	22.87	1.35
TP53	0.78	23.15	0.63	23.21	1.24	0.82	23.18	1.04
HIF1A	0.92	22.74	0.77	22.20	1.20	0.83	22.18	1.11
ADM	2.16	24.34	1.98	23.68	1.09	1.07	22.82	2.01
HMOX1	1.18	26.18	1.09	25.66	1.08	1.00	25.62	1.19
PRKAA1	1.11	25.06	1.03	24.37	1.08	0.97	24.35	1.14
PHD1	0.84	23.73	0.78	23.04	1.06	0.69	23.01	1.22
ARNT	1.24	24.81	1.22	24.33	1.02	1.26	24.30	1.01
GAPDH	1.21	17.40	1.20	16.61	1.02	1.05	16.57	1.16
FIH	0.89	23.57	0.90	22.78	1.01	1.08	22.76	1.21
PTEN	1.01	26.45	1.02	25.66	1.01	0.94	25.63	1.08
EPO	1.25	34.06	1.31	33.18	1.05	1.46	33.14	1.17
PHD2	1.97	21.90	2.07	21.03	1.05	1.57	21.00	1.26
FRAP1	0.84	23.48	0.90	22.56	1.07	0.78	22.53	1.08
VHL	0.60	25.73	0.72	24.64	1.19	0.60	24.61	1.01
HYOU1	0.82	23.72	1.19	22.40	1.44	1.04	22.37	1.27
ATP1B1	1.03	24.62	1.71	23.08	1.66	0.91	23.05	1.13
CREBBP	1.01	22.81	1.77	21.61	1.75	0.59	21.58	1.72
EP300	0.97	23.19	1.73	21.76	1.79	0.93	21.72	1.04
PHD3	2.57	25.36	5.40	23.49	2.10	3.46	23.46	1.35
NOTCH1	0.78	25.78	1.69	23.84	2.17	1.14	23.80	1.47

The data from the two arrays was directly compared to assess the effect of each HIF isoform on the transcription of the hypoxia-related genes studied. A heat map of this data was produced to visualise the expression of these genes in hypoxia, relative to their expression in normoxia, following treatment with Dox, HIF-2α siRNA or both (**Figure 91**). Genes were grouped by function so changes in cell behaviour could be assessed.

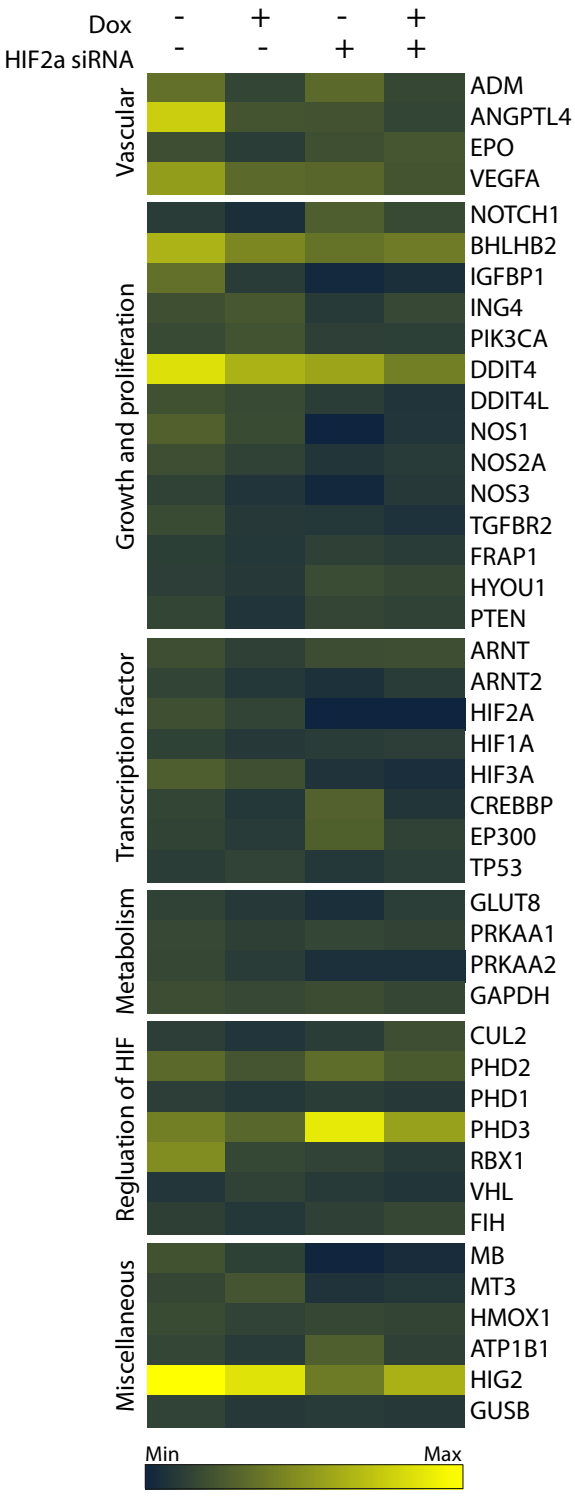

Figure 91: Heat map of relative gene expression in T-REx-HRE cells treated with Dox and HIF-2α siRNA. Colours represent ΔΔCt compared to normoxic expression and normalised to expression of 18S, where blue is low and yellow is high. Genes are grouped according to cellular function.

Comparison of the effect of inhibition of HIF-1 dimerisation to the effect of HIF-2α knockdown on gene induction can also yield information about the isoform specificity of the HIF subunits. Genes whose expression under hypoxic conditions was downregulated following Dox treatment or siRNA knockdown compared to untreated cells, may be targets of HIF-1 or HIF-2, respectively. In contrast, the expression of genes that were upregulated following Dox treatment of HIF-2α knockdown compared to untreated cells, may be supressed by HIF-1 or HIF-2 respectively. The relative effect of disruption of each isoform on the hypoxic expression of genes in the array was assessed. This analysis is summarised in Table 5.

Table 5: HIF isoform specificity in transcriptional activation of genes in hypoxia in T-REx-HRE cells.

Activated by HIF-1 only		Activated by HIF-2 only		Activated by HIF-1 and HIF-2		
HIF-2 appears to have no effect	HIF-2 appears to repress expression	HIF-1 appears to have no effect	HIF-1 appears to repress expression	HIF-1 and HIF-2 have similar effects	HIF-1 has more effect	HIF-2 has more effect
HMOX1	FRAP1	NOS1	MT3	BHLHB2	EGLN2	IGFBP1
PRKAA1	HYOU1	MB	ING4	DDIT4		NOS3
ARNT	ATP1B1	HIF3A	PIK3CA	RBX1		PRKAA2
HIF1AN	EP300	HIG2	TP53	TGFBR2		SLC2A8
EGLN1	CREBBP	DDIT4L		VEGFA		NOS2A
EPO	EGLN3			EDN1		ARNT2
PTEN	NOTCH1			ANGPTL4		
ADM	CUL2			GUSB		
				HIF1A		
				CASP1		

Following treatment of T-REx-HRE cells with HIF-2α siRNA, HIF-2α expression was diminished. The expression of HIF-1α in siRNA and Dox treated cells was 1.2-fold of that in untreated cells; supporting earlier findings that HIF-2α siRNA does not significantly affect HIF-1α expression. In addition, treatment of cells with HIF-2α siRNA and Dox resulted in a 2.4-fold decrease in VEGF expression, reflecting qRT-PCR analyses, which also showed a 2.4-fold decrease in VEGF expression (Figure 84A).

Interestingly, treatment of T-REx-HRE cells with HIF-2α siRNA resulted in a three-fold decrease in HIF-3α expression whereas treatment with Dox only resulted in a 1.3-fold decrease (Figure 92A). These results were validated by qRT-PCR analyses, which also showed a three-fold reduction in HIF-3α expression following siRNA treatment, compared to 1.3-fold with Dox, suggesting that hypoxic upregulation of HIF-3α is principally mediated by HIF-2 in T-REx-HRE cells (Figure 92B). Up to ten splice variants of HIF-3α mRNA have been identified;[28, 30] the TaqMan probe used in the hypoxia array bound to HIF-3α at the splice junction between exons 9-10 and so would be able to detect expression of all identified splice variants except HIF-3α4, which lacks the ODDD. In contrast to the array results, hypoxic

expression of HIF-3α was modulated by HIF-1 and not HIF-2 in Caki-1 renal carcinoma and Hep3B hepatoma cells.[28, 29] Therefore inhibition of HIF-3α expression with HIF-2α siRNA suggests a novel role for HIF-2 in regulation of HIF-3α in HEK cells.

A

Gene	Hypoxia	Hypoxia +Dox	Hypoxia +HIF-2α siRNA	Hypoxia +HIF-2α siRNA +Dox
HIF-3α	1.67	1.27	0.53	0.41

B

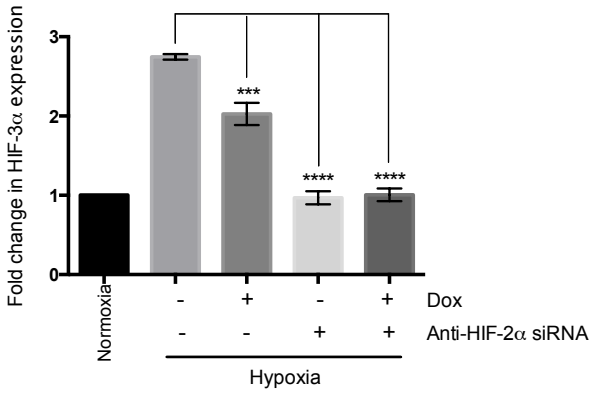

Figure 92: HIF-3α expression is mediated by the HIF-2 transcription factor in hypoxic conditions. (A) Array results of expression of HIF-3α under hypoxia untreated or treated with Dox or HIF-2α siRNA relative to normoxic expression. Experiments were conducted in duplicate and results normalised to expression of 18S. (B) qRT-PCR analyses of HIF-3α expression with and without Dox and HIF-2α siRNA treatment, relative to normoxic expression. Experiments were conducted in triplicate (n=3) and results normalised to expression of 18S and β-actin. Error bars represent ±SEM. Stars denote significant differences between means: ***$p \leq 0.001$, ****$p \leq 0.0001$.

In addition to VEGF, HIF-2α siRNA treatment reduced expression ANGPTL4, which has also been implicated in promoting angiogenesis, metastasis and cancer growth and progression. Treatment of T-REx-HRE cells with HIF-2α siRNA resulted in a 3.4-fold decrease in ANGPTL4 expression, suggesting that HIF-2 may also have a role in transactivation of ANGPTL4 (Figure 93A). There was a greater decrease in ANGPTL4 expression following combined Dox and siRNA treatment, 4.7-fold. This result was supported by qRT-PCR analyses where hypoxia-induced ANGPTL4 expression was reduced 2.2-fold when cells were treated with Dox and HIF-2α siRNA, compared to a 1.9-fold reduction with Dox alone and a 1.3-fold reduction with HIF-2α siRNA alone (Figure 93B). Following HIF-2α siRNA and Dox treatment, ANGPTL4 expression under hypoxia was not significantly different to normoxic ANGPTL4 expression.

In contrast, in the array, treatment of cells with HIF-2α siRNA did not significantly impact ADM expression and this result was validated by qRT-PCR analyses (Figure 93A and C). The array data also suggested that the combination of HIF-2α siRNA and Dox treatment reduced ADM expression two-fold, to normoxic levels. In contrast, qRT-PCR analyses indicated that

treatment of cells with HIF-2α siRNA and Dox resulted in only a 1.4-fold reduction in ADM expression compared to untreated cells under hypoxia. ADM has previously been identified as a target of HIF-1 and HIF-2 transcription factors,[32] however, array data and qRT-PCR analyses suggest that in T-REx-HRE cells, ADM expression in hypoxia is only dependent on HIF-1, not HIF-2, for hypoxic transactivation.

A similar result was recorded for EPO, the hormone responsible for erythropoiesis. In the array, EPO expression increased 1.3-fold under hypoxia, compared to normoxia. This increase was attenuated by disruption of HIF-1 dimerisation, but not by treatment of cells with HIF-2α siRNA (Figure 93A). Analysis of EPO expression by qRT-PCR also showed that hypoxic induction of EPO transcription was reduced 1.5-fold by Dox, but not by HIF-2α siRNA treatment of cells (Figure 93D). HIF-1 was first identified as an activator of EPO in Hep3B and HeLa cells.[3, 274] Later work suggested that EPO was a target of both HIF-1 and HIF-2 in a cell type specific manner.[275] In infant mouse hepatocytes, EPO expression required HIF-2α but not HIF-1α. However, erythropoiesis was found to be impaired in mice deficient in HIF-1α only.[276] The array and qRT-PCR data suggest that transactivation of EPO in hypoxia is mediated by HIF-1, and not HIF-2, in T-REx-HRE cells.

A

Gene	Hypoxia	Hypoxia +Dox	Hypoxia +HIF-2α siRNA	Hypoxia +HIF-2α siRNA +Dox
ANGPTL4	4.69	1.42	1.39	1.00
ADM	2.16	1.01	1.98	1.07
EPO	1.25	0.80	1.31	1.46

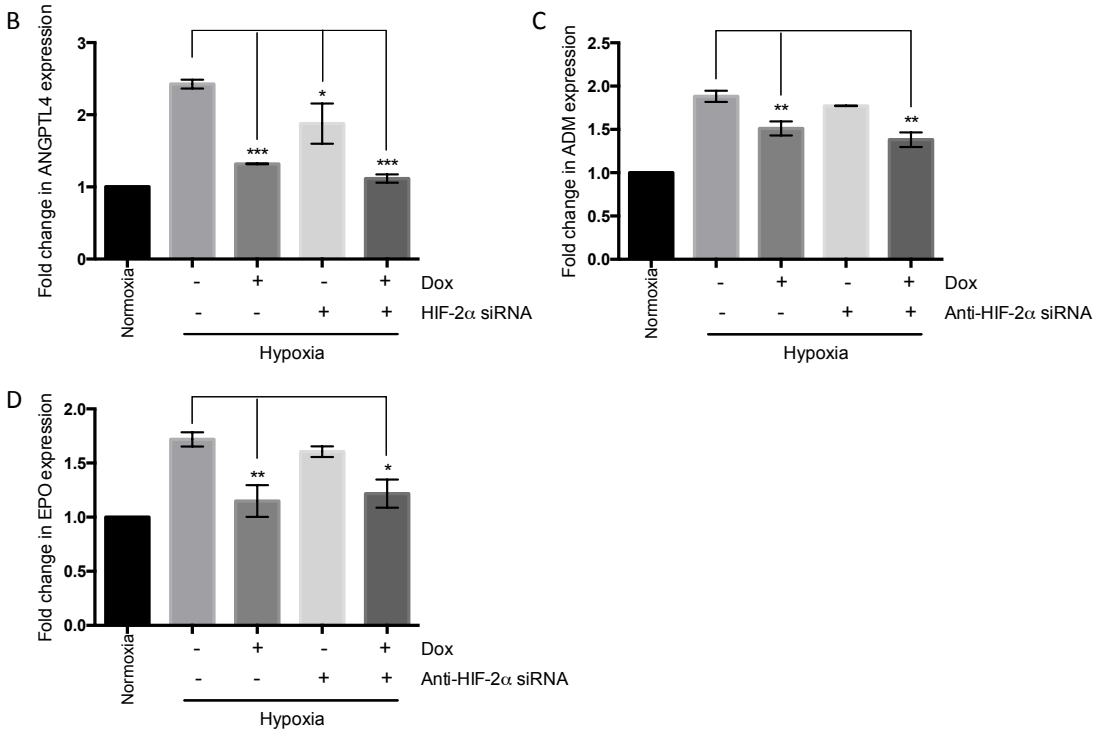

Figure 93: Inhibition of HIF-1 dimerisation decreases expression of genes involved in vascularisation. (A) Array results of expression of ANGPLT4, ADM and EPO under hypoxia, untreated or treated with Dox, HIF-2α siRNA, or both, relative to normoxic expression. Experiments were conducted in duplicate and results normalised to expression of 18S. qRT-PCR analyses of ANGPLT4 (B), ADM (C) and EPO (D) expression with and without Dox and HIF-2α siRNA treatment, relative to normoxic expression. Experiments were conducted in triplicate (n=3) and results normalised to expression of 18S and β-actin. Error bars represent ±SEM. Stars denote significant differences between means: *$p \leq 0.05$, **$p \leq 0.01$, ***$p \leq 0.001$.

Expression of cyclo-CLLFVY, and HIF-2α siRNA treatment, resulted in a decrease in a number of genes involved in growth and proliferation. The array data showed that following treatment with Dox, insulin growth factor binding protein 1 (IGFBP1) expression under hypoxia decreased 2.6-fold (Table 6). The effect of HIF-2α siRNA was even larger, resulting in an eight-fold reduction in IGFBP1. IGFBP1 is a secreted protein that binds insulin-like growth factor (IGF) and inhibits the activities of IGF on cell growth.[277] IGFBP1 expression is upregulated in hypoxic conditions and is negatively correlated with foetal size.[277] A putative HRE has been identified in the promoter of IGFBP1 and it has been suggested that HIF-1 is responsible for hypoxia-induced IGFBP expression.[277, 278] The large effect of inhibition of HIF-

1 dimerisation and of HIF-2α siRNA on IGFBP1 expression indicates that HIF-1 and HIF-2 are involved in the upregulation of IGFBP1 in hypoxic conditions.

In addition, in the array HIF-2α siRNA also resulted in depletion of nitric oxide synthase 1 (NOS1) mRNA, a 14-fold decrease compared to untreated cells (Table 6). NOS1 (also known as neuronal NOS) is one of three isozymes (along with NOS2A (inducible NOS) and NOS3 (endothelial NOS)) that catalyse the l-arginine dependent synthesis of nitric oxide (NO), in an oxygen-dependent process.[279] NO stabilises HIF-1α protein in normoxic conditions and has been shown to increase HIF-1 binding activity.[83] No published literature was found that suggests NOS1 is a HIF-1 or HIF-2 target. However, the array data showed that inhibition of HIF-1 dimerisation resulted in a decrease in NOS1 expression from 1.7 to 1.2-fold normoxic expression, suggesting that NOS1 is a target of HIF-1 in T-REx cells.

As reduction of NOS1 mRNA in HIF-2α siRNA treated cells was so large, it may be a result of off target effects of the siRNA. This should not affect gene expression in hypoxia as NO stabilises HIF-1 under normoxia. Alternatively, the decrease in NOS1 expression recorded following HIF-2α siRNA treatment could be a result of experimental error. The combination of HIF-2α siRNA and Dox treatment resulted in a decrease of NOS1 expression from 1.7 to 0.6-fold normoxic expression, a larger decrease than Dox treatment alone. This suggests that NOS1 is a target of both HIF-1 and HIF-2.

In the array NOS2A expression was only induced 1.2-fold in hypoxia compared to normoxic expression, however, inhibition of HIF-1 dimerisation reduced NOS2A expression to normoxic levels (Table 6). In addition, HIF-2α siRNA halved the hypoxic expression of NOS2A although both treatments together did not have an additive effect. A HRE has been identified in the promoter region of the NOS2A gene and NOS2A was identified as a target of HIF-1 in cardiac monocytes.[280, 281] Together these results suggest that NOS2A is a target of both HIF isoforms in T-REx-HRE cells, but is principally reliant on HIF-2α for hypoxic expression.

Array data showed that the expression of the third NOS isoform, NOS3 appeared to be constitutive, hypoxia did not increase NOS3 mRNA levels. However, Dox and HIF-2α siRNA treatment of cells inhibited hypoxic NOS3 expression (Table 6), perhaps indicating a reliance on HIFs for maintenance of hypoxic NOS expression. Combination of the two treatments resulted in less suppression of NOS3 expression than either treatment alone. In human dermal microvascular endothelial cells (HMEC-1) and human umbilical vein endothelial cells (HUVEC) levels of NOS3 mRNA were increased in hypoxia compared to normoxia.[282] In HMEC-1 and HUVEC cells, luciferase reporter assays with the NOS3 promoter showed an increase in gene expression with exogenous HIF-2 expression, and two contiguous HREs were identified in the NOS3 promoter,[282] suggesting that hypoxic NOS3 expression was

stimulated through HIF-2. The array results also indicate that NOS3 expression in hypoxic conditions is maintained by HIF-2.

In contrast to genes involved in the promotion of growth and proliferation, the expression of the tumour suppressor ING4 was increased 1.2-fold following inhibition of HIF-1 dimerisation (Table 6). ING4 has previously been shown to supress activation of HIF-1 through association with prolyl hydroxylases.[283] Once activated, HIF-1 may supress ING4 expression in hypoxia to prevent inhibition of HIF-1 activity by ING4 upon reoxygenation. Conversely, ING4 expression was decreased following treatment with HIF-2α siRNA.

Table 6: Effect of inhibition of HIF-1 dimerisation and of knockdown of HIF-2α expression on expression of genes involved in growth and proliferation. Array results of expression of IGFBP1, NOS1, NOS2A, NOS3 and ING4 under hypoxia untreated or treated with Dox or HIF-2α siRNA relative to normoxic expression. Experiments were conducted in duplicate and results normalised to expression of 18S.

Gene	Hypoxia	Hypoxia +Dox	Hypoxia +HIF-2α siRNA	Hypoxia +HIF-2α siRNA +Dox
IGFBP1	2.16	0.77	0.26	0.43
NOS1	1.74	1.18	0.12	0.58
NOS2A	1.24	0.93	0.59	0.75
NOS3	0.94	0.55	0.22	0.69
ING4	1.28	1.48	0.72	1.09

Inhibition of HIF-1 dimerisation decreased expression of the stress response gene DDIT4, however, following treatment of T-REx-HRE cells with Dox the array data showed that DDIT4 expression was still 3.9-fold increased compared to normoxic cells (Figure 94A). Treatment of T-REx-HRE cells with HIF-2α siRNA reduced DDIT4 expression to 3.6-fold that in normoxia and treatment of cells with HIF-2α siRNA and Dox decreased DDIT4 expression to 2.6-fold that in normoxia. Validation of this result by qRT-PCR analyses showed that DDIT4 was upregulated 6.9-fold in hypoxic conditions compared to normoxia and this upregulation was inhibited by Dox and HIF-2α siRNA treatment of cells (Figure 94B). qRT-PCR analyses showed that treatment of T-REx-HRE cells with Dox resulted in a 1.4-fold reduction in DDIT4 expression. In addition, treatment of T-REx-HRE cells with HIF-2α siRNA also led to a 1.4-fold decrease in DDIT4 expression. Following treatment with both Dox and HIF-2α siRNA, DDIT4 expression was 1.6-fold decreased compared to untreated hypoxic cells, but still 4.3-fold increased compared to untreated normoxic cells. Together these results suggest that although HIF-1 and HIF-2 have a role in hypoxic upregulation of DDIT4, other cellular pathways also contribute to increase DDIT4 expression in hypoxia. DDIT4 is also induced in response to endoplasmic reticulum (ER) stress and DNA damage related to the regulation of

reactive oxygen species,[284, 285] which may be a result of hypoxic exposure, particularly when HIF response pathways are disrupted.[285] Therefore, in hypoxic conditions, with Dox or HIF-2α siRNA treatment, DDIT4 may be upregulated via alternative stress response pathways.

In addition, in the array, HIF-2α siRNA treatment resulted in a 1.3-fold decrease in expression of the oncogene PIK3CA and a combination of Dox and HIF-2α siRNA also led to a 1.3-fold decrease in PIK3CA (Figure 94A). This is in contrast to the 1.3-fold increase in PIK3CA expression following treatment with Dox. Validation of array data via qRT-PCR analyses revealed that HIF-2α siRNA did not significantly impact PIK3CA expression (Figure 94C). However, the combination of Dox and HIF-2α siRNA treatment prevented the significant increase in PIK3CA expression recorded following Dox treatment alone, indicating opposing roles of the HIF isoforms.

A

Gene	Hypoxia	Hypoxia +Dox	Hypoxia +HIF-2α siRNA	Hypoxia +HIF-2α siRNA +Dox
DDIT4	5.17	3.92	3.56	2.58
PIK3CA	1.12	1.38	0.86	0.87

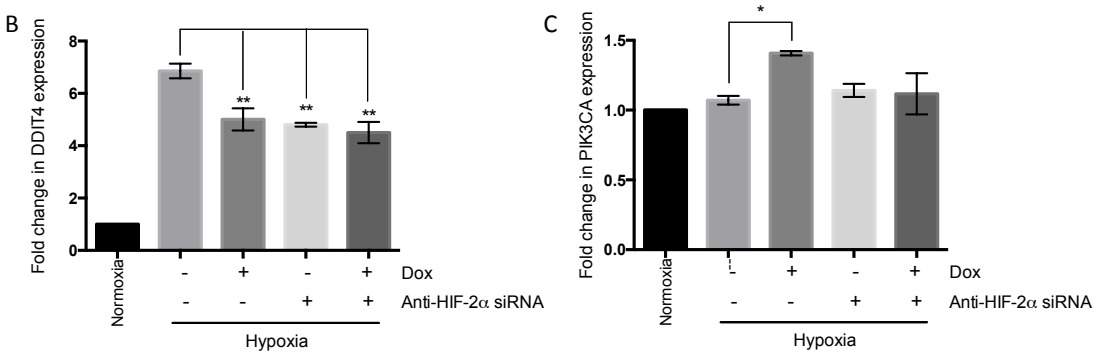

Figure 94: Effect of inhibition of HIF-1 dimerisation and knockdown of HIF-2α expression on DDIT4 and PIK3CA expression. (A) Array results of expression of DDIT4 and PIK3CA under hypoxia untreated or treated with Dox or HIF-2α siRNA relative to normoxic expression. Experiments were conducted in duplicate and results normalised to expression of 18S. qRT-PCR analyses of DDIT4 (B) and PIK3CA (C) expression with and without Dox and HIF-2α siRNA treatment, relative to normoxic expression. Experiments were conducted in triplicate (VHL: n=3; PIK3CA n=2) and results normalised to expression of 18S and β-actin. Error bars represent ±SEM. Stars denote significant differences between means: *$p \leq 0.05$, **$p \leq 0.01$.

Interestingly, disruption of HIF-1 an HIF-2 pathways had markedly different impacts on NOTCH1 expression. Array data showed that inhibition of HIF-1 dimerisation halved hypoxic expression of NOTCH1 whereas treatment of cells with HIF-2α siRNA doubled it (Figure 95A). This result was supported by qRT-PCR analyses, which revealed a 1.6-fold decrease in NOTCH1 expression following Dox treatment, in contrast to a 1.4-fold increase in NOTCH1 expression following treatment of cells with HIF-2α siRNA (Figure 95B). Contrasting

properties of HIFs in NOTCH1 regulation have also been noted in glioma stem cells. Notch signalling plays a key role in the maintenance of pluripotency in stem cells and is required for hypoxia-induced maintenance of stem cell characteristics.[108] In glioma stem cells, HIF-1α activated Notch signalling whilst HIF-2α repressed it. This difference was attributed to differential (competitive) binding of the two transcription factors to Notch intracellular domain receptors.[107] This differential regulation of NOTCH1 by HIFs indicates opposing roles of the transcription factors in differentiation.

A

Gene	Hypoxia	Hypoxia +Dox	Hypoxia +HIF-2α siRNA	Hypoxia +HIF-2α siRNA +Dox
NOTCH1	0.78	0.42	1.69	1.14

B

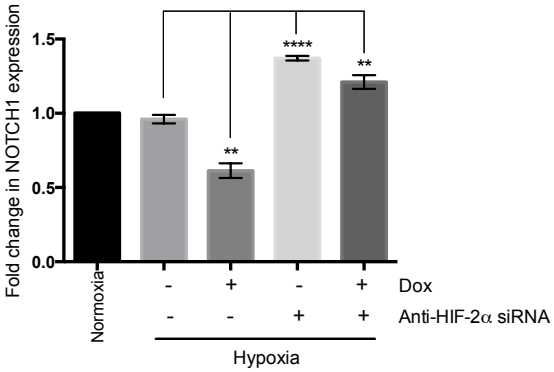

Figure 95: HIF-1 and HIF-2 have conflicting roles in hypoxic NOTCH1 regulation. (A) Array results of expression of NOTCH1 in hypoxia untreated or treated with Dox or HIF-2α siRNA relative to normoxic expression. Experiments were conducted in duplicate and results normalised to expression of 18S. (B) qRT-PCR analyses of NOTCH1 expression with and without Dox and HIF-2α siRNA treatment, relative to normoxic expression. Experiments were conducted in triplicate (n=3) and results normalised to expression of 18S and β-actin. Error bars represent ±SEM. Stars denote significant differences between means: ***$p \leq 0.001$, ****$p \leq 0.0001$.

In the array, treatment of T-REx-HRE cells with Dox also decreased RBX1 expression three-fold, to normoxic levels. In addition, following treatment with HIF-2α siRNA RBX1 expression was reduced three-fold compared to untreated cells, suggesting that RBX1 expression can be induced by HIF-1 or HIF-2 transcription factors in hypoxic conditions (Figure 96A). Disruption of HIF-1 and HIF-2 (Dox and HIF-2α siRNA treatment) had a cumulative effect, leading to a reduction of RBX1 to below normoxic levels. These results were validated by qRT-PCR analyses. qRT-PCR data showed that RBX1 expression was induced 1.8-fold under hypoxia compared to normoxia. However, following treatment of cells with Dox or HIF-2α siRNA, expression of RBX1 in hypoxic conditions was not significantly different to normoxic RBX1 expression (Figure 96B). As described earlier, RBX1 is a core component of the VHL complex, which is responsible for the polyubiquitination of hydroxylated HIF-1α, which leads

to its degradation in normoxia.[40, 286] Upregulation of RBX1 and other VHL components such as CUL2 in hypoxic conditions may aid rapid degradation of HIF-1α upon cellular re-oxygenation.

However, VHL, the gene encoding pVHL, was the only gene analysed in the array whose expression was increased following both Dox treatment and HIF-2α siRNA treatment. Array data showed that inhibition of HIF-1 dimerisation increased VHL expression in hypoxic conditions 1.6-fold and HIF-2α siRNA treatment increased VHL expression under hypoxia 1.2-fold (Figure 96A). Together these results suggest that HIFs have a suppressive role on VHL expression. However, qRT-PCR analyses indicated that Dox and HIF-2α siRNA treatments had no significant effect on expression of VHL (Figure 96C).

A

Gene	Hypoxia	Hypoxia +Dox	Hypoxia +HIF-2α siRNA	Hypoxia +HIF-2α siRNA +Dox
RBX1	2.93	1.06	0.96	0.72
CUL2	0.82	0.58	0.80	1.25
VHL	0.60	0.93	0.72	0.60

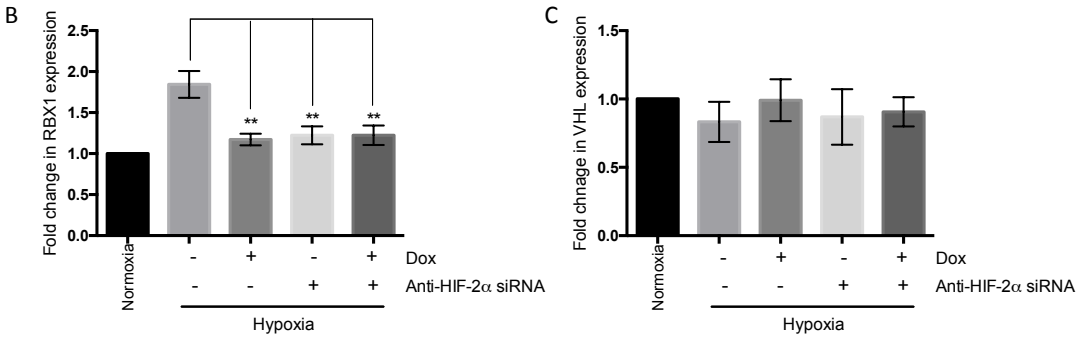

Figure 96: Inhibition of HIF-1 dimerisation, and knockdown of HIF-2α expression, decreases expression of components of VHL complex but not of the gene encoding pVHL. (A) Array results of expression of RBX1, CUL2 and VHL in hypoxia untreated or treated with Dox, HIF-2α siRNA, or both, relative to normoxic expression. Experiments were conducted in duplicate and results normalised to expression of 18S. (B) qRT-PCR analyses of RBX1 and (C) qRT-PCR analysis of VHL expression with and without Dox and HIF-2α siRNA treatment, relative to normoxic expression. Experiments were conducted in triplicate (n=3) and results normalised to expression of 18S and β-actin. Error bars represent ±SEM. Stars denote significant differences between means: **p ≤ 0.01.

In contrast, inhibition of HIF-1 dimerisation and HIF-2α siRNA treatment did significantly impact upstream effectors of oxygen-dependent regulation of HIF-1, prolyl and asparaginyl hydroxylases. Inhibition of HIF-1 and HIF-2-mediated transactivation had conflicting roles on PHD3 expression in T-REx-HRE cells. In the array, following treatment with Dox, expression of PHD3 was decreased 1.4-fold compared to untreated cells, in contrast, following treatment with HIF-2α siRNA, PHD3 expression increased two-fold (Figure 97A). This suggests that in

T-REx-HRE cells, HIF-1 induces PHD3 expression whereas HIF-2α represses it. The effect of inhibition of HIF-1 dimerisation on PHD3 expression was supported by qRT-PCR analyses, which showed that following treatment of T-REx-HRE cells with Dox, PHD3 expression was reduced 1.6-fold (Figure 97B). However, qRT-PCR analyses did not indicate any repressive effect of HIF-2 on PHD3 expression, there was no significant difference in the expression of PHD3 in hypoxic conditions following HIF-2α siRNA treatment compared to untreated cells.

HIF-1 also appeared to positively regulate PHD2 expression whereas HIF-2α had no effect. The array data showed that treatment of cells with Dox resulted in a 1.4-fold decrease in PHD2 expression whereas treatment of cells with HIF-2α siRNA did not affect PHD2 expression (Figure 97A). This result was supported by qRT-PCR analyses, which showed that following treatment of cells with Dox, PHD2 expression decreased 1.5-fold, whereas expression of PHD2 in cells treated with HIF-2α siRNA in hypoxic conditions was not significantly different to that in untreated cells. (Figure 97B) Similarly, treatment of cells with Dox resulted in a 1.3-fold decrease in factor inhibiting HIF-1 (FIH) expression whereas HIF-2α siRNA has no significant effect (Figure 97A). Array results indicated that PHD1 expression was not upregulated in hypoxic conditions.

Expression of PHD2 and 3 has previously been shown to be induced by hypoxia, and PHD1 expression has been shown to be constitutive, in a number of cell lines.[39, 49] In U2OS cells a two-fold induction of PHD2 and 3 expression in hypoxia was abrogated by transfection of HIF-1α siRNA but not HIF-2α siRNA, suggesting that PHD2 and PHD3 are hypoxic targets of HIF-1 only, in agreement with the array data.[49] However in U2OS cells no repressive effect of HIF-2α on PHD enzyme expression was identified, in agreement with the qRT-PCR data. HIF-1 is thought to mediate response to acute hypoxia whereas HIF-2 is the prominent driver of adaptation to prolonged periods of hypoxic conditions.[78, 105] Upregulation of hydroxylases by HIF-1 in hypoxia may lead to more rapid degradation of HIF-1α and HIF-2α upon reoxygenation, to prevent HIF-1-mediated transactivation in normoxia. However, HIF-2 may have no such effect on hydroxylases as it is associated with chronic hypoxia.

A

Gene	Hypoxia -Dox	Hypoxia +Dox	Hypoxia +HIF-2α siRNA	Hypoxia +HIF-2α siRNA +Dox
PHD1	0.84	0.63	0.78	0.69
PHD2	1.97	1.43	2.07	1.57
PHD3	2.57	1.92	5.40	3.46
FIH	0.89	0.65	0.90	1.08

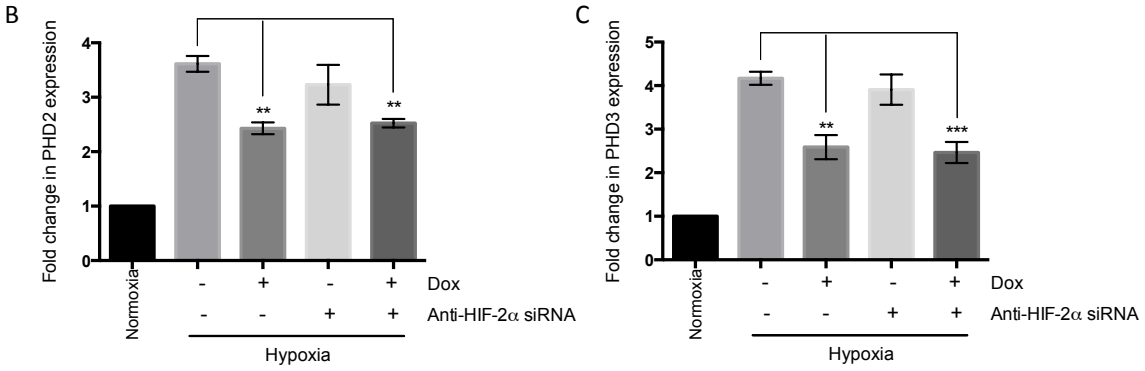

Figure 97: Inhibition of HIF-1 dimerisation decreases expression of prolyl and asparaginyl hydroxylases involved in regulation of HIF-1α and HIF-2α in normoxia. (A) Array results of expression of PHD1, PHD2, PHD3 and FIH under hypoxia untreated or treated with Dox, HIF-2α siRNA, or both, relative to normoxic expression. Experiments were conducted in duplicate and results normalised to expression of 18S. (B) qRT-PCR analyses of PHD2 and (C) qRT-PCR analysis of PHD3 expression with and without Dox and HIF-2α siRNA treatment, relative to normoxic expression. Experiments were conducted in triplicate (n=3) and results normalised to expression of 18S and β-actin. Error bars represent ±SEM. Stars denote significant differences between means: **p ≤ 0.01, ***p ≤ 0.001.

2.2.8 Effect of inhibition of HIF-1 dimerisation on cell growth in hypoxia

The hypoxia-focused microarray revealed that inhibition of HIF-1 dimerisation in T-REx-HRE cells decreased the expression of many genes activated in hypoxia. This decrease in hypoxia-activated genes may prevent cellular adaptation to hypoxia, reducing cell growth, proliferation and viability.

2.2.8.1 Competitive growth assay

To assess the effect of inhibition of HIF-1 dimerisation on the survival of T-REx cells, a competition assay was devised. If two populations of T-REx cells, one expressing the Npu-CLLFVY construct and one not, were mixed a difference in survival may be observed when the peptide is expressed in hypoxia. In normoxia, HIF-1α is degraded and so the HIF-1 transcription factor cannot form therefore no difference in the growth of the two populations would be expected following cyclo-CLLFVY expression. In hypoxia however, where HIF-1 induces the upregulation of genes required for cellular adaptation to hypoxia, expression of

the peptide may inhibit cell growth and decrease survival. If each cell line expressed a different fluorescent protein, the relative number of cells of each cell line present in the population could be analysed by fluorescent microscopy and flow cytometery.

For a negative cell line, that does not express cyclo-CLLFVY, the fluorescent protein mCherry was encoded on to the plasmid pcDNA5/FRT/TO and integrated on to the chromosome of T-REx-293 cells, via Flp-FRT recombination. Positive clones were selected with hygromycin in high dilution culture. Inducible expression of mCherry in the resulting cell line, T-REx-mCherry, was demonstrated by fluorescent microscopy (Figure 98). In the absence of Dox, no fluorescence was visible in cells, however following treatment with 1 µg / mL Dox for 24 h, strong fluorescence was visualised, indicating successful integration of mCherry into the cell line.

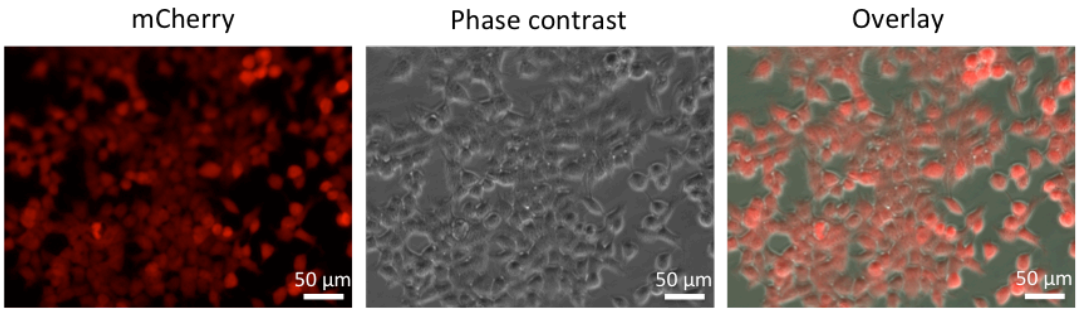

Figure 98: Expression of mCherry in T-REx-mCherry cells treated with 1 µg / mL Dox. Micrographs demonstrate strong, widespread mCherry expression indicative of successful integration of the construct.

Next, a mixed population of T-REx-GFP (cells expressing the Npu-CLLFVY construct and the fluorescent protein GFP on the same open reading frame) and T-REx-mCherry cells was seeded and visualised by fluorescent microscopy following 24 h treatment with 1 µg / mL Dox. Visualisation of the individual cells lines in both GFP and mCherry fluorescence channels (with excitation/ emission 500/535 nm and 565/620 nm respectively) showed that there was no cross over of fluorescent signals between the two proteins (Figure 99). In addition, in the mixed population of cells, GFP or mCherry expressing cells could be clearly distinguished, although mCherry fluorescence was more intense than that of GFP.

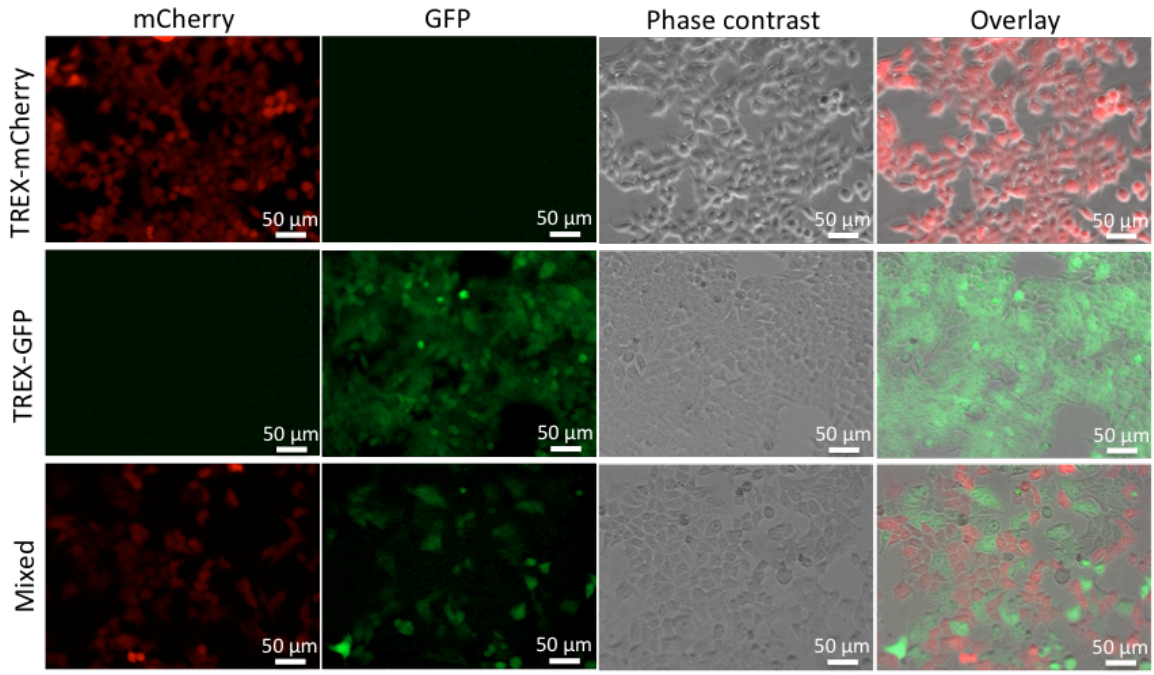

Figure 99: Cells expressing mCherry or GFP can be distinguished by fluorescence microscopy. Top and middle rows demonstrates that there is no cross talk between mCherry and GFP fluorescence. Bottom row demonstrates the visualisation of individual cells expressing mCherry or GFP, indicating that in a mixed population of cells, the two cell types can be distinguished.

A 1:1 mixed population of T-REx-mCherry and T-REx-GFP cells was seeded and incubated in normoxia for 24 h. Cells were then treated with vehicle or 1 µg / mL Dox and maintained in normoxia or hypoxia for four weeks, passaging twice weekly. Cells incubated in hypoxia were maintained in hypoxic conditions during passaging. Following the four-week incubation period, it was difficult to visualise any difference in cell populations by fluorescence microscopy. There appeared to be mostly GFP expressing cells and few mCherry expressing cells in all samples, suggesting T-REx-GFP cells grew faster in all conditions (Figure 100). Although fluorescence microscopy gave an idea of the proportion of each cell line in each population, it was not possible to quantify cell numbers. Therefore flow cytometery was employed to count the number of cells expressing each fluorescent protein.

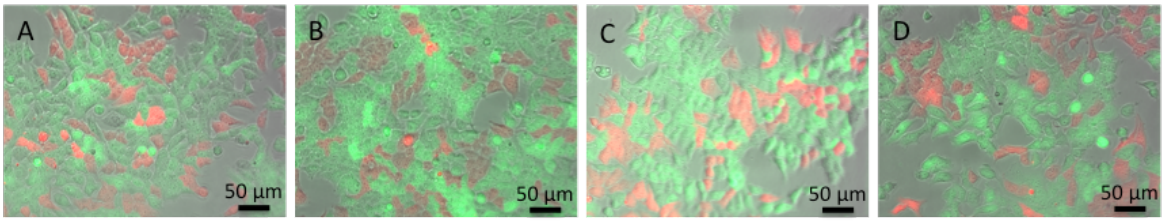

Figure 100: T-REx-GFP cell growth outcompetes mCherry cell growth in normoxia and hypoxia. T-REx-GFP and T-REx-mCherry cells were mixed in a 1:1 ratio and cultured in/ with normoxia –Dox (A), normoxia +Dox (B), hypoxia –Dox (C) or hypoxia +Dox (D) for 4 weeks, then incubated in normoxia or hypoxia with Dox for 24 h.

The data collected from flow cytometery of samples is shown in Figure 101 and is summarised in Table 7. For all samples, there were more T-REx-GFP cells than T-REx-mCherry cells (up to 11-fold more GFP than mCherry expressing cells). There was a lower percentage of T-REx-GFP cells in hypoxia than normoxia, but expression of the peptide made no difference to this. The fact that T-REx-GFP cells out compete T-REx-mCherry cells in normoxia and hypoxia (83% GFP in normoxia and 63-65% GFP in hypoxia), regardless of peptide expression, suggests that the difference in cell survival is not a result of inhibition of HIF-1 activity but that the T-REx-GFP cells inherently grow faster than T-REx-mCherry cells. This difference could be a result of selecting faster growing colonies after integration. There does appear to be more mCherry expressing cells in hypoxic cells expressing the peptide than not, despite a similar percentage of GFP expressing cells.

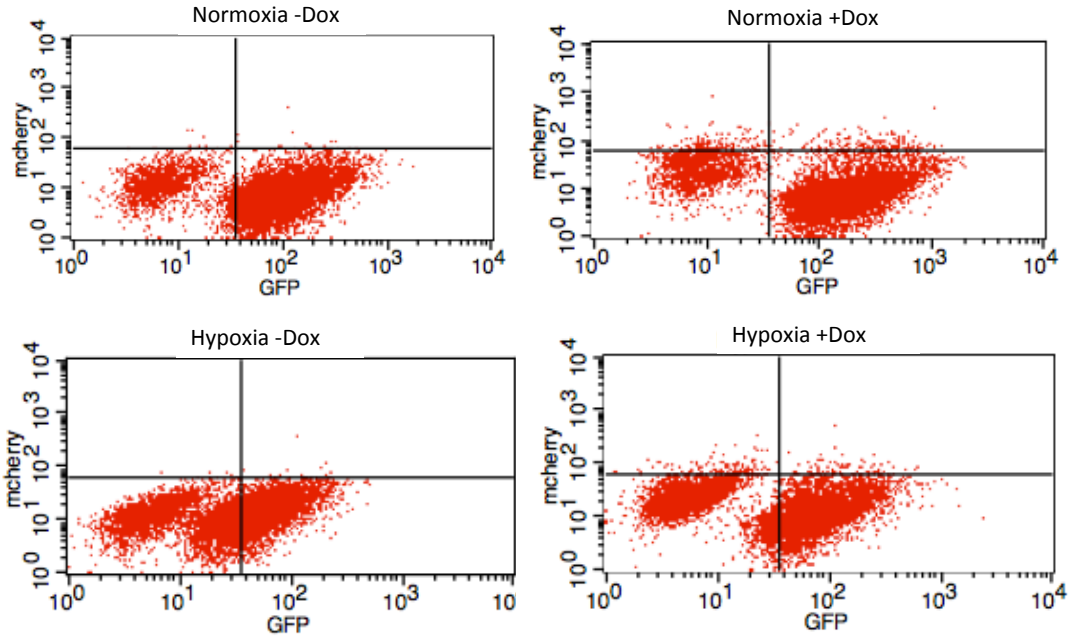

Figure 101: Flow cytometery data for mixed population of T-REx-GFP and T-REx-mCherry cells. Cells were mixed in a ratio of 1:1 and seeded in T25 flasks. Cells were maintained in normoxia or hypoxia with vehicle (-Dox) or 1 µg / mL Dox (+Dox) for 4 weeks. All cells were then exposed to 1 µg / mL Dox for 24 h. Cells were collected, fixed and analysed on a FACSCalibur instrument.

Table 7: Summary data collected from analysis of mixed populations of T-REx-GFP and T-REx-mCherry using a flow cytometer.

Sample	%GFP expressing cells	% mCherry expressing cells
Normoxia -Dox	83	7
Normoxia +Dox	83	7
Hypoxia -Dox	63	6
Hypoxia +Dox	65	14

Analysis was conducted on a FACSCalibur instrument that operates with a two-laser system. This was suitable to detect GFP but the excitation wavelength of mCherry was on the limit of the excitation ability of the instrument. Therefore, it is possible that during analysis, not all the mCherry expressing cells were sufficiently excited to be detected and were counted as negative cells. Comparison of the data collected from negative control cells (T-REx-CLLFVY) with a mixed population of T-REx-GFP and T-REx-mCherry cells shows a clearly distinguishable population of GFP expressing cells, but no mCherry cells (Figure 102). Fluorescence microscopy suggested that all cells were fluorescent, therefore it could be assumed that all the 'not GFP' cells were mCherry expressing cells. With this assumption, it appears that T-REx-mCherry cells are less disadvantaged compared to T-REx-GFP expressing cells in hypoxia than normoxia. As this effect is peptide independent, it is also likely a result of the cells selected during integration, not a result of inhibition of HIF-1 dimerisation. Overall, no firm conclusions can be drawn from this data.

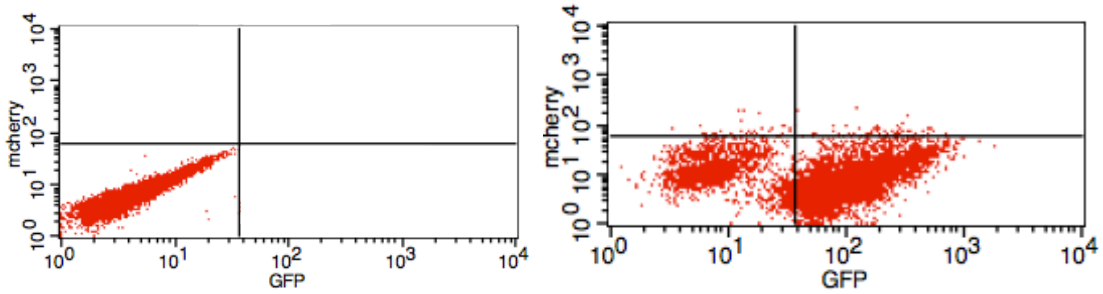

Figure 102: Flow cytometery data for negative control (T-REx-CLLFVY) and mixed population of T-REx-mCherry and T-REx-GFP cells. Cells were incubated with Dox (1 µg/mL) for 24 h, collected, fixed then analysed using a FACSCalibur instrument.

2.2.8.2 Cell counting

A different technique was employed to measure the effect of inhibition of HIF-1 dimerisation on cell growth and viability. T-REx-HRE cells were exposed to normoxia or hypoxia, with or without Dox treatment, for 24 or 48 h. Cells were then collected and counted using a Moxi cell counter instrument. As well as measuring cell number, the instrument provides a Moxi population index ratio (MPI), which uses the size of particles to assess the proportion of live to dead cells.

Cell counting revealed that there was no significant difference in cell number after both 24 and 48 h treatment with Dox compared to untreated cells (Figure 103A). However, there was a significant decrease in the MPI ratio after 24 h in treated compared to untreated cells (Figure 103B), suggesting that inhibition of HIF-1 dimerisation decreased cell viability.

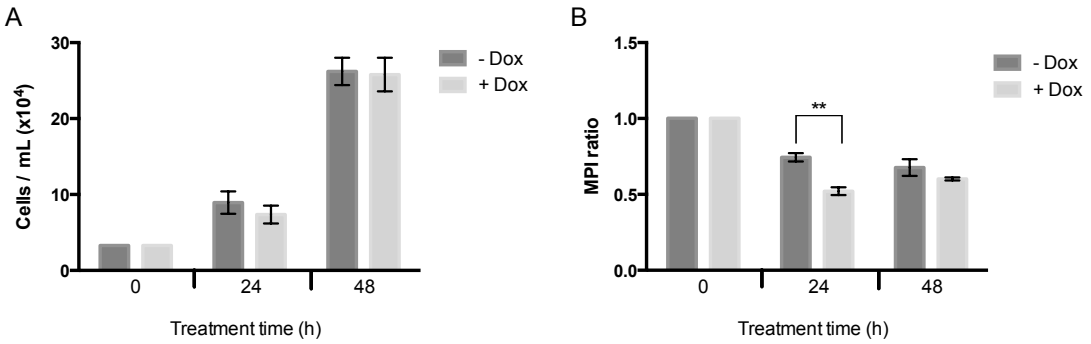

Figure 103: Inhibition of HIF-1 dimerisation in T-REx-HRE cells does not affect cell number but does decrease cell viability. T-REx-HRE cells were plated at equal densities and incubated with vehicle (-Dox) or 1 μg / mL Dox (+Dox) for 24 or 48 h. Post treatment, cells were collected in a set volume, cell number (A) and MPI ratio (B) were assessed using a Moxi-Z instrument. Bars represent means (n=3) ± SEM. Stars denote significant differences between means: **p ≤ 0.01.

2.2.8.3 MTT assay

To further assess the effect of inhibition of HIF-1 dimerisation on cell viability, a colorimetric assay using MTT (3-(4,5-dimethylthiazol-2-yl)-2-5-diphenyltetrazolium bromide) was conducted. NAD(P)H-dependent cellular oxidoreductase enzymes in metabolically active cells can convert the tetrazolium dye MTT to its insoluble formazan (Figure 104), giving an indication of the number of viable cells. The assay was also conducted with T-REx-Scram cells, as a control, to ensure that any effect on number of viable cells was a result of expression of cyclo-CLLFVY, not expression of the inteins or Dox treatment.

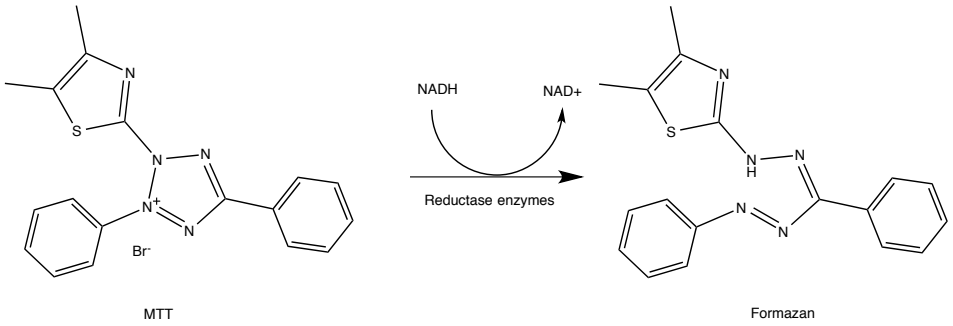

Figure 104: MTT is reduced to a formazan in viable cells. Oxidoreductase enzymes in metabolically active cells reduce MTT (tetrazolium salt) to the insoluble formazan, which can be visualised as a blue precipitate.

Following treatment with Dox for 24 or 48 h, there was no significant difference in the cell viability of T-REx-HRE or T-REx-Scram cells, indicating that expression of neither cyclo-CLLFVY nor cyclo-CFVLYL affected cell viability of T-REx cells under normoxia or hypoxia (Figure 105). It should be noted that although the number of viable of cells incubated in normoxic conditions continued to increase from 0-48 h, the number of viable cells exposed to hypoxia increased for the first 24 h hours, then stopped. Regardless of HIF-1 activity, hypoxia reduces cell proliferation. The same effect was seen in T-REx-HRE and T-REx-Scram cells, and both cell types increased to a similar maximum number of viable cells in both normoxia and hypoxia, supporting that they are comparable in this assay.

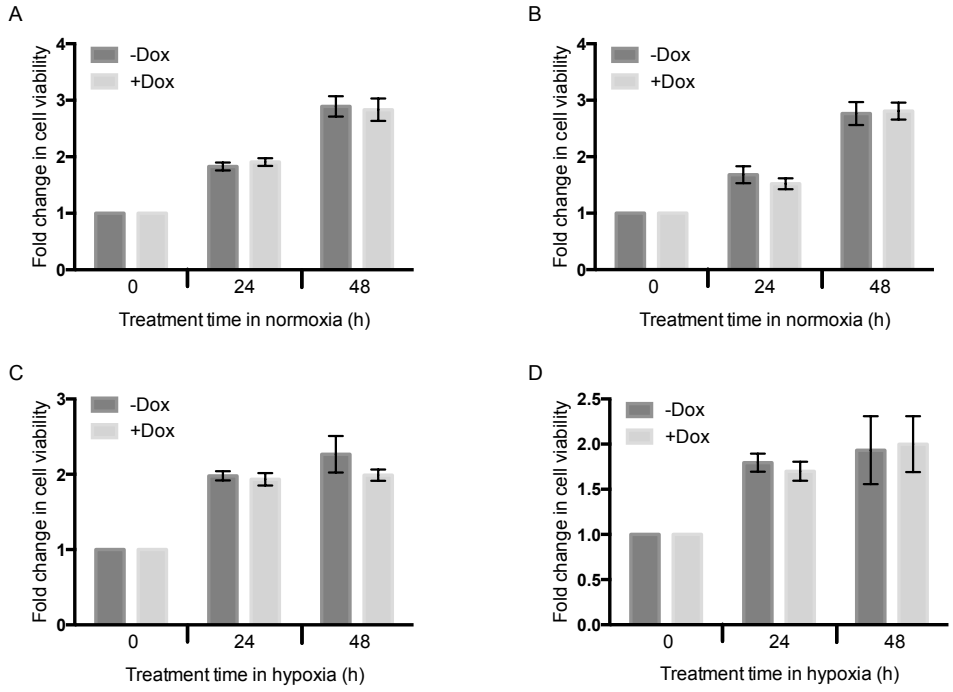

Figure 105: Expression of cyclo-CLLFVY or cyclo-CFVLYL does not affect cell growth. T-REx-HRE (A and C) and T-REx-Scram (B and D) cells were exposed to normoxia (A and B) or hypoxia (C and D) for 0, 24 or 48 h. Cells were incubated with vehicle (-Dox) or 1 μg/ mL Dox (+Dox) for the treatment period (n=4). Cell viability was analysed by MTT assay. Error bars show ± SEM.

To further investigate the effect of inhibition of HIF-1 dimerisation on the growth of T-REx-HRE cells, the assay was extended to longer incubation periods (Figure 106). T-REx-HRE cells continued to proliferate when incubated in normoxic conditions for 72 or 96 h. After 96 h incubation in normoxic conditions, the number of viable cells was 15-fold that at the start of the experiment. The number of viable cells continued to increase under hypoxic conditions, too, however, treatment with Dox significantly impacted cell proliferation, after 96 h incubation. After 96 h incubation, the nutrients, in particular glucose, in the cell media may become limited. The hypoxia-focused microarray showed a number of genes that contribute to cellular adaptation to hypoxia were downregulated when cyclo-CLLFVY was expressed. In the context of a tumour, where concentrations of critical nutrients are heterogeneous,[89] this could prevent angiogenesis, glucose uptake and tumour vascularisation. Such inhibition can result in reduction of tumour size, as has been shown in previous studies with HIF-1α knockdown and dominant negative HIF-1α.[237, 287] However in cell culture, where cells are grown in monolayer, nutrients are readily available to all cells. When these cells are exposed to increased stress, such as glucose deprivation, inability to activate hypoxia-induced genes may have more of an effect, as seen after the extended period of incubation.

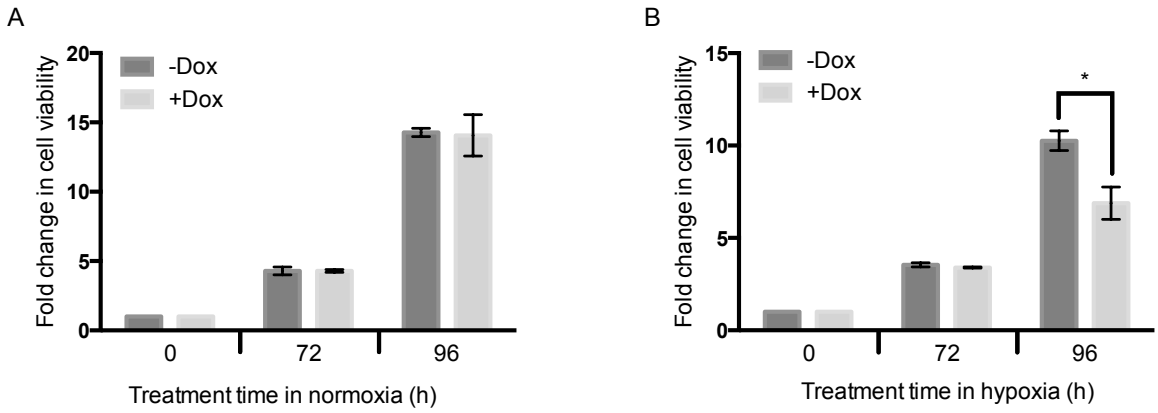

Figure 106: Inhibition of HIF-1 dimerisation supresses growth of T-REx-HRE cells under hypoxia after long incubation periods. T-REx-HRE cells were treated with vehicle (-Dox) or 1μg / mL Dox (+Dox) under normoxia (A) or hypoxia (B) for 0, 72 or 96 h. Cell viability was analysed by MTT assay (n=2). Error bars show ± SEM. Stars denote significant differences between means: *p ≤ 0.05.

The MTT assay was repeated with T-REx-HRE and T-REx-Scram cells cultured in glucose-free medium. In normoxic conditions, glucose deprivation reduced T-REx-HRE and T-REx-Scram cell viability compared to cells cultured in glucose containing medium, but addition of Dox had no significant effect in either cell line (Figure 107A and B). Under normoxia, the number of viable cells increased in the treatment period, but in hypoxia, cell viability decreased, suggesting hypoxia supressed cell proliferation in T-REx-HRE and T-REx-Scram cells lines (Figure 107C and D). However, Dox treatment only had an effect in T-REx-HRE cells (Figure 107C). In T-REx-HRE cells, treatment with Dox, and expression of cyclo-CLLFVY, resulted in a

1.3-fold decrease in cell viability as compared to untreated cells at 24 h. This difference was larger at 48 h, where treatment of cells with Dox resulted in a 1.5-fold decrease in cell viability compared to untreated cells. In contrast, treatment of T-REx-Scram cells with Dox, in hypoxia, in glucose-free conditions, did not affect cell viability.

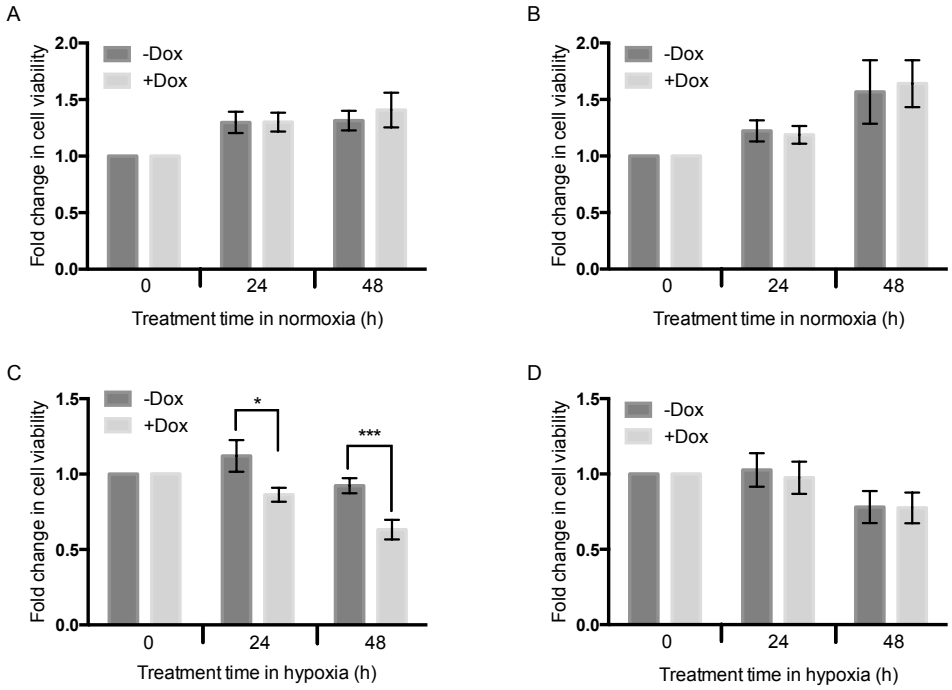

Figure 107: Expression of cyclo-CLLFVY increases sensitivity to glucose deprivation. T-REx-HRE (A and C) and T-REx-Scram (B and D) cells were exposed to normoxia (A and B) or hypoxia (C and D) for 0, 24 or 48 h in medium containing no glucose. Cells were incubated with vehicle (-Dox) or 1 μg/ mL Dox (+Dox) for the treatment period (n=4). Cell viability was analysed by MTT assay. Error bars show ± SEM. Stars denote significant differences between means: *$p \leq 0.05$, ***$p \leq 0.001$.

The cell viability assay with glucose withdrawal was repeated after 72 and 96 h incubation under normoxia or hypoxia to assess if there was any increase in the effect of inhibition of HIF-1 dimerisation (Figure 108). Treatment of T-REx-HRE cells with Dox resulted in a reduction in the number of viable cells by 1.5-fold after 72 h incubation and 1.3-fold after 96 h incubation. These changes were similar to the effect of Dox treatment after 24 and 48 h incubation, 1.3 and 1.4-fold decreases respectively. As the cells were grown in glucose deficient medium, prolonged incubation would not further deprive cells. There was no significant change in the number of viable cells following Dox treatment in normoxic conditions. Together, these results suggest that inhibition of HIF-1 dimerisation increases sensitivity to glucose deprivation in hypoxia.

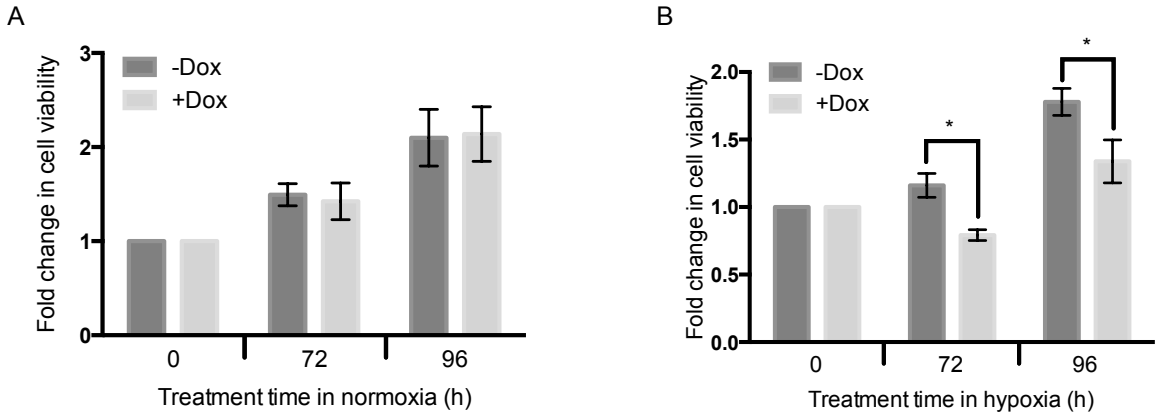

Figure 108: The effect of inhibition of HIF-1 dimerisation on viability of T-REx-HRE cells incubated in glucose-free medium for 0-96 h. T-REx-HRE cells were treated with vehicle (-Dox) or 1µg / mL Dox (+Dox) under normoxia (A) or hypoxia (B) for 0, 72 or 96 h, in glucose-free medium. Cell viability was analysed by MTT assay (n=3). Error bars show ± SEM. Stars denote significant differences between means: *$p \leq 0.05$.

The hypoxia phenotype is characterised by a switch from aerobic to anaerobic metabolism; hypoxic cells become more reliant on glycolysis to meet their energy needs when oxygen is limited.[89] Previous work has shown that treatment of HeLa cells with siRNA targeting HIF-1α increases cell sensitivity to treatment with the glycolysis inhibitor 2-deoxy-d-glucose (2-DG).[151] 2-DG has a hydrogen atom in place of the hydroxyl group on C2 of glucose; therefore it cannot undergo glycolysis and acts as a metabolic block. To assess the synthetic lethality of 2-DG in hypoxic cells with inhibited HIF-1 activity, the MTT assay was repeated with T-REx-HRE and T-REx-Scram cells in glucose containing media, with and without 2-DG treatment.

Unlike with glucose depravation, the number of viable cells continued to increase from 0- 48 h treatment when treated with 2-DG, suggesting 2-DG did not supress cell proliferation in hypoxia. However, in hypoxia, treatment of T-REx-HRE cells with Dox reduced cell growth by 1.4-fold after 24 h and 1.3-fold after 48 h (Figure 109C), suggesting that even though cells under hypoxia could adapt to inhibition of glycolysis by 2-DG, when HIF-1 dimerisation was inhibited, this adaptation was hindered. Dox treatment of T-REx-Scram cells did not significantly change viability of 2-DG treated cells in normoxia or hypoxia (Figure 109B and D).

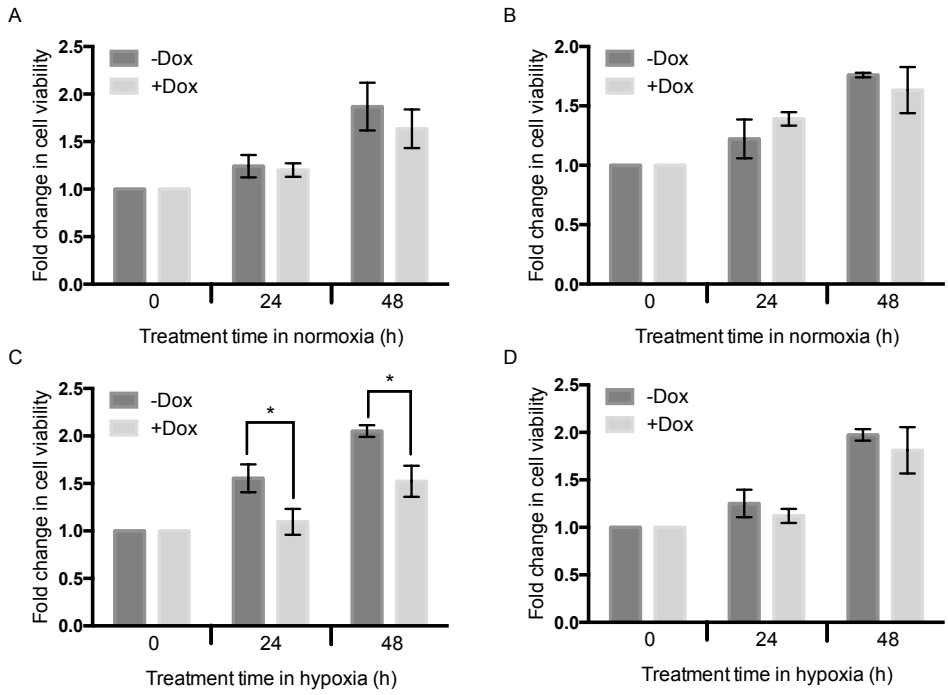

Figure 109: Expression of cyclo-CLLFVY increases sensitivity to 2-DG treatment. T-REx-HRE (A and C) and T-REx-Scram (B and D) cells were exposed to normoxia (A and B) or hypoxia (C and D) for 0, 24 or 48 h in medium containing 3mg/ mL 2-DG. Cells were incubated with no Dox or 1 µg/ mL Dox for the treatment period (n=3). Cell viability was analysed by MTT assay. Error bars show ± SEM. Stars denote significant differences between means: *$p \leq 0.05$.

The assay was repeated in T-REx-HRE cells at longer incubation periods (Figure 110). Following Dox treatment, there was no significant difference in the number of viable cells incubated under normoxia for 72 or 96 h. However, treatment of T-REx-HRE cells with Dox resulted in a 1.6-fold reduction in cell viability after 72 h and a 2.1-fold reduction in cell viability after 96 h. Between 72 and 96 h incubation, there was 4.1-fold increase in the number of viable cells in hypoxia, compared to a 2.8 fold increase in normoxia. This suggests that after 72 h, cells begin to adapt to hypoxic conditions and are able to proliferate rapidly despite inhibition of glycolysis. Inhibition of HIF-1 dimerisation after 96 h appears to prevent this adaptation, but the lower number of viable cells under hypoxia after 96 h could be a result of earlier inhibition of cell proliferation (at 24 and 48 h), leading to a lower cell number when proliferation begins.

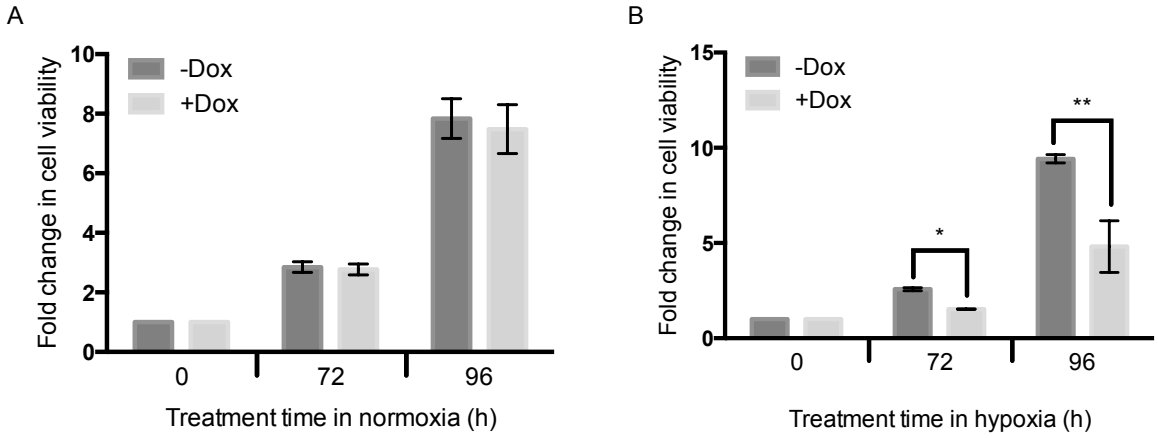

Figure 110: Inhibition of HIF-1 dimerisation in combination with 2-DG glucose treatment has a larger effect on cell viability after longer incubation periods . T-REx-HRE cells were exposed to normoxia (A) or hypoxia (C) for 0, 24, 48, 72 or 96 h in medium containing 3mg / mL 2-DG. Cells were incubated with vehicle (-Dox) or 1 µg / mL Dox (+Dox) for the treatment period (n=2). Cell viability was analysed by MTT assay. Error bars show ± SEM. Stars denote significant differences between means: *$p \leq 0.05$, **$p \leq 0.01$.

These results add to a growing body of evidence that inhibition of HIF-1, or re-direction of cellular pathways away from HIF-1 controlled mechanisms, may improve the anticancer effects of current chemotherapeutic agents. A study in glioblastoma-derived xenograft model showed that resistance to the anti-angiogenic agent Bevacizumab was associated with increased HIF expression and a shift from mitochondrial respiration to glycolysis.[288] Treatment of cells with dichloroacetate to reactivate mitochondrial respiration enhanced the effect of Bevacizumab.[288] This study also found that 2-DG had no additive effect to Bevacizumab, whereas directly knocking down HIF-1α expression was shown to decrease resistance to 2-DG itself in HeLa cells.[151] A similar effect was shown with CCI-779, an analogue of rapamycin, which increased the toxicity of 2-DG through the downregulation of HIF-1α in lung cancer cell lines.[55] In addition, the HIF inhibitors digoxin and acriflavine were shown to decrease resistance to cytotoxic chemotherapeutic agents paclitaxel and gemcitabine in triple negative breast cancer cell lines.[150] Therefore, inhibition of HIF-1 dimerisation could be highly advantageous as a therapeutic strategy by impairing the metabolic plasticity of tumorigenic cells, increasing their sensitivity to chemotherapeutics.

2.3 Adaptation of mammalian SICLOPPS system for transient transfection

Stable integration into mammalian cell lines is a difficult, time-consuming process. The availability of HEK-293 cells integrated with the FRT site for targeted integration facilitated fast, reliable incorporation of the intein-peptide constructs on to the genome of the cell. However, there are few cell lines currently available with this pre-integrated site. To enable study of the effect of inhibition of HIF-1 dimerisation in a range of cancer cell types, the feasibility of using transient transfection to deliver cyclo-CLLFVY was assessed. Transiently transfected genes are not integrated into the host chromosome and so are not replicated with the host genome, and are only expressed for 1-2 days. However, as the peptide was shown to have an effect after 16 h treatment, this period should be sufficient to analyse the activity of the peptide expressed from a plasmid. Variability in transfection efficiencies may also affect the reproducibility of results, and therefore careful controls will be necessary to analyse results.

A mammalian expression vector encoding the cyclic peptide CLLFVY as the extein between Npu inteins with an in-frame CBD at the C-terminus of the N-intein was constructed. The backbone from SV40-Luc was used, replacing the luciferase gene with the Npu-intein construct to give SV40-Npu-CLLFVY (SV40-CLLFVY). To demonstrate expression of the Npu-CLLFVY construct in MCF-7 cells, the DNA sequence encoding mCherry was cloned, in frame, downstream of the N-intein resulting in an intein-mCherry fusion construct. The expression of this construct in MCF-7 cells was visualised by fluorescent microscopy (Figure 111). Although the fluorescent fusion protein permitted observation of intein expression, it does not indicate whether the inteins were able to splice *in vivo*. Previous work in the integrated cell line demonstrated that the inteins can splice in vivo and cyclise the peptide, and so this was assumed in MCF-7 cells too.

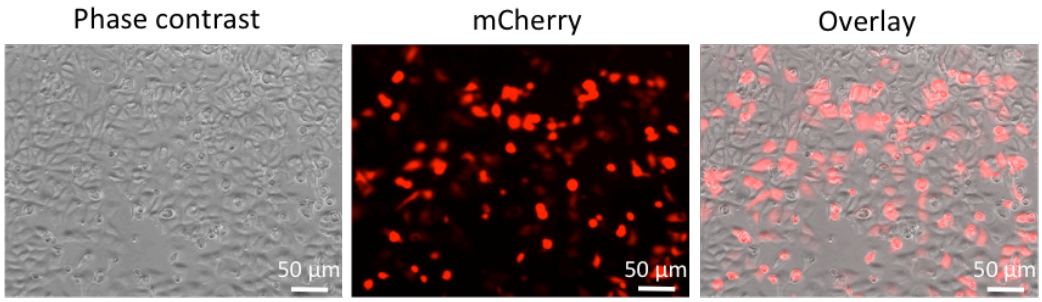

Figure 111: Expression of intein-mCherry fusion protein in MCF-7 cells. MCF-7 cells were transfected with pmCherry-Npu-CLLFVY and incubated for 24 h. Fluorescent signal indicated transfection of the plasmid and expression of the Npu-CLLFVY-mCherry construct.

To maintain a simple system that can be used in any cell line, the TetO2 was not included in the construct. Repression at the TetO2 requires binding of the TET repressor molecule. The gene for the TET repressor molecule (TetR) was stably integrated into T-REx-293 cells, so TetR was endogenously expressed and repressed expression of integrated constructs in the absence of Dox. Repression in MCF-7 cells would require co-transfection of a plasmid expressing the TET repressor molecule, which would complicate assays and potentially result in low reproducibility of results because of differences in transfection efficiencies. However, physiological control of peptide expression was achieved via a HRE promoter. The Npu-CLLFVY construct from SV40-CLLFVY was cloned into HRE-Luc, downstream of the HRE promoter, replacing the DNA sequencing encoding luciferase. Expression of the Npu construct in HRE-CLLFVY was therefore under the control of the HRE promoter.

2.3.1 Extraction of inteins from transiently transfected MCF-7 cells

In order to demonstrate intein splicing from the transiently transfected Npu-CLLFVY construct, a pull-down assay was conducted on protein extracted from MCF-7 cells transfected with SV40-CLLFVY. The proteins eluted from chitin binding beads were visualised by Western immunoblotting. However, immunofluorescence imaging of the blot did not show any bands. Western blotting is a sensitive technique; the enhanced chemiluminescent (ECL) substrate used can detect low picogram levels of protein. However, there is some loss of product during the chitin bead purification process, with a low amount of material to start with, the percentage loss of material may have been too great. Instead, total protein extracted from SV40-CLLFVY transfected cells visualised by Western immunoblotting. Unfortunately, no bands were visible upon immunofluorescent imaging of the blot. Probing of the blot with anti-β-actin HRP gave strong bands at the expected size, verifying that protein extraction and transfer onto the nitrocellulose membrane was successful.

Isolation of the inteins or peptide from mammalian cells may have been limited by the low amount produced because of a low number of cells in the adherent cell layer. Synthetic Tat-cyclo-CLLFVY has been shown to prevent the dimerisation between HIF-1α and HIF-1β in MCF-7 cells.[140] Assessment of downstream effects of inhibition of HIF dimerisation with transfection of the Npu-P1 construct could allow indirect analysis of peptide expression and its effect in MCF-7 cells.

2.3.2 Activity of peptide expressed from transiently transfected construct in MCF-7 cells

2.3.2.1 HRE dependent luciferase assay

The HRE-dependent luciferase assay was adapted to demonstrate the expression and splicing of the Npu-CLLFVY construct and the activity of the peptide in MCF-7 cells. The reporter construct used was HRE-Luc, where the expression of luciferase is controlled by a HRE. Luciferase expression is only induced in hypoxic conditions where HIF-1α is stabilised and can dimerise with HIF-1β forming the HIF-1 transcription factor. However, co-transfection of HRE-CLLFVY would, if the intein construct is expressed and splices, prevent dimerisation of HIF-1α and HIF-1β, preventing the formation of HIF-1 and so expression of luciferase from HRE-Luc would be dampened, even in hypoxia.

Transfection was first optimised with the promoter vector SV40-Luc. Luciferase expression, and therefore transfection efficiency, was highest when 200,000 cells were plated and transfected with a 1:6 ratio DNA: transfection reagent (Figure 112). Therefore this cell number and ratio was used for further MCF-7 experiments.

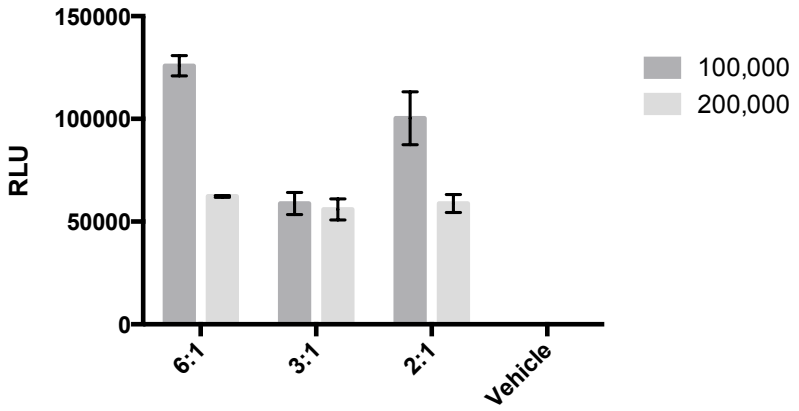

Figure 112: Optimisation of transfection efficiency in MCF-7 cells. MCF-7 cells were plated at 100,000 or 200,000 cells per plate and transfected with a ratio of transfection reagent: plasmid (SV40-Luc) of 6:1, 3: or 2:1, or with a water control and luciferase expression measured after incubation. Experiments were conducted in triplicate (n=2). Error bars represent ±SEM.

The reporter construct HRE-Luc was co-transfected with HRE-CLLFVY or HRE- Scramble in to MCF-7 cells. The luciferase plasmid SV40-Luc was also co-transfected in MCF-7 cells with the intein-peptide encoding plasmids, to ensure any effect of the inhibitor construct was a result of HRE dependent inhibition. The expression of luciferase in SV40-Luc is not dependent on a HRE so inhibition of HIF-1 dimerisation should not affect luciferase expression. Each luciferase construct was also co-transfected with pARCBD-Npu-CLLFVY, a bacterial expression vector encoding the inhibitor that should not be expressed in MCF-7 cells, as a

negative control. Transfected cells were incubated in hypoxia or normoxia for 16 h prior to quantification of luciferase expression.

Co-transfection of HRE-CLLFVY with HRE-Luc resulted in a 2.4-fold decrease in luciferase activity compared to the transfection of HRE-Luc with the control vector (Figure 113A), suggesting that the Npu-CLLFVY construct is expressed in mammalian cells and successfully splices to form the active cyclic peptide. Co-transfection of HRE-Scram with HRE-Luc did not significantly impact luciferase activity, indicating that the decrease in luciferase activity with HRE-CLLFVY transfection is caused by cyclo-CLLFVY, not the inteins. In addition, HRE-CLLFVY and HRE-Scramble did not significantly change the expression of luciferase under the control of an SV40 promoter (hypoxia independent) element (Figure 113A). This corroborates splicing of the inteins, to form the active peptide, cyclo-CLLFVY, which prevents formation of the HIF-1 transcription factor, as the linear peptide has been shown to be inactive.[140]

Interestingly, SV40 controlled luciferase expression was two-fold decreased in cells incubated in hypoxic conditions compared to normoxic conditions (Figure 113B). This is in contrast to results from T-REx cell lines where SV40 controlled luciferase expression was not significantly different under hypoxia compared to normoxia. Similarly, in HeLa cells, SV40 promoted luciferase expression in hypoxia was not significantly different to expression under normoxia.[289] However, in A293T (human embryonic kidney) cells, SV40 promoted gene expression from a transfected plasmid was 50 % lower under hypoxia than normoxia, and this difference was a result of decreased nuclear transport of the transfected DNA.[290] The SV40 DNA targeting sequence has been shown to mediate nuclear transport of plasmid DNA in a cell type specific manner,[291, 292] which may result in differential activity of the SV40 promoter in hypoxia is different cell types.

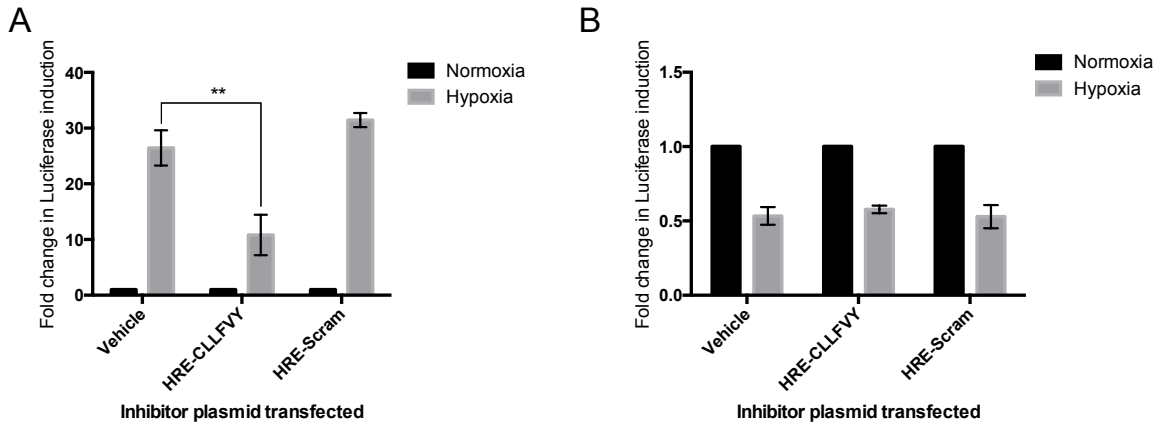

Figure 113: Expression of CLLFVY from a transiently transfected construct inhibits HRE-dependent luciferase expression. MCF-7 cells were co-transfected with either HRE-Luc or SV40-Luc and either pARCBD-Npu-CLLFVY control plasmid, HRE-CLLFVY or HRE-Scram. Transfected cells were incubated in hypoxia (A) or normoxia (B) for a further 16 h and luciferase activity measured. Data is shown relative to luciferase expression with co-transfection of the control plasmid. Experiments were performed in triplicate (n=3). Error bars represent ±SEM. Stars denote significant differences between means: **$p \leq 0.01$.

The impact of cyclo-CLLFVY on luciferase expression in MCF-7 cells was greater than that in TREX cell lines. This may suggest more peptide expression from the transiently transfected HRE-CLLFVY plasmid than the integrated construct in TREX cell lines. In stable transfection, only one copy of the gene is present in each cell whereas with transient transfection, more than one plasmid may enter each cell leading to multiple copies of the gene. Alternatively this increased inhibition could be a result of the format of the experiment. Previously, issues were encountered with this HRE dependent luciferase assay in TREX-HRE cells where luciferase expression was induced before peptide expression. In this co-transfection format of the assay, peptide and luciferase expression may be induced at the same time.

2.3.2.2 qRT-PCR of HIF-1 target genes

To further examine the activity of genetically-encoded cyclo-CLLFVY expression in MCF-7 cells, expression of downstream targets of HIF-1, VEGF and CAIX, were analysed by qRT-PCR. MCF-7 cells were transfected with HRE-CLLFVY or HRE-Scramble and exposed to normoxia or hypoxia for 16 h. Transfection of HRE-CLLFVY, and expression of cyclo-CLLFVY, supressed VEGF expression 2.7-fold, decreasing its expression to normoxic levels (Figure 114A). CAIX expression under hypoxia was reduced 1.4-fold by inhibition of HIF-1 dimerisation (Figure 114B), similar to that in T-REx-CLLFVY cells (1.3-fold).

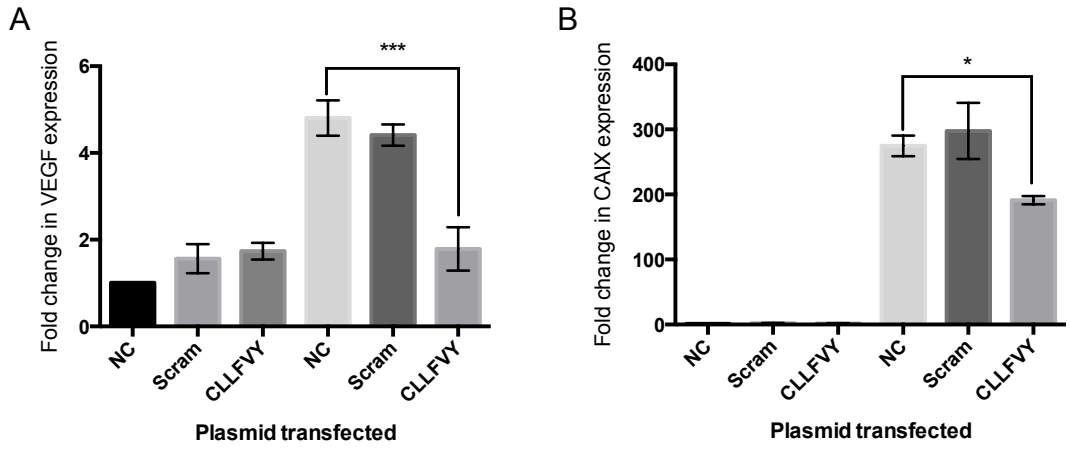

Figure 114: Transfection of HRE-Npu-CLLFVY decreases hypoxia-induced VEGF and CAIX expression. MCF-7 cells were transfected with HRE-CLLFVY (CLLFVY), HRE-Scram (Scram) or a negative control (pARCBD-Npu-CLLFVY; NC) and incubated in normoxia or hypoxia for 16 h, VEGF (A) and CAIX (B) expression was quantified by qRT-PCR. Experiments were conducted in triplicate (n=3) and results were normalised to expression of 18S and β-actin. Error bars represent ±SEM. Stars denote significant differences between means: *$p \leq 0.05$, ***$p \leq 0.001$.

Hypoxic induction of VEGF and CAIX was higher in MCF-7 cells than T-REx-CLLFVY cells (approximately five-fold and 275-fold in MCF-7 cells compared to three-fold and 80-fold in T-REx-CLLFVY cells, respectively). Increased hypoxic induction could be due to lower background expression and stabilisation of HIF-1αin MCF-7 cells leading to lower expression of HIF-1 target genes in normoxia. qRT-PCR analysis of HIF-1α expression in MCF-7 and T-REx-293 cells showed that normoxic expression of HIF-1α was 1.6-fold higher in T-REx-293 cells than MCF-7 cells (Figure 115). After 16 h hypoxia, HIF-1α expression increased 1.7-fold in MCF-7s and 1.4-fold in T-REx-293 cells.

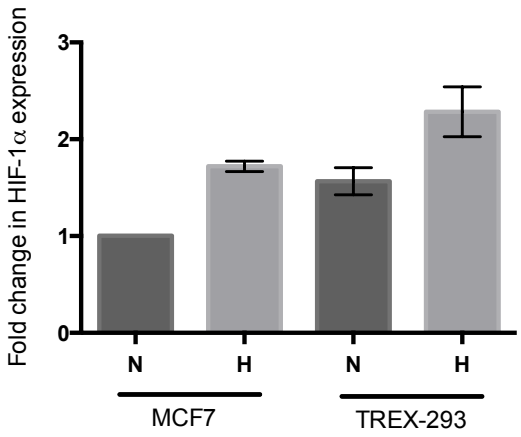

Figure 115: Expression of HIF-1α in MCF-7 and T-REx-293 cells. Cells were incubated in normoxia (N) or hypoxia (H) for 16 h and HIF-1α expression analysed by qRT-PCR. Experiments were conducted in triplicate (n=3) and results were normalised to expression of 18S and β-actin. Error bars represent ±SEM

The activity of the genetically expressed peptide was compared to that of its synthetic equivalent using previous work in MCF-7 cells with synthetic Tat-tagged cyclo-CLLFVY.[140] When compared to qRT-PCR analysis of VEGF expression in MCF-7 cells dosed with synthetic Tat-cyclo-CLLFVY, the 2.6-fold change in VEGF expression recorded in this study with co-transfection of HRE-CLLFVY, aligns with a synthetic peptide dose of ~50-100 μM.[140] The actual amount of peptide produced is likely less than this, as the 100 μM figure refers to the concentration of peptide in the cell media rather than concentration in the cell. The genetically-encoded peptide is produced directly in cells, so there is no issue with low cell permeability of the peptide requiring a higher dose of the synthetic peptide to achieve the same biological response. However, if the total concentration of peptide expressed from HRE-CLLFVY was assumed to be a maximum of 100 μM, this corresponds to 0.1 mg / mL of the peptide.

2.4 Specificity of peptide activity- transfection into 786-O cells

The transient transfection system was applied to 786-O cells to assess the specificity of cyclo-CLLFVY activity. 786-O renal carcinoma cells do not express HIF-1α;[40]this was verified experimentally by qRT-PCR (Figure 116A). 786-O cells are also VHL deficient and thus strongly express HIF-2α, which has been shown to activate the expression of VEGF and GLUT-1 in hypoxia, whereas CAIX requires HIF-1α for transactivation.[97, 265, 286, 293] qRT-PCR analysis of mRNA extracted from 786-O cells exposed to hypoxia showed hypoxic upregulation of VEGF and GLUT-1 but not CAIX (Figure 116B), therefore, GLUT-1 was used instead of CAIX as a reporter gene of cyclo-CLLFVY activity for transfection studies in 786-O cells.

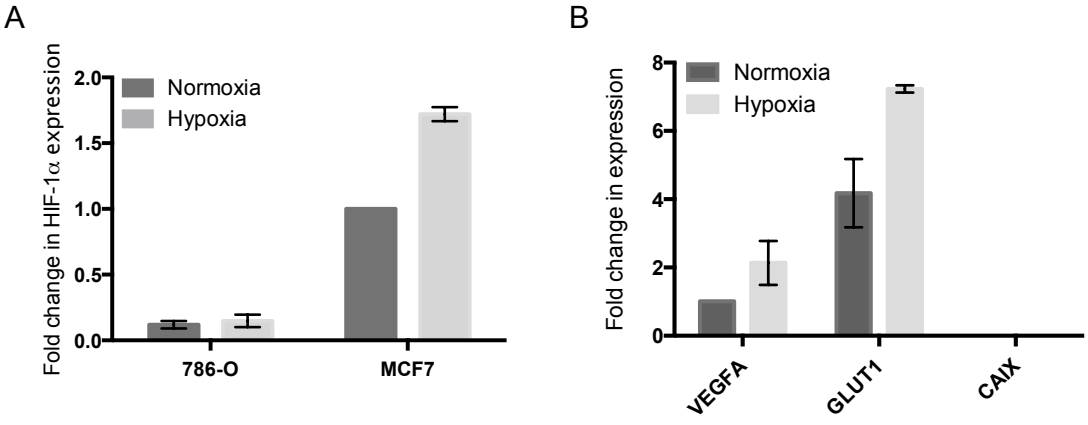

Figure 116: HIF-1α and CAIX are not expressed in 786-O cells. 786-O and MCF-7 cells were incubated in normoxia or hypoxia for 16 h. qRT-PCR was used to analyse expression of HIF-1α in both cell lines (A) and VEGF, GLUT1 and CAIX expression in 786-O cells (B). Experiments were conducted in triplicate (n=2) and results were normalised to expression of 18S and β-actin. Error bars represent ±SEM

786-O cells were transfected with the Npu-CLLFVY/mCherry construct and expression of the construct visualised by fluorescent microscopy (Figure 117). 786-O cells were then transfected with HRE-CLLFVY, or pARCBD-Npu-CLLFVY as a negative control, and exposed to hypoxia for 16 h. VEGF and GLUT-1 expression, under hypoxia, in cells transfected with HRE-CLLFVY was not significantly different to that in untreated cells (Figure 118), suggesting specificity of the peptide for HIF-1α over HIF-2α. In addition transfection of the peptide did not impact normoxic expression of VEGF or GLUT-1.

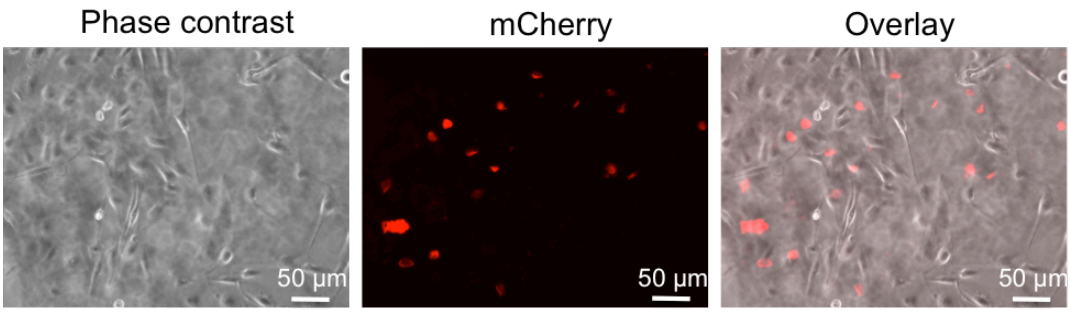

Figure 117: Expression of intein-mCherry fusion protein in 786-O cells. 786-O cells were transfected with pmCherry-Npu-CLLFVY and incubated for 24 h. Fluorescent signal indicated transfection of the plasmid and expression of the Npu-CLLFVY-mCherry construct.

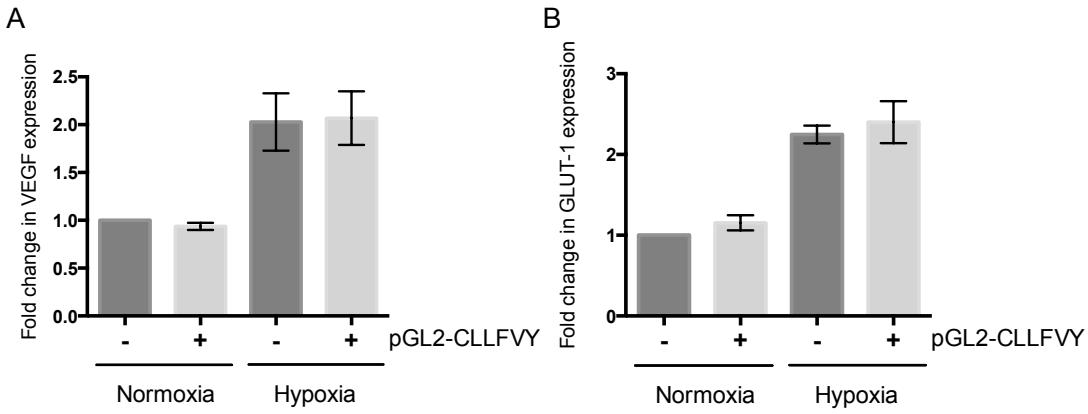

Figure 118: Transfection of Npu-CLLFVY construct into 786-O cells does not affect VEGF or GLUT-1 expression. 786-O cells were transfected with pGL2-Npu-CLLFVY (+) or pARCBD-Npu-CLLFVY as a negative control (-) for 24h then incubated in normoxia or hypoxia for 16h. VEGF (A) and GLUT-1 (B) expression was analysed by qRT-PCR. Experiments were conducted in triplicate (n=3) and results were normalised to expression of 18S and β-actin. Error bars represent ±SEM.

2.5 Chapter 2 discussion

The response to hypoxia in mammalian cells is principally orchestrated by the HIF-1 transcription factor. Over 100 direct targets of HIF-1 have been identified and HIF signalling is also linked to multiple other cellular pathways. HIF-1 activity is often de-regulated in human cancers, and this is associated with tumour progression and resistance to chemotherapy. Therefore, a detailed understanding of the role of HIF-1 in hypoxic response is key to developing cancer therapeutics. Chapter 2 describes the construction and validation of a mammalian expression system for the production of the HIF-1 dimerisation inhibitor cyclo-CLLFVY in mammalian cells (HEK-293). In addition, described in the chapter is the use of *in situ* cyclo-CLLFVY production to study the effect of inhibition of HIF-1 dimerisation on the transcriptional program and the metabolic flexibility of hypoxic HEK-293 cells.

Analysis of HIF-1 target genes was used to assess the downstream effect of inhibition of HIF-1 dimerisation. In T-REx-HRE cells, hypoxic induction of VEGF and CAIX expression was reduced 1.3-fold after 16 h Dox treatment, and 1.7 and two-fold, respectively, after 24 h Dox treatment. In contrast, there was no significant difference in VEGF and CAIX expression in T-REx-HRE cells after 4 or 8 h Dox treatment. Expression of both target genes was similar to that in normoxia at 4 and 8 h, then significantly increased compared to normoxia at 16 and 24 h. Together these results suggested that the level of inhibitory effect of cyclo-CLLFVY on HIF-1 target gene expression was dependent on the timing of peptide and target expression in hypoxia rather than the amount of peptide expressed. Such an effect was also noted for Topotecan (a topoisomerase inhibitor with HIF-1 inhibitory activity) in U251 cells.[260] Hypoxic accumulation of HIF-1α protein was inhibited 70% by topotecan at 6 h and completely abrogated at 24 h.[260] However, many studies of HIF-1 inhibitors conduct hypoxic experiments at only one time point.[139, 140, 146, 148, 258] Consideration of temporal effects on the activity of HIF inhibitors may aid translation of such compounds to the clinic by allowing optimisation of dosing regime, or through the use of a compound with inducible activity.

Having demonstrated the inhibition of HIF-1 dimerisation by genetically-encoded cyclo-CLLFVY in T-REx-HRE cells, the role of HIF-2α in the system was analysed. Hypoxic induction of VEGF was decreased in T-REx-HRE cells treated with HIF-2α siRNA, and a combination of HIF-2α siRNA and Dox treatment significantly decreased VEGF expression further. When T-REx-HRE cells were treated with Dox and HIF-2α siRNA, hypoxic VEGF expression was not significantly different to that in normoxia. The same effect was recorded in T-REx-CLLFVY cells. In contrast, HIF-2α siRNA had no significant impact on CAIX expression in hypoxia in T-REx-HRE cells, whereas Dox treatment halved it, which is in agreement with reports of CAIX as a HIF-1-specific target.[97, 265]

Separating the effects of disruption of HIF-1 dimerisation and HIF-2-mediated transcriptional activation allowed identification of VEFG as a target of both transcription factors and CAIX as HIF-1-specific. Therefore it was hypothesised that this methodology could allow the identification of other HIF-1 or HIF-2-specific targets in T-REx-HRE cells. A microarray was used to gain an overall view of the effect of inhibition of HIF-1 dimerisation and of knockdown on HIF-2α siRNA on the transcription of hypoxia-related genes in T-REx-HRE cells.

Inhibition of HIF-1 dimerisation prevented expression of genes involved in angiogenesis, ADM, ANGPLT4 and VEGFA, and erythropoiesis, EPO. Following Dox treatment of cells, expression of ADM and EPO was decreased to normoxic levels, whereas following treatment of cells with HIF-2α siRNA, there was no significant change. In contrast, although inhibition of HIF-1 dimerisation significantly reduced ANGPLT4 and VEGF expression, three-fold and 1.7-fold respectively, a combination of both Dox and HIF-2α siRNA treatments was required to reduce gene expression to normoxic levels. These genes are well characterised as HIF targets;[87, 267, 268] these results suggest that ADM and EPO expression is principally mediated by HIF-1 in these cells whereas ANGPTL4 and VEGF expression is transactivated by HIF-1 and HIF-2, in hypoxia. Together, the inhibitory affect of cyclo-CLLFVY expression on genes involved in the promotion of angiogenesis and erythropoiesis indicates the potential of targeting HIF-1 dimerisation as a therapeutic strategy to prevent tumour vascularisation.

Expression of cyclo-CLLFVY also resulted in a decrease in a number of genes involved in growth and proliferation. The expression of IGFBP1 and TGFBR2, genes involved in growth factor signal transduction, was decreased following Dox treatment of cells. In addition, following treatment of cells with Dox expression of synthases NOS1, NOS2A and NOS3 was reduced. NOS2A and NOS3 have previously been identified as direct transcriptional targets of HIF-1 and HIF-2,[280-282] but these results suggest that NOS1 expression is also upregulated by HIF-1 in hypoxia. NO stabilises HIF-1α protein in normoxic conditions and has been shown to increase HIF-1 binding activity.[83] HIF-1-mediated transactivation of NOS1 may result in positive feedback of HIF-1 activity.

In contrast to genes involved in the promotion of growth and proliferation, the expression of the tumour suppressor ING4 was increased following inhibition of HIF-1 dimerisation. ING4 has previously been shown to supress activation of HIF-1 through association with prolyl hydroxylases.[283] These results further demonstrate the altered behaviour of the cell line with disrupted HIF-1 signalling.

Of note was the expression of NOTCH-1, which halved following Dox treatment but doubled following HIF-2α siRNA treatment, suggesting positive regulation by HIF-1 but suppression

by HIF-2. Contrasting properties of HIFs in NOTCH1 regulation have also been noted in glioma stem cells. Notch signalling plays a key role in the maintenance of pluripotency in stem cells and is required for hypoxia-induced maintenance of stem cell characteristics.[108] In glioma stem cells, HIF-1α activated Notch signalling HIF-2α repressed it. This difference was attributed to differential (competitive) binding of the two transcription factors to Notch intracellular domain receptors.[107] Such conflicting roles of HIF isoforms underline the need for specific therapeutics that can distinguish between them, such as cyclo-CLLFVY. In addition, this data demonstrates the value of the cell line as a biological probe.

Inhibition of HIF-1 dimerisation and HIF-2α siRNA treatment also significantly impacted upstream effectors of oxygen-dependent regulation of HIF-1. Following treatment with Dox, the expression of PHD2 and PHD3 was decreased whereas HIF-2α siRNA treatment had no effect. Expression of PHD2 and 3 has previously been shown to be induced by hypoxia, and PHD1 expression has been shown to be constitutive, in a number of cell lines.[39, 49] In U2OS cells a two-fold induction of PHD2 and 3 expression in hypoxia was abrogated by transfection of HIF-1α siRNA but not HIF-2α siRNA, suggesting that PHD2 and PHD3 are hypoxic targets of HIF-1 only, in agreement with the array data.[49] This concordance with of the effect of inhibition of HIF-1 dimerisation via the genetically-encoded peptide, on hypoxic gene expression, further supports the validity of this technique to study HIF-1 biology.

Similarly, treatment of cells with Dox resulted in a 1.3-fold decrease in FIH expression whereas HIF-2α siRNA had no significant effect. HIF-1 is thought to mediate response to acute hypoxia whereas HIF-2 is the prominent driver of adaptation to prolonged periods of hypoxic conditions.[78, 105] Upregulation of hydroxylases by HIF-1 in hypoxia allows more rapid degradation of HIF-1α and HIF-2α upon reoxygenation, to prevent HIF-1-mediated transactivation in normoxia. However, HIF-2 may have no such effect on hydroxylases because it is associated with chronic hypoxia.

As cyclo-CLLFVY expression reduced the expression of many hypoxia-induced genes, including those involved in growth factor signalling TGFBR2 and IGFBP1 and proliferation DDIT4 and FRAP1, it was postulated that the peptide could impact cell growth. Expression of cyclo-CLLFVY made no significant difference to the growth of T-REx-HRE or T-REx-Scram (used as a negative control) cells in normoxia or hypoxia. However, when cells were subjected to glucose deprivation, Dox treatment resulted in a significant decrease in T-REx-HRE cell growth after 24- 72 h treatment in hypoxia. In contrast, Dox treatment made no significant difference to cell growth of T-REx-Scram cells in hypoxia, or that of normoxic cells, in glucose-free conditions. The hypoxia-focused microarray showed that hypoxic induction of genes related to metabolism PRKAA1, PRKAA2 and GLUT8 were inhibited by Dox treatment.

This downregulation of metabolism-regulated genes may increase sensitivity of T-REx-HRE cells to glucose withdrawal leading to reduced cell growth.

There was also a significant difference in cell growth with Dox treatment of T-REx-HRE cells incubated with 2-deoxyglucose (2-DG). T-REx-HRE cells continued to grow in the presence of 2-DG alone, but in combination with Dox treatment, cell growth was inhibited, further indicating that inhibition of HIF-1 dimerisation decrease the metabolic flexibility of hypoxic cells. Therefore targeting cancer cells with aberrant metabolic activity with HIF-1 inhibitors may improve activity of therapeutics and decrease resistance to them.

The transcriptional micro-array and cell viability assays demonstrated the application of *in situ* cyclo-CLLFVY production to studying HIF-1 pathways. However, it was noted that some results that contrasted with findings in T-REx-HRE cells had previously been reported in other cell lines. For example disruption of HIF-1 dimerisation by cyclo-CLLFVY led to the identification of HIF-3α as a target of the HIF-2 transcription factor in hypoxia in T-REx-HRE cells whereas HIF-3α had been identified as a target of HIF-1 in other cell lines. This highlights the importance of studying HIF pathways in different cell lines to act as models for different cancer phenotypes. To facilitate the application of this methodology to other cell lines, the *in situ* cyclo-CLLFVY expression system was adapted for transient transfection of the Npu-CLLFVY construct.

A vector encoding Npu-CLLFVY under the control of a HRE promoter was constructed. Co-transfection of this plasmid with HRE-Luc into MCF-7 cells resulted in a decrease in HRE dependent luciferase expression, indicative of cyclo-CLLFVY expression and inhibition of HIF-1 dimerisation in MCF-7 cells from the transiently transfected vector. In addition, transfection of HRE-CLLFVY and into MCF-7 cells resulted in suppression of VEGF expression in hypoxia to that recorded in normoxic MCF-7 cells. An inhibitory effect of HRE-CLLFVY transfection on CAIX expression was also recorded. In contrast, transfection of HRE-CLLFVY into HIF-1α deficient 786-O cells resulted in no significant difference in hypoxic VEGF or GLUT-1 expression, supporting the selectivity of the inhibitor peptide for HIF-1 over HIF-2. Together these results demonstrate the ability to study inhibition of HIF-1 dimerisation in other cancer cell lines via expression of cyclo-CLLFVY from a transiently transfected genetically-encoded construct.

Overall, a novel technique to study the HIF-1 pathway in a tumorigenic cell line was developed. A cell line expressing the HIF-1 dimerisation inhibitor cyclo-CLLFVY under a hybrid HRE/TetO2 promoter was engineered and the peptide was shown to be active in cells. Previous approaches to explore the HIF pathway by disrupting HIF-1 have targeted transcription with techniques such as siRNA and antisense mRNA, but these methods prevent

expression of HIF-1α or HIF-1β entirely, rather than specifically modulating their role in hypoxia.[237, 238] Evidence of roles of HIF-1α independent of its canonical function as a transcription factor is emerging. For example, in U2OS cells and xenografts, HIF-1α was shown to supress DNA repair by counteracting c-Myc transcriptional activity, in a mechanism independent of HIF-1β.[294] In addition, HIF-1α was found to bind to p53 via its ODDD and disrupt p53 binding to DNA.[295] These alternative roles of HIF-1α in hypoxia underlie the advantage of specifically inhibiting HIF-1 dimerisation compared to genetic ablation of the protein. Therefore the approach presented here has great potential to inform on monomer functions of HIF-1α or roles of HIF-1α with binding partners other than HIF-1β. Furthermore, not only is this cell line a useful tool to study HIF biology, it provides a framework methodology that can be applied to other cyclic peptide inhibitors of mammalian signalling pathways.

Chapter 3: Probing the epigenetic regulation of HIF-1α

DNA methylation in cancer cell lines appears to dampen their response to hypoxia by preventing binding of HIF-1 to the HREs of target genes and subsequent transcriptional activation.[94, 185] During normal mammalian development, cells experience hypoxic conditions due to rapid cell division.[242] This is comparable to cells in tumour tissue. Analysis of the epigenetic control of these genes in embryonic DNA can shed light on their regulation in cancer. As the epigenetic status of the HIF-1α HRE in developing tissue was unknown, the aim of this section of work was to analyse the methylation status of HIF-1α and its target EPO in embryonic DNA samples. The embryonic samples were bisulfite treated, then analysed by methylation specific PCR (MSP) and bisulfite sequencing (BS).

3.1 Bisulfite conversion

Treatment of DNA with sodium bisulfite in basic conditions leads to conversion of unmethylated cytosine residues to uracil by deamination at the C4 position of the pyrimidine ring (Figure 119). However, 5-methyl-cytosine (5mC) does not react with sodium bisulfite as the inductive effect of the methyl group at C5 prevents sulfonation at C6 and subsequent deamination at C4.[296-298] Bisulfite treated DNA can be used for downstream analysis of methylation status. PCR amplification of the treated DNA will distinguish between methylated and unmethylated native DNA. Unmethylated cytosine residues that have been converted to uracil will base pair with adenine on the antisense strand and therefore be amplified by PCR as thymine on the sense strand (Figure 120). 5mC however, which remains 5mC after bisulfite treatment will base pair to guanine on the antisense strand and be amplified as cytosine on the sense strand. Therefore, the methylation status of the native DNA can be inferred from the bisulfite treated DNA by PCR with specific primers or sequencing of resulting PCR amplicons.

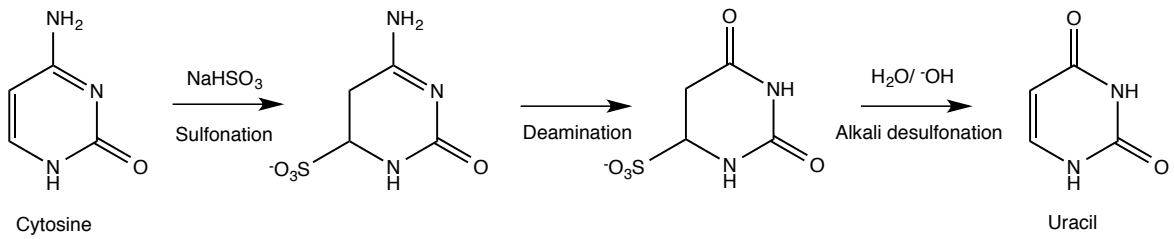

Figure 119: Mechanism of bisulfite conversion of cytosine to uracil. The pyridine ring is activated by sulfonation, which in aqueous conditions results in deamination at the C4 position. Alkali conditions lead to de-sulfonation and formation of Uracil.

	Unmethylated	Methylated
Native DNA	ATCGTG	ATCGTG
Bisulphite treated DNA	ATUGTG	ATCGTG
PCR template	ATUGTG	ATCGTG
Antisense	TAACAC	TAGCAC
Sense	ATTGTG	ATCGTG

Figure 120:Bisulfite conversion followed by PCR allows differentiation of unmethylated and methylated DNA. Unmethylated cytosine residues are converted to uracil and during PCR amplification will base pair with adenine on the antisense strand and so be amplified as thymine on the sense strand. Methylated cytosine residues will not be converted and so remain at cytosine residues in the PCR amplified product.

3.2 Methylation specific PCR

In MSP, modified DNA is amplified with primers specific for methylated or unmethylated DNA.[299] Unmodified or incompletely modified DNA can also be distinguished, as there are marked differences between these DNA sequences as cytosine methylation predominately takes place at CpG dinucleotides in vertebrates.[300] Therefore the presence of cytosine residues that are not part of CpG dinucleotides in bisulfite treated DNA is indicative of failed modification.[301] In contrast, the presence of cytosine residues in CpG dinucleotides in treated DNA shows methylation of these residues in native DNA. The primers are designed such that in those specific for methylated DNA (M primers), the cytosine residues that are conserved because of their methylation are placed at the 3' end and in the primers specific for unmethylated DNA (U primers), thymidine derived from converted cytosine residues are placed at the 3' end.[302] This positioning results in greatest discrepancy between methylated and unmethylated DNA because any mismatches will impede PCR amplification. Agarose gel electrophoresis of PCR products should show products only for the primer set that match the methylation status of the DNA.

Primers specific to methylated or unmethylated DNA were designed to amplify the 200 bp region around the HRE of the HIF-1αgene using methprimer, a web-based primer design software (Figure 121, Table 8).[303] Each set of primers were used to amplify the HRE containing region of the HIF-1α gene promoter from bisulfite converted MCF7 DNA. The HRE of HIF-1α is unmethylated in MCF7 cell lines and therefore should only be amplified by the U primer set.[140]

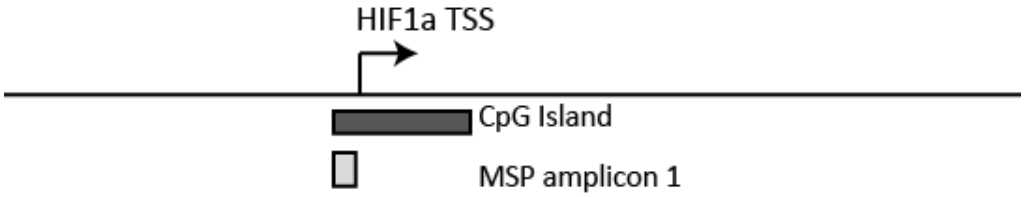

Figure 121: Graphical representation of the region of the HIF-1α promoter analysed. The M and U primers (1) amplify the portion of the CpG island in the promoter of HIF-1α that contained the HIF-1α HRE.

Table 8: Sequences of M and U primers (1) for the 200 bp region surrounding the HIF-1α HRE.

Primer	Sequence
Left M primer (1)	5'GATGTATGTTTGGGATTAGGTAATC 3'
Right M primer (1)	5'TCAACTAAAACACAACTAAAACGAA 3'
Left U primer (1)	5' TGTATGTTTGGGATTAGGTAATTGA 3'
Right U primer (1)	5' ATCAACTAAAACACAACTAAAACAAA 3'

Surprisingly, there were no PCR products for either set of primers, despite varying the annealing temperature of the reaction between 40 and 60 °C to optimise binding of primers to the target DNA region. Low molecular weight bands were visualised for all samples, particularly for the M primer pair (Figure 122). When the 3' end of one primer anneals to itself or to the second primer it can lead to primer extension, resulting in 'primer-dimers'. There is a degree of complementarity between the left and right primers of each set so the primers could be forming primer dimers preferentially to priming the DNA for extension by DNA polymerase. The addition of 5% DMSO and varying the concentration of $MgCl_2$ did not reduce primer dimer formation.

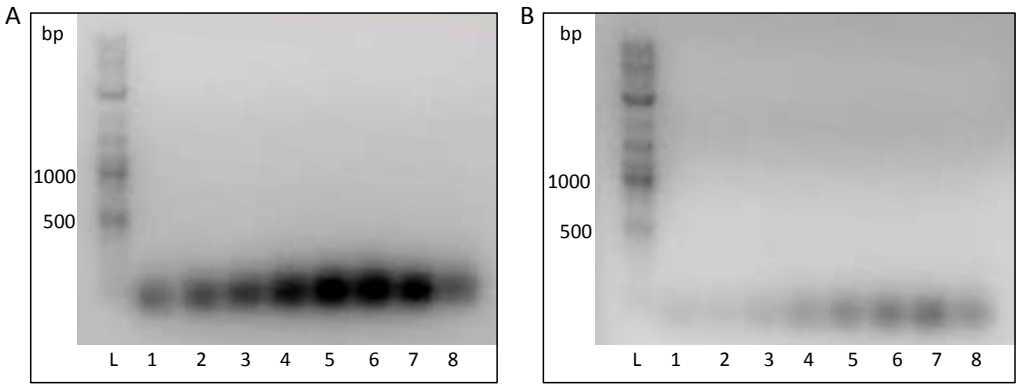

Figure 122: Representative agarose gel electrophoresis visualisation of PCR products. PCR amplification of bisulfite treated MCF7 DNA with M (A) and U (B) primer sets (1) only gave rise to primer-dimer products. Here, annealing temperature was varied from 50 °C (lane 1) to 60 °C (lane 8). Products are shown relative to a 2-log DNA ladder (lane L).

Alternative primers with less hetero-complementarity were designed (Figure 123, Table 9). They also contained more CpG sites, so that the M and U sets of primers were more dissimilar and could distinguish between methylated and unmethylated DNA with more stringency. Each set of primers was used to amplify bisulfite treated MCF7 DNA. Although there was less primer dimer formation, there were still no products of the expected length of 200 bp (Figure 124).

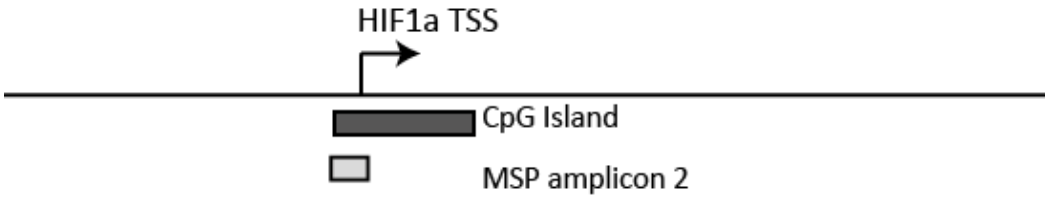

Figure 123: Graphical representation of the region amplified by M and U primers (2). The amplicon (325 bp) is larger than that of primers (1) but overlaps the same CpG island region of the HIF-1α promoter.

Table 9: Sequences of alternative M and U primer sets (2) for amplification of HIF-1α HRE. The primers have lower hetero-complementarity, and cover more CpG dinucleotide sites on the target DNA than the M and U (1) primers.

Primer	Sequence
Left M primer (2)	5'AGGCGTAGAGTTTTTAGATTC3'
Right M primer (2)	5'AAACGAACAAAAACGAAAAC 3'
Left U primer (2)	5'TGTAGAGTTTTTAGATTT 3'
Right U primer (2)	5'AAATGAATAAAAATGAAAAT3'

GoTaq DNA polymerase (Promega) was used for PCR amplification, this is not a 'Hot-start' polymerase and this may be the cause of the lack of products. 'Hot start' polymerases are coupled with an antibody that blocks polymerase activity at ambient temperatures. An initial denaturation step is added to the reaction, prior to PCR cycling, in order to activate the polymerase. This additional hot start step is useful for GC rich sequences as it allows the highly stable DNA to denature more fully. The target region of DNA is GC rich (it is part of a CpG island in the promoter of the HIF-1α gene), so the use of a hot start enzyme may be beneficial. The bisulfite treated DNA was amplified with both sets of M and U primers with Platinum Taq DNA polymerase (LifeTechnologies). With the HotStart enzyme no primer dimers were formed, however, the target region was not amplified either.

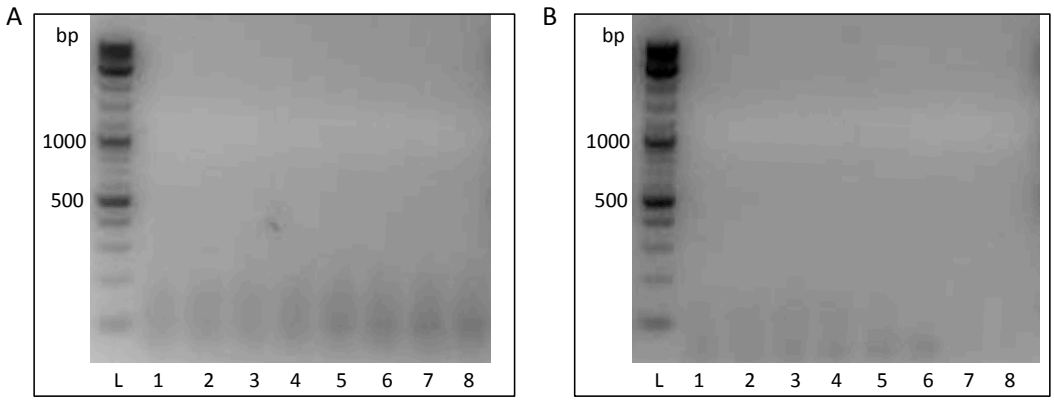

Figure 124: Representative agarose gel electrophoresis visualisation of PCR products. PCR amplification of bisulfite treated MCF7 DNA with M (A) and U (B) primer sets (2) resulted in less primer dimer formation but still no amplification of the HIF-1α HRE. Here, annealing temperature was varied from 45 °C (lane 1) to 55 °C (lane 8). Products are shown relative to a 2-log DNA ladder (lane L).

This region of DNA may not be suitable for analysis by MSP as it is GC rich. The target might not fully denature during PCR so primers cannot bind. Alternatively, the primers may not be optimal for PCR because they contain regions of repeated residues. Repeats in the primers can cause mis-priming and inefficient PCR amplification. As a specific region of DNA is targeted, the design of the primers is limited so they cannot be improved further. As the MSP was not successful despite extensively optimising PCR conditions including the primers and polymerase, it was decided that bisulfite sequencing would be used to investigate the methylation status of the HIF-1α HRE.

3.3 Bisulfite sequencing

3.3.1 Method optimisation

For bisulfite sequencing, bisulfite treated DNA is amplified by 'universal' primers: PCR primers that amplify bisulfite treated DNA regardless of methylation status. The primers target regions of the DNA that do not contain CpG dinucleotides so should not be different in unmethylated or methylated DNA. The PCR amplification is conducted with a Taq family DNA polymerase that has inherent non-template dependent terminal transferase activity that preferentially adds a single deoxyadenosine residue to the 3' ends of PCR products.[304] This allows the use of TA-cloning of the PCR products into plasmids for full-length sequencing.[305] The use of a linearised 'T' vector that has single 3' thymine overhangs on both ends allows high efficiency cloning of PCR products without the need for restriction digest of the PCR product. The vector is then sequenced over the region containing the insert. Cytosine residues that were unmethylated in the native DNA would be tyrosine in the sequence

whereas 5mC would still be cytosine in the sequence. Thus the methylation status of the native DNA can be deduced.

Universal primers were designed to amplify the 220 bp region around the HIF-1α HRE in the promoter region of the HIF-1α gene (Figure 125, Table 10). To validate the bisulfite sequencing method, the methylation status of the HIF-1α HRE in MCF7 breast cancer cells and HCT-116 colon cancer cells was first assessed. MCF7 DNA, known to contain an unmethylated HIF-1α HRE,[95] was used a negative control, and HCT-116 DNA, known to contain a methylated HIF-1α HRE[94] was used as a positive control.

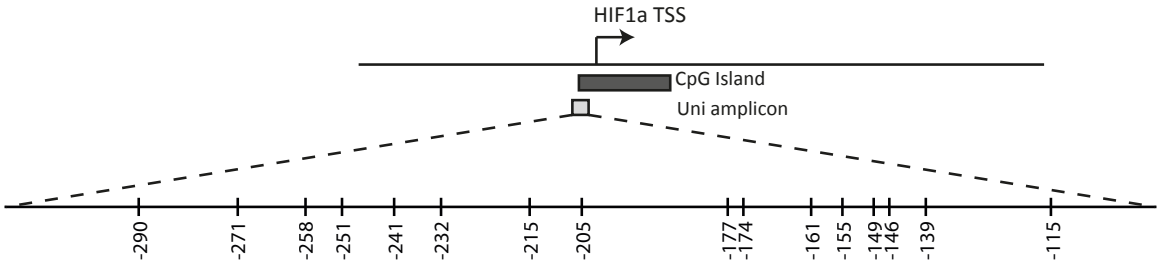

Figure 125: Graphical representation of the region of the HIF-1α promoter amplified by the universal primers. An expanded view of the universal primer (Uni) amplicon shows the position of the CpG dinucleotides analysed, relative to the TSS of HIF-1α.

Table 10: Primer sequences to amplify the region surrounding the HIF-1α HRE regardless of its methylation status.

Primer	Sequence
HIF-1α Universal FP	5'TGATGTATGTTTGGGATTAGGTAAT3'
HIF-1α Universal RP	5'CTCTCAACCAATCAAAAAAC3'

PCR amplification of bisulfite treated genomic DNA with Platinum Taq DNA polymerase gave the correct sized products when analysed by agarose gel electrophoresis (Figure 126A). The enzyme was used for the remainder of PCR amplifications of bisulfite treated DNA. The HIF-1α HRE fragments were then ligated into a pGem Easy-T vector (Promega) and cloned into chemically competent DH5α cells. Colony PCR of resulting bacterial colonies confirmed that the HIF-1α HRE fragments had been ligated into the vectors (Figure 126B). Sequencing of recombinant plasmids verified that the cytosine residues in CpG dinucleotides in the HIF-1α promoter region, and in particular, that the cytosine in the CpG dinucleotide in the HIF-1α HRE (A<u>CG</u>TG) was unmethylated in MCF7s and methylated in HCT-116s in all three clones sequenced (Figure 127).

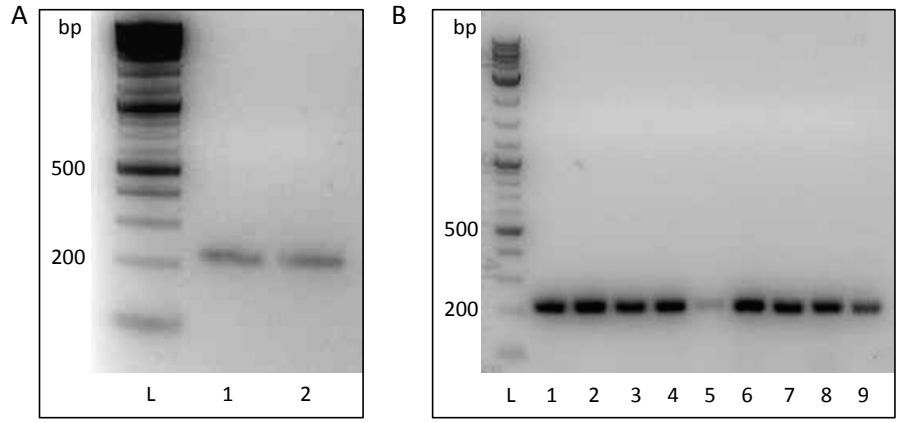

Figure 126: Visualisation of agarose gel electrophoresis of PCR products. (A) Amplification of HIF-1α HRE region from MCF7 (lane 1) and HCT-116 (lane 2) genomic DNA using universal primers. (B) Colony PCR of TA-cloned vectors containing HIF-1α HRE insert, from MCF7 (lanes 1-4) and HCT-116 (lanes 5-9), all colonies contained the correct insert. Products are shown relative to a 2-log DNA ladder (both, lane L).

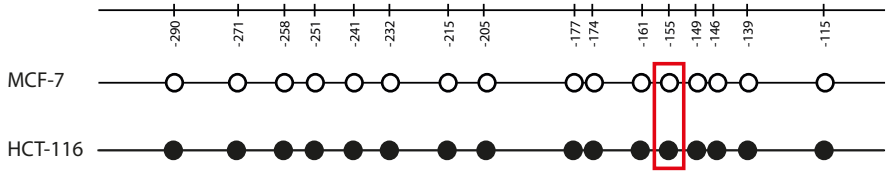

Figure 127: Verification of bisulfite sequencing method. The HIF-1α promoter fragment was amplified from bisulfite treated genomic DNA from MCF7 and HCT-116 cells and analysed by sequencing. Each circle represents a CpG site (numbered relative to HIF-1α TSS), where white = unmethylated and black = unmethylated. The CpG site within the HRE is highlighted with a red box.

3.3.2 Analysis of the HIF-1α HRE in developing tissue

The technique was the applied to embryonic DNA samples. The samples were from 4 different embryos (H1251, H1279, H1297 and H1328) and DNA was extracted from 5 different tissues from each (5 from bowel, brain, kidney, stomach, muscle, adrenal, lung or tongue). Five clones for each of the 20 DNA samples were sequenced.

The 220bp region of the HIF-1α promoter amplified contains 15 CpG dinucleotides. The sequencing data for each clone was analysed by BiQ analyser. This software compares the sequencing file to the native DNA sequence and identifies sequences with a low bisulfite conversion rate.[306] Incomplete bisulfite conversion can lead to false positive results as some unmethylated cytosine residues are not converted to uracil residues, therefore when they are read as cytosine during sequencing, they are interpreted as methylated in the native DNA. As cytosine methylation occurs predominately in CpG dinucleotides in vertebrates, if the sequencing shows any methylated cytosine residues that are not in CpG dinucleotides, the DNA sample was likely incompletely converted.[301] If a sequence had an unacceptably low

conversion rate (below 96%) it was discounted from the analysis. In addition, any incorrect sequencing was discounted. The CpG island region of the HIF-1α promoter was largely unmethylated; on average, 1.1% of CpGs were methylated (Figure 128).

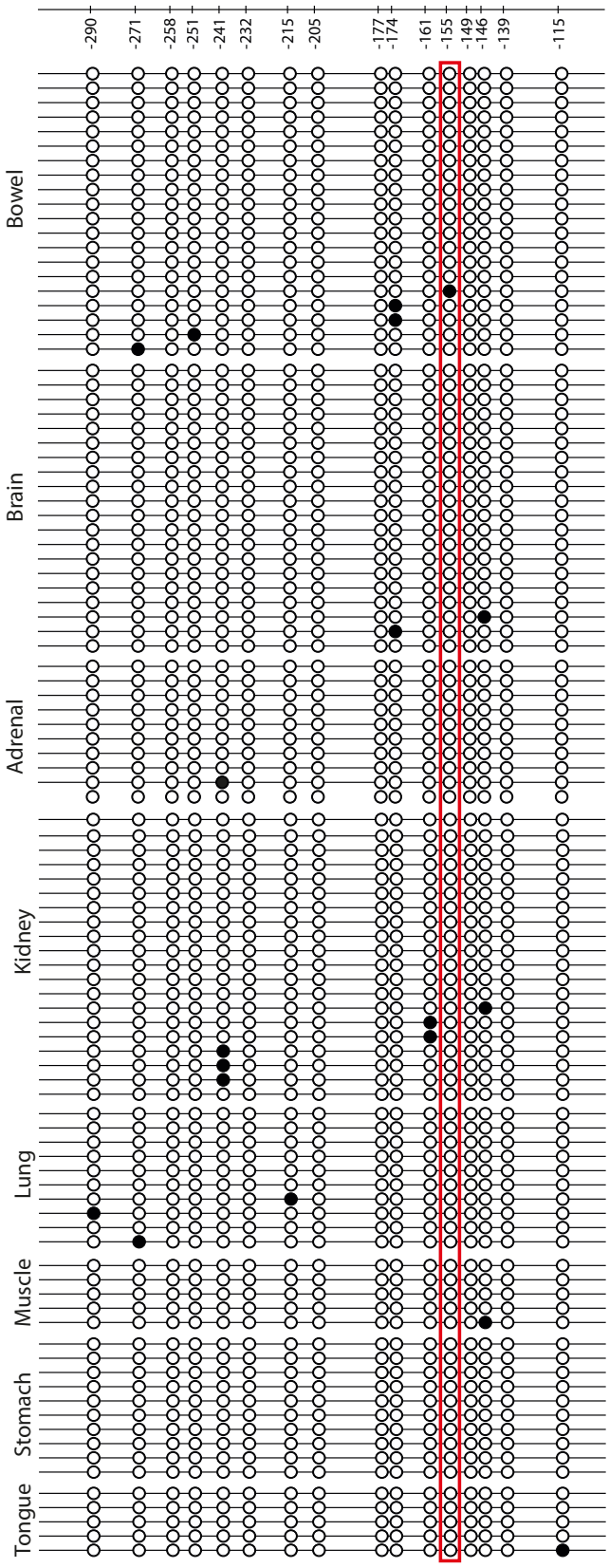

Figure 128: Methylation status of HIF-1α HRE in DNA extracted from embryonic tissue.
Methylation status of each CpG site is represented by each circle, where white is unmethylated and black is methylated. The numbered bars above represent the position of each CpG site in the promoter region of HIF-1α, relative to its TSS. The CpG situated in the HIF-1α HRE is highlighted with a red box. Each row represents data from one clone sequenced, clones are grouped by tissue: Adrenal, Bowel, Brain, Kidney, Lung, Muscle, Stomach and Tongue; 5 clones of each DNA sample were sequenced.

As the samples were from foetuses of similar age (55-59 days post conception), and no major epigenetic events are thought to take place in this period of development,[214] the samples were grouped by tissue type rather than sample origin. Therefore the epigenetic status of the HIF-1α promoter in the different tissues could be compared, in addition to an overall view of the methylation status of HIF-1α promoter in embryonic cells.

There was no more than 2% methylation in each tissue (Figure 129B). The proportion of methylated CpGs at each position of the HIF-1α promoter was more varied (Figure 129A), with a maximum of 3.8% methylation at position -146 bp, and similarly 3.1% methylation at position -241 bp, relative to the HIF-1α TSS. However the large errors associated with these values indicate that methylation percentages at these positions are positively skewed by few highly methylated samples, and they are not significantly different to unmethylated positions. The CpG site in the HIF-1α HRE, 155 bp upstream of the HIF-1α TSS (Figure 128 and Figure 129A), was unmethylated in 99% of clones sequenced, suggesting that the HIF-1 transactivation loop is active in the embryonic tissue.

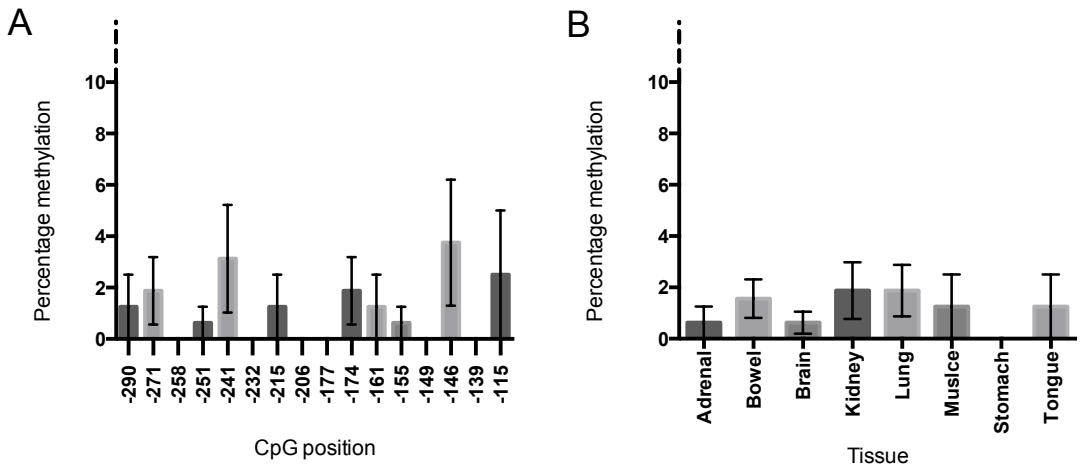

Figure 129: Percentage methylation of CpG sites within the HIF-1α promoter region analysed. Samples are grouped by CpG position relative to HIF-1α TSS (A) and tissue (B). Bars represent mean proportion of methylated clones at each position of in each tissue ±SEM.

A methylation free HRE permits HIF-1α (as part of the HIF-1 complex) to transactivate its own transcription and amplifies the activation of hypoxia response genes.[94] Histoimmunochemical analysis of mouse embryos using the hypoxia marker pimonidazole and its associated antibody have shown that hypoxic cells are widespread in the early stages of embryo development, and that these hypoxic regions co-localise with HIF expression.[307, 308] The bisulfite sequencing data suggests that the HIF-1α transactivation loop is active in embryonic tissue, with the HIF-1 transcription factor able to bind to the unmethylated HRE and upregulate expression of HIF-1α. Previous chromatin immunoprecipitation assays with

HCT-116 cells have shown that HIF-1 is only recruited to an unmethylated HIF-1α promoter.[94] In addition, the methylation status of the HRE in particular has been shown to be a key determinant of HIF-1-mediated transactivation of target genes.[185, 235, 309] The lack of methylation in these samples suggests that HIF-1 is active in embryonic tissue. This is expected, as normal mammalian development occurs in an hypoxic environment and HIF activates genes that are responsible for cell migration, differentiation, angiogenesis, erythropoiesis and other key processes in development.[11, 242, 276, 307, 308]

3.3.3 Analysis of the methylation status of the HIF-1α HRE in adult tissue

To better understand the relevance of the methylation status of the HIF-1α HRE during development, the methylation status of the sequence in (non-cancerous) adult tissue was assessed. Cells in these tissues would typically be normoxic because of sufficient vascularisation and regulated growth.[243] The samples available were limited, so not all the same tissue types that were analysed from embryonic tissue could be analysed from adult tissue. Bisulfite sequencing was used to assess the methylation status of the HIF-1α HRE in genomic DNA extracted from the adult tissue samples.

The promoter region of HIF-1α containing the HRE was unmethylated in the four tissue types analysed (bowel, colon, skeletal and stomach; Figure 130). This result is contrary to previous statements that the HRE of HIF-1α is usually supressed by methylation,[94] however no published data was found to support a default state of HRE methylation. In contrast, the HIF-1α promoter was shown to be unmethylated in histopathologically unchanged colon tissue and normal uterine cervical tissue consistent with the results here.[310, 311] Interestingly, both of these studies showed that, despite the presence of an unmethylated HRE, HIF-1α mRNA and protein levels were low in normal tissue and upregulated in equivalent cancerous tissue.[310, 311]

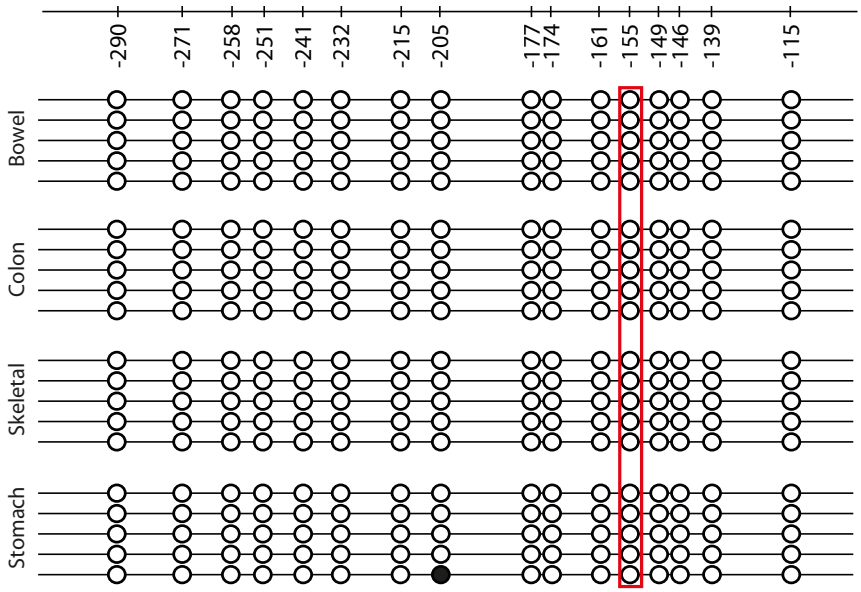

Figure 130: Methylation status of HIF-1α HRE in adult tissue. Methylation status of each CpG site is represented by each circle, where white is unmethylated and black is methylated. The numbered bars above represent the position of each CpG site in the promoter region of HIF-1α, relative to its TSS. The CpG situated in the HIF-1α HRE is highlighted with a red box. Each row represents data from one clone sequenced, clones are grouped by tissue: Bowel, Colon, Skeletal and Stomach; 5 clones of each DNA sample were sequenced.

3.3.4 Analysis of the methylation status of the EPO HRE in embryonic tissue

To evaluate whether the unmethylated status of the HIF-1α promoter was a reflection of global demethylation of HREs in embryonic tissue, the methylation status of EPO was analysed. The gene encoding EPO resides on chromosome 7, whereas the HIF-1α gene resides on chromosome 14. There is no CpG island in the 3' enhancer of EPO,[185] but previous studies have shown that hypermethylation in the 3' enhancer region of EPO leads to a decrease in its expression in primary cancer cell lines and that EPO requires an unmethylated HRE for HIF-1 binding and EPO transcriptional activation.[185, 312, 313] EPO, the principal growth factor regulating bone marrow differentiation and erythrocyte production, is a target of HIF-1.[3] Therefore analysis of the methylation status of the EPO HRE will also give an insight into the implication of the theorised positive autoregulation of HIF-1 in developing tissue.

Primers were designed to amplify the EPO HRE containing region of the EPO enhancer (Table 11). The methylation status of the HRE in the 3' enhancer region of the EPO gene in embryonic tissue samples was determined by bisulfite sequencing. The same bisulfite treated DNA used in the HIF-1α study was used for evaluation of EPO to ensure consistency between the analysis of the two genes. The amplified region of the EPO enhancer contains 5 CpG dinucleotides (Figure 131). The sequencing data was analysed by BiQ analyser as with HIF-1α, to discount erroneous results.

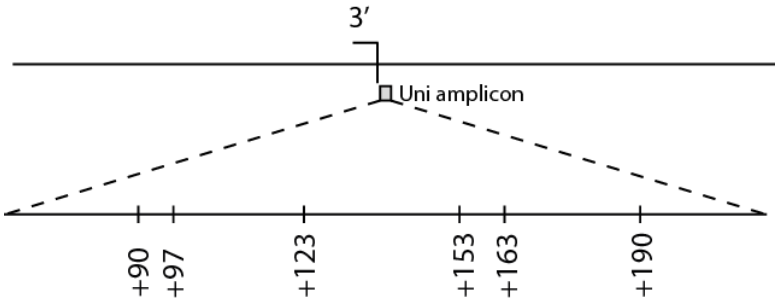

Figure 131: Graphical representation of the region of the EPO enhancer amplified by the EPO universal primers. An expanded view of the universal primer (Uni) amplicon shows the position of the CpG dinucleotides analysed, relative to the 3' polyadenylation site of EPO.

Table 11: Primer sequences to amplify the region surrounding the EPO HRE region regardless of its methylation status.

Primer	Sequence
EPO Universal FP	5'TGGTAGTAGTGTAGTAGGTTTAGGTT3'
EPO Universal RP	5'AAATAAAACCACCTTATTAACCAAC3'

There was a high degree of methylation in the EPO enhancer, with overall 47% methylation across all CpG sites (Figure 132). Therefore the unmethylated state of the HIF-1α promoter is likely not indicative of global demethylation, but a result of specific epigenetic regulation in the region. Interestingly, there were significant differences (ranging between 21% and 63%) in the methylation state of individual CpG sites within the EPO enhancer for each tissue, and between tissues (Figure 133). The CpG situated within the HRE of EPO had the lowest average methylation in the locus studied; only 21%, compared to the average 47%, this value was significantly lower than other EPO CpG sites, excepting the site adjacent to the EPO HRE (97 bp downstream from the EPO 3' polyadenylation site). The relative lack of methylation of the CpG site in the EPO HRE indicates that despite methylation of the enhancer region, binding of HIF-1 and transcriptional activation of EPO is still available.

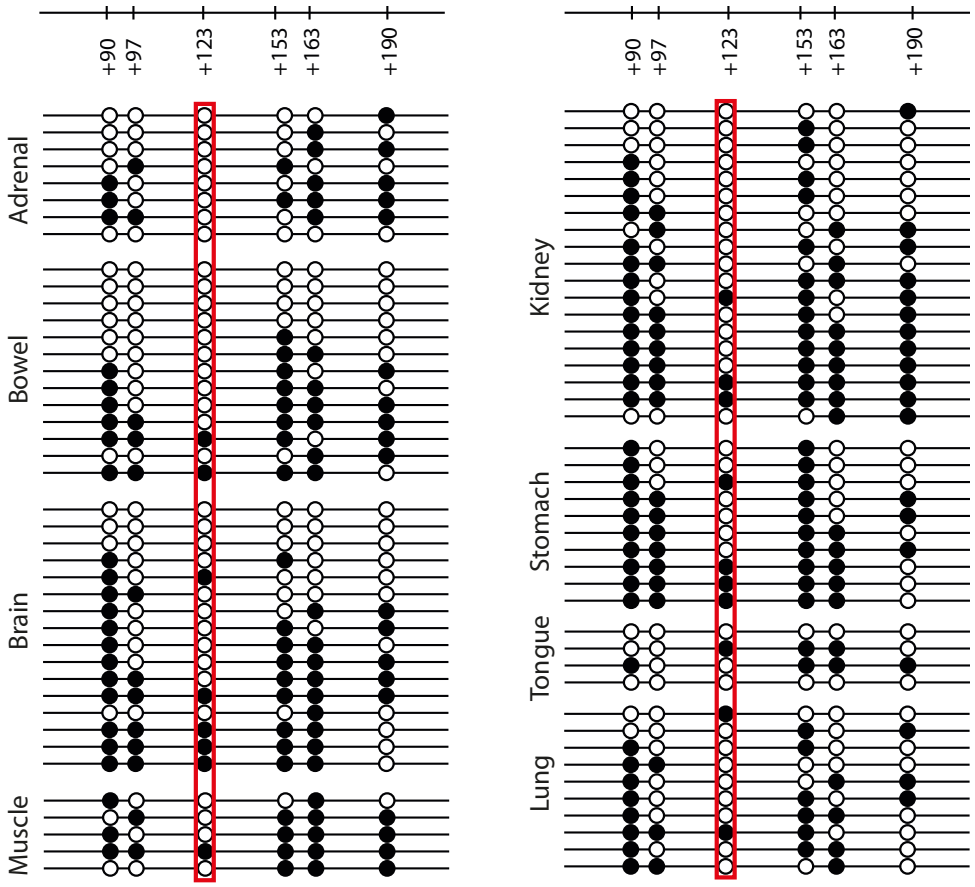

Figure 132: Analysis of the methylation status of the EPO enhancer via bisulfite sequencing.
Methylation status of each CpG site is represented by each circle, where white is unmethylated and black is methylated. The numbered bars above represent the position of each CpG site in the promoter region of EPO, relative to its 3' polyadenylation site. The CpG situated in the EPO HRE is highlighted with a red box. Each row represents data from one clone sequenced, clones are grouped by tissue: Adrenal, Bowel, Brain, Kidney, Lung, Muscle, Stomach and Tongue; 5 clones of each DNA sample were sequenced.

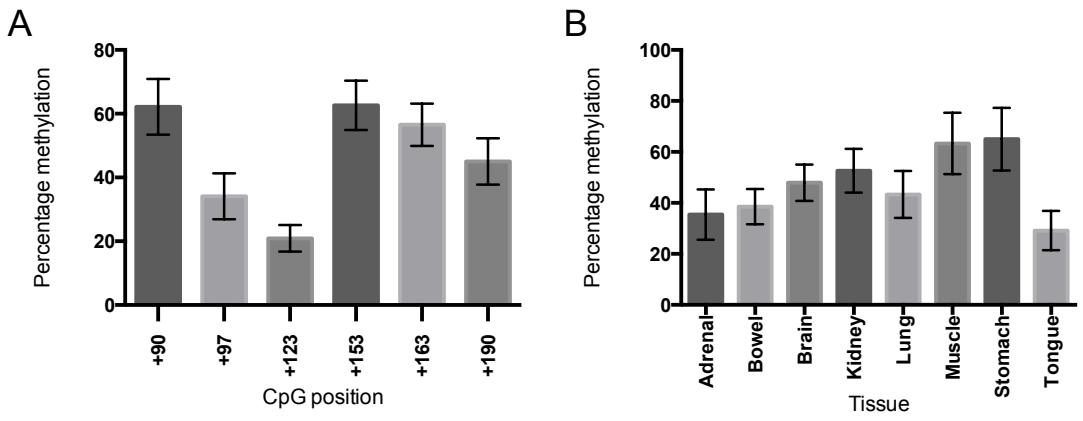

Figure 133: Percentage methylation of CpG sites within the EPO promoter region analysed.
Samples are grouped by CpG position relative to EPO 3' polyadenylation site (A) and tissue (B). Bars represent mean proportion of methylated clones at each position of in each tissue ±SEM.

Previous studies have shown that methylation of the CpG residue within the core HRE (A<u>CG</u>TG) alone prevents binding of HIF-1 to the EPO enhancer region,[185] indicating the importance of the HRE in dictating HIF-1 association with DNA. The level of methylation in the EPO enhancer varied between tissues from 29% in tongue to 65% in stomach (Figure 133B). This disparity between tissues may be a result of differing degrees of hypoxia throughout the developing embryo. For example, areas of low oxygen are more consistently detected in specific regions of the embryo such as the developing heart, gut and skeleton.[242, 314] This is likely due the incredible growth and energy demands of these tissues.[242] While the molecular basis of such selective demethylation events are not clear, the increased methylation in the region as a whole may dampen transcriptional activation by recruiting methyl binding proteins and histone deacetylases, exemplifying the complexity of the interlinking epigenetic mechanisms of gene regulation.[312]

3.4 Chapter 3 discussion

There is increasing evidence that epigenetics play a crucial part in the cellular response to hypoxia including the impact of the hypoxic environment on global histone and DNA methylation patterns and the role of epigenetics in HIF stability and function.[315-317] In particular the methylation status of HREs in the DNA of HIF target genes has been demonstrated to be a key determinant of HIF-1 binding to the promoters of these genes and inducing their transactivation.[185, 235, 309] One such target gene of HIF-1 is its subunit component HIF-1α, leading to positive autoregulation of HIF-1 in hypoxia.[94, 95] However, HIF-1 is only recruited to an unmethylated HIF-1α promoter.[94, 95] During mammalian development cells experience hypoxia due to rapid division.[307] Chapter 3 aimed to determine the methylation status of the HIF-1α HRE in embryonic tissue in order to shed light on the epigenetic regulation of HIF-1 in development. In addition, the methylation status of the HRE in the 3' enhancer of the EPO gene was assessed to aid understanding of the downstream effects of HIF-1α autoregulation.

Bisulfite sequencing was used to analyse the methylation status of the DNA. The bisulfite sequencing method was first verified by analysis of the HIF-1α HRE region from MCF7 and HCT-116 genomic DNA, which were unmethylated and methylated respectively, as expected. Subsequent evaluation of the methylation status of HIF-1α HRE region of embryonic DNA showed the HIF-1α promoter was unmethylated and the CpG site within the HRE in particular was unmethylated in 99% of clones analysed. This suggested that the HIF-1α autoregulation loop was active in developing tissue.

Having established the methylation status of the HIF-1α HRE region in developing tissue, a comparison to that in normal adult tissue was sought. Previous work in cancer cell lines has shown that an unmethylated HIF-1α HRE allows positive autoregulation of HIF-1α (whereas a methylated HRE prevents autoregulation).[94, 95, 236] Therefore, it was hypothesised that in normal adult tissue the HIF-1α HRE region would be methylated to prevent HIF-1-mediated transactivation. However, bisulfite sequencing of this region from normal adult DNA revealed an unmethylated HIF-1α promoter in all clones of all tissues analysed. This suggests that HIF-1 is able to transactivate HIF-1α expression in these cells; however, this relies on the stabilisation of HIF-1α protein to form the HIF-1 transcription factor. As cells experience hypoxia during mammalian development, HIF-1α can be stabilised and a methylation free HRE may lead to positive autoregulation. However, in normal adult cells, which are typically normoxic, HIF-1α would be degraded via the PHD/VHL pathway preventing formation of HIF-1.[41] This was demonstrated in histopathologically unchanged colon tissue and in normal uterine cervical tissue, where HIF-1α mRNA and protein levels were low despite the presence

of an unmethylated HIF-1α HRE.[310, 311] In addition, in the equivalent cancerous tissues, both HIF-1α mRNA and protein levels were increased, suggesting transcriptional upregulation of HIF-1α in addition to protein stabilisation.[310, 311]

To further understand the impact of the unmethylated status of the HIF-1α HRE in the embryonic tissue analysed, the methylation status of the HRE of the HIF-1 target gene EPO was assessed. There were varying degrees of methylation in the EPO enhancer region, however, the CpG site with the EPO HRE displayed the lowest degree of methylation (21%), more than half the average across all sites (47%) and significantly lower than most other sites.. As HIF-1 binding to the EPO enhancer has been shown to require an unmethylated HRE, the relatively low methylation at the EPO HRE CpG suggests that despite methylation in the enhancer region as a whole, the HRE is still available for HIF-1 binding.[185]

Overall, these findings underline the importance of post-translational regulation of HIF-1α, and suggest that there may be selective pressure for the HIF-1α HRE site to remain methylation free, independent of HIF-1α expression. Selective pressure for an unmethylated HRE independent of gene expression levels was also suggested for the EPO HRE, where a methylation free EPO HRE was found in human cell lines and mouse tissues that do not express EPO.185 Maintaining an unmethylated HRE (in the promoter of HIF-1α or HIF-1 target genes) may allow for more rapid recovery of oxygen homeostasis at the onset of hypoxia.

.

Chapter 4: Conclusions and further work

The aim of chapter 2 was to extend current understanding of the role of HIF-1 dimerisation in hypoxic response. This was achieved through the construction of mammalian cell lines that expressed the HIF-1 dimerisation inhibitor cyclo-CLLFVY, which was cyclised *in situ* by SICLOPPS. The peptide sequence was encoded downstream of a tetracycline operator (TetO2), resulting in inducible expression with doxycycline (Dox). Physiological control of peptide expression was achieved through the construction of a hybrid hypoxia response element (HRE)/TetO2 promoter in T-REx-HRE cells. The cell line was used to study the effect of inhibition of HIF-1 dimerisation on the transcription of HIF target genes under hypoxia. In addition, the role of HIF-1 signalling in the metabolic activity of cells was explored. It was found that inhibition of HIF-1 dimerisation increased cellular sensitivity to glucose withdrawal and to inhibition of glycolysis in hypoxia. These results improve current understanding of the HIF pathway but the methodology described, and its components, could be applied to further study of hypoxia response and to other gene networks.

The engineered hybrid HRE/TetO2 promoter was used to control expression of the Npu-CLLFVY construct in T-REx-HRE cells such that it was only expressed in hypoxia with Dox treatment. This promoter could be highly advantageous in gene therapy applications in a clinical setting where the ability to regulate gene expression tightly is vital. In gene therapy, therapeutic genes are introduced into target cells with the aim of efficient, stable expression with minimal cytotoxic side effects.[318] The use of a HRE promoter for tumour selective gene therapy has previously been suggested.[319, 320] Such controlled expression could be used, for example, for the expression of an enzyme that converts a non-toxic pro-drug into a drug in hypoxic cells only.[320, 321] Therapeutic DNA could be delivered via viral vectors, cationic lipids or polymers. The use of the HRE/TetO2 promoter could lead to more specifically targeted expression, as cells will also require the presence of Dox for gene induction. For such applications, further characterisation of the kinetics of the HRE/TetO2 promoter would be necessary. Visualisation of Npu-CLLFVY expression in T-REx-CLLFVY and T-REx-HRE cells suggested differing kinetics of the CMV/TetO2 promoter (which has previously been characterised)[256] to the HRE/TetO2 promoter. Cloning of a reporter gene such as firefly luciferase into the vector constructed here pcDNA5/HRE/CLLFVY, would give the expression vector pcDNA5/HRE/Luc. Integration of pcDNA5/HRE/Luc in to the chromosome of T-ReX-293 cells via Flp-FRT recombination would lead to a cell line that conditionally expressed luciferase in hypoxia with Dox treatment. This cell line could be used to characterise the response of the HRE/TetO2 promoter to Dox concentration and expression over time by

monitoring luciferase activity. In addition, such a cell line would facilitate the characterisation of the activation of the HRE promoter at differing concentrations of oxygen.

The hypoxia-focused microarray and cell viability assays demonstrated the T-REx-HRE cell line as a novel, valuable tool to study the effect of HIF-1 dimerisation inhibition in cells. Further experiments with the cell line could yield a wealth of information about HIF-1 in hypoxic response. It is suggested that a wider transcriptional array be carried out, particularly examining the effect of HIF-1 dimerisation inhibition on the expression of glycolytic genes. Cell viability assays in T-REx-HRE cells suggested that HIF-1 dimerisation inhibition increased cellular sensitivity to glucose withdrawal and information on the causes of these effects can be found by transcriptional analysis of genes involved in glycolysis and the tricarboxylic acid cycle. In addition, analysis of the proteome of hypoxic T-REx-HRE cells will show the downstream effects, at the protein level, inhibition of HIF-1 dimerisation. For these studies, it would be interesting to also treat cells with HIF-1α siRNA. HIF-1α siRNA would prevent HIF-1α protein production, so comparison of the effect of HIF-1α knockdown to inhibition of HIF-1 dimerisation on the transcriptome and proteome of the cells, would identify monomer functions of the α subunit. Furthermore, treatment of cells with both HIF-1α siRNA and endogenously expressed cyclo-CLLFVY would target the HIF-1 pathway at both the mRNA and protein levels.

Cell viability assays of T-REx-HRE cells also showed that disruption of HIF-1 dimerisation resulted in increased growth inhibition by the glycolysis inhibitor 2-DG. Upregulation of HIF-1α has been associated with poor prognosis and resistance to chemotherapy and inhibition of HIF-1 signalling has been shown to increase activity of and decrease resistance to a number of chemotherapeutic agents. The T-REx-HRE cell line provides a facile method of testing the activity of therapeutic agents with and without disruption of HIF signalling. The MTT assay used is a convenient, inexpensive method to assess cell viability however it does not provide information on the mechanism of cell death. The use of an alternative assay, such as ApoToxGlo assay (Promega) would allow multiplex detection of viability, necrosis and apoptosis in cells.[322] Alternatively, cells could be stained with a dye such as fluorescein conjugated to the protein annexin A5 which binds to cells that have expressed phosphatidylserine on the cell surface, which is characteristic of apoptosis.[323] Flow cytometery could be used to quantify the number of cells undergoing apoptosis following treatment.

The T-REx-CLLFVY and T-REx-HRE cell lines provide novel tools to study the hypoxia pathway by expression and *in situ* cyclisation of the HIF-1 dimerisation inhibitor CLLFVY. However, this methodology is not limited to this cyclic peptide. A 6-mer cyclic peptide that inhibits HIF-1 and HIF-2 dimerisation has recently been identified in the Tavassoli

laboratory. Integration of this inhibitor as the extein sequence between Npu split inteins would result in a cell line expressing this the peptide, induced by doxycycline and cyclised *in situ* by SICLOPPS as with cyclo-CLLFVY in T-REx-CLLFVY cells. These two cell lines could be used to compare and contrast the effect of inhibiting HIF-1 only and inhibiting HIF-1 and HIF-2.

Furthermore, the methodology is not limited to the HIF pathway; it has wide ranging applications to directly study the cellular consequences of inhibiting any protein-protein interaction with a suitable cyclic peptide. For example the peptide cyclo-SGWTVVRMY (CP61), a potent inhibitor of C-terminal binding protein (CtBP) dimerisation identified through screening of a SICLOPPS library in a bacterial RTHS.[154] CtBP1 and CtBP2 are closely related, evolutionarily conserved, transcriptional co-repressors that have been linked to tumourigenesis and tumour progression.[324] A well as CtBP dimers, a number of distinct roles of CtBP monomers have been identified, demonstrating the value of a CtBP dimerisation inhibitor to study CtBP mediated gene expression, compared to siRNA techniques.[325, 326] The integration of the CP61 sequence as the extein sequence between split inteins onto the chromosome would allow facile study of the role of CtBP dimers and monomers on tumour progression, in particular on the expression of tumour suppressor genes.

Chapter 3 aimed to expand the knowledge of the transcriptional regulation of HIF-1 in developing tissue by analysis of the methylation status of the HIF-1α and EPO HREs. This was achieved through bisulfite sequencing of the HRE containing region of the HIF-1α promoter, which was unmethylated, and the EPO enhancer, which was partially methylated. Also, bisulfite sequencing of the HIF-1α promoter from normal adult tissue revealed the HRE was unmethylated in these samples too. These results suggested the HIF-1α transactivation loop was active in developing tissue and that this could lead to increased expression of HIF-1 target genes such as EPO. In addition, partial methylation of the EPO HRE in embryonic tissue, and the lack of methylation of the HIF-1α HRE in adult tissue highlighted the importance of post-transcriptional regulation of HIF-1α expression.

Sequencing of the HRE regions of other HIF-1 target genes such as VEGF and CAIX would allow these conclusions to be expanded upon. The analysis of methylation status of the HIF-1α HRE in adult tissue was limited by the samples available. Further bisulfite sequencing of this region from different adult tissue types would allow a more detailed comparison of cell function and HIF-1α HRE methylation status. In addition, the use of tissue types with direct tumorigenic cell line equivalents would allow direct analysis of the effect of tumourigenesis on the methylation status of HIF-1.[310, 311]

Chapter 5: Materials and methods

5.1 Equipment

5.1.1 Molecular Biology

All equipment and media was sterilised in a Touchclave-R autoclave (LTE Scientific Ltd, UK). A Hydrus 300 pH meter (Fisher Scientific, UK) was used to measure pH of buffers. A Cary 100 Bio UV-Visible Spectrometer (Agilent Technologies, UK) was used to measure optical density of cell cultures.

Bacterial cultures were centrifuged in a ThermoScientific Heraeus Biofuge Primo R. A Nanodrop ND-1000 Spectrometer (Nanodrop technologies, USA) was used to measure nucleic acid concentrations. Enzyme X was used for choosing restriction sites and to aid primer design and pDraw software was used to calculate annealing temperatures for primers for PCR reactions. Standard PCR reactions were carried out on a Bio-Rad MyCycler™ Thermal Cycler (Bio-Rad, USA). Reverse transcription reactions were carried out on a Mastercycler personal (Eppendorf, UK). A Bio-Rad CFX Connect Real Time System was used to carry out qRT-PCR reactions. The associated CFX software was used to set the threshold for C_T calculations. Agarose gels were run with Bio-Rad sub-cell systems and power packs. Quantity One software and a Bio-Rad Gel Doc were used to image the gels. SDS-PAGE electrophoresis and Western blotting was carried out using a Bio-Rad Mini Protean 3 Cell system and power pack. DNA purification was carried out using GeneJET miniprep and GeneJET PCR purification kits (both ThermoScientific, UK). DNA gel purification was achieved with GeneJET gel extraction kits (ThermoScientific, UK). Sequencing and primer synthesis were carried out by Eurofins MWG Operon (Germany).

5.1.2 Cell Culture

Mammalian cells were incubated in normoxia in a HeraCell 150I incubator (Fisher Scientific, UK). Mammalian cells were incubated and manipulated under hypoxia in a H35 Hypoxystation (Don Whitley Scientific, UK). A Trinocular Inverted Microscope for 96 well plates (Fisher Scientific, UK) was used to view mammalian cells. Mammalian cell cultures were centrifuged in a Heraeus Biofuge Primo Centrifuge (ThermoScientific). Plates were agitated on a IKA VIBRAX VXR basic orbital shaker. Fluorescence microscopy was carried out on a Zeiss Axio Vert.A1 microscope fitted with a HXP 120V light box and 10X, 20X and 40X phase contrast objectives. Zeiss fluorescence filter sets used (with excitation/ emission

wavelengths in nm) were: Filter set 02 (365/420), Filter set 31 (565/ 620) and Filter set 46 (500/535).

RNA extraction and purification was carried out with Reliaprep RNA Miniprep systems (Promega, UK). Luciferase activity was measured using a GLOMAX MULTI+ detection system (Promega, UK). Cells were sonicated in a Clifton Ultrasonc SW1H Bath.

5.1.3 Peptide synthesis

Reverse phase HPLC was carried out on a Waters HPLC system (Waters, UK). Samples were manually injected into a Waters flex inject system into the HPLC system containing a Waters 1525 binary pump. Elution was monitored by a Waters 2998 photo diode array detector at 220 nm (amide backbone) and 280 nm (aromatic amino acids). Solvent was removed *in vacuo* on a Buchi rotary evaporator.

ESI-MS samples were analysed using a ZMD (Waters, Manchester, UK) mass spectrometer equipped with a single quadrupole analyser. Electrospray ionisation mass spectrometry (ESI-MS) samples were analysed using a ZMD (Waters, UK) mass spectrometer equipped with a single quadrupole analyser, samples were injected via flow injection using a Waters 600 pump (flow rate 0.1 ml /minutes MeCN) and Waters 2700 autosampler.

5.2 Materials

All chemicals were purchased from Fisher Scientific (UK), unless otherwise stated. Restriction enzymes and buffers were bought from New England Biolabs (UK). Polymerase enzymes were purchased from Promega (UK) or Life Technologies (UK). Primers were synthesised by Eurofins MWG Operon (Germany). Mammalian cell culture reagents were bought from Life Technologies (UK). MCF7 cells were gifted by Dr. Jeremy Blades' Group (Southampton General Hospital, UK). T-REx-293 cells were gifted by Dr Noel Howarth (Institute for Life Sciences, Southampton, UK). RNA purification and reverse transcription reagents were purchased from Promega (UK). TaqMan qRT-PCR reagents were purchased from Life Technologies and SYBR qRT-PCR reagents from Promega (UK). For peptide synthesis all amino acids and Wang resins were purchased from Novabiochem, UK or Matrix Innovations, Canada. All DMF and acetonitrile used was HPLC grade, purchased from Fisher Scientific, UK.

5.3 Statistical analysis

Statistical analysis of data was performed with Prism 6 (GraphPad Software Inc.). Statistical significance was evaluated with an unpaired *t*-test for comparisons between two means and analysis of variance followed by Bonferroni method for multiple comparisons. A value of $P < 0.05$ was considered to denote statistical significance. Significant differences between means are indicated on figures, *P ≤0.05, **P ≤0.01, ***P ≤0.001 or ****P≤0.0001.

5.4 General methods for Molecular Biology

5.4.1 Preparation of Luria Broth (LB) Medium

A suspension of 6.25 g of LB powder in 250 mL deionised water was autoclaved at 121°C on the media cycle and left to cool to room temperature prior to use.

5.4.2 Preparation of Luria Broth (LB) Agar plates

A suspension of 10 g LB agar powder in 250 mL deionised water was autoclaved at 121°C on the media cycle. Prior to use, the LB agar was melted in a microwave and allowed to cool to approximately 50°C before the relevant antibiotic was added. Around 25 mL of agar was used for each plate.

5.4.3 Preparation of SOC Medium

To 50 mL of freshly autoclaved LB broth, 500 µL 1 M $MgCl_2$, 500 µL $MgSO_4$ and 500 µL 20% glucose solution (w/v) were added. All solutions were made with autoclaved deionised water. The solution was filtered through a 0.22 µm sterile filter (Millipore, UK) and stored in 10 mL aliquots at 4°C.

5.4.4 Preparation of Antibiotics

The antibiotics used were made up to the concentrations shown in Table 12 using sterile deionised water and filtered through a 0.22 µm sterile filter (Millipore, UK) and stored at 4°C.

Table 12: Concentrations of antibiotics used.

Antibiotic	Stock concentration (mg/mL)	Volume for 10 mL culture (µL)	Working concentration (µg/mL)
Ampicillin	20	50	100
Chloramphenicol	10	35	35

5.4.5 Preparation of TBFI buffer

The buffer was prepared according to the quantities given in Table 13. The resulting solution was then adjusted to pH 5.8 with 1% acetic acid and made up to 200 mL with sterile deionised water.

Table 13: Composition of TBFI buffer.

Component	Quantity	Final concentration
Calcium chloride	0.29 g	10 mM
Manganese chloride	2.00 g	50 mM
Potassium acetate	0.59 g	30 mM
Rubidium chloride	2.42 g	100 mM
Glycerol	30 mL	15% v/v

5.4.6 Preparation of TBFII buffer

The buffer was prepared according to the quantities given in Table 14. The resulting solution was then adjusted to pH 6.5 with 1 M NaOH and made up to 100 mL with sterile deionised water.

Table 14: Composition of TBFII buffer.

Component	Quantity	Final concentration
MOPS	0.21 g	10 mM
Calcium chloride	1.10 g	10 mM
Rubidium chloride	0.12 g	75 mM
Glycerol	30 mL	15% v/v

5.4.7 Strains and plasmids

DH5α (chromosomal genotype:fhuA2 lac(del)U169 phoA glnV44 Φ80' lacZ(del)M15 gyrA96 recA1 relA1 endA1 thi-1 hsdR17) was from the *E. coli* Genetic Stock Centre (Yale, USA). pARCBD-Npu was constructed by J. Townend, University of Southampton. pcDNA5/FRT/TO, pIRES2-eGFP and pOG44 were kind gifts from Dr. N. Wortham, University of Southampton.

5.4.8 Preparation of *E. coli* Strain Culture Stocks

Stocks of each strain were prepared by adding 100 µL dimethyl sulfoxide (DMSO) to 900 µL of the culture (grown from a single colony from a plate, in 10 mL LB broth with the relevant antibiotic, overnight). The stocks were stored at –80°C. Strains were re-grown by inoculating 10 mL LB broth, containing the relevant antibiotic, with a small amount of the frozen stock.

5.4.9 Preparation of Chemically Competent Bacterial cells

A culture of the strain was grown by inoculating 10 mL LB broth with a small amount of the frozen stock and incubated overnight at 37°C, with agitation. The overnight culture was then used to make a 1% culture in 250 mL LB broth and incubated at 37°C, with agitation, until an OD_{600} of 0.5-0.7 was reached. The culture was then centrifuged (3100 rpm, 4°C, 15 minutes) to pellet the cells. The supernatant was discarded and the cell pellet resuspended in 5 mL TBFI buffer before repeating centrifugation. The supernatant was discarded, and the cell pellet resuspended in 1 mL TBFII buffer. The cell solution was then flash frozen in aliquots of 100 µL in PCR tubes and stored at -80°C.

5.4.10 Bisulfite treatment of DNA

DNA was bisulfite treated using Imprint DNA modification kit (Sigma Aldrich, UK) according to the manufacturers instructions.

5.4.11 General procedure for PCR

Genes for cloning were amplified by the polymerase chain reaction (PCR) using the general procedure in Table 15.

Table 15: Reagents for general PCR reaction.

Component	Volume (µL)	Final concentration
Polymerase buffer (5X or 10X)	5 or 10	1X
dNTP mix (10 mM)	2	200 µM
Forward primer (10 pmol/µL)	2	0.2 µM
Reverse primer (10 pmol/ µL)	2	0.2 µM
Template	1	Variable
DNA polymerase	0.1-1	~1.25 units
Deionised water	Up to 50 µL	

All reagents were allowed to thaw completely, on ice. The buffer, primers and dNTPs were mixed with a vortex and briefly centrifuged before use. The reaction was run on a thermocycler according to the protocol in Table 16 or as described in the enzymes' general protocol (from the manufacturers' website).

Table 16: General running protocol for PCR reactions. The annealing temperature 'X' varies depending on the melting temperature of the primers. The extension time 'Y' varies according to the product length.

Step	Temperature (°C)	Time	Cycle
Initial denaturation	95	6 minutes	1
Denature	95	30 s	20-35
Anneal	X	30 s	
Extend	72	Y	
Final extension	72	5 minutes	1

5.4.12 General procedure for colony PCR

A 10 µL scale PCR reaction was made up on ice as described in Table 17 and half a colony picked off a plate was added as the template.

Table 17: Reagents for colony PCR reaction.

Reagent	Volume (µL)
Deionised water	6.25
GoTaq 5X green buffer	2
dNTPs (10 mM)	1
Forward primer (10 pmol/ µL)	0.25
Reverse primer (10 pmol/ µL)	0.25
GoTaq DNA polymerase	0.05
Template	Colony

All reagents were allowed to thaw completely, on ice. The buffer, primers and dNTPs were mixed with a vortex and briefly centrifuged before use. The reaction was run on a thermocycler according to the protocol in Table 18.

Table 18: Running protocol for colony PCR reactions. The annealing temperature 'X' varies depending on the melting temperature of the primers. The extension time 'Y' varies according to the product length.

Step	Temperature (°C)	Time	Cycle
Initial denaturation	95	6 minutes	1
Denature	95	30 s	25
Anneal	X	30 s	
Extend	72	Y	

5.4.13 General procedure for qRT-PCR

qRT-PCR was carried out using TaqMan gene expression assays (Invitrogen, UK) specific to the gene being studied. Reactions were prepared according to the proportions given in Table 19, per sample, for each gene expression assay. All samples were run in triplicate, alongside a no template control and two housekeeper genes.

Table 19: Reagents for TaqMan qRT-PCR reactions.

Reagent	Vol (µL)1X
cDNA	1
2X TaqMan gene expression master mix	10
20X TaqMan gene expression assay	1
Nuclease free water	Up to 20 µL

Reactions were set up in the dark, as the fluorophore on the TaqMan probes are light sensitive. The 20 µL PCR samples were loaded into a 96 well plate, taking care not to allow any bubbles to form in the wells and the plate was sealed. The plate was loaded into the qRT-PCR instrument immediately, and run according to the protocol given in Table 20. Relative quantitation of gene expression was calculated using the comparative C_T method ($\Delta\Delta C_T$) and normalised to the expression of the housekeeper genes.

Table 20: General running protocol for qRT-PCR reactions.

Step	Temperature (°C)	Time
Hold	50°C	2 minutes
Initial denature	95°C	10 minutes
Cycle (x 40)	95°C	15 s
	60°C (+ plate read)	1 minute
(Melt curve starts)		
Hold	95°C	10 s
Melt	65°C to 95°C, increment 0.5°C for 5 s each (+ plate read)	5 s per increment
END		

Alternatively, qRT-PCR was carried out using GoTaq qRT-PCR master mix. With primers specific for the gene (or integrated construction) being studied. For qRT-PCR of inteins FP: GTTGTTAAGCTTGGCCGCCACCATGGGCATG and RP: GGAATTCAAGCTTTCATTGAAGCTGCCACAAGG were used. For qRT-PCR of β-actin FP: ATTGGCAATGAGCGGTCCCG and RP: AGGGCAGTGATCTCCCTCTG. Reactions were prepared according to the proportions given in Table 21, per sample, for each primer pair. All samples

were run in triplicate, alongside a no template control, expression of β-actin was used to normalise expression of the inteins.

Table 21: Reagents for SYBR qRT-PCR reactions

Reagent	Vol (µL) 1X
GoTaq qRT-PCR Master Mix	25
Nuclease free water	Up to 40
FP (10 pmol/ µL)	1.25
RP (10 pmol/ µL)	1.25

cDNA was diluted 1:10 in sterile dH_2O and 10 µL added to appropriate wells. qRT-PCR master mix was added to each well, the plate sealed and run according to the protocol above (Table 20).

5.4.14 General procedure for site directed mutagenesis

Mutation of a single base pair on a plasmid was achieved by site-directed mutagenesis. Primers were designed with the desired mutation at the centre of the primer, flanked by 15 bp of the plasmid sequence either side of where the mutation. Forward and reverse primers were complementary to each other such that they annealed to complimentary locations on opposite strands of the template.

A PCR reaction was set up on ice as described below (Table 22).

Table 22: Reagents for site directed mutagenesis PCR reaction.

Reagent	Quantity
Pfu DNA polymerase buffer (10X)	5 µL
dNTP mix (100 mM)	1 µL
Forward primer (10 pmol/µL)	1.25 µL
Reverse primer (10 pmol/ µL)	1.25 µL
Template	50 ng
DNA polymerase	1 µL
Deionised water	Up to 50 µL

All reagents were allowed to thaw completely, on ice. The buffer, primers and dNTPs were mixed with a vortex and briefly centrifuged before use. The reaction was run on a thermocycler according to the protocol given in Table 23.

Table 23: Running protocol for site directed mutagenesis PCR. The annealing temperature 'X' varies depending on the melting temperature of the primers. The extension time 'Y' varies according to the product length: 1 minute/kb plasmid length.

Step	Temperature (°C)	Time	Cycle
Initial denaturation	95	2 minutes	1
Denature	95	30 s	18
Anneal	X	1 minute	
Extend	68	Y	
Final extension	68	20 minutes	1

The reaction was cooled to 37°C and treated with 2 µL DpnI (37°C, 3 hours). The reaction was then purified and transformed into DH5α chemically competent cells.

5.4.15 General procedure for Reverse Transcription

Reverse transcription (RT) reactions were carried out using GoScript cDNA synthesis kit (Promega, UK). The kit components and purified RNA were defrosted in an ice/water bath. Each component was briefly mixed and centrifuged before use. RNA/ primer mix was prepared on ice for each reaction according to the quantities in Table 24. The mix was heated at 70°C for 5 minutes then chilled in ice/water for 5 minutes and centrifuged for 10 s to collect the condensate.

Table 24: Reagents for RNA/primer mix for reverse transcription reaction.

Reagent	Quantity
Experimental RNA	1 µg
Primer oligo dT (500 µg/ mL)	1 µL
Random primer (500 µg / mL	1 µL
Nuclease free water	To 11.5 µL

A reverse transcription master mix was prepared on ice for each reaction, according to the quantities in Table 25. 8.5 µL of reverse transcription mix was added to each RNA/primer mix sample on ice for a final reaction volume of 20 µL. The reaction was run on a

thermocycler according to the protocol in Table 26. The cDNA was then used for qRT-PCR reactions or stored at -20°C.

Table 25: Reagents for master mix for reverse transcription reaction.

Reagent	Volume (µL)
GoScript 5X reaction buffer	4.0
$MgCl_2$ (25 mM)	2
dNTPs (10 mM)	1
RNasin (40 U/ µL)	0.5
GoScript reverse transcriptase	1

Table 26: Running protocol for reverse transcription reaction.

Step	Temperature (°C)	Time
Anneal	25	5 minutes
Extend	42	1 h
Reverse transcriptase inactivation	70	15 minutes

5.4.16 Preparation of Plasmids

The strain containing the plasmid was grown from the frozen stock in 10 mL LB broth with the relevant antibiotic at 37°C with agitation, overnight. The culture was centrifuged (3100 rpm, 4°C, 15 minutes) to pellet the cells, and the pellet was then gel purified.

5.4.17 General Procedure for Restriction Digests

Restriction digests of plasmids/ PCR products were set up as detailed below (Table 27). All reagents were allowed to thaw completely and the buffer was thoroughly mixed with a vortex mixer prior to use.

Table 27: Reagents for restriction digest of plasmid/ PCR product.

Reagent	Quantity
Plasmid/ PCR product	500 ng
Appropriate buffer	5 µL
BSA (if required)	5 µL
Restriction enzyme 1	1 µL
Restriction enzyme 2	1 µL
Deionised water	Up to 50 µL

Information on the buffer and BSA requirements and the time for digestion was found on the NEB website. The digestions were carried out at 37°C in a water bath for the time required by each enzyme. This was followed by heat inactivation as stated in the enzyme properties on the NEB website. The digestion were then analysed and purified by agarose gel electrophoresis.

Dephosphorylation of digested plasmids using thermosensitive alkaline phosphatase

After heat inactivation of the digested plasmid, 1 µL of thermosensitive alkaline phosphatase (TSAP) was added directly to the reaction mixture, and the reaction incubated at 37°C for a further 45 minutes. The TSAP was irreversibly inactivated by heating at 74°C for 15 minutes. The digested, TSAP treated plasmid was then analysed and purified by agarose gel electrophoresis and gel purification using the GeneJET gel purification kit, according to the manufacturer's instructions.

5.4.18 Preparation of Agarose Gels for Electrophoresis

1% agarose gels were prepared by dissolving 1 g of agarose in 100 mL tris-acetate-EDTA (TAE) buffer (Table 28) by heating in a microwave. The solution was left to cool for 10 minutes then 2 drops of ethidium bromide solution (0.625 mg/ mL) were added and the solution swirled before pouring into an appropriate mould and allowing to set.

Table 28: Composition of TAE buffer for agarose gel electrophoresis.

Component	Quantity	Final concentration
Tris base	242 g	2 M
Glacial acetic acid	57.1 mL	1 M
EDTA (0.5 M)	100 mL	50 mM
Deionised water	Up to 1 L	

The samples (generally 5 µL mixed with 1 µL loading dye) were loaded onto the gel with 2-Log DNA ladder (NEB, UK)

5.4.19 Gel Purification of digested DNA

DNA was extracted from agarose gels and purified using GeneJET gel extraction kit (ThermoScientific, UK) according to the manufacturer's instructions.

5.4.20 Preparation of SDS-PAGE gels for protein visualisation

A Mini Protean 3 Cell instrument (Bio-Rad, UK) was used according to the manufacturers instructions to carry out sodium dodecyl sulfate-polyacrylamide gel electrophoresis (SDS-PAGE). SDS-PAGE gels (10 or 15%) were made using the quantities shown in Table 29and Table 30. The resolving gel was moulded and allowed to set for ~30 minutes before the stacking gel was added. Protein samples were prepared by heating for 10 minutes at 100°C with an equal volume of 2X Laemmli buffer (100 mM Tris-HCl, 4% SDS, 2% glycerol, 50 mM Dithiothreitol (DTT) and trace bromophenol blue, pH 6.8). The gels were run at 100 V for 40 minutes, or until the dye front had reached the end of the gel in 1X SDS running buffer (25 mM Tris base, 192 mM Glycine, 0.1% SDS, pH 8.3).

Table 29: Composition of 10 and 15% resolving gels for SDS-PAGE. Volumes are sufficient for four gels.

Component	Volume (mL)	
	10%	15%
Deionised water	14.35	10.6
1.5 M Tris-HCl, pH 8.8	7.5	7.5
10% (w/v) SDS	0.3	0.3
Acrylamide/ bisacrylaminde (40%/ 0.8%) (w/v)	7.5	11.25
10% (w/v) ammonium persulfate	0.15	0.15
TEMED	0.02	0.02

Table 30: Composition of stacking gel for SDS –PAGE. Volumes are sufficient for four gels.

Component	Volume (mL)
Deionised water	6.18
0.5 M Tris-HCl, pH 6.8	2.5
10% (w/v) SDS	0.1
Acrylamide/ bisacrylaminde (40%/ 0.8%) (w/v)	1.26
10% (w/v) ammonium persulfate	0.05
TEMED	0.01

Gels were then stained with blue Coomassie dye (50 methanol, 10% acetic acid, 0.05% brilliant blue) for 8 minutes and visualised after soaking in destain solution (50% methanol, 40% water, 10% glacial acetic acid) for 1 hour.

5.4.21 General sticky end ligation protocol

Ligation of the restriction enzyme digest plasmid backbone (vector) and PCR product (insert) were set up as shown in Table 31. T4 DNA ligase buffer was thawed and separated into aliquots of 10 µL after purchase to minimise freeze-thaw of the buffer. Before use, the aliquot of T4 ligase buffer was fully thawed and mixed well using a vortex mixer.

The amount of vector and insert required was calculated using the following equations:

$$Amount\ of\ vector\ (\mu L) = Amount\ of\ vector\ to\ be\ taken\ (ng) / Concentration\ of\ vector\ (ng\ \mu L^{-1})$$

Where the amount of vector to be taken is 90.0 ng

$$Amount\ of\ insert\ (ng\ \mu L^{-1}) = \frac{(Amount\ of\ vector\ (ng) \times Size\ of\ insert\ (bp) \times Ratio) / Size\ of\ vector\ (bp)}{Concentration\ of\ insert\ (ng\ \mu L^{-1})}$$

Where molar ratio varied from 1:1 to 1:6

Table 31: General reagents for sticky end ligation. Volume of vector and insert is dependent on size and concentration.

Reagent	Volume (µL)			
	No insert	1:1	1:3	1:6
Vector	Dependent on size and concentration			
Insert	-	Dependent on size and concentration		
T4 DNA ligase buffer	1.5	1.5	1.5	1.5
T4 DNA ligase	1.5	1.5	1.5	1.5
Water	Up to 15 µL			

The ligation reactions were incubated at 4°C overnight then the ligase inactivated by heating at 70°C for 10 minutes.
5 µL of each mixture was transformed directly into competent cells.

5.4.22 General TA ligation protocol

TA ligations of PCR products amplified with a Taq family polymerase into pGEM vectors was carried out using pGEM Easy-T vector system (Promega, UK) according to the volumes in Table 32. The 2X rapid ligation buffer was thawed and mixed by vortex vigorously before use. The amount of vector and insert required was calculated using the following equations:

$$Amount\ of\ vector\ (\mu L) = Amount\ of\ vector\ to\ be\ taken\ (ng) / Concentration\ of\ vector\ (ng\ \mu L^{-1})$$

Where the amount of vector to be taken is 50.0 ng

$$Amount\ of\ insert\ (ng\ \mu L^{-1}) = \frac{(Amount\ of\ vector\ (ng) \times Size\ of\ insert\ (bp) \times 1) / Size\ of\ vector\ (bp)}{Concentration\ of\ insert\ (ng\ \mu L^{-1})}$$

Table 32: General reagents for TA ligation. Volume of insert 'X' is dependent on its size and concentration.

Reagent	Volume (µL)
2X buffer	5
pGEM Vector (50 ng)	1
Insert	X
T4 DNA ligase	1
Water	Up to 10 µL

The reaction was made up according to quantities in Table 20, mixed by pipetting and incubated at 4°C overnight then the ligase inactivated by heating at 70°C for 10 minutes.

5 µL of each mixture was transformed directly into competent cells. Sequencing of recombinant TA vectors was carried out by Eurofins MWG Operon (Germany) using T7 promoter forward primer (TAATACGACTCACTATAGGG).

5.4.23 Transformation of plasmids into Chemically Competent Cells

5 µL of plasmid or ligation reaction mixture was added to one 100 µL aliquot of chemically competent cells and left on ice for 30 minutes before heat shocking at 42°C for 30 seconds in a water bath. The cells were then transferred into 895 µL of room temperature SOC media and the cultures incubated at 37°C with agitation for 1 hour. 100 µL of each culture was spread onto LB agar containing the relevant antibiotic and the plates incubated overnight at 37°C. For each set of cells, a water control was carried out to confirm their sterility.

5.5 General methods for Cell culture

5.5.1 Mammalian cell culture conditions

All cell culture reagents were purchased from Life Technologies unless otherwise stated. All cells were cultured at 37°C in a humidified 5% CO_2 atmosphere. T-REx-293 cells were maintained in DMEM containing 10% foetal bovine serum (FBS), 100 µg/ mL zeocin and 15 µg/ mL blasticidin and integrated T-REx cell lines were cultured in DMEM containing 10% FBS, 100 µg/ mL hygromycin B and 15 µg/ mL blasticidin. MCF-7 cells were maintained in DMEM supplemented with 10% FBS and 1% penicillin/ streptomycin. 786-O cells were

maintained in RPMI-1640 medium containing 10% FBS. Unless otherwise stated, T-REx cells were dosed with 1 μg/ mL doxycycline to induce expression of integrated constructs.

5.5.2 Mammalian cell passaging

Cell passaging was achieved by removing the culture medium, washing the cells with PBS (10 mL) and then incubating the cells at room temperature with 4 mL trypsin (0.05%) for 2 minutes or until all cells had detached from the surface of the flask. The trypsin was neutralised and the cells resuspended by the addition of 6 mL culture medium. The resuspended cell solution was transferred to a 15 mL centrifuge tube and centrifuged (1000 rpm, 4 minutes). The supernatant was removed and the cell pellet resuspended in 4- 10 mL fresh medium and the desired amount of cells were transferred into a fresh 75 cm^3 flask. Culture medium was then added to the flask to make the total culture volume 12 mL.

5.5.3 Preparation of Mammalian cell stocks

Cell culture medium was aspirated from the cell culture flask and the cells washed with PBS (10 mL) then incubated with 4 mL trypsin (0.05%) at room temperature for 2 minutes or until all cells had detached from the flask surface. The trypsin was neutralised and the cells resuspended by the addition of 6 mL culture medium. The resuspended cell solution was transferred to a 15 mL falcon tube and centrifuged (1000 rpm, 4 minutes). The supernatant was removed and the cell pellet was resuspended in 10 mL fresh culture medium. The cells were counted using a haemocytometer and the required amount of cells were transferred to a falcon tube (3 million cells per stock). The cells were centrifuged (1000 rpm, 4 minutes) to form a pellet, and the supernatant was removed. The pellet was resuspended in freezing solution (50% FBS, 10% DMSO (v/v); 1 mL per stock) and separated into 1 mL aliquots in cryotubes. The stocks were then cooled to -80°C slowly in an isopropanol box, then transferred to liquid nitrogen for storage.

5.5.4 Thawing of frozen mammalian cell stocks for cell culture

The frozen stock was thawed rapidly in a 37°C water bath and immediately added to culture medium (10 mL). The cells were spun down (1000 rpm, 4 minutes) and the supernatant removed. The pellet was resuspended in culture medium (12 mL), transferred to a 75 cm^3 flask and incubated at 37°C.

5.5.5 Extraction and purification of RNA from mammalian cells

Cells were collected by trypsinisation, transferred to a 15 mL falcon tube and centrifuged (1000 rpm, 4 minutes). The supernatant was removed and the cell pellet was washed in 2 x 2 mL PBS then resuspended in 500 µL lysis buffer 'BL' containing 5 µL thioglycerol (Reliaprep RNA miniprep kit, Promega, UK). To homogenise the cells, the mixture was mixed by vortex thoroughly and passed through a 19-gauge syringe five times and snap frozen in liquid nitrogen.

The extracted total RNA was thawed quickly in cold water and purified using Reliaprep RNA miniprep kit spin columns according to the manufacturers instructions (Promega, UK). RNA was eluted in DEPC (diethylpyrocarbonate) treated deionised water (1% v / v) to avoid the introduction of any RNase enzymes to the RNA or stored at -20°C with the addition of 1% RNasin.

5.5.6 Transient transfection of plasmids

Transfection of plasmid DNA into mammalian cells was achieved using Fugene 6 transfection reagent (Promega, UK). Cells were plated in 6 well plates with 2 x 10^5 MCF7 cells, 6 x 10^5 T-REx cells or 3 x 10^5 786-O cells per well 24 hours prior to transfection. Cell densities were optimised to reach 50-80% confluency on the day of transfection. The transfection mixtures were then prepared: to serum free media, the Fugene 6 and plasmids to be transfected were added (in a 6:1 transfection reagent: plasmid ratio). The total volume of each transfection mixture was 200 µL. The solutions were incubated at room temperature for 15 minutes then added drop wise to the plated cells and the cells incubated for a further 24 hours (37°C). In co-transfection experiments total amount of DNA was constant.

For transfected cells being using in luciferase assays, the media was aspirated from the cells and each well was washed with PBS (2 mL) then trypsin (0.05%, 1.5 mL). The cells were incubated at 37°C for 2 minutes or until all the cells had detached from the plate, then the trypsin neutralised and the cells suspended by the addition of fresh media (2 mL). The cells were counted and re-plated in an opaque 96 well plate in triplicate with 5000 cells per well in culture medium, with a total volume of 100 µL per well. The cells were incubated for a further 24 hours (37°C) then transfection efficiency calculated by measuring the firefly luciferase activity using the bright-glo assay system according to the manufacturer's instructions.

5.5.7 Transient transfection of siRNA

T-REx cells were plated in 6 well plates at a density of 2 x10^5 cell per well in a total volume of 1.5 mL per well, 24 hours prior to transfection. Cell densities were optimised to reach 50-80% confluency on the day of transfection. Silencer Select EPAS-1 siRNA (s4700, Life Technologies) or Silencer Select Negative Control No. 2 siRNA (4398047, Life Technologies) was diluted in 200 µL OptiMEM to allow a final concentration of 5 nM in the well. Lipofectamine RNAiMax transfection reagent (Life Technologies) was diluted in 200 µL OptiMEM to allow a final concentration of 25 pmol in the well. Both dilutions were incubated at RT for 5 minutes. The diluted siRNA and the Lipofectamine solutions were mixed together and incubated at RT with gentle agitation for 10 minutes. The cell culture medium was changed to 1 mL OptiMEM then 400 µL siRNA/Lipofectamine solution was added for each well. Cells were incubated for 24 h, then treated.

For HIF-2α knockdown studies, 24 h post transfection, the media was replaced with DMEM or DMEM containing 1 µg / mL Dox and incubated in normoxia or hypoxia for 24 h, then, RNA was extracted for downstream analysis.

5.5.8 Extraction and purification of proteins via the chitin binding domain

Transfected cells were scraped in 6 mL cold PBS, collected and snap frozen in liquid nitrogen. Cell suspensions were then defrosted under cold running water then centrifuged (3200 rpm, 4°C, 4 minutes). The resulting pellet was resuspended in 30 µL radioimmunoprecipitation assay (RIPA) buffer (50 mM Tris-HCl pH 7.5, 150 mM NaCl, 1% NP-40, 0.5% Sodium Deoxycholate, 0.1% SDS, 1 mM DTT, 1 X protease inhibitor cocktail) and incubated on ice for 20 minutes to lyse the cells. The cells were further lysed by sonication in a sonicator ice water bath (2 x 30 s). The sample was then centrifuged (10,500 rpm, 4°C, 10 minutes) to pellet the insoluble membrane, and the lysate collected. Chitin beads (NEB, UK) were re-suspended four times in 1 mL chitin buffer (20 mM Tris-HCl, 1 mM tris(2-carboxyethyl)phosphine (TCEP), 0.5 mM NaCl, pH 7.8), removing the supernatant after each centrifugation (2500 rpm, 4°C, 5 minutes). The protein lysate was added to 50 µL washed beads and incubated on ice for 1 hour with gentle mixing. The supernatant (unbound fraction) was then decanted and stored on ice and the beads washed four times with chitin buffer. After the last wash, 20 µL chitin buffer was left in the bead sample. The 20 µL beads or 20 µL unbound fraction were combined with 20 µL of 2X Laemmli buffer and the protein solution denatured by heating at 90°C for 10 minutes. Samples were then loaded onto a 15% SDS-PAGE gel along with a 170 kDa PageRuler Prestained Protein Ladder (ThermoScientific, UK) and run at 150 V for 45 minutes in SDS running buffer. The gel was stained for 8 minutes in Coomassie dye stain, then destained overnight and visualised.

5.5.9 Analysis of cell viability by MTT assay

T-REx cells were plated at a density of 15,000 cells per well in a 96 well plate in a total volume of 100 µL per well, 24 h prior to treatment. The cell culture medium was replaced with DMEM or no glucose DMEM containing no drug, 1 µg/ mL Dox or 3 mg/ mL 2DG and incubated for a further 24 h in normoxia or hypoxia. A treatment of 4% DMSO was used as a positive control. Cells were media changed to no phenol red DMEM and 10 µL of12 mM MTT (3-(4, 5-dimethylthiazolyl-2)-2,5-diphenyltetrazolium bromide) in PBS was added to each well. Plates were returned to incubation (normoxia or hypoxia) for 4 h. Cells were visualised to ensure the presence of intracellular punctate purple precipitate. After incubation, 75 µL media was removed carefully as to not disturb or remove the precipitate from the well then 100 µL DMSO was added to each well. Plates were shaken on an orbital shaker for 5 minutes until all the precipitate had dissolved then the absorbance of each well measured at 570 nm in a microtitre plate reader. Experiments were conducted in triplicate and results were normalised to the absorbance of a media only control.

5.6 Specific procedures

5.6.1 Construction of the HRE-Npu-CLLFVY vector (pGL2 backbone)

The Npu-CLLFVY construct was made via PCR of the plasmid pARCBD-Npu (constructed by Jaime Townend, University of Southampton) using GoTaq DNA polymerase (annealing temperature 55°C, extension time 45 s, 30 cycles) with the primers NpuCLLFVY-FP: TTCATTGCTAGCAACTGCCTGCTGTTTGTGTATTGCCTGTGCTATGAT and CBDrev: GGAATTCAAGCTTTCATTGAAGCTGCCACAAGG. This produced a PCR fragment with the peptide sequence CLLFVY between the split Npu intein.

The PCR product and the pARCBD-Npu vector were then simultaneously digested with HindIII and NheI in accordance with the manufacturers instructions. The pARCBD-Npu vector was treated with TSAP and the digestion products purified and ligated at a ratio of 1:3 (vector: insert).

5 µL of the ligation mixture was then transformed into DH5α chemically competent cells and plated onto chloramphenicol selective agar. After incubation overnight, colony PCR was carried out with 5AF1 (GCATTTTTGTCCATAAGATTAGC) and 5AR1 (CATGTTTGACAGCTTATCATCG) primers to verify the ligation had been successful. Two colonies that contained the insert were grown overnight and miniprepped. Sequencing with 5AF1 primer confirmed the presence of the Npu-CLLFVY construct in pARCBD with no mutations.

The Npu-CLLFVY construct was then amplified from the pARCBD-Npu-CLLFVY vector via PCR using GoTaq DNA polymerase (annealing temperature 60°C, extension time 1 minute, 30 cycles) with the primers NpuCLLFVY-FP-PstI: GTTGTTCTGCAGGCCGCCACCATGGGCATGATTAAAATCGCCAC and NpuCLLFVY-RP-ClaI: GTTGTTATCGATTTGAAGCTG.

The Npu-CLLFVY PCR product and the plasmid pGL2-TK-HRE were simultaneously digested with PstI and ClaI in accordance with the manufacturer's instructions. The pGL2-HREx3 vector contained three copies of the HRE (5'-GTGACTACGTGCTGCCTAG-3') from the inducible nitric oxide synthase promoter [260]. The pGL2 vector was treated with TSAP and the digestion products purified and ligated at a ratio of 1:3 (vector: insert).

5 μL of the ligation mixture was then transformed into DH5α chemically competent cells and plated onto ampicillin selective agar. After incubation overnight, colony PCR was carried out with NpuCLLFVY-FP-PstI and NpuCLLFVY-RP-ClaI primers to verify that the ligation had been successful. Two colonies that contained the insert were grown overnight, miniprepped and sequenced with NpuCLLFVY-FP-PstI, however they both showed a point mutation at position 351 bp of guanine substituted for adenine. The mutation was in the N-intein region of construct and would cause a glutamic acid to glycine amino acid mutation, so would likely affect intein splicing.

Site-directed mutagenesis was conducted on the mutated pGL2-Npu-CLLFVY plasmid with Pfu DNA polymerase (annealing temperature 56°C, extension time 5 minutes, 18 cycles) with the primers pGL2 SDM FP: ACCGTGGCGAACAGGAAGTGTTTGAGTATTGC and pGL2 SDM RP: GCAATACTCAAACACTTCCTGTTCGCCACGGT. The reaction was then treated with DpnI and the digestion products purified.

5 μL of the purified DNA was then transformed into DH5α chemically competent cells and plated onto ampicillin selective agar. Sequencing with NpuCLLFVY-FP-PstI confirmed the presence of the Npu-CLLFVY construct in pGL2 with no mutations .

5.6.2 Construction of the HRE-Npu-Scramble vector (pGL2 backbone)

As with HRE-Npu-CLLFVY, HRE-Npu-Scramble (CFVLYL) was constructed from pARCBD-Npu

using GoTaq DNA polymerase (annealing temperature 55°C, extension time 45 s, 30 cycles) with the primers Npu-CFVLYL -FP: TTCATTGCTAGCAACTGCTTTGTGCTGTATCTGTGCCTGTCGTATGAT and CBDrev: GGAATTCAAGCTTTCATTGAAGCTGCCACAAGG. This produced a PCR fragment with the peptide sequence CFVLYL between the split Npu intein.

The PCR product and the pARCBD-Npu vector were then simultaneously digested with HindIII and NheI in accordance with the manufacturers instructions. The pARCBD-Npu vector was treated with TSAP and the digestion products purified and ligated at a ratio of 1:3 (vector: insert).

5 μL of the ligation mixture was then transformed into DH5α chemically competent cells and plated onto chloramphenicol selective agar. After incubation overnight, colony PCR was carried out with 5AF1 (GCATTTTTGTCCATAAGATTAGC) and 5AR1 (CATGTTTGACAGCTTATCATCG) primers to verify the ligation had been successful. Two colonies that contained the insert were grown overnight and miniprepped. Sequencing with 5AF1 primer confirmed the presence of the Npu-CFVLYL construct in pARCBD with no mutations.

The Npu-CFVLYL construct was then amplified from the pARCBD-Npu-CFVLYL vector via PCR using GoTaq DNA polymerase (annealing temperature 60°C, extension time 1 minute, 30 cycles) with the primers NpuCLLFVY-FP-PstI: GTTGTTCTGCAGGCCGCCACCATGGGCATGATTAAAATCGCCAC and NpuCLLFVY-RP-ClaI: GTTGTTATCGATTTGAAGCTG.

The Npu-CFVLYL PCR product and pGL2-HREx3 were simultaneously digested with PstI and ClaI in accordance with the manufacturer's instructions. 5 μL of the ligation mixture was then transformed into DH5α chemically competent cells and plated onto ampicillin selective agar. After incubation overnight, colony PCR was carried out with NpuCLLFVY-FP-PstI and NpuCLLFVY-RP-ClaI primers to verify that the ligation had been successful. Sequencing with NpuCLLFVY-FP-PstI confirmed the presence of the Npu-CFVLYL construct in pGL2 with no mutations.

5.6.3 Construction of the SV40-Npu-CLLFVY vector (pGL3 backbone)

The Npu-CLLFVY construct was amplified from the pGL2-HRE-NpuCLLFVY vector using GoTaq DNA polymerase (annealing temperature 55°C, extension time 1 minute, 30 cycles) with primers: CLLFVY Npu HindIII FP: GTTGTTAAGCTTGGCCGCCACCATGGGCATG and CLLFVY Npu Xbal RP: GTTGTTTCTAGATTGAAGCTGCCACAAGGCAG.

The PCR product and the plasmid pGL3 SV40 promoter vector (Promega, UK) were simultaneously digested with HindIII and Xbal according to the manufacturer's instructions. The pGL3 vector was treated with TSAP and the digestion products purified and ligated at a ratio of 1:3 (vector: insert). 5 μL of the ligation mixture was then transformed into DH5α chemically competent cells and plated on to ampicillin selective agar. After incubation overnight, colony PCR was carried out with pGL2 seq FP (CCTCGGCCTCTGAGCTATTCC) and

CLLFVY Npu XbaI RP primers to verify that the ligation had been successful. Two colonies that contained the insert were grown overnight and miniprepped. Sequencing with pGL2 seq FP confirmed the presence of the Npu-CLLFVY construct in pGL3 with no mutations.

5.6.4 Construction of pmCherry-Npu-CLLFVY vector

The Npu-CLLFVY construct as amplified from pGL2-HRE-NpuCLLFVY using GoTaq DNA polymerase (annealing temperature 65°C, extension time 1 minute,30 cycles) with primers CLLFVY Npu SacI FP: GAGCTCGGCCGCCACCATGGGCATGATTAAAATC and CLLFVY Npu Gly linker SalI RP: GTCGACGCCGCCGCCGCCTTTAATTTTAATGGTAC to introduce SacI and SalI restriction sites to the construct. The RP also encoded a 4 amino acid linker (GlyGlyGlyGly) at the 3' end of the construct to prevent the inteins interfering with mCherry folding once the insert was cloned to make an mCherry fusion construct. As the insert lacked overhang for restriction digest, the PCR fragment was TA cloned into a pGem vector, transformed into DH5A chemically competent cells and plated onto AMP selective agar. A positive colony was grown overnight and miniprepped. The resulting plasmid (pGEM-Npu-CLLFVY) and pmCherry were simultaneously digested with SacI and SalI according to the manufacturer's instructions. Digested pmCherry was then treated with TSAP, the digestion products gel purified and ligated at a ratio of 1:3 (vector: insert). 5 µL of the ligation mixture was then transformed into DH5α chemically competent cells and plated on to ampicillin selective agar. After incubation overnight, colony PCR was carried out with internal primers to verify that the ligation had been successful. Two colonies that contained the insert were grown overnight and miniprepped. Sequencing with CLLFVY Npu SacI FP and CLLFVY Npu Gly linker SalI RP confirmed the presence of the Npu-CLLFVY construct fused to mCherry in pmCherry with no mutations (Figure 12).

5.6.5 Construction of pcDNA/FRT/TO/Npu/CLLFVY

The intein construct was first cloned into pcDNA5/FRT/TO (from Dr. Noel Wortham IFLS, Southampton; commercially available from Invitrogen, USA), an inducible expression vector encoding a CMV promoter followed by a tetracycline operator upstream of a multiple cloning site. The vector also encodes an FRT recombination site upstream of a hygromycin resistance gene to allow site-specific FRT recombination into a suitable cell line, and polyclonal selection using hygromycin.

The Npu-CLLFVY construct was amplified from pGL2-Npu-CLLFVY with Npu CLLFVY FP (GTTGTTAAGCTTGGCCGCCACCATGGGCATG) and Npu CLLFVY RP XhoI (GCTTCTCGAGTCATTGAAGCTGCCAGAA) by PCR (Ta= 65°C, extension time 1 minute, 30 cycles) to introduce HindIII and XhoI restriction sites. The PCR product was then used as the

template in another PCR reaction with CLLFVY Npu FP and Npu CLLFVY RP ApaI NotI (ATTATTGGGCCCGCGGCCGCTTCTCGA; Ta=59°C, extension time 1 minute, 30 cycles) to introduce NotI and ApaI restriction sites to the 3' end of the fragment. The PCR product and the vector pcDNA5/FRT/TO were digested with ApaI and HindIII according to the manufacturer's instructions (NEB). The vector was treated with TSAP and the digestion products ligated at a ratio of 1:3 (vector: insert). 5 μL of the ligation reaction was transformed into DH5α chemically competent cells and plated at 10% dilution on to carbenicillin selective agar and incubated at 37°C overnight. Colony PCR with internal primers (Npu CLLFVY FP and Npu CLLFVY RP ApaI NotI) suggested successful ligation and one positive colony was grown up overnight miniprepped. Sequencing with CMV FP and BGH RP confirmed the presence of the Npu-CLLFVY construct in pcDNA5/FRT/TO with no mutations.

5.6.6 Construction of pcDNA/FRT/TO/Npu/CLLFVY/IRES/GFP

An internal ribosome entry site (IRES) followed by GFP was then cloned into pcDNA5/FRT/TO/NpuCLLFVY (pCDNA5/NpuCLLFVY) to use as a secondary marker of successful integration and to quantify levels of gene expression after induction with doxycycline. pIRES2-eGFP (Dr. Noel Wortham) was digested with XhoI and NotI-HF according to the manufacturers instructions (NEB) and the digestion products separated on a 1% agarose gel. The band at ~1300 bp, containing the IRES-GFP DNA fragment was isolated and purified. pcDNA5/ NpuCLLFVY was also digested with XhoI and NotI-HF then treated with TSAP. The digested vector and IRES-GFP fragment were ligated at a ration of 1:1 (vector: insert). 5 μL of the ligation reaction was transformed into DH5α chemically competent cells and plated at 10% dilution on to carbenicillin selective agar and incubated at 37°C overnight. Colony PCR with external primers (CMV FP and BHG RP) suggested successful ligation and one positive colony was grown up overnight miniprepped. Sequencing with CMV FP and BHG RP confirmed presence of IRES-GFP downstream of Npu-CLLFVY with no mutations.

5.6.7 Construction of pcDNA5/FRT/HRE/TO/Npu/CLLFVY

A DNA fragment encoding three copies of the HRE from the inducible nitric oxide synthase promoter (5'-GTGACTACGTGCTGCCTAG-3') upstream of two copies of the Tet Operator 2 promoter (5'TCCCTATCAGTGATAGAGA-3') was synthesised by IDT. The promoter fragment was amplified by PCR with HRE TET FP SpeI (ATCGTAACAAACTAGTGTGAC) and HRE TET RP HindIII (CAGTAAGCTTAAGTTTAAACGC) to introduce SpeI and Hind III restriction sites. The HRE-TOx2 PCR product and the vector pcDNA5/FRT/TO/NpuCLLFVY were digested with SpeI and HindIII according to the manufacturer's instructions (NEB). The vector was treated with TSAP and the digestion products ligated at a ratio of 1:3 (vector: insert). 5 μL of the

ligation reaction was transformed into DH5α chemically competent cells and plated at 10% dilution on to carbenicillin selective agar and incubated at 37°C overnight. Colony PCR with internal primers (HRE TET FP SpeI and HRE TET RP HindIII) suggested successful ligation and one positive colony was grown up overnight miniprepped. Sequencing with CMV FP and BGH RP confirmed the presence of the HRE-TOx2 promoter in pcDNA5/FRT/TO/Npu-CLLFVY with no mutations.

5.6.8 Construction of pcDNA5/FRT/TO/mCherry

pcDNA5/NpuCLLFVY was digested with HindIII and NotI according to the manufacturer's instructions (NEB) to remove the intein construct; the 5058 bp plasmid backbone was treated with TSAP and gel purified. pmCherry was digested with HindIII and NotI according to the manufacturer's instructions (NEB) and the 741 bp mCherry sequence insert was gel purified. Digested backbone and insert were ligated at a ratio of 1:3 (vector: insert) then transformed into DH5α chemically competent cells and plated at 10% dilution on to carbenicillin selective agar and incubated at 37°C overnight. Colony PCR with external primers (CMV FP and BHG RP) suggested successful ligation and one positive colony was grown up overnight miniprepped. Sequencing with CMV FP and BHG RP confirmed presence mCherry in pcDNA5 with no mutations.

5.6.9 Integration of intein constructs into T-REx-293 cell line

Integration plasmids (pcDNA5/NpuCLLFVY, pcDNA5/NpuScram, pcDNA5/GFP, pcDNA/HRE/NpuCLLFVY and pcDNA5/mCherry) were maxi-prepped from a 250 mL culture in LB broth using GeneJET maxiprep kit (Thermo Scientific). Flp-In T-REx 293 cells (from Dr. Noel Wortham) were plated in 6 cm plates with 8 x 10^5 cells per plate, in DMEM complete medium. The cell line expresses the Tet repressor from pcDNA6/TR (Invitrogen) and contains a single integrated FRT site. After 24 hours incubation, the cells were co-transfected with integration plasmid and pOG44 at a ratio of 1 :9 µg (pcDNA5 to pOG44) a total of 3 µg of DNA was used. A no-recombinase control transfected with pcDNA5 only, and a no DNA control treated with transfection reagent only, were also performed. 24 hours post transfection, each integration or control plate was passaged at a 1:4 dilution into selective DMEM complete medium containing 15 µg/ mL blasticidin and 200 µg/ mL hygromycin to select for positive transformants. Cells were maintained in selective media (200 µg/mL hygromycin) until defined foci became visible on integration plates, at which point cells on control plates were detached and had stopped growing. Once confluent, integrated T-REx-Npu-CLLFVY, T-REx-Npu-Scram, T-REx-GFP, T-REx-HRE-Npu-CLLFVY and T-REx-mCherry cells were passaged and hygromycin concentration reduced to 100 µg/ mL. Stocks of each cell

line were prepared in freezing media (50% FBS, 10% DMSO, 40% DMEM complete with no antibiotics).

5.6.10 Procedure for Western immunoblotting for HIF-1α and HIF-2α protein

MCF7 cells plated on 6 well plates with 0.8 x 10^6 cells per plate and incubated overnight in normoxia (20 % O_2, 37°C). Cells were then incubated for 16 h in hypoxic conditions, scraped in 1 mL cold PBS and collected. Collected cells were snap frozen in liquid nitrogen then defrosted in cold water and the cells pelleted (3200 rpm, 4 minutes, 4°C). Cells were then further lysed by incubation with 30 µL RIPA buffer for 1h on ice, then sonication in an ice water bath (2 x 6 x 30 s). Cell debris was pelleted (13000 rpm, 4°C, 4 minutes) and the supernatant containing soluble proteins collected. 30 µg protein was then incubated with 2X Laemmli buffer and the proteins denatured by heating at 90°C for 10 minutes. Proteins were separated on a 10% SDS-PAGE gel under denaturing conditions (150 V, 40 minutes) and transferred to a PVDF membrane (Invitrogen; 250 mA, 2 h). The membrane was blocked with 5% nonfat powdered milk and 0.1% Tween-20 in PBS and subjected to immunoblot analysis. Rabbit Anti-Human HIF-1α (NB100-449, Novus Biologicals) or Mouse Anti-Human HIF-2α (NB100-132, Novus Biologicals) was diluted (1:200) in 5% milk-PBS/Tween and then incubated with the membrane overnight at 4°C. anti-Rabbit horseradish peroxidase secondary antibody (7074, Cell Signalling) was used for HIF-1α and anti-Mouse horseradish peroxidase conjugated secondary antibody (7076, Cell Signalling) was used for HIF-2α. Bound immunocomplexes were detected using ECL prime Western blot detection reagent (RPN2232, GE Healthcare).

5.6.11 Procedure for Western immunoblotting for CBD-labelled proteins

Either, protein from transfected cells were extracted as purified on chitin binding beads as described above (5.5.8) and 20 µL beads or 20 µL unbound fraction were combined with 20 µL of 2X Laemmli buffer and the protein solution denatured by heating at 100°C for 10 minutes.

Alternatively, treated T-REx cells were collected via trypsinisation and the cell pellet washed twice in PBS. Cells were then lysed in intein extraction buffer and incubated on ice with agitation for 20 minutes then sonication in an ice water bath (2 x 6 x 30 s). Cell debris was pelleted (13000 rpm, 4°C, 4 minutes) and the supernatant containing soluble proteins collected. 30 µg protein was then incubated with 2X Laemmli buffer and the proteins denatured by heating at 90°C for 10 minutes.

For both, proteins were separated on a 15% SDS-PAGE gel under denaturing conditions (140 V, 40 minutes) and transferred to a PVDF membrane (Invitrogen; 250 mA, 2 h). The membrane was blocked with 5% nonfat powdered milk and 0.1% Tween-20 in PBS and subjected to immunoblot analysis. Mouse monoclonal anti-CBD (E8034S, NEB) was diluted (1:500) in 5% milk-PBS/Tween and then incubated with the membrane overnight at 4°C. anti-Mouse horseradish peroxidase conjugated secondary antibody (7076, Cell Signalling) was used. Bound immunocomplexes were detected using ECL prime Western blot detection reagent (RPN2232, GE Healthcare).

5.6.12 Procedure for detection of cyclo-CLLFVY in cell lysate

T-REx-CLLFVY and T-REx-293 cells were seeded in T75 flasks and left to settle for 24 h. Cells were then media changed to DMEM containing 1 µg/ mL Dox and incubated for a further 24 h. Cells were scraped and collected in 2 x 2mL ice cold PBS and pelleted (1000 rpm, 4 minutes). The PBS was removed and the pellet frozen in liquid nitrogen.

A stock solution of PMSF lysis buffer was prepared according to the quantities in Table 33. A working solution was prepared of 895 µL PMSF lysis buffer stock, 100 µL protease inhibitor cocktail (to a final concentration of 1 X) and 5 µL 100 mM PMSF (to a final concentration of 0.4 mM). Cells were thawed and resuspended in 400 µL working solution PMSF lysis buffer. Cells were lysed by freeze thaw in liquid nitrogen followed by warm water for three minutes each, three times. One drop of TFA was added to precipitate proteins. Lysate was centrifuged (8000 rpm, 30 minutes, 4°C) to pellet cell debris and proteins. The supernatant was collected and passed through a 10 kDa cut off filter. The flow through was collected for analysis.

Table 33: PMSF lysis buffer stock solution.

Component	Volume	Final concentration
PBS (-$MgCL_2$, -$CaCl_2$)	5 mL	1X
EDTA (0.5 M)	50 µL	5 mM
EGTA (100 mM)	20 µL	2 mM

Cell lysates were analysed by running on a Waters Atlantis T3, amide capped C18, 5 µm, 6 x100 mm column using the solvent system HPLC program 2 described below (Table 35). Seven one-minute fractions were collected between 20 and 27 minutes of the run and analysed by ESI+ mass spectrometry.

5.6.13 Procedure for Duolink proximity ligation assay

8 well chamber slides (177445, Nuc Lab-Tek) were pretreated with poly-D-lysine (50 µg/mL in PBS, 100 µL per well) for 30 minutes then each well washed with 2 x 200 µL PBS. T-REx-HRE cells were plated on the slides at a density of 2 x 10^4 cells per well, with a total volume of 300 µL per well and incubated in normoxia overnight. Wells were then media changed to DMEM or DMEM contained 1 µg/ mL Dox and incubated in normoxia or hypoxia for 24 h.

Following incubation, the media was removed and cells washed in PBS twice. Washing steps were performed gently, using a pastette to add PBS then tapping off the solution after washing. Cells were then fixed in 100 µL 2% formaldehyde in PBS, RT 10 minutes. Cells were washed once in PBS. Cells were permeabilised with 0.5% Triton-X 100 in PBS, RT 10 minutes. Cells were incubated with Duolink Blocking Reagent for 1h then treated with the primary antibodies Rabbit Anti-Human HIF-1α (NB100-449, Novus Biologicals) and Mouse Anti-Human HIF-1β (H00000405-B01P, Abnova) were diluted (1:500) in PBS, overnight at 4°C. A technical control with no antibodies and a negative control with anti-HIF-1β only were included on each slide (normoxia and hypoxia). Slides were placed on a wet tissue and covered with a box during incubation at 4°C to provide humidity, this arrangement was also used during the following incubation steps at 37°C.

For the remainder of this protocol, treatments were tapped off and washing steps conducted in (separate) boxes containing 70 mL of the appropriate wash buffer on an orbital shaker, after washing, excess wash buffer was tapped off before the next treatment. Fresh wash buffer was used for each wash step. Reactions were conducted on a scale of 40 µL per well.

PLA probes were diluted 1:5 in antibody diluent. The chambers were removed from the slides and the slides washed in 1X wash buffer A for 2 x 5 minutes. PLA probe solution was added to each sample and the slides incubated at 37°C for 1h. The slides were washed in 1X Wash Buffer A for 2 x 5 minutes. The ligation stock was diluted 1:5 in sterile dH_2O and 1 µL Ligase per reaction added to this solution. The ligation-ligase solution was added to each sample and the slides incubated at 37°C for 30 minutes. The slides were washed in 1X Wash Buffer A for 2 x 2 minutes. The Amplification stock was diluted 1:5 in sterile dH_2O and 0.5 µL Polymerase per reaction added to this solution. The Amplification-Polymerase solution was added to each sample and the slides incubated at 37°C for 100 minutes.

The slides were washed in 1X Wash Buffer B for 2 x 10 minutes followed by 0.01X Buffer B for 1 minute, then left to dry at RT in the dark. Once dry, the slides were mounted with Duolink In Situ Mounting Medium with DAPI and the coverslip sealed with nail varnish. Once dry, the samples were visualised by fluorescent microscopy. To allow comparison between

hypoxic and normoxic samples, the same fluorescence brightness level, exposure time and processing settings were used for all samples on both slides.

5.6.14 Hypoxia Focused Microarray

Hypoxia focused microarray was conducted with TaqMan Array 96- well plate Human Hypoxia (Applied Biosystems). A master mix of TaqMan qRT-PCR master mix (1080 μL) and cDNA and nuclease free water (1080 μL) was made up. 20 μL of this master mix was added to each well of the array plate. The plate was run according to the protocol in Table 20. Each plate contained a duplicate of one sample; separate samples were run on the same day to improve consistency. Each plate was prepared just prior to running. Data was analysed using BioRad CFX connect software.

5.6.15 Solid phase peptide synthesis of cyclo-CLLFVY

5.6.15.1 Fmoc deprotection

During solid-phase peptide synthesis, 20% piperidine/ dimethylformamide (DMF) (v/v)(20 ml) was added to the protected peptidyl resin in a sinter funnel to remove the N-terminal fluorenylmethyloxycarbonyl (Fmoc) groups. The mixture was bubbled with argon for 30 minutes. The solution was then filtered and washed with DMF (3 x 10 ml) followed by alternating dichloromethane (DCM) (3 x 10 ml) and diethyl ether (3 x 10 ml) washes. The ninhydrin test was used to confirm complete deprotection. If the ninhydrin test showed incomplete Fmoc deprotection, the process was repeated.

5.6.15.2 Amino acid coupling

The Fmoc protected amino acid (1.5 mmol), Hydroxybenzotriazole (HOBt) (203 mg, 1.5 mmol) and then N,N-Diisopropylcarbodiimide (232 μl, 1.5 mmol) were added to DMF (3 ml). The solution was stirred for 15 minutes and then added to Fmoc deprotected peptidyl resin (0.5 mmol) in a sinter funnel. The coupling reaction was bubbled with argon for 2 hours. The resin was filtered, washed with DMF (3 x 10 ml) and alternating DCM (3 x 10 ml) and diethyl ether (3 x 10 ml). Ninhydrin test was used to detect complete coupling, if free amines were detected the process was repeated.

5.6.15.3 Ninhydrin test: Test for free amines

Solution A (100 μl) and solution B (25 μl) were added to a small sample of resin and then heated to 125°C for 1-2 minutes. A resin colour change from yellow/colourless to blue/purple indicated the presence of free amines.[327]

Solution A: $KCN_{(aq)}$ (0.4 mL, 0.001 M) in 20 mL pyridine.

Solution B: Ninhydrin (1.25 g, 7.02 mmol) in ethanol (25 ml).

5.6.15.4 Peptide cleavage from resin and side chain deprotection

A cleavage cocktail of TFA (9.5 ml), water (0.25 ml) and triisopropylsilane (0.25 ml) was added to the Fmoc deprotected peptidyl resin. The mixture was stirred for 2 hours under argon. The resin was then filtered and the solvent removed from the filtrate liquor *in vacuo*. In order to remove traces of TFA, DCM (10 ml) was added to the residue, and removed *in vacuo*, this was repeated 3 times. The residue was finally dissolved in minimal DCM (3-4 ml) and added to cold diethyl ether (80 ml) drop-wise. The solution was incubated at -80°C for 20 minutes and the precipitated peptide was collected by centrifugation (4000 rpm, 20 minutes). The supernatant was removed and the pellets dried *in vacuo* overnight, to leave the crude peptide.

5.6.15.5 Cysteine aldrithiol (spy) protection

After cleavage from the resin the free thiol of cysteine was protected by a pyridinesulfenyl group (spy) using 2,2'dipyridyl sulfide (aldrithiol-2, 10 equivalents (eq)). The protected crude peptide was dissolved in DMF (30 ml) and aldrithiol-2 was added to the mixture and stirred for 16 hours. Solvent was removed *in vacuo* and the solution filtered. The solution was then purified using HPLC program 1 (Table 34) and lyophilised, yielding a colourless solid.

5.6.15.6 Linear peptide cyclisation

Linear spy protected peptide was dissolved in DMF in high dilution (1 ml/mg), N-(3-Dimethylaminopropyl)-N-ethylcarbodiimide hydrochloride (3 eq) and HOBt (6 eq). The reaction mixture was stirred for 24 hours under argon; after which the solvent was removed *in vacuo*. The remaining solution was filtered and purified by HPLC using HPLC program 1 (Table 34), the solvents were then removed by lyophilisation.

5.6.15.7 Removal of aldrtihiol (spy) protection from cyclo-CLLFVY

Cyclo-CLLFVY(spy) (1 eq) was dissolved in DMF (100 μl/mg), and water (10 μl/mg) was added followed by TCEP (1 eq). After approximately 1 hour MeCN (0.5 ml) and water (0.5-1 ml) were added to the reaction mixture, which was filtered and purified using HPLC program 1 (Table 34) and solvents were removed by lyophilisation yielding a colourless solid.

5.6.15.8 HPLC purification and peptide analysis

Linear and cyclic peptides were purified using a prep reverse-phase HPLC with a Waters Atlantis prep OBD T3 amide capped C18, 5 μm, 19 x100 mm column (Waters, UK) and the solvent system HPLC program 1 described below (Table 34).

Table 34: HPLC program 1. HPLC solvent program used to purify linear and cyclic peptides.

Time (minutes)	Flow (ml / minute)	% A (H_2O, 0.1% TFA)	% B (MeCN, 0.1% TFA)
0	17	95	5
1.0	17	95	5
10.0	17	40	60
15.0	17	40	60
15.5	17	95	5
20.0	17	95	5
20.1	0	95	5

Peptide purity was analysed by running samples of the compound on a Waters Atlantis T3, amide capped C18, 5 μm, 6 x100 mm column using the solvent system HPLC program 2 described below (Table 35). This program was also used to detect cyclo-CLLFVY in T-REx-CLLFVY cell lysate (5.6.13).

Table 35: HPLC program 2. Solvent system used to analyse the purity of synthesised peptides.

Time (minutes)	Flow (ml / minute)	% A (H_2O, 0.1% TFA)	% B (MeCN, 0.1% TFA)
0	1	95	5
10.0	1	95	5
20.0	1	40	60
30.0	1	40	60
31.0	1	95	5
34.5	1	95	5
35.0	0	95	5

References

1. G. L. Semenza, *Curr Opin Genet Dev*, 1998, 8, 588-594.

2. R. H. Wenger, *Faseb J*, 2002, 16.

3. G. L. Semenza and G. L. Wang, *Molecular and Cellular Biology*, 1992, 12, 5447-5454.

4. G. L. Wang, B. H. Jiang, E. A. Rue and G. L. Semenza, *Proc. Natl. Acad. Sci.*, 1995, 92, 5510-5514.

5. E. C. Hoffman, H. Reyes, F. F. Chu, F. Sander, L. H. Conley, B. A. Brooks and O. Hankinson, *Science*, 1991, 252, 954-958.

6. H. Tian, S. L. McKnight and D. W. Russell, *Gene Dev*, 1997, 11, 72-82.

7. Y. Z. Gu, S. M. Moran, J. B. Hogenesch, L. Wartman and C. A. Bradfield, *Gene Expression*, 1998, 7, 205-213.

8. C. Frelin, A. Ladoux and C. Bauters, *Med Sci*, 1997, 13, 886-890.

9. M. Ema, S. Taya, N. Yokotani, K. Sogawa, Y. Matsuda and Y. Fujii-Kuriyama, *Proc. Natl. Acad. Sci.*, 1997, 94, 4273-4278.

10. D. Shweiki, A. Itin, D. Soffer and E. Keshet, *Nature*, 1992, 359, 843-845.

11. H. Tian, R. E. Hammer, A. M. Matsumoto, D. W. Russell and S. L. McKnight, *Gene Dev*, 1998, 12, 3320-3324.

12. H. E. Ryan, J. Lo and R. S. Johnson, *Embo J*, 1998, 17, 3005-3015.

13. C. C. L. Wong, D. M. Gilkes, H. F. Zhang, J. Chen, H. Wei, P. Chaturvedi, S. I. Fraley, C. M. Wong, U. S. Khoo, I. O. L. Ng, D. Wirtz and G. L. Semenza, *Proc. Natl. Acad. Sci.*, 2011, 108, 16369-16374.

14. R. Bos, P. J. van Diest and E. van der Wall, *J Natl Cancer I*, 2001, 93, 1177-1177.

15. M. C. Lauzier, M. D. Michaud, M. A. C. Dery and D. E. Richard, *B Cancer*, 2006, 93, 349-356.

16. J. B. Hogenesch, W. K. Chan, V. H. Jackiw, R. C. Brown, Y.-Z. Gu, M. Pray-Grant, G. H. Perdew and C. A. Bradfield, *J. Biol. Chem.*, 1997, 272, 8581-8593.

17. D. L. Wu, N. Potluri, J. P. Lu, Y. C. Kim and F. Rastinejad, *Nature*, 2015, 524, 303-+.

18. P. J. A. Erbel, P. B. Card, O. Karakuzu, R. K. Bruick and K. H. Gardner, *Proc. Natl. Acad. Sci.*, 2003, 100, 15504-15509.

19. A. Chapman-Smith, J. K. Lutwyche and M. L. Whitelaw, *J. Biol. Chem y*, 2004, 279, 5353-5362.

20. J. S. Yang, L. Zhang, P. J. A. Erbel, K. H. Gardner, K. Ding, J. A. Garcia and R. K. Bruick, *J. Biol. Chem y*, 2005, 280, 36047-36054.

21. R. Cardoso, R. Love, C. L. Nilsson, S. Bergqvist, D. Nowlin, J. L. Yan, K. K. C. Liu, J. Zhu, P. Chen, Y. L. Deng, H. J. Dyson, M. J. Greig and A. Brooun, *Protein Sci*, 2012, 21, 1885-1896.

22. T. H. Scheuermann, D. R. Tomchick, M. Machius, Y. Guo, R. K. Bruick and K. H. Gardner, *Proc. Natl. Acad. Sci.*, 2009, 106, 450-455.

23. R. H. Wenger, D. P. Stiehl and G. Camenisch, *Science's STKE : Signal Transduction Knowledge Environment*, 2005, 2005, re12.

24. B.-H. Jiang, J. Z. Zheng, S. W. Leung, R. Roe and G. L. Semenza, *J. Biol. Chem.*, 1997, 272, 19253-19260.

25. C. W. Pugh, J. F. O'Rourke, M. Nagao, J. M. Gleadle and P. J. Ratcliffe, *J. Biol. Chem.*, 1997, 272, 11205-11214.

26. C. J. Hu, A. Sataur, L. Wang, H. Chen and M. C. Simon, *Mol Biol Cell*, 2007, 18, 4528-4542.

27. M. Ema, K. Hirota, J. Mimura, H. Abe, J. Yodoi, K. Sogawa, L. Poellinger and Y. Fujii-Kuriyama, *Embo J*, 1999, 18, 1905-1914.

28. M. Heikkila, A. Pasanen, K. I. Kivirikko and J. Myllyharju, *Cell. Mol. Life Sci.*, 2011, 68, 3885-3901.

29. T. Tanaka, M. Wiesener, W. Bernhardt, K. U. Eckardt and C. Warnecke, *Biochem. J.*, 2009, 424, 143-151.

30. A. Pasanen, M. Heikkila, K. Rautavuoma, M. Hirsila, K. I. Kivirikko and J. Myllyharju, *Int J Biochem Cell B*, 2010, 42, 1189-1200.

31. L. E. Huang, J. Gu, M. Schau and H. F. Bunn, *Proc. Natl. Acad. Sci.*, 1998, 95, 7987-7992.

32. C. J. Hu, L. Y. Wang, L. A. Chodosh, B. Keith and M. C. Simon, *Mol. Cell. Biol.*, 2003, 23, 9361-9374.

33. A. C. R. Epstein, J. M. Gleadle, L. A. McNeill, K. S. Hewitson, J. O'Rourke, D. R. Mole, M. Mukherji, E. Metzen, M. I. Wilson, A. Dhanda, Y.-M. Tian, N. Masson, D. L. Hamilton, P. Jaakkola, R. Barstead, J. Hodgkin, P. H. Maxwell, C. W. Pugh, C. J. Schofield and P. J. Ratcliffe, *Cell*, 2001, 107, 43-54.

34. N. Masson, C. Willam, P. H. Maxwell, C. W. Pugh and P. J. Ratcliffe, *Embo J*, 2001, 20, 5197-5206.

35. M. Ivan, K. Kondo, H. F. Yang, W. Kim, J. Valiando, M. Ohh, A. Salic, J. M. Asara, W. S. Lane and W. G. Kaelin, *Science*, 2001, 292, 464-468.

36. M. A. McDonough, V. Li, E. Flashman, R. Chowdhury, C. Mohr, B. M. R. Lienard, J. Zondlo, N. J. Oldham, I. J. Clifton, J. Lewis, L. A. McNeill, R. J. M. Kurzeja, K. S. Hewitson, E. Yang, S. Jordan, R. S. Syed and C. J. Schofield, *Proc. Natl. Acad. Sci.*,, 2006, 103, 9814-9819.

37. H. Tarhonskaya, A. M. Rydzik, I. K. H. Leung, N. D. Loik, M. C. Chan, A. Kawamura, J. S. O. McCullagh, T. D. W. Claridge, E. Flashman and C. J. Schofield, *Nat Commun*, 2014, 5.

38. E. Berra, E. Benizri, A. Ginouves, V. Volmat, D. Roux and J. Pouyssegur, *Embo J*, 2003, 22, 4082-4090.

39. R. J. Appelhoff, Y. M. Tian, R. R. Raval, H. Turley, A. L. Harris, C. W. Pugh, P. J. Ratcliffe and J. M. Gleadle, *J. Biol. Chem.*, 2004, 279, 38458-38465.

40. P. H. Maxwell, M. S. Wiesener, G. W. Chang, S. C. Clifford, E. C. Vaux, M. E. Cockman, C. C. Wykoff, C. W. Pugh, E. R. Maher and P. J. Ratcliffe, *Nature*, 1999, 399, 271-275.

41. P. Jaakkola, D. R. Mole, Y. M. Tian, M. I. Wilson, J. Gielbert, S. J. Gaskell, A. von Kriegsheim, H. F. Hebestreit, M. Mukherji, C. J. Schofield, P. H. Maxwell, C. W. Pugh and P. J. Ratcliffe, *Science*, 2001, 292, 468-472.

42. M. Ohh, C. W. Park, N. Ivan, M. A. Hoffman, T. Y. Kim, L. E. Huang, N. Pavletich, V. Chau and W. G. Kaelin, *Nat Cell Biol*, 2000, 2, 423-427.

43. D. E. Foxler, K. S. Bridge, V. James, T. M. Webb, M. Mee, S. C. K. Wong, Y. F. Feng, D. Constantin-Teodosiu, T. E. Petursdottir, J. Bjornsson, S. Ingvarsson, P. J. Ratcliffe, G. D. Longmore and T. V. Sharp, *Nat Cell Biol*, 2012, 14, 201-208.

44. P. C. Mahon, K. Hirota and G. L. Semenza, *Gene Dev*, 2001, 15, 2675-2686.

45. D. Lando, D. J. Peet, D. A. Whelan, J. J. Gorman and M. L. Whitelaw, *Science*, 2002, 295, 858-861.

46. D. Lando, D. J. Peet, J. J. Gorman, D. A. Whelan, M. L. Whitelaw and R. K. Bruick, *Gene Dev*, 2002, 16, 1466-1471.

47. P. Koivunen, M. Hirsila, V. Gunzler, K. I. Kivirikko and J. Myllyharju, *J. Biol. Chem*., 2004, 279, 9899-9904.

48. S. A. Dames, M. Martinez-Yamout, R. N. De Guzman, H. J. Dyson and P. E. Wright, *Proc. Natl. Acad. Sci.*,2002, 99, 5271-5276.

49. J. H. Marxsen, P. Stengel, K. Doege, P. Heikkinen, T. Jokilehto, T. Wagner, W. Jelkmann, P. Jaakkola and E. Metzen, *The Biochemical Journal*, 2004, 381, 761-767.

50. J. S. Isaacs, Y. J. Jung, D. R. Mole, S. Lee, C. Torres-Cabala, Y. L. Chung, M. Merino, J. Trepel, B. Zbar, J. Toro, P. J. Ratcliffe, W. M. Linehan and L. Neckers, *Cancer Cell*, 2005, 8, 143-153.

51. M. A. Selak, S. M. Armour, E. D. MacKenzie, H. Boulahbel, D. G. Watson, K. D. Mansfield, Y. Pan, M. C. Simon, C. B. Thompson and E. Gottlieb, *Cancer Cell*, 2005, 7, 77-85.

52. S. M. Wood, J. M. Gleadle, C. W. Pugh, O. Hankinson and P. J. Ratcliffe, *J. Biol. Chem*, 1996, 271, 15117-15123.

53. D. Chilov, G. Camenisch, I. Kvietikova, U. Ziegler, M. Gassmann and R. H. Wenger, *Journal of Cell Science*, 1999, 112, 1203-1212.

54. R. Depping, A. Steinhoff, S. G. Schindler, B. Friedrich, R. Fagerlund, E. Metzen, E. Hartmann and M. Kohler, *Biochim Biophys Acta*, 2008, 1783, 394-404.

55. S. K. Burroughs, S. Kaluz, D. Wang, K. Wang, E. G. Van Meir and B. Wang, *Future Medicinal Chemistry*, 2013, 5, 10.4155/fmc.4113.4117.

56. A. Ladoux and C. Frelin, *Biochem Bioph Res Co*, 1997, 240, 552-556.

57. R. H. Wenger, I. Kvietikova, A. Rolfs, M. Gassmann and H. H. Marti, *Kidney Int*, 1997, 51, 560-563.

58. A. M. Arsham, J. J. Howell and M. C. Simon, *J. Biol. Chem.*, 2003, 278, 29655-29660.

59. S. C. Land and A. R. Tee, *J. Biol. Chem*., 2007, 282, 20534-20543.

60. J. Brugarolas, K. Lei, R. L. Hurley, B. D. Manning, J. H. Reiling, E. Hafen, L. A. Witter, L. W. Ellisen and W. G. Kaelin, *Gene Dev*, 2004, 18, 2893-2904.

61. H. Lu, R. A. Forbes and A. Verma, *J. Biol. Chem*., 2002, 277, 23111-23115.

62. V. L. Dengler, M. D. Galbraith and J. M. Espinosa, *Crit Rev Biochem Mol*, 2014, 49, 1-15.

63. D. E. Richard, E. Berra, E. Gothie, D. Roux and J. Pouyssegur, *J. Biol. Chem*, 1999, 274, 32631-32637.

64. P. W. Conrad, T. L. Freeman, D. Beitner-Johnson and D. E. Millhorn, *J. Biol. Chem*, 1999, 274, 33709-33713.

65. K. Gradin, C. Takasaki, Y. Fujii-Kuriyama and K. Sogawa, *J. Biol. Chem*, 2002, 277, 23508-23514.

66. A. Kalousi, I. Mylonis, A. S. Politou, G. Chachami, E. Paraskeva and G. Simos, *Journal of Cell Science*, 2010, 123, 2976-2986.

67. D. Flugel, A. Gorlach, C. Michiels and T. Kietzmann, *Molecular and Cellular Biology*, 2007, 27, 3253-3265.

68. D. Z. Xu, Y. X. Yao, L. Lu, M. Costa and W. Dai, *J. Biol. Chem*, 2010, 285, 38944-38950.

69. H. Geng, Q. Liu, C. Xue, L. L. David, T. M. Beer, G. V. Thomas, M. S. Dai and D. Z. Qian, *J. Biol. Chem*, 2012, 287, 35496-35505.

70. J. H. Lim, Y. M. Lee, Y. S. Chun, J. Chen, J. E. Kim and J. W. Park, *Mol Cell*, 2010, 38, 864-878.

71. H. Geng, C. T. Harvey, J. Pittsenbarger, Q. Liu, T. M. Beer, C. Xue and D. Z. Qian, *J. Biol. Chem*, 2011, 286, 38095-38102.

72. J. W. Jeong, M. K. Bae, M. Y. Ahn, S. H. Kim, T. K. Sohn, M. H. Bae, M. A. Yoo, E. J. Song, K. J. Lee and K. W. Kim, *Cell*, 2002, 111, 709-720.

73. Y. V. Liu and G. L. Semenza, *Cell Cycle*, 2007, 6, 656-659.

74. J. S. Isaacs, Y. J. Jung, E. G. Mimnaugh, A. Martinez, F. Cuttitta and L. M. Neckers, *J. Biol. Chem*, 2002, 277, 29936-29944.

75. E. Minet, D. Mottet, G. Michel, I. Roland, M. Raes, J. Remacle and C. Michiels, *Febs Lett*, 1999, 460, 251-256.

76. W. B. Luo, J. Zhong, R. Chang, H. X. Hu, A. Pandey and G. L. Semenza, *J. Biol. Chem*, 2010, 285, 3651-3663.

77. M. Y. Koh, B. G. Darnay and G. Powis, *Molecular and Cellular Biology*, 2008, 28, 7081-7095.

78. M. Y. Koh, R. Lemos, Jr., X. Liu and G. Powis, *Cancer Res*, 2011, 71, 4015-4027.

79. H. Kimura, A. Weisz, T. Ogura, Y. Hitomi, Y. Kurashima, K. Hashimoto, F. D'Acquisto, M. Makuuchi and H. Esumi, *J. Biol. Chem.*, 2001, 276, 2292-2298.

80. E. Minet, I. Ernest, G. Michel, I. Roland, J. Remacle, M. Raes and C. Michiels, *Biochem Biophys Res Commun*, 1999, 261, 534-540.

81. J. Schodel, D. R. Mole and P. J. Ratcliffe, *Biological Chemistry*, 2013, 394, 507-517.

82. D. R. Mole, C. Blancher, R. R. Copley, P. J. Pollard, J. M. Gleadle, J. Ragoussis and P. J. Ratcliffe, *J. Biol. Chem*, 2009, 284, 16767-16775.

83. H. Kimura, A. Weisz, Y. Kurashima, K. Hashimoto, T. Ogura, F. D'Acquisto, R. Addeo, M. Makuuchi and H. Esumi, *Blood*, 2000, 95, 189-197.

84. X. B. Xia and A. L. Kung, *Genome Biol*, 2009, 10.

85. W. Liu, S. M. Shen, X. Y. Zhao and G. Q. Chen, *International Journal of Biochemistry and Molecular Biology*, 2012, 3, 165-178.

86. N. Takeda, K. Maemura, Y. Imai, T. Harada, D. Kawanami, T. Nojiri, I. Manabe and R. Nagai, *Circ Res*, 2004, 95, 146-153.

87. M. Garayoa, A. Martinez, S. M. Lee, R. Pio, W. G. An, L. Neckers, J. Trepel, L. M. Montuenga, H. Ryan, R. Johnson, M. Gassmann and F. Cuttitta, *Mol Endocrinol*, 2000, 14, 848-862.

88. J. A. Forsythe, B. H. Jiang, N. V. Iyer, F. Agani, S. W. Leung, R. D. Koos and G. L. Semenza, *Mol. Cell. Biol.*, 1996, 16, 4604-4613.

89. R. A. Cairns, I. S. Harris and T. W. Mak, *Nature Reviews Cancer*, 2011, 11, 85-95.

90. Y. Benita, H. Kikuchi, A. D. Smith, M. Q. Zhang, D. C. Chung and R. J. Xavier, *Nucleic Acids Res*, 2009, 37, 4587-4602.

91. B. Keith, R. S. Johnson and M. C. Simon, *Nature Reviews Cancer*, 2012, 12, 9-22.

92. K. L. Covello, J. Kehler, H. Yu, J. D. Gordan, A. M. Arsham, C. J. Hu, P. A. Labosky, M. C. Simon and B. Keith, *Genes Dev*, 2006, 20, 557-570.

93. M. V. Gustafsson, X. Zheng, T. Pereira, K. Gradin, S. Jin, J. Lundkvist, J. L. Ruas, L. Poellinger, U. Lendahl and M. Bondesson, *Dev Cell*, 2005, 9, 617-628.

94. M. Koslowski, U. Luxemburger, O. Tureci and U. Sahin, *Oncogene*, 2011, 30, 876-882.

95. D. J. Asby, F. Cuda, F. Hoakwie, E. Miranda and A. Tavassoli, *Mol Biosyst*, 2014, 10, 2505-2508.

96. I. Papandreou, R. A. Cairns, L. Fontana, A. L. Lim and N. C. Denko, *Cell Metabolism*, 2006, 3, 187-197.

97. K. Grabmaier, A. d. W. MC, G. W. Verhaegh, J. A. Schalken and E. Oosterwijk, *Oncogene*, 2004, 23, 5624-5631.

98. V. Wang, D. A. Davis, M. Haque, L. E. Huang and R. Yarchoan, *Cancer Res*, 2005, 65, 3299-3306.

99. R. R. Raval, K. W. Lau, M. G. B. Tran, H. M. Sowter, S. J. Mandriota, J. L. Li, C. W. Pugh, P. H. Maxwell, A. L. Harris and P. J. Ratcliffe, *Molecular and Cellular Biology*, 2005, 25, 5675-5686.

100. M. J. Hsieh, K. S. Chen, H. L. Chiou and Y. S. Hsieh, *Eur J Cell Biol*, 2010, 89, 598-606.

101. C. J. Hu, S. Iyer, A. Sataur, K. L. Covello, L. A. Chodosh and M. C. Simon, *Molecular and Cellular Biology*, 2006, 26, 3514-3526.

102. E. B. Rankin, J. Rha, T. L. Unger, C. H. Wu, H. P. Shutt, R. S. Johnson, M. C. Simon, B. Keith and V. H. Haase, *Oncogene*, 2008, 27, 5354-5358.

103. M. S. Wiesener, J. S. Jurgensen, C. Rosenberger, C. K. Scholze, J. H. Horstrup, C. Warnecke, S. Mandriota, I. Bechmann, U. A. Frei, C. W. Pugh, P. J. Ratcliffe, S. Bachmann, P. H. Maxwell and K. U. Eckardt, *Faseb J*, 2003, 17, 271-273.

104. K. Brusselmans, F. Bono, P. Maxwell, Y. Dor, M. Dewerchin, D. Collen, J. M. Herbert and P. Carmeliet, *J. Biol. Chem*, 2001, 276, 39192-39196.

105. T. Uchida, F. Rossignol, M. A. Matthay, R. Mounier, S. Couette, E. Clottes and C. Clerici, *J. Biol. Chem*, 2004, 279, 14871-14878.

106. T. N. Seagroves, H. E. Ryan, H. Lu, B. G. Wouters, M. Knapp, P. Thibault, K. Laderoute and R. S. Johnson, *Molecular and Cellular Biology*, 2001, 21, 3436-3444.

107. Y. Y. Hu, L. A. Fu, S. Z. Li, Y. Chen, J. C. Li, J. Han, L. Liang, L. Li, C. C. Ji, M. H. Zheng and H. Han, *Cancer Lett*, 2014, 349, 67-76.

108. M. V. Gustafsson, X. W. Zheng, T. Pereira, K. Gradin, S. B. Jin, J. Lundkvist, J. L. Ruas, L. Poellinger, U. Lendahl and M. Bondesson, *Developmental Cell*, 2005, 9, 617-628.

109. H. Zhong, A. M. De Marzo, E. Laughner, M. Lim, D. A. Hilton, D. Zagzag, P. Buechler, W. B. Isaacs, G. L. Semenza and J. W. Simons, *Cancer Res*, 1999, 59, 5830-5835.

110. V. Ramachandran, T. Arumugam, R. F. Hwang, J. K. Greenson, D. M. Simeone and C. D. Logsdon, *Cancer Res*, 2007, 67, 2666-2675.

111. C. Berenguer, F. Boudouresque, C. Dussert, L. Daniel, X. Muracciole, M. Grino, D. Rossi, K. Mabrouk, D. Figarella-Branger, P. M. Martin and L. Ouafik, *Oncogene*, 2008, 27, 506-518.

112. J. Szenajch, G. Wcislo, J. Y. Jeong, C. Szczylik and L. Feldman, *Bba-Rev Cancer*, 2010, 1806, 82-95.

113. J. Mathieu, Z. Zhang, W. Y. Zhou, A. J. Wang, J. M. Heddleston, C. M. A. Pinna, A. Hubaud, B. Stadler, M. Choi, M. Bar, M. Tewari, A. Liu, R. Vessella, R. Rostomily, D. Born, M. Horwitz, C. Ware, C. A. Blau, M. A. Cleary, J. N. Rich and H. Ruohola-Baker, *Cancer Res*, 2011, 71, 4640-4652.

114. M. J. Tan, Z. Q. Teo, M. K. Sng, P. C. Zhu and N. S. Tan, *Molecular Cancer Research*, 2012, 10, 677-688.

115. H. Zhang, C. C. L. Wong, H. Wei, D. M. Gilkes, P. Korangath, P. Chaturvedi, L. Schito, J. Chen, B. Krishnamachary, P. T. Winnard, V. Raman, L. Zhen, W. A. Mitzner, S. Sukumar and G. L. Semenza, *Oncogene*, 2012, 31, 1757-1770.

116. R. Bos, P. van der Groep, A. E. Greijer, A. Shvarts, S. Meijer, H. M. Pinedo, G. L. Semenza, P. J. van Diest and E. van der Wall, *Cancer*, 2003, 97, 1573-1581.

117. G. Gruber, R. H. Greiner, R. Hlushchuk, D. M. Aebersold, H. J. Altermatt, G. Berclaz and V. Djonov, *Breast Cancer Research*, 2004, 6, R191-198.

118. T. Fillies, R. Werkmeister, P. J. van Diest, B. Brandt, U. Joos and H. Buerger, *BMC Cancer*, 2005, 5, 84.

119. J. A. Wells and C. L. McClendon, *Nature*, 2007, 450, 1001-1009.

120. A. C. Cheng, R. G. Coleman, K. T. Smyth, Q. Cao, P. Soulard, D. R. Caffrey, A. C. Salzberg and E. S. Huang, *Nat. Biotechnol.*, 2007, 25, 71-75.

121. L. Lo Conte, C. Chothia and J. Janin, *J Mol Biol*, 1999, 285, 2177-2198.

122. J. Janin and C. Chothia, *J. Biol. Chem.*, 1990, 265, 16027-16030.

123. M. R. Arkin and J. A. Wells, *Nat Rev Drug Discov*, 2004, 3, 301-317.

124. T. Clackson and J. A. Wells, *Science*, 1995, 267, 383-386.

125. A. A. Bogan and K. S. Thorn, *J Mol Biol*, 1998, 280, 1-9.

126. E. J. Sundberg and R. A. Mariuzza, *Structure*, 2000, 8, R137-142.

127. Y. Xia, H. K. Choi and K. Lee, *Eur J Med Chem*, 2012, 49, 24-40.

128. Y. Z. Hu, J. Liu and H. Huang, *Journal of Cellular Biochemistry*, 2013, 114, 498-509.

129. G. N. Masoud and W. Li, *Acta Pharmaceutica Sinica. B*, 2015, 5, 378-389.

130. L. M. Greenberger, I. D. Horak, D. Filpula, P. Sapra, M. Westergaard, H. F. Frydenlund, C. Albaek, H. Schroder and H. Orum, *Mol Cancer Ther*, 2008, 7, 3598-3608.

131. W. Jeong, A. Rapisarda, S. R. Park, R. J. Kinders, A. Chen, G. Melillo, B. Turkbey, S. M. Steinberg, P. Choyke, J. H. Doroshow and S. Kummar, *Cancer Chemotherapy and Pharmacology*, 2014, 73, 343-348.

132. A. Rapisarda, B. Uranchimeg, O. Sordet, Y. Pommier, R. H. Shoemaker and G. Melillo, *Cancer Res*, 2004, 64, 1475-1482.

133. B. I. Rini, *Clin Cancer Res*, 2008, 14, 1286-1290.

134. D. Del Bufalo, L. Ciuffreda, D. Trisciuoglio, M. Desideri, F. Cognetti, G. Zupi and M. Milella, *Cancer Res*, 2006, 66, 5549-5554.

135. J. R. Porter, J. E. Ge, J. Lee, E. Normant and K. West, *Curr Top Med Chem*, 2009, 9, 1386-1418.

136. D. Z. Qian, S. K. Kachhap, S. J. Collis, H. M. W. Verheul, M. A. Carducci, P. Atadja and R. Pili, *Cancer Res*, 2006, 66, 8814-8821.

137. G. L. Semenza, *Trends Pharmacol Sci*, 2012, 33, 207-214.

138. E. J. Park, D. Kong, R. Fisher, J. Cardellina, R. H. Shoemaker and G. Melillo, *Cell Cycle*, 2006, 5, 1847-1853.

139. K. Lee, H. Zhang, D. Z. Qian, S. Rey, J. O. Liu and G. L. Semenza, *Proc Natl Acad Sci U S A*, 2009, 106, 17910-17915.

140. E. Miranda, I. K. Nordgren, A. L. Male, C. E. Lawrence, F. Hoakwie, F. Cuda, W. Court, K. R. Fox, P. A. Townsend, G. K. Packham, S. A. Eccles and A. Tavassoli, *J. Am. Chem. Soc.*, 2013, 135, 10418-10425.

141. D. Kong, E. J. Park, A. G. Stephen, M. Calvani, J. H. Cardellina, A. Monks, R. J. Fisher, R. H. Shoemaker and G. Melillo, *Cancer Res*, 2005, 65, 9047-9055.

142. B. J. Foster, K. Clagett-Carr, D. D. Shoemaker, M. Suffness, J. Plowman, L. A. Trissel, C. K. Grieshaber and B. Leyland-Jones, *Investigational New Drugs*, 1985, 3, 403-410.

143. J. Drevs, J. Fakler, S. Eisele, M. Medinger, G. Bing, N. Esser, D. Marme and C. Unger, *Anticancer Research*, 2004, 24, 1759-1763.

144. K. Lee, D. Z. Qian, S. Rey, H. Wei, J. O. Liu and G. L. Semenza, *Proc Natl Acad Sci U S A*, 2009, 106, 2353-2358.

145. D. H. Shin, Y. S. Chun, D. S. Lee, L. E. Huang and J. W. Park, *Blood*, 2008, 111, 3131-3136.

146. C. D. Befani, P. J. Vlachostergios, E. Hatzidaki, A. Patrikidou, S. Bonanou, G. Simos, C. N. Papandreou and P. Liakos, *J Mol Med*, 2012, 90, 45-54.

147. S. H. Li, D. H. Shin, Y. S. Chun, M. K. Lee, M. S. Kim and J. W. Park, *Molecular Cancer Therapeutics*, 2008, 7, 3729-3738.

148. Y. S. Chun, E. J. Yeo, E. Choi, C. M. Teng, J. M. Bae, M. S. Kim and J. W. Park, *Biochemical Pharmacology*, 2001, 61, 947-954.

149. H. L. Sun, Y. N. Liu, Y. T. Huang, S. L. Pan, D. Y. Huang, J. H. Guh, F. Y. Lee, S. C. Kuo and C. M. Teng, *Oncogene*, 2007, 26, 3941-3951.

150. D. Samanta, D. M. Gilkes, P. Chaturvedi, L. Xiang and G. L. Semenza, *Proc Natl Acad Sci U S A*, 2014, 111, E5429-5438.

151. J. C. Maher, M. Wangpaichitr, N. Savaraj, M. Kurtoglu and T. J. Lampidis, *Molecular Cancer Therapeutics*, 2007, 6, 732-741.

152. C. Falciani, L. Lozzi, A. Pini and L. Bracci, *Chem Biol*, 2005, 12, 417-426.

153. A. Tavassoli and S. J. Benkovic, *Nat Protoc*, 2007, 2, 1126-1133.

154. C. N. Birts, S. K. Nijjar, C. A. Mardle, F. Hoakwie, P. J. Duriez, J. P. Blaydes and A. Tavassoli, *Chem Sci*, 2013, 4, 3046-3057.

155. A. Tavassoli, Q. Lu, J. Gam, H. Pan, S. J. Benkovic and S. N. Cohen, *ACS Chem. Biol.*, 2008, 3, 757-764.

156. C. P. Scott, E. Abel-Santos, M. Wall, D. C. Wahnon and S. J. Benkovic, *Proc. Natl. Acad. Sci.,*, 1999, 96, 13638-13643.

157. T. W. Muir, D. Sondhi and P. A. Cole, *Proc. Natl. Acad. Sci.,*, 1998, 95, 6705-6710.

158. H. D. Mootz, *Chembiochem*, 2009, 10, 2579-2589.

159. S. Elleuche and S. Poggeler, *Appl Microbiol Biot*, 2010, 87, 479-489.

160. X.-Q. Liu, *Annual Review of Genetics*, 2000, 34, 61-76.

161. H. Wu, Z. M. Hu and X. Q. Liu, *P Natl Acad Sci USA*, 1998, 95, 9226-9231.

162. B. S. Chevalier and B. L. Stoddard, *Nucleic Acids Res*, 2001, 29, 3757-3774.

163. T. M. T. Hall, J. A. Porter, K. E. Young, E. V. Koonin, P. A. Beachy and D. J. Leahy, *Cell*, 1997, 91, 85-97.

164. P. Sun, S. Ye, S. Ferrandon, T. C. Evans, M. Q. Xu and Z. Rao, *J Mol Biol*, 2005, 353, 1093-1105.

165. F. B. Perler, G. J. Olsen and E. Adam, *Nucleic Acids Res*, 1997, 25, 1087-1093.

166. S. Pietrokovski, *Protein Sci*, 1998, 7, 64-71.

167. M. Kawasaki, S. Nogami, Y. Satow, Y. Ohya and Y. Anraku, *J. Biol. Chem*, 1997, 272, 15668-15674.

168. Z. H. Liu, S. Frutos, M. J. Bick, M. Vila-Perello, G. T. Debelouchina, S. A. Darst and T. W. Muir, *Proc. Natl. Acad. Sci.,*, 2014, 111, 8422-8427.

169. Y. Ding, M. Q. Xu, I. Ghosh, X. H. Chen, S. Ferrandon, G. Lesage and Z. H. Rao, *J. Biol. Chem*, 2003, 278, 39133-39142.

170. M. W. Southworth, J. Benner and F. B. Perler, *Embo J*, 2000, 19, 5019-5026.

171. K. Tori, B. Dassa, M. A. Johnson, M. W. Southworth, L. E. Brace, Y. Ishino, S. Pietrokovski and F. B. Perler, *J. Biol. Chem*, 2010, 285, 2515-2526.

172. K. Tori and F. B. Perler, *J Bacteriol*, 2011, 193, 2035-2041.

173. P. Carvajal-Vallejos, R. Pallisse, H. D. Mootz and S. R. Schmidt, *J. Biol. Chem*, 2012, 287, 28686-28696.

174. H. Iwai, S. Zuger, J. Jin and P. H. Tam, *Febs Lett*, 2006, 580, 1853-1858.

175. J. Zettler, V. Schutz and H. D. Mootz, *Febs Lett*, 2009, 583, 909-914.

176. Q. Wu, Z. Q. Gao, Y. Wei, G. L. Ma, Y. C. Zheng, Y. H. Dong and Y. Z. Liu, *Biochemical Journal*, 2014, 461, 247-255.

177. S. W. Lockless and T. W. Muir, *Proc Natl Acad Sci U S A*, 2009, 106, 10999-11004.

178. J. E. Townend and A. Tavassoli, *ACS Chemical Biology*, 2016, DOI: 10.1021/acschembio.6b00095.

179. Y. Z. Kunes, W. R. Gion, E. Fung, J. G. Salfeld, R. R. Zhu, P. Sakorafas and G. R. Carson, *Biotechnol Progr*, 2009, 25, 735-744.

180. C. M. Yuen, S. J. Rodda, S. A. Vokes, A. P. McMahon and D. R. Liu, *Journal of the American Chemical Society*, 2006, 128, 8939-8946.

181. D. F. Selgrade, J. J. Lohmueller, F. Lienert and P. A. Silver, *Journal of the American Chemical Society*, 2013, 135, 7713-7719.

182. D. C. Jones, I. N. Mistry and A. Tavassoli, *Mol Biosyst*, 2016, DOI: 10.1039/C6MB00007J.

183. T. M. Kinsella, C. T. Ohashi, A. G. Harder, G. C. Yam, W. Q. Li, B. Peelle, E. S. Pali, M. K. Bennett, S. M. Molineaux, D. A. Anderson, E. S. Masuda and D. G. Payan, *J. Biol. Chem*, 2002, 277, 37512-37518.

184. F. H. Gohard, D. J. St-Cyr, M. Tyers and W. C. Earnshaw, *Open Biol*, 2014, 4.

185. R. H. Wenger, I. Kvietikova, A. Rolfs, G. Camenisch and M. Gassmann, *Eur. J. Biochem.*, 1998, 253, 771-777.

186. I. Mimura, M. Nangaku, Y. Kanki, S. Tsutsumi, T. Inoue, T. Kohro, S. Yamamoto, T. Fujita, T. Shimamura, J. Suehiro, A. Taguchi, M. Kobayashi, K. Tanimura, T. Inagaki, T. Tanaka, T. Hamakubo, J. Sakai, H. Aburatani, T. Kodama and Y. Wada, *Mol. Cell. Biol.*, 2012, 32, 3018-3032.

187. H. Choudhry, J. Schodel, S. Oikonomopoulos, C. Camps, S. Grampp, A. L. Harris, P. J. Ratcliffe, J. Ragoussis and D. R. Mole, *EMBO reports*, 2014, 15, 70-76.

188. R. Jaenisch and A. Bird, *Nature Genetics*, 2003, 33, 245-254.

189. L. He and G. J. Hannon, *Nature Reviews. Genetics*, 2004, 5, 522-531.

190. V. Pelechano and L. M. Steinmetz, *Nature Reviews. Genetics*, 2013, 14, 880-893.

191. H. Choudhry and D. R. Mole, *Briefings in Functional Genomics*, 2015, DOI: 10.1093/bfgp/elv050, 1-12.

192. X. Huang, L. Ding, K. L. Bennewith, R. T. Tong, S. M. Welford, K. K. Ang, M. Story, Q. T. Le and A. J. Giaccia, *Mol Cell*, 2009, 35, 856-867.

193. J. A. Foekens, A. M. Sieuwerts, M. Smid, M. P. Look, V. de Weerd, A. W. Boersma, J. G. Klijn, E. A. Wiemer and J. W. Martens, *Proc Natl Acad Sci U S A*, 2008, 105, 13021-13026.

194. X. Huang and J. Zuo, *Acta Biochimica et Biophysica Sinica*, 2014, 46, 220-232.

195. T. K. Barth and A. Imhof, *Trends Biochem Sci*, 2010, 35, 618-626.

196. A. B. Johnson, N. Denko and M. C. Barton, *Mutat Res-Fund Mol M*, 2008, 640, 174-179.

197. E. Baxter, K. Windloch, F. Gannon and J. S. Lee, *Cell Biosci*, 2014, 4.

198. H. B. Chen, Y. Yan, T. L. Davidson, Y. Shinkai and M. Costa, *Cancer Res*, 2006, 66, 9009-9016.

199. J. Xu, B. Wang, Y. Xu, L. Sun, W. Tian, D. Shukla, R. Barod, J. Grillari, R. Grillari-Voglauer, P. H. Maxwell and M. A. Esteban, *Oncogene*, 2012, 31, 1065-1072.

200. S. Beyer, M. M. Kristensen, K. S. Jensen, J. V. Johansen and P. Staller, *J. Biol. Chem*, 2008, 283, 36542-36552.

201. A. J. Krieg, E. B. Rankin, D. Chan, O. Razorenova, S. Fernandez and A. J. Giaccia, *Molecular and Cellular Biology*, 2010, 30, 344-353.

202. N. S. Kenneth, S. Mudie, P. van Uden and S. Rocha, *J. Biol. Chem*, 2009, 284, 4123-4131.

203. A. Melvin, S. Mudie and S. Rocha, *Molecular Biology of the Cell*, 2011, 22, 4171-4181.

204. T. H. Kim, L. O. Barrera, M. Zheng, C. X. Qu, M. A. Singer, T. A. Richmond, Y. N. Wu, R. D. Green and B. Ren, *Nature*, 2005, 436, 876-880.

205. J. G. Herman and S. B. Baylin, *New Engl J Med*, 2003, 349, 2042-2054.

206. H. Leonhardt, A. W. Page, H. U. Weier and T. H. Bestor, *Cell*, 1992, 71, 865-873.

207. M. Schaefer, T. Pollex, K. Hanna, F. Tuorto, M. Meusburger, M. Helm and F. Lyko, *Gene Dev*, 2010, 24, 1590-1595.

208. F. Tuorto, F. Herbst, N. Alerasool, S. Bender, O. Popp, G. Federico, S. Reitter, R. Liebers, G. Stoecklin, H. J. Grone, G. Dittmar, H. Glimm and F. Lyko, *Embo J*, 2015, 34, 2350-2362.

209. M. Okano, D. W. Bell, D. A. Haber and E. Li, *Cell*, 1999, 99, 247-257.

210. S. Sharma, T. K. Kelly and P. A. Jones, *Carcinogenesis*, 2010, 31, 27-36.

211. X. Nan, H. H. Ng, C. A. Johnson, C. D. Laherty, B. M. Turner, R. N. Eisenman and A. Bird, *Nature*, 1998, 393, 386-389.

212. P. O. Esteve, H. G. Chin, A. Smallwood, G. R. Feehery, O. Gangisetty, A. R. Karpf, M. F. Carey and S. Pradhan, *Gene Dev*, 2006, 20, 3089-3103.

213. A. P. Bird and A. P. Wolffe, *Cell*, 1999, 99, 451-454.

214. W. Reik, *Nature*, 2007, 447, 425-432.

215. M. Tahiliani, K. P. Koh, Y. H. Shen, W. A. Pastor, H. Bandukwala, Y. Brudno, S. Agarwal, L. M. Iyer, D. R. Liu, L. Aravind and A. Rao, *Science*, 2009, 324, 930-935.

216. Y. F. He, B. Z. Li, Z. Li, P. Liu, Y. Wang, Q. Tang, J. Ding, Y. Jia, Z. Chen, L. Li, Y. Sun, X. Li, Q. Dai, C. X. Song, K. Zhang, C. He and G. L. Xu, *Science*, 2011, 333, 1303-1307.

217. S. Ito, L. Shen, Q. Dai, S. C. Wu, L. B. Collins, J. A. Swenberg, C. He and Y. Zhang, *Science*, 2011, 333, 1300-1303.

218. H. Hashimoto, Y. Liu, A. K. Upadhyay, Y. Chang, S. B. Howerton, P. M. Vertino, X. Zhang and X. Cheng, *Nucleic Acids Res*, 2012, 40, 4841-4849.

219. D. Bourc'his, G. L. Xu, C. S. Lin, B. Bollman and T. H. Bestor, *Science*, 2001, 294, 2536-2539.

220. Z. D. Smith, M. M. Chan, T. S. Mikkelsen, H. Gu, A. Gnirke, A. Regev and A. Meissner, *Nature*, 2012, 484, 339-344.

221. F. M. Piccolo, H. Bagci, K. E. Brown, D. Landeira, J. Soza-Ried, A. Feytout, D. Mooijman, P. Hajkova, H. G. Leitch, T. Tada, S. Kriaucionis, M. M. Dawlaty, R. Jaenisch, M. Merkenschlager and A. G. Fisher, *Mol Cell*, 2013, 49, 1023-1033.

222. K. P. Koh, A. Yabuuchi, S. Rao, Y. Huang, K. Cunniff, J. Nardone, A. Laiho, M. Tahiliani, C. A. Sommer, G. Mostoslavsky, R. Lahesmaa, S. H. Orkin, S. J. Rodig, G. Q. Daley and A. Rao, *Cell Stem Cell*, 2011, 8, 200-213.

223. G. Ficz, M. R. Branco, S. Seisenberger, F. Santos, F. Krueger, T. A. Hore, C. J. Marques, S. Andrews and W. Reik, *Nature*, 2011, 473, 398-U589.

224. J. Madzo, H. Liu, A. Rodriguez, A. Vasanthakumar, S. Sundaravel, D. B. D. Caces, T. J. Looney, L. Zhang, J. B. Lepore, T. Macrae, R. Duszynski, A. H. Shih, C. X. Song, M. Yu, Y. T. Yu, R. Grossman, B. Raumann, A. Verma, C. He, R. L. Levine, D. Lavelle, B. T. Lahn, A. Wickrema and L. A. Godley, *Cell Reports*, 2014, 6, 231-244.

225. T. P. Gu, F. Guo, H. Yang, H. P. Wu, G. F. Xu, W. Liu, Z. G. Xie, L. Y. Shi, X. Y. He, S. G. Jin, K. Iqbal, Y. J. G. Shi, Z. X. Deng, P. E. Szabo, G. P. Pfeifer, J. S. Li and G. L. Xu, *Nature*, 2011, 477, 606-U136.

226. K. Iqbal, S. G. Jin, G. P. Pfeifer and P. E. Szabo, *Proc. Natl. Acad. Sci.,*, 2011, 108, 3642-3647.

227. P. A. Jones and P. W. Laird, *Nature Genetics*, 1999, 21, 163-167.

228. E. N. Gal-Yam, G. Egger, L. Iniguez, H. Holster, S. Einarsson, X. M. Zhang, J. C. Lin, G. N. Liang, P. A. Jones and A. Tanay, *P Natl Acad Sci USA*, 2008, 105, 12979-12984.

229. S. Rainier, L. A. Johnson, C. J. Dobry, A. J. Ping, P. E. Grundy and A. P. Feinberg, *Nature*, 1993, 362, 747-749.

230. M. Makos, B. D. Nelkin, M. I. Lerman, F. Latif, B. Zbar and S. B. Baylin, *Proc. Natl. Acad. Sci.,*, 1992, 89, 1929-1933.

231. S. Shahrzad, K. Bertrand, K. Minhas and B. L. Coomber, *Epigenetics*, 2007, 2, 119-125.

232. K. Skowronski, S. Dubey, D. Rodenhiser and B. L. Coomber, *Epigenetics*, 2010, 5.

233. Q. Liu, L. Liu, Y. Zhao, J. Zhang, D. Wang, J. Chen, Y. He, J. Wu, Z. Zhang and Z. Liu, *Mol. Cancer Ther.*, 2011, 10, 1113-1123.

234. Q. Y. Liu, K. L. Wu, Y. Zhu, Y. M. He, J. G. Wu and Z. S. Liu, *Hepatol Res*, 2007, 37, 376-388.

235. C. J. Mariani, A. Vasanthakumar, J. Madzo, A. Yesilkanal, T. Bhagat, Y. Yu, S. Bhattacharyya, R. H. Wenger, S. L. Cohn, J. Nanduri, A. Verma, N. R. Prabhakar and L. A. Godley, *Cell Reports*, 2014, 7, 1343-1352.

236. A. Walczak-Drzewiecka, M. Ratajewski, L. Pulaski and J. Dastych, *Biochem Bioph Res Co*, 2010, 391, 1028-1032.

237. J. Li, M. X. Shi, Y. Cao, W. S. Yuan, T. X. Pang, B. Z. Li, Z. Sun, L. Chen and R. C. H. Zhao, *Biochem Bioph Res Co*, 2006, 342, 1341-1351.

238. X. Sun, J. R. Kanwar, E. Leung, K. Lehnert, D. Wang and G. W. Krissansen, *Gene Ther*, 2001, 8, 638-645.

239. O. Stoeltzing, M. F. McCarty, J. S. Wey, F. Fan, W. Liu, A. Belcheva, C. D. Bucana, G. L. Semenza and L. M. Ellis, *J Natl Cancer Inst*, 2004, 96, 946-956.

240. M. W. Halterman, C. C. Miller and H. J. Federoff, *The Journal of neuroscience : the official journal of the Society for Neuroscience*, 1999, 19, 6818-6824.

241. G. L. Semenza, *Nature Reviews Cancer*, 2003, 3, 721-732.

242. S. L. Dunwoodie, *Dev. Cell*, 2009, 17, 755-773.

243. M. C. Simon and B. Keith, *Nat Rev Mol Cell Bio*, 2008, 9, 285-296.

244. T. Schlake and J. Bode, *Biochemistry-Us*, 1994, 33, 12746-12751.

245. N. L. Craig, *Annual Review of Genetics*, 1988, 22, 77-105.

246. D. Schnappinger and W. Hillen, *Arch Microbiol*, 1996, 165, 359-369.

247. A. Yamaguchi, T. Udagawa and T. Sawai, *J. Biol. Chem*, 1990, 265, 4809-4813.

248. B. Eckert and C. F. Beck, *J. Biol. Chem*, 1989, 264, 11663-11670.

249. B. Eckert and C. F. Beck, *J Bacteriol*, 1989, 171, 3557-3559.

250. A. Wissmann, R. Baumeister, G. Muller, B. Hecht, V. Helbl, K. Pfleiderer and W. Hillen, *Embo J*, 1991, 10, 4145-4152.

251. T. Lederer, M. Takahashi and W. Hillen, *Anal Biochem*, 1995, 232, 190-196.

252. P. Orth, D. Schnappinger, W. Hillen, W. Saenger and W. Hinrichs, *Nat Struct Biol*, 2000, 7, 215-219.

253. M. Gossen, S. Freundlieb, G. Bender, G. Muller, W. Hillen and H. Bujard, *Science*, 1995, 268, 1766-1769.

254. J. Degenkolb, M. Takahashi, G. A. Ellestad and W. Hillen, *Antimicrobial Agents and Chemotherapy*, 1991, 35, 1591-1595.

255. T. Lederer, M. Kintrup, M. Takahashi, P. E. Sum, G. A. Ellestad and W. Hillen, *Biochemistry-Us*, 1996, 35, 7439-7446.

256. M. Gossen, S. Freundlieb, G. Bender, G. Muller, W. Hillen and H. Bujard, *Science*, 1995, 268, 1766-1769.

257. S. S. S. Alwi, B. E. Cavell, U. Telang, M. E. Morris, B. M. Parry and G. Packham, *Brit J Nutr*, 2010, 104, 1288-1296.

258. N. M. Chau, P. Rogers, W. Aherne, V. Carroll, I. Collins, E. McDonald, P. Workman and M. Ashcroft, *Cancer Res*, 2005, 65, 4918-4928.

259. X. H. Wang, B. E. Cavell, S. S. Syed Alwi and G. Packham, *Biochemical Pharmacology*, 2009, 78, 261-272.

260. A. Rapisarda, B. Uranchimeg, D. A. Scudiero, M. Selby, E. A. Sausville, R. H. Shoemaker and G. Melillo, *Cancer Res*, 2002, 62, 4316-4324.

261. M. P. Mongiardi, V. Stagni, M. Natoli, D. Giaccari, I. D'Agnano, M. L. Falchetti, D. Barila and A. Levi, *Cell Cycle*, 2011, 10, 4311-4320.

262. Y. J. Cao, T. Shibata and N. G. Rainov, *Gene Ther*, 2001, 8, 1357-1362.

263. D. E. Post and E. G. Van Meir, *Gene Ther*, 2001, 8, 1801-1807.

264. P. Jaakkola, D. R. Mole, Y. M. Tian, M. I. Wilson, J. Gielbert, S. J. Gaskell, A. von Kriegsheim, H. F. Hebestreit, M. Mukherji, C. J. Schofield, P. H. Maxwell, C. W. Pugh and P. J. Ratcliffe, *Science*, 2001, 292, 468-472.

265. C. C. Wykoff, N. J. Beasley, P. H. Watson, K. J. Turner, J. Pastorek, A. Sibtain, G. D. Wilson, H. Turley, K. L. Talks, P. H. Maxwell, C. W. Pugh, P. J. Ratcliffe and A. L. Harris, *Cancer Res*, 2000, 60, 7075-7083.

266. K. W. Lau, Y. M. Tian, R. R. Raval, P. J. Ratcliffe and C. W. Pugh, *Brit J Cancer*, 2007, 96, 1284-1292.

267. M. Uemura, H. Yamamoto, I. Takemasa, K. Mimori, T. Mizushima, M. Ikeda, M. Sekimoto, Y. Doki and M. Mori, *Anticancer Research*, 2011, 31, 507-514.

268. K. A. Kocemba, H. van Andel, A. de Haan-Kramer, K. Mahtouk, R. Versteeg, M. J. Kersten, M. Spaargaren and S. T. Pals, *Leukemia*, 2013, 27, 1729-1737.

269. T. Kamura, M. N. Conrad, Q. Yan, R. C. Conaway and J. W. Conaway, *Gene Dev*, 1999, 13, 2928-2933.

270. M. Tan, Q. Gu, H. He, D. Pamarthy, G. L. Semenza and Y. Sun, *Oncogene*, 2008, 27, 1404-1411.

271. T. Shoshani, A. Faerman, I. Mett, E. Zelin, T. Tenne, S. Gorodin, Y. Moshel, S. Elbaz, A. Budanov, A. Chajut, H. Kalinski, I. Kamer, A. Rozen, O. Mor, E. Keshet, D. Leshkowitz, P. Einat, R. Skaliter and E. Feinstein, *Molecular and Cellular Biology*, 2002, 22, 2283-2293.

272. K. Geiger, A. Leiherer, A. Muendlein, N. Stark, S. Geller-Rhomberg, C. H. Saely, M. Wabitsch, P. Fraunberger and H. Drexel, *Plos One*, 2011, 6.

273. M. Alvarez-Tejado, S. Naranjo-Suarez, C. Jimenez, A. C. Carrera, M. O. Landazuri and L. del Peso, *J. Biol. Chem*, 2001, 276, 22368-22374.

274. G. L. Semenza, P. H. Roth, H. M. Fang and G. L. Wang, *J. Biol. Chem*, 1994, 269, 23757-23763.

275. K. Franke, M. Gassmann and B. Wielockx, *Blood*, 2013, 122, 1122-1128.

276. D. Yoon, Y. D. Pastore, V. Divoky, E. Liu, A. E. Mlodnicka, K. Rainey, P. Ponka, G. L. Semenza, A. Schumacher and J. T. Prchal, *J. Biol. Chem*, 2006, 281, 25703-25711.

277. S. Kajimura, K. Aida and C. M. Duan, *Proc. Natl. Acad. Sci.,*, 2005, 102, 1240-1245.

278. S. I. Tazuke, N. M. Mazure, J. Sugawara, G. Carland, G. H. Faessen, L. F. Suen, J. C. Irwin, D. R. Powell, A. J. Giaccia and L. C. Giudice, *Proc. Natl. Acad. Sci.,*, 1998, 95, 10188-10193.

279. D. J. Stuehr, *Bba-Bioenergetics*, 1999, 1411, 217-230.

280. G. Melillo, T. Musso, A. Sica, L. S. Taylor, G. W. Cox and L. Varesio, *J Exp Med*, 1995, 182, 1683-1693.

281. F. Jung, L. A. Palmer, N. Zhou and R. A. Johns, *Circ Res*, 2000, 86, 319-325.

282. F. Coulet, S. Nadaud, M. Agrapart and F. Soubrier, *J. Biol. Chem*, 2003, 278, 46230-46240.

283. A. Ozer, L. C. Wu and R. K. Bruick, *Proc. Natl. Acad. Sci.,*, 2005, 102, 7481-7486.

284. Z. Q. Wang, M. H. Malone, M. J. Thomenius, F. Zhong, F. Xu and C. W. Distelhorst, *J. Biol. Chem*, 2003, 278, 27053-27058.

285. L. W. Ellisen, K. D. Ramsayer, C. M. Johannessen, A. Yang, H. Beppu, K. Minda, J. D. Oliner, F. McKeon and D. A. Haber, *Mol Cell*, 2002, 10, 995-1005.

286. Y. D. Jiang, W. Zhang, K. Kondo, J. M. Klco, T. B. St Martin, M. R. Dufault, S. L. Madden, W. G. Kaelin and M. Nacht, *Molecular Cancer Research*, 2003, 1, 453-462.

287. J. Chen, S. J. Zhao, K. Nakada, Y. Kuge, N. Tamaki, F. Okada, J. X. Wang, M. Shindo, F. Higashino, K. Takeda, M. Asaka, H. Katoh, T. Sugiyama, M. Hosokawa and M. Kobayashi, *Am J Pathol*, 2003, 162, 1283-1291.

288. K. Kumar, S. Wigfield, H. E. Gee, C. M. Devlin, D. Singleton, J. L. Li, F. Buffa, M. Huffman, A. L. Sinn, J. Silver, H. Turley, R. Leek, A. L. Harris and M. Ivan, *Journal of Molecular Medicine*, 2013, 91, 749-758.

289. J. Y. Lee, Y. S. Lee, J. M. Kim, K. Kim, J. S. Lee, H. S. Jang, I. S. Shin, W. Suh, E. S. Jeon, J. Byun and D. K. Kim, *Gene Ther*, 2006, 13, 857-868.

290. C. B. Sacramento, J. Z. Moraes, P. M. A. Denapolis and S. W. Han, *Braz J Med Biol Res*, 2010, 43, 722-727.

291. T. K. Prasad and N. M. Rao, *Cell Mol Biol Lett*, 2005, 10, 203-215.

292. D. A. Dean, *Experimental Cell Research*, 1997, 230, 293-302.

293. T. Shinojima, M. Oya, A. Takayanagi, R. Mizuno, N. Shimizu and M. Murai, *Carcinogenesis*, 2007, 28, 529-536.

294. Y. G. Yoo, J. Christensen and L. E. Huang, *Cancer Res*, 2011, 71, 1244-1252.

295. N. Sanchez-Puig, D. B. Veprintsev and A. R. Fersht, *Mol Cell*, 2005, 17, 11-21.

296. R. Y. H. Wang, C. W. Gehrke and M. Ehrlich, *Nucleic Acids Res*, 1980, 8, 4777-4790.

297. M. Frommer, L. E. McDonald, D. S. Millar, C. M. Collis, F. Watt, G. W. Grigg, P. L. Molloy and C. L. Paul, *Proc. Natl. Acad. Sci.*, 1992, 89, 1827-1831.

298. R. Shapiro, Braverma.B, J. B. Louis and R. E. Servis, *J. Biol. Chem*, 1973, 248, 4060-4064.

299. J. G. Herman, J. R. Graff, S. Myohanen, B. D. Nelkin and S. B. Baylin, *P Natl Acad Sci USA*, 1996, 93, 9821-9826.

300. A. P. Bird, *Nature*, 1986, 321, 209-213.

301. D. Cooper and M. Krawczak, *Hum Genet*, 1989, 83, 181-188.

302. E. Smith, T. Bianco-Miotto, P. Drew and D. Watson, *Biotechniques*, 2003, 35, 32-33.

303. L. C. Li and R. Dahiya, *Bioinformatics*, 2002, 18, 1427-1431.

304. G. X. Hu, *DNA Cell Biol*, 1993, 12, 763-770.

305. M. Y. Zhou and C. E. Gomez-Sanchez, *Current Issues in Molecular Biology*, 2000, 2, 1-7.

306. C. Bock, S. Reither, T. Mikeska, M. Paulsen, J. Walter and T. Lengauer, *Bioinformatics*, 2005, 21, 4067-4068.

307. Y. M. Lee, C. H. Jeong, S. Y. Koo, M. J. Son, H. S. Song, S. K. Bae, J. A. Raleigh, H. Y. Chung, M. A. Yoo and K. W. Kim, *Developmental Dynamics*, 2001, 220, 175-186.

308. K. G. Pringle, K. L. Kind, J. G. Thompson and C. T. Roberts, *Placenta*, 2007, 28, 1147-1157.

309. A. Horiuchi, T. Hayashi, N. Kikuchi, A. Hayashi, C. Fuseya, T. Shiozawa and I. Konishi, *International Journal of Cancer*, 2012, 131, 1755-1767.

310. A. A. Rawluszko-Wieczorek, K. Horbacka, P. Krokowicz, M. Misztal and P. P. Jagodzinski, *Molecular Cancer Research : MCR*, 2014, 12, 1112-1127.

311. M. W. Luczak, A. Roszak, P. Pawlik, H. Kedzia, M. Lianeri and P. P. Jagodzinski, *Oncology reports*, 2011, 26, 1259-1264.

312. K. Steinmann, A. M. Richter and R. H. Dammann, *Genes & Cancer*, 2011, 2, 65-73.

313. J. Rossler, I. Stolze, S. Frede, P. Freitag, L. Schweigerer, W. Havers and J. Fandrey, *Journal of Cellular Biochemistry*, 2004, 93, 153-161.

314. M. Ream, A. M. Ray, R. Chandra and D. M. Chikaraishi, *American journal of physiology. Regulatory, Integrative and Comparative Physiology*, 2008, 295, R583-595.

315. M. P. Nguyen, S. Lee and Y. M. Lee, *Arch. Pharm. Res.*, 2013, 36, 252-263.

316. Y. P. Tsai and K. J. Wu, *Int. J. Cancer*, 2013, 134, 249-256.

317. J. A. Watson, C. J. Watson, A. McCann and J. Baugh, *Epigenetics*, 2010, 5, 293-296.

318. S. Goverdhana, M. Puntel, W. Xiong, J. M. Zirger, C. Barcia, J. F. Curtin, E. B. Soffer, S. Mondkar, G. D. King, J. Hu, S. A. Sciascia, M. Candolfi, D. S. Greengold, P. R. Lowenstein and M. G. Castro, *Molecular Therapy*, 2005, 12, 189-211.

319. T. Shibata, A. J. Giaccia and J. M. Brown, *Gene Ther*, 2000, 7, 493-498.

320. K. Binley, Z. Askham, L. Martin, H. Spearman, D. Day, S. Kingsman and S. Naylor, *Gene Ther*, 2003, 10, 540-549.

321. T. Shibata, A. J. Giaccia and J. M. Brown, *Neoplasia*, 2002, 4, 40-48.

322. T. L. Riss, R. A. Moravec and A. L. Niles, *Methods Mol Biol*, 2011, 740, 103-114.

323. I. Vermes, C. Haanen, H. Steffensnakken and C. Reutelingsperger, *J Immunol Methods*, 1995, 184, 39-51.

324. G. Chinnadurai, *Cancer Res*, 2009, 69, 731-734.

325. K. G. R. Quinlan, M. Nardini, A. Verger, P. Francescato, P. Yaswen, D. Corda, M. Bolognesi and M. Crossley, *Molecular and Cellular Biology*, 2006, 26, 8159-8172.

326. D. Corda, A. Colanzi and A. Luini, *Trends Cell Biol*, 2006, 16, 167-173.

327. E. Kaiser, Colescot.Rl, Bossinge.Cd and P. I. Cook, *Analytical Biochemistry*, 1970, 34, 595-598.